AE3200 Design Synthesis Exercise (2012-2013)

Final Report

DelFFi Delta & Phi: Two Nanosatellites for Formation Flying in Low-Earth Orbit

Group Delta

July 2, 2013

Delft University of Technology

TU Delft Delft University of Technology

Challenge the future

AE3200 Design Synthesis Exercise (2012-2013)

Final Report

DelFFi Delta & Phi: Two Nanosatellites for Formation Flying in Low-Earth Orbit

Group Delta
July 2, 2013

M.H.G. Akerboom	4008766
M. Deklerck	4106989
J.R. Hess	4087321
F. Paredis	4093941
S.D. Petrovic	4003349
A.D.T. Rijndorp	4098927
A. Schulz	4124251
M.G. Talboom	1522396
R.L.P. Wildvank	1320343

A. Cervone	Principal Tutor
O. Stroosma	Coach
D. Dirkx	Coach

Change Record

Version	Date	Paragraphs affected	Changes
0.1	15/06/2013	All	New Final Report
0.2	21/06/2013	All	Internal comments processed
1.0	01/07/2013	All	Tutor comments processed

PREFACE

This document is the one in relation with the course AE3200 Design Synthesis Excercise (DSE), a course taught at the Faculty of Aerospace Engineering of Delft University of Technology, The Netherlands. The DSE concludes the Bachelor (BSc) head phase of the Aerospace Engineering program. It is intended to facilitate students in gaining design experience. To realize this, it takes students through the complete design process of an aerospace project in a structured and iterative manner.

In general, groups of eight to ten students take on one specific project. In this case, the project envelopes the design of one out of two satellites that are actually being designed by Delft University of Technology and will be part of the QB50 mission.

The Von Karman Institute (VKI) set up a mission with the name QB50 which consists of 50 CubeSats. CubeSats are small scale satellites (nanosatellites) with a mass between one and ten kilograms that feature a modular, cube-like design. The CubeSats related to the QB50 mission will be launched into a Low Earth Orbit (LEO) and they will perform measurements in the thermosphere. Next to these measurements, other mission objectives will also be performed by the individual CubeSats. Delft University of Technology designs two of these nanosatellites, with the primary goal of demonstrating a coordinated formation flight.

This is the Final Report of the Design Synthesis Exercise: DelFFi Delta & Phi: Two Nanosatellites for Formation Flying in Low-Earth Orbit (Delta Group). The project objective is to generate a complete design, down to the sub-system level, of two CubeSats. Being the Delta group, the Delta satellite was designed. In addition to the objectives described before, a secondary (DSE) mission is performed. Previously created documents for the Design Synthesis Exercise: DelFFi Delta & Phi: Two Nanosatellites for Formation Flying in Low-Earth Orbit (Delta Group)" are the Project Plan, the Baseline Report and the Mid-term Report.

This document is intended to be read by university staff involved in the course for grading and guidance purposes. Furthermore, future students enrolled in the same course might want to use this document as a guideline on how to set up similar documents. Lastly, anyone with an interest in the topic might want to give this document a read. The academic level coincides with the knowledge of students with a BSc in the field of aerospace engineering.

We would like to express our gratitude to our principal tutor, Angelo Cervone, for his guidance during the DSE. We would also like to thank Dominic Dirkx and Olaf Stroosma for being our coaches and for answering our questions. Furthermore, we would like to thank the university staff members who we have talked to, as the information they gave us was very valuable; those were Jasper Bouwmeester, Ron Noomen, Eelco Doornbos, Pieter Visser, Kees Sudmeijer and Prem Sundaramoorthy. Finally, we would like to thank Delft University of Technology for providing us with its facilities and resources.

SUMMARY

The QB50 program consists of 50 CubeSats that will be launched in 2015. The CubeSats will be injected into an orbit with an altitude of 320 km to perform different objectives. Delft University of Technology proposed to design two CubeSats. These are named Delta and Phi and together they are referred to as the DelFFi mission. The phase A design of the Delta satellite is presented in this report.

The primary mission is the QB50 mission. For this mission, the satellite will be equipped with a Flux-Φ-Probe and a set of thermocouples, which will be used to investigate the properties of the lower thermosphere.

Next to the thermospheric measurements, Delta and Phi will perform a formation flying demonstration. The formation flying requirements state that the satellites should remain at a distance of 1000 km relative to each other. This should be done within a control box of 100 km.

The third objective of the Delta satellite is to perform a secondary (DSE) mission objective. The choice has been made to carry a re-entry capsule inside the satellite and eject it just before the satellite will burn-up in the lower atmosphere.

A number of goals were achieved to design different aspects of the Delta mission. These goals are:

- Analyze the astrodynamic properties of the satellite and its orbit
- Formulate a formation flying strategy
- Determine subsystem characteristics in terms of mass, power, volume, and cost
- Investigate potential design solutions on a subsystem level that respect the established budgets
- Design a re-entry capsule to carry out the partial non-destructive re-entry mission
- Create a post-DSE schedule for the satellite design and mission operation
- Perform a market and financial analysis

From analyzing the astrodynamic properties it was concluded that the mission lifetime will be approximately 100 days. In these 100 day the three mission objectives will be performed, namely the QB50 measurements, formation flying mission and the partial non-destructive re-entry. The formation flying mission will be demonstrated for 7 consecutive days. The ΔV budget for each satellite is set to be 15 m/s. And the end of the satellites life, partial non-destructive re-entry will be demonstrated.

The solar panel configuration will consist of two body mounted and two deployable solar panels, which are all placed on one side of the satellite. Therefore, the satellite is controlled along the long axis by the AOCS, in order to obtain the most power and still fly in low drag attitude. Furthermore, the AOCS is able to detumble the satellite during initialization. To do this, three magnetorquers and three reaction wheels are used as actuators. The senors of the AOCS consist of a magnetometer and six sun sensors. For obtaining the ΔV during the formation flight, a propulsion system is used. It will consist of 18 Cold-Gas Generators and 16 MEMS Resistojets.

For the partial non-destructive re-entry, a capsule with a custom designed ejection system is used. The capsule and the ejection system will be located at the bottom of the satellite. The capsule will be ejected with the heat shield facing the direction of flight. The heat shield has a 9 mm layer of PICA and a thermal insulation of 3 mm. The heat shield will protect the capsule components from heat generated during re-entry. The capsule will land with a velocity of 17 m/s in a landing zone with a footprint of 1850 km by 107 km. To locate the capsule, the Argos network will be used.

The cost analysis showed that the nanosatellite markets are growing and are expected to keep growing in the future. A growth of 16.8% to 23.5% per year is expected during the next seven years. The total cost of the mission is estimated to be €1,772,000 and includes a 10% margin.

LIST OF SYMBOLS

Greek symbols

α	Absorption	[−]
χ	Heading angle	[rad]
γ	Flight path angle	[rad]
γ_h	Specific heat ratio	[−]
Λ	Mass ratio	[−]
λ	Longitude	[rad]
μ	Bank angle	[rad]
μ_E	Earth's gravitational parameter	[m^3/s^2]
ν	True anomaly	[rad]
Ω	Right ascension of the ascending node	[rad]
ω	Rotational rate	[rad/s]
Φ	Solar constant	[W/m^2]
ϕ	Angle of incidence	[rad]
ϕ	Argument of latitude	[rad]
ϕ	Carrier phase	[rad]
ϕ	Latitude	[rad]
ρ	Density	[kg/m^3]
σ	Normal stress	[Pa]
σ	Ratio of densities	[−]
σ_{boltz}	Boltzmann constant	[$m^2kgs^{-2}K^{-1}$]
ε	Oblateness	[−]
ε_{emit}	Emittance	[−]

Roman symbols

A	Area	[m^2]
a	Acceleration	[m/s^2]
a	Semi-major axis	[m]
A_{mp}	Amplitude	[m]
B	Bandwidth capacity	[bps]
B	Magnetic field strength	[T]
C	Channel capacity	[bps]
c	Speed of light	[m/s]
C/N	Carrier-to-Noise ratio	[−]
C^*	Characteristic velocity	[m/s]

C_d	Drag coefficient	[−]
cm	Center of mass	[m]
cp_a	Center of aerodynamic pressure	[m]
cp_s	Center of solar radiation pressure	[m]
D	Dipole moment	$[\mathrm{A} \cdot \mathrm{m}^2]$
D	Drag	[N]
d	Depth	[m]
d	Diameter	[m]
$d_{\theta,\mathrm{drift}}$	Along track drift	[m]
E	Elastic modulus	[Pa]
e	Eccentricity	[−]
F	Force	[N]
f	Daylight fraction	[−]
f	Frequency	[Hz]
G	Gain	[dB]
H	Effective heat ablation	[J/kg]
h	Altitude	[m]
h	Height	[m]
I	Inertia	$[\mathrm{m}^4]$
i	Inclination	[unit]
I_{sp}	Specific impulse	[s]
J	Radiation intensity	$[\mathrm{W}/\mathrm{m}^2]$
J_2	Orbit perturbation	[−]
L	Lift	[N]
L	Loss	[dB]
l	Length	[m]
M	Magnetic moment of the Earth multiplied by the magnetic constant	$[\mathrm{T} \cdot \mathrm{m}^3]$
M	Molar mass	[kg/mol]
m	Mass	[kg]
m	Modulation signal	[−]
P	Period	[s]
P	Power	[W]
P	Pressure	[s]
Q	Heat load	$[\mathrm{J}/\mathrm{m}^2]$
q	Dynamic pressure	[Pa]
q	Heat rate	$[\mathrm{W}/\mathrm{m}^2]$
q	Reflectance factor	[−]
R	General gas constant	[J/mol/K]
r_a	Distance to apogee	[m]
R_E	Earth radius	[m]

r_p	Distance to perigee	[m]
S	Surface area	[m^2]
S/N	Signal-to-Noise ratio	[−]
s_d	Decay	[m/rev]
T	Temperature	[K]
t	Thickness	[m]
t	Time	[s]
T_a	Atmospheric Drag Torque	[Nm]
T_m	Magnetic torque	[Nm]
T_s	Solar Radiation Pressure Torque	[Nm]
u	Velocity in x-direction	[m/s]
V	Velocity	[m/s]
v	Velocity in y-direction	[m/s]
w	Velocity in z-direction	[m/s]
w	Width	[m]

LIST OF ACRONYMS

1U,2U,3U	1-Unit, 2-Unit and 3-Unit CubeSat size, respectively
AOCS	Attitude and Orbital Control System
ASK	Amplitude Shift Keying
BER	Bit Error Rate
BPSK	Binary Phase Shift Keying
C&DH	Command and Data Handling
CCR	Corner Cube laser Reflector
CD	Command and Data
COM	Communication
COTS	Commercial off-the-shelf
CVCM	Collected Volatile Condensible Material
DC	Direct Current
DOD	Dept-of-Discharge
DSE	Design Synthesis Exercise
ECSS	European Cooperation for Space Standardization
EIRP	Equivalent Isotropic Radiated Power
EPS	Electrical Power System
FIPEX	Flux-Φ-Probe Experiment
FSK	Frequency Shift Keying
G-EPS	Global Electric Power System
GaAs	Gallium Arsenide
GENSO	Global Educational Network of Satellite Operations
GMT	Greenwich Mean Time
GPS	Global Positioning System
GS	Ground Station
GSE	Ground Support Equipment
I^2C	Inter Integrated Circuit
IC	Integrated Circuit
IOD	In Orbit Demonstration
ISIS	Innovative Solution In Space
ISL	Inter-Satellite Link
LA	Launcher
LEO	Low Earth Orbit
LNA	Low-Noise Amplifier
MATLAB	Matrix Laboratory
MEMS	Micro-Electro-Mechanical Systems
MPPT	Maximum Power Point Trackers
NASA	National Aeronautics and Space Administration
OBC	On-Board Computer
OBDH	On-Board Data Handling
P-POD	Poly Picosatellite Orbital Deployer
PAY	Payload
PCB	Printed Circuit Board
PICA	Phenolic Impregnated Carbon Ablator
PNR	Partial Non-destructive Re-entry
PPT	Pulsed Plasma Thruster
PR	Propulsion

PWR	Power
QPSK	Quadrature Phase Shift Keying
RCC	Reinforced Carbon-Carbon
RO	Radio Occultation
RTD	Resistance Temperature Detectors
SB	Space Bus
SD	Secure Data
SDHC	Secure Data High Capacity
SDXC	Secure Data eXtended Capacity
SLA	Super Light Weight Ablator
SS	Space System
STR	Structure
TBC	To Be Confirmed
tbd	To Be Determined
TML	Total Mass Loss
TPS	Thermal Protection System
TT&C	Telemetry, Tracking and Command
UHF	Ultra High Frequency
UTC	Universal Time
VCE	Vehicle Carried normal Earth reference frame
VHF	Very High Frequency
VKI	von Karman Institute for Fluid Dynamics
XTJ	NeXt Triple Junction

TABLE OF CONTENTS

CHAPTER 1

INTRODUCTION

The QB50 program consists of 50 CubeSats that will be launched in 2015. The CubeSats will be injected into an orbit with an altitude of 320 km to perform different mission objectives and will be equipped with a predefined set of sensors. These sensors will perform measurements in the Low Earth Orbit (LEO) and will continue the measurements until the CubeSats burn up upon re-entry. Considering the amount of CubeSats that will be launched, a significant amount of data will be obtained. This data is intended to provide more insight into the thermosphere.

Furthermore, within the QB50 project ten CubeSats will be performing an In-Orbit Demonstration (IOD). Delft University of Technology proposed to design two CubeSats. These are named Delta and Phi and together they are referred to as the DelFFi mission. During the DSE, these two satellites will be designed by two separate teams. Besides the QB50 mission, Delta and Phi will perform formation flying demonstration. The last objective of the Delta satellite is to perform a secondary (DSE) mission objective: Partial non-destructive re-entry will be demonstrated. This mission objective can give an impulse to hypersonic research due to the low cost of CubeSats when compared to larger satellites.

The purpose of this report is to give a detailed design of the DelFFi mission, after the conceptual design of the subsystems in the Mid-term report. Furthermore, the report elaborates on how the mission objective of formation flight is achieved. Finally, a detailed design of the partial non-destructive re-entry mission is given.

Chapter 2 gives an outline on the QB50 mission, formation flying and partial non-destructive re-entry. Furthermore, Chapter 2 also contains technical risk management and the mass, volume and power budget. In Chapter 3, the astrodynamics of the mission are explained. In particular, the air density prediction method and the strategy to perform formation flying are presented. Chapter 4 gives the detailed design of the satellite. This contains the design of the different subsystems, but also the sensitivity analysis. Within Chapter 5, the DSE mission is treated in detail. Next to the flight profile and heat shield determination, the deployment of the capsule, its retrieval and general layout is treated. The subsystem integration and the physical appearance is shown in Chapter 6. This is followed by the post-design phase in Chapter 7, which gives an overview of all activities that will be executed after the DSE has been finished. Chapter 8 provides information on the sustainable development strategy, while Chapter 9 presents the cost analysis. Subsequently, Chapter 10 will verify the requirements that were set up in the Baseline report [1] and validate the mathematical models that were set up. Finally, conclusions and recommendations are stated in Chapter 11.

CHAPTER 2

MISSION OUTLINE

DelFFi Delta is part of the QB50 mission and performs different mission objectives during its lifetime. In the following section an outline of these mission objectives will be given.

Starting with the primary payload, the Von Karman Institute mission objective will be discussed in Section 2.1. This includes the different payload sets which will be used on-board of all the CubeSats. Afterwards, the formation flying mission will be elaborated on, which presents an overview of the formation flying strategy. Subsequently, the DSE mission objective of partial non-destructive re-entry is presented in Section 2.3. In Section 2.4 a technical risk assessment is performed. Risk mitigation strategies are presented here as well. Finally the power, mass and volume budgets are presented in Section 2.5

Table 2.1 gives a time line of the DelFFi mission and the performed tasks throughout the mission. A functional flow diagram and functional breakdown diagram are given in Chapter A.

Table 2.1: Timetable of satellite mission life time

Timing	**Activity**
T_0 - Δt_1	Launch
T_0	Orbit injection of Phi
T_0 + Δt_2	Orbit injection Delta
T_0 + 1 hour	Initialize EPS
T_0 + 1 hour	Initialize C&DH
T_0 + 1 hour	Initialize AOCS
T_0 + 1 hour	Start of detumbling
T_0 + 25 hours	End of detumbling
T_0 + 26 hours	Deployment of solar arrays and antennas
T_0 + 27 hours	Initialize TT&C Delta & Phi
T_0 + 36 hours	Switch on QB50 payload on both Delta & Phi
T_0 + 40 hours	Completed check-out of Delta & Phi
T_0 + 42 hours	Start formation acquisition using differential drag (7 days)
T_0 + 3 days	Determination of relative motion and drift
T_0 + 4 days	Propulsion test run
T_0 + 4 days	End of initialization phase
T_0 + 8 days	Formation acquired, start of formation flight demonstration
T_0 + 15 days	End of formation flight demonstration
T_0 ± 100 days	End of primary payload mission
T_0 ± 100 days	Begin re-entry mission
T_0 ± 100 days	Heating of Delta
T_0 ± 100 days	Capsule deployment
T_0 ± 100 days	Delta burn-up
T_0 ± 100 days	Capsule re-entry
T_0 ± 100 days	Burning heat shield
T_0 ± 100 days	Send radio beacon to retrieve capsule
T_0 ± 100 days	Landing on ground

2.1 QB50 Mission

The QB50 mission has the scientific objective to study in situ the temporal and spatial variations of a number of key constituents and parameters in the lower thermosphere with a network of 40 2U and 10 3U CubeSats [2]. QB50 will also study the re-entry process by measuring a number of key parameters during re-entry and by comparing predicted and actual CubeSat trajectories as well as orbital lifetimes. QB50 will also accommodate 10 double or triple unit CubeSats that will perform an In-Orbit Demonstration (IOD) of technologies and miniaturized science sensors. The DelFFi Delta satellite will carry a predefined QB50 payload. The IOD of choice for the Delft University of Technology satellites is a formation flying demonstration.

The 50 satellites will be equipped with sensor payloads for measurements in the lower thermosphere, as well as during re-entry. There are three sets of payloads that can be integrated into the satellite. These three sensor payload sets will be distributed among the 50 satellites. In Table 2.2 the three different sets are shown. The DelFFi Delta satellite will accommodate payload set 2, which focuses on in situ measurements in the lower thermosphere.

Table 2.2: The three sensors payload sets for atmospheric research

Set 1	**Set 2**	**Set 3**
Neutral Mass Spectrometer	Flux-Φ-Probe Experiment	A set of 4 Langmuir probes
2 Corner Cube Retroreflectors*	2 Corner Cube Retroreflectors*	2 Corner Cube Retroreflectors*
Thermistors/thermocouples/RTD	Thermistors/thermocouples/RTD	Thermistors/thermocouples/RTD)

*Optional

The Flux-Φ-Probe (FIPEX) is able to distinguish and measure the time resolved behavior of atomic and molecular oxygen as a key parameter of the lower thermosphere. The FIPEX should point in the direction of flight and to obtain as little drag as possible it should be mounted on the top of the satellite.

Furthermore, the Corner Cube Retroreflector (CCR) is a passive device that is used to reflect back laser beams originating from a ground laser ranging station. This could be used to measure the distance and position with respect to the satellite tracking station, since the location of the satellite can immediately be added to the measured data. The CCR is not implemented on the Delta satellite.

Finally, thermistors/thermocouples are used to measure the temperature on-board of the spacecraft [3]. These are added in the QB50 payload.

2.2 Formation Flying

One of the primary goals of the DelFFi mission is to demonstrate a coordinated formation flight. The required parameters of this formation flight are that the two DelFFi satellites should remain at a 1,000 km along track distance during the mission. The satellites are to be positioned within a control window of 100 km with an accuracy of $\pm$ 10 km. Furthermore, in agreement with the DelFFi Phi team it was decided that the formation demonstration duration is set to 7 days, which will commence after the satellite initialization phase of approximately 9 days, directly after the orbit injection. The 7 day formation flying requirement was set up in order to comply with the ΔV budget based on preliminary calculations and the 9 day initialization phase was based on a preliminary detumbling calculation made by the DelFFi Phi team.

Due to the low altitude, formation flying can also be realized through the use of differential drag as corrective force, though it has been decided to not use differential drag for the purpose of formation keeping. The reason for this decision is that formation flying through differential drag poses a lot of requirements on main satellite functions as there are conflicts between the required attitudes of the satellite. Another aspect is that differential drag will decrease the mission lifetime as the satellites will fly with a higher angle of attack on average. However, realizing the 1,000 km along track distance[1] is a task that requires a lot of ΔV as calculated previously [4]. It has been decided that formation acquisition will be partly realized through the use of differential drag. A full elaboration on the formation flying strategy, along with an estimation for the mission lifetime, can be found in Chapter 3.

[1] The satellites are ejected from the same launcher with a small ejection velocity. Therefore, the along track distance that is accumulated over time is very low if no specific action is taken.

2.3 Partial Non-Destructive Re-entry

Besides the QB50 mission, which was the drive from the Von Karman Institute to launch the CubeSats, the TU Delft satellites have an additional primary mission next to demonstrating formation flying with CubeSats. The DSE team designing the Delta satellite, had the option of adding an additional mission: the DSE mission. During the course of the DSE project, several mission options were presented. Three were found to be the most viable; GPS radio occultation, creating an inter-satellite link and partial non-destructive re-entry. In the Midterm Report [4], the final choice for the DSE mission resulted in partial non-destructive re-entry.

The mission objective of partial non-destructive re-entry is to prove that a part of the satellite can survive re-entry. Since a satellite experiences high temperatures during re-entry, it will burn up entirely in the atmosphere. However, in this mission objective a capsule will survive re-entry. To achieve this, a small re-entry capsule will be fitted into the Delta satellite that will be ejected during the final stage of operations of the satellite. After ejection, this capsule will follow a re-entry path that is computed in Section 5.1. During this re-entry path, the capsule will experience large heat rates. To be able to withstand the heat coming from these heat loads, a heat shield needs to be designed. This heat shield will make sure that the internal capsule temperatures are in a reasonable range, being below a maximum temperature at which the internal materials or components fail. Besides the heat shield, a safe landing mechanism needs to be implemented in the capsule. This is to make sure that the capsule survives landing. Furthermore, retrieval of the capsule is of utmost importance. Without capsule retrieval, there will be no proof to see if the mission was successful. Therefore, a retrieval strategy needs to be implemented in the mission, together with a locating device inside the capsule. The entire mission outline and design will be discussed in Chapter 5.

2.4 Technical Risk Management

After the final design is completed, the satellite will be built, launched and it will perform its mission. However, there are events that can occur during launch and operation that can impact the performance of the satellite in a negative way. These events are risks and should be taken into account while designing the satellite. Knowing the risks before designing the satellite is necessary to mitigate the probability of occurrence and/or the impact on the mission. Several technical risks can be identified. They are listed in Table 2.3, together with their probability of occurrence and the impact on the mission execution. In some cases, failure probabilities were estimated unacceptably high during the Mid-term phase. Table 2.3 shows how these probabilities have changed during the Final phase. Afterwards, the risks are elaborated and their mitigation strategy, if required, is explained.

Table 2.3: Technical risks with their probability of occurrence and impact on the mission

	Risk	**Probability (Mid-term)**	**Impact**	**Probability (Final)**
1	Failure of electrical circuits	Low	Significant	Low
2	Power supply failure	Very Low	Critical	Very Low
3	Failure to deploy solar panels	High	Significant	Low
4	Failure of AOCS	Low	Significant	Low
5	Failure of propulsion system	Medium	Significant	Low
6	Thermal system failure	Very Low	Significant	Very Low
7	Failure of communication devices	Low	Critical	Very Low
8	Degradation of materials	Very Low	Significant	Very Low
9	Partial Phi satellite failure	-	Minor	Medium
10	Capsule deployment failure	-	Moderate	Medium
11	Capsule aerodynamic instability	-	Moderate	High
12	OBC crash	-	Significant	Very low

1 - Failure of electrical circuits There is a risk that the electrical circuits fail due to short circuiting of the system or insufficient electrical connections. However, since all satellites contain a large amount of electronics, the knowledge of building durable electrical circuits is extensive. Therefore, the probability of occurrence of electrical circuit failure is low. However, the impact of electrical circuit failure can be significant if a vital system element is affected.

The electrical systems can be tested thoroughly on the ground, reducing the failure probability. Connections will be vibration tested, assuring that the electrical connections will survive the launch loads.

2 - Power supply failure Another risk is that the power system fails partially or entirely. This can be caused by various power system components. This includes partial or total failure of solar panels, which would cause lower or even no power generation, but also energy storage failure and power converter failure. However, if a power system component should fail, the satellite will have only partial or even no operating power. This means that the mission can partly or entirely fail, which leads to a critical impact on the mission execution.

The electrical power system features inherent redundancy through using multiple solar panels and multiple batteries, assuring that the most likely failure mode is partial failure, leading to a reduced performance, rather than complete mission failure.

3 - Failure to deploy solar panels In case of failure of solar panel deployment, the satellite will generate less power than predicted. This will lead to a reduced ability to successfully perform the mission. The probability of occurrence of solar panel deployment failure is high, since mechanisms are involved. However, the impact on the mission execution is moderate since the mission can still be partly completed.

The risk was mitigated by selecting commercial off-the-shelf solar panels (featuring a deployment mechanism) that have a proven track record. If deployment does fail, the TT&C antennas can still be deployed through slots inside the solar panels. In case reduced power is available due to deployment failure, some power saving options are:

- *reducing the formation flying mission duration*
- *reducing the amount of QB50 mission data while still complying with the minimum requirement of 8 Mb per day*
- *limiting the amount of downlink data to the minimum necessary to keep the satellite operational (i.e. reducing the sampling rate of housekeeping data on stable subsystems)*

4 - Failure of AOCS Failure of the AOCS can lead to incomplete or incorrect attitude knowledge and inability of attitude control. This in turn can lead to pointing errors, which cause thrust vector errors. Since the AOCS is a system that has been validated on other satellites and undergoes extensive testing, the probability of occurrence is low. The impact on the mission in case of AOCS failure is significant. The formation flying objective will also be heavily affected as it will not be possible to direct the thrust vector.

Even though the probability of failure is still estimated to be the same, some changes have been made to the system to make it more reliable.

- Sun sensors to the satellite. The solar panels now serve as a fallback system for added redundancy. The solar panels are, however, less precise than the sun sensors.
- The magnetic torquers can also change the attitude of the satellite in case of reaction wheel failure. However, the performance will be lower in terms of both accuracy and adjustment speed.

5 - Failure of propulsion system In case of propulsion system failure, the satellite will not be able to actively change its orbit. This is not a problem for the QB50 mission, but will pose problems for the formation flying mission. As formation flying is a primary mission objective, the impact of propulsion system failure is significant. The chosen propulsion method will have been extensively tested on the ground, and will probably have been used on another nanosatellite. Together with the fact that propulsion systems always have a relatively high uncertainty, the probability of propulsion system failure is medium.

The propulsion system now features multiple cold gas generators and multiple thrusters. In the event that one of the generators fails, the total available ΔV will be reduced. If one of the thrusters fails, the thrust time will have to increase to obtain the same ΔV per thrust.

6 - Thermal system failure Delta features a passive thermal system, which uses material properties to regulate the internal satellite temperature. Thermal regulators such as heat sinks and thermal tape are used. These have been proved to work in the previous Delfi missions. This leads to a very low probability of failure. However, since most of the equipment on the satellite has an operational and non-operational temperature range that lies far from the temperature extremes in the thermosphere, the impact on the mission execution is significant, should the thermal system fail.

7 - Failure of communication devices The communication system can fail in case the antennas fail to deploy or if a processing error occurs. Since the communication system will be based on previous nanosatellites, the probability of failure will be low. However, the impact on the mission is critical, since the data could not be sent in this case, rendering the satellite useless.

The communication system hardware is designed to be partially redundant. With two transceivers on board, a fail safe system is implemented, which reduces the probability of failure. The antennas are positioned in a double dipole configuration in order to provide omni-directional coverage. If one antenna pair would fail, signals can still be transmitted, but there will be singularities in the radiation pattern.

8 - Degradation of materials Degradation of materials over time is the result of possible launch postponements, launch vibrations and environment interactions. Satellites are usually made from materials that have a long degradation time and are to a large extent resistant to the space environment. Therefore, the probability of material degradation over time is very low. However, should this occur, the impact on the satellite systems can be significant.

The degradation effects of solar cells is well known. Internal components are shielded from radiation by using an enclosed outer structure, rather than commercially available structures that feature holes in order to save weight.

9 - Partial Phi satellite failure Even though (partial) failure of the Phi satellite is out of the control of the Delta team, the impact on the formation flying mission objective can be discussed. Even if the Phi satellite would become uncontrollable, a formation flight might still be demonstrated. In this case, Delta would track Phi and adjust its orbit to that of Phi. This is assuming Phi's attitude determination, downlink, and on board computer are still functioning. Therefore, the impact on the total mission is estimated to be minor, but depends on the exact failure mode. Enough propellant is provided on board of Delta to compensate for a (partial) failure of Phi with respect to the formation flying objective.

10 - Capsule deployment failure The capsule deployment system is brand new. It was designed specifically for this mission and is currently in a conceptual design phase. Thus, the probability of failure is high. The capsule might get stuck during deployment, or might not deploy before the satellite has burnt up. This would be potentially catastrophic for the PNR mission objective as the propulsion system might explode in close proximity of the capsule. Nevertheless, the impact was rated only moderate as the objective is only of secondary importance to the mission. *Succesful deployment is ensured by having a passive (backup) deployment mechanism that does not rely on any satellite subsystem to execute.*

11 - Capsule aerodynamic instability No detailed analysis was done yet with respect to the aerodynamic characteristics of the re-entry capsule. An effort was made to keep the center of mass as low as possible, and the geometry resembles that of many blunt body re-entry vehicles. However, the probability of serious instability problems is still high at this stage. Uncontrollable tumbling of the capsule during re-entry will very likely cause the capsule to burn op in the atmosphere. As the objective is only of secondary importance to the mission, the impact was rated moderate. *This risk should be mitigated in the future by making a detailed design of the capsule and careful analysis of the center of pressure and center of gravity, which should result in a lower probability of instability.*

12 - OBC crash The on-board computer might crash for any number of reasons. Permanent failure of both OBCs is a catastrophic event which would render the satellite useless. The event that is considered here is a crash that is recoverable by an OBC reset. As the C&DH is equipped with redundant processors, the event of having both computers crash at the same time is unlikely. In case this does happen, satellite functions will

temporarily be halted. However, a watchdog timer that resets the processors is also implemented in order to recover from crashes. The probability of failure is therefore estimated to be very low.

Risk Map

All risks in Table 2.3 can be put into a risk map. On a risk map, the probability of occurrence of an event, which is found on the horizontal axis, is plotted against the impact of the event on the mission, which is found on the vertical axis. The risk map for the Delta satellite can be found in Table 2.4. The numbers in the risk map correspond to the numbers in Table 2.3. Events that are in the right top corner have a high risk. This means that a rather large part of the resources should be spent on mitigating these risks. The events in the left bottom corner have a low risk and less resources should be spent on mitigating these risks. Values previously determined at the time of writing of the Mid-term Report [4] are shown like 'x', while new or adjusted risks are shown as '**(x)**'.

Table 2.4: Technical Risk Map

Impact	Very low	Low	Medium	High	Very high
Critical	**(7)**, 2	7			
Significant	**(12)**, 6, 8	**(3)**, **(5)**, 1, 4	5	3	
Moderate		**(10)**	**(11)**		
Minor		**(9)**			
Minimal					

Probability of event

2.5 Budgets

Within this section the power, mass and volume budget per subsystem are discussed. The power budget will be presented in Section 2.5.1 and the mass and volume budget will be discussed in Section 2.5.2

2.5.1 Power Budget

The power budget is an important tool in the design of the power supply system. The power supply system should be able to deliver the required power to all the subsystems. Therefore, the power budget shown in Table 2.5a gives an overview of the maximum required power by all subsystems in their active mode. The extensive power budgets per mode are given in Chapter D and are also elaborated in Section 4.2.

2.5.2 Mass and Volume budget

The mass and volume budget are tools to control the layout of the satellite. In the beginning of the project, each subsystem had its predestined mass and volume budget to make sure the requirements were met. After the design phase, the final budgets were set up which can be seen in Table 2.5b. The volume budget is defined based on the thickness. This can be done due to the general layout of a CubeSat. It is based on a layer composition of 10 x 10 cm plates which are placed above each other. Therefore the thickness is more important than the actual volume occupied by the subsystems.

Table 2.5: Budgets

Subsystem	**Max Power [W]**
Power	0.063
C&DH	0.167
Communication	1.7
AOCS	2.061
Propulsion	13.2
QB50 Payload	0.53
DSE Payload	0
System bus	0.25

(a) Power budget

Subsystem	**Mass [g]**	**Thickness [mm]**
Power	650	24
C&DH	161	15
TT&C	270	37
AOCS	438	42
Propulsion	418	58
Structural	630	16
QB50 payload	600	30
Re-entry capsule	150	75
Spacing	0	20
Used	3317	317
Total	3600	340.5
Excess	283	23.5

(b) Mass and volume budget

This chapter will discuss the astrodynamics of the mission. Astrodynamics deals with the general dynamics of the satellite during its mission duration. This includes the formation flight and the general decay of the satellite. The orbital decay is an important part of the astrodynamics of the satellite. The orbital decay is based on the aerodynamic drag of the satellite which is why the air density is an important factor. First a good estimation of the density at the location of the satellite must be acquired. In order to achieve this an air density model is set up in Section 3.1. Once the density is known at all different positions, an orbital decay model can be set up. This model is set up in Section 3.2 and determines the position of the satellite over time. Now that the general movement of the satellite is known, the strategy and ΔV budget for the formation flight can be set up. This is done in Section 3.3. Within this section, the first thing which is described are the possible ways to do formation flying. After this the coordination of the two satellites and their roles with respect to each other are defined. Furthermore, as formation flight is performed it is important to be aware of the possible disturbances which may occur over the duration of the formation flight. These disturbances are also described in Section 3.3. Next, within that section, formation acquisition and keeping are discussed. Within these parts a ΔV budget for countering velocity differences due to aerodynamic drag is set up together with an approach for passive formation acquisition. After this a strategy for command and data flow is established. With this a correction scheme is suggested which leads up to a ΔV budget estimate to adjust for secular drifts. Next a justification for impulsive shots is provided. Lastly the results for the astrodynamics are given in Section 3.4

3.1 Air Density Prediction Method

To be able to predict the trajectory of the satellite over the mission duration, an air density model is set up. This is mainly because the decay of the satellite is caused by aerodynamic drag. This drag has a linear relation with respect to the density and therefore, an accurate density model is necessary. The used model,the NRLmsise-00 model, incorporates many different data bases in order to determine the air density as accurate as possible. More information on the model and the reason for the implementations of different data bases can be found in [5]. This model uses the solar activity, time of the year and location of the satellite as input to determine the density and temperature at the location of the satellite. The model can be found in the aerospace toolbox of MATLAB.

The reason that this model is selected is mainly due to the fact that it incorporates changes in density due to the solar activity. The thermosphere is the layer in the Earth's atmosphere that is most influenced by solar activity. As the satellite will fly within the thermosphere, solar activity should certainly be accounted for. The main solar activity characteristics which influence the air density of the thermosphere are the solar radio flux and the geomagnetic index. The NRLmsise-00 model inputs and outputs are listed below.

NRLmsise-00 inputs
- Altitude [m]
- Latitude [rad]
- Longitude [rad]
- Year
- Day of the year [1-365]
- Seconds in day, in universal time [s]
- Local apparent solar time
- Solar radio flux f81 - values
- Solar radio flux f10.7 - values
- Magnetic index
- FLAGS
- Otype
- Action

NRLmsise-00 outputs
- Air density [kg/m^3]
- Temperature [K]

The determination of the solar radio flux and magnetic index is shown in Section 3.1.1. To obtain the longitude and latitude values, transformations need be performed. These transformations are described in Section 3.1.2. Furthermore, it is assumed that the satellite gets in orbit on the first of April at '00:00:01'

universal time. This implies that the initial day of the year is 90, the seconds in day is 1 second. $f10.7$ stands for the solar radio flux with a wave length of 10.7 cm. $f81$ is the average solar radio flux over 81 days.

3.1.1 Geomagnetic Index and Solar Radio Flux

The air density in the thermosphere is strongly affected by solar activity. The geomagnetic index and solar radio flux are the two variables following from the solar activity which have an influence on the thermospheric air density. Therefore, the solar activity cannot be neglected in the air density model. In order to have values for these variables, the prediction made by NASA for the solar radio flux was analyzed, which is shown in Figure 3.1.

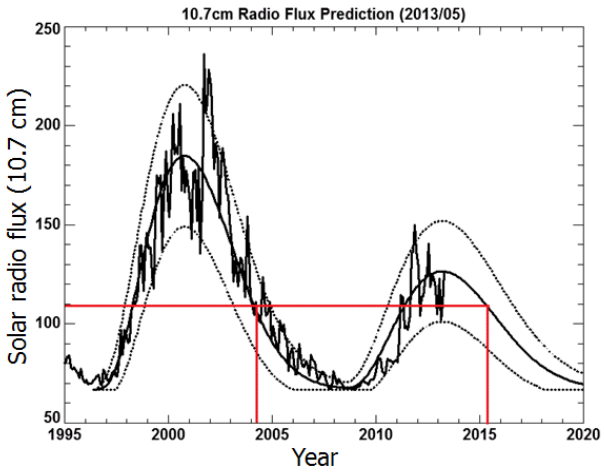

Figure 3.1: Predicted of the solar radio flux made by NASA [6]

Using this graph it can be stated that the same solar activity values, as predicted for April to June 2015, can be found in the same period of the year 2004. Therefore, the historic values from 2004 are used as input for the model [7]. Note that the geomagnetic index has a period of 1 year. Thus the data from April to June 2004 was used for an accurate prediction of the density during the mission duration.

3.1.2 Satellite Location in Atmosphere

The air density is not only a function of the solar activity but it is also based on the location of the satellite in the atmosphere. In case of natural decay, in which the satellite will lower its orbit due to drag, the density will increase. In order to predict this decay, a model is made in Section 3.2. This will result in the altitude of the satellite as a function of time.

In addition to the altitude, the longitude and latitude of the satellite should be known as input for the model. To determine the longitude and latitude, a transformation sequence is required. This sequence is shown in Equation (3.1).

$$\begin{bmatrix} a \\ e \\ i \\ \omega \\ \Omega \\ \nu \end{bmatrix} \Rightarrow \begin{bmatrix} x \\ y \\ z \\ u \\ v \\ w \end{bmatrix} ; \begin{bmatrix} x \\ y \\ z \end{bmatrix} \Rightarrow \begin{bmatrix} \varphi \\ \lambda \\ h \end{bmatrix} \tag{3.1}$$

The initial eccentricity e is set to 0 under the assumption that one revolution is nearly circular. The initial true anomaly ν is set to 1.31 radians (75°) and the Right Ascension of the Ascending Node Ω changes over time and is initially set to 0.698 radians (40°). The values for ν and Ω are extracted from the FAQ of the QB50 website [8]. The difference in Ω is calculated using Equation (3.2), which gives the change in Right Ascension of the Ascending Node for a subsequent $\frac{1}{8}^{th}$ revolution. Within this equation, J_2 represents the irregularities in the Earth's gravity field and R_E is the Earth's radius. This equation also has to be implemented into

a loop for an accurate density computation. The changes in eccentricity and true anomaly will be further discussed in Section 3.2.

$$\Delta\Omega_{rev} = \frac{-3\pi J_2(\frac{R_E}{a})^2 cos(i)}{8} \tag{3.2}$$

The scripts used to perform the transformations steps were found on the MATLAB website [9, 10].

3.2 Orbital Decay

The orbital decay is the effect that describes the descend of the satellite due to drag. To compute the orbital decay, Equations (3.3) to (3.5) are used. These equations give the difference in the semi major axis a, the period P and the velocity V that will occur over the next $\frac{1}{8}^{th}$ revolution. These equations are a variations of equations which give the same parameters per revolution [11].This is done to have more points on one orbit. These equations are derived by means of energy equations where the work performed by the drag is assumed to be done on a circular orbit. This introduces a small error that becomes larger the more iterations are done and the more the orbit becomes elliptical.

$$\Delta a = \frac{-\pi \cdot C_d \cdot A \cdot \rho \cdot a^2}{4 \cdot m} \tag{3.3}$$

$$\Delta P = \frac{-3 \cdot \pi^2 \cdot C_d \cdot A \cdot \rho \cdot a^2}{4 \cdot m \cdot V} \tag{3.4}$$

$$\Delta V = \frac{\pi \cdot C_d \cdot A \cdot \rho \cdot a \cdot V}{8 \cdot m} \tag{3.5}$$

Where C_d is the drag coefficient of the satellite, A is the frontal area of the satellite and ρ is the air density at that point.

To use this in a loop within MATLAB first the initial values need to be computed. This is done using Equations (3.6) and (3.7). From the requirements it follows that the initial altitude is 320 km which represents a semi-major axis of 6691 km. Note that the transformation mentioned in Section 3.1.2 is also implemented within the loop to calculate the air density at the respective location.

$$V = \sqrt{\frac{\mu}{a}} \tag{3.6}$$

$$P = 2 \cdot \pi \cdot \sqrt{\frac{a^3}{\mu_E}} \tag{3.7}$$

Where the Earth's gravitational parameter μ_E is determined with Equation (3.8).

$$\mu_E = G \cdot M_E \tag{3.8}$$

With G being the gravitational constant and M_E the mass of the Earth.

Within the loop, the velocity, semi-major axis and period is then calculated by simply subtracting the difference per orbit from the parameters of the previous orbit. This is done using Equations (3.9) to (3.11).

$$a_2 = a_1 - \Delta a_{rev} \tag{3.9}$$

$$P_2 = P_1 - \Delta P_{rev} \tag{3.10}$$

$$V_2 = V_1 - \Delta V_{rev} \tag{3.11}$$

Knowing these parameters the drag can be computed during each part using Equation (3.12).

$$D = \frac{1}{2} \cdot \rho \cdot C_d \cdot V^2 \cdot A \tag{3.12}$$

To account for eccentricity, the first three points of the initial orbit are set to an eccentricity of 0. This is because the initial orbit is assumed to be circular and the eccentricity can only be computed over half a revolution. For every point after these initial three points, the eccentricity at that point can be computed using Equation (3.13).

$$e = \frac{r_a - r_p}{r_a + r_p} \tag{3.13}$$

In this equation r_a is the distance to the apogee, this is considered the semi-major axis of 3 points before the point at which the eccentricity is calculated. r_p is the distance to the perigee which is the semi-major axis of the orbit at the point the eccentricity is examined. The eccentricity is also taken into account in the air density prediction model.

Since the mean anomaly changes over time, the computation is done using the fact that there are eight points per orbit. As eight points are taken per orbit, the mean anomaly varies $\pi/4$ radians per point starting at a value of 1.31 radians as mentioned in Section 3.1.2.

3.3 Formation Flying Strategy

This section deals with developing a strategy with respect to the formation flying objective. First, different types of formations are being discussed and one will be selected. Afterwards, different approaches towards coordinating the formation will be treated and one method will be selected. The influence of the J_2 and differential drag effects with respect to formation flying will be discussed and finally, a protocol will be suggested in order to determine when orbit corrections should be performed.

3.3.1 Formations

Several different formations are possible. The simplest formation is known as the in-plane formation (see Figure 3.2). In this formation, the satellites orbit in the exact same orbital plane and are separated only by a true anomaly. When an unperturbed, circular orbit is assumed, the along track distance will remain constant [12].

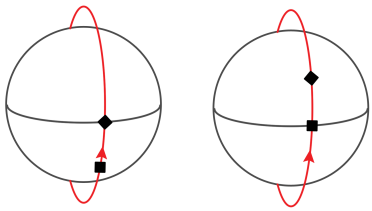

Figure 3.2: In-plane formation. Note how the satellites have the same orbital parameters, except for their true anomaly (or argument of latitude).

Another possible formation is the in-track formation (see Figure 3.3). The main principle of this formation is that the satellites feature the same ground track. In order to have the same ground track, the orbits need to be different with respect to the right ascension of the ascending node in order to compensate for the rotation of Earth [12].

A third formation flying technique is eccentricity / inclination vector separation (see Figure 3.4). As the name suggests, the main principle of this method is that the orbits of two or more satellites have differences in inclination and eccentricity. In this formation, the satellites have distinct trajectories but can remain relatively close together [13].

To determine which formation should be chosen for the DelFFi mission, the goals of the different formations should be discussed. In-track formation flying serves a clear purpose when Earth observation goals are considered for which the satellites should pass over the same landmarks, which is not the case for the DelFFi mission. Eccentricity / inclination vector separation is a formation flying technique that was designed in order

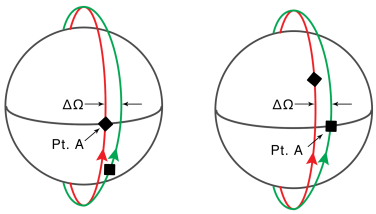

Figure 3.3: In-track formation. Note the difference in right ascension of the ascending node $\Delta\Omega$ between the two orbits to compensate for Earth's rotation, and how Pt. A is being covered by each satellite [12].

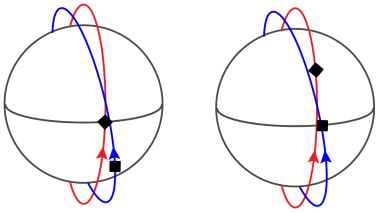

Figure 3.4: Eccentricity / inclination separated formation. Note how the satellites have different inclinations (exaggerated in this figure), in order to minimize potential collision hazard.

to mitigate collision hazard [13]. As the separation between the Delta and Phi satellites is required to be approximately 1000 km, or equivalently, 130 seconds (using $V = \sqrt{\mu/a}$), the collision hazard is much smaller than for formation flying missions that require smaller temporal separations. Furthermore, eccentricity / inclination separation introduces additional disturbances that cause a secular drift (see Section 3.3.3). This drift would need to be compensated using additional ΔV. For these reasons, an in-plane formation will be assumed.

3.3.2 Coordination

Several methods to coordinate a formation flight have been developed [14]. Some of these patterns are Leader/Follower, Virtual Structure, and Swarming patterns. In the Leader/Follower pattern, the leader orbits in some desired orbit, while the follower adjusts its orbit in order to maintain the desired formation. A direct effect of this approach is that the fuel consumption of the follower spacecraft is inherently larger than that of the leader. However, this problem (it is a problem as the DelFFi assumes two identical spacecraft configurations) can be solved by alternating the roles of leader and follower, as it is not required that the leader is located in front of the follower.
The Virtual Structure coordination method [15] considers a reference structure and a total position error estimate with respect to this reference structure. The advantage of this method is that fuel balancing methods can be implemented [14]. A virtual structure is a very good candidate, if an in-track formation is necessary, as either satellite might drift away from the designated ground track, and the error estimate could be taken with respect to the ground track.
Swarming algorithms are based on simple control laws and are an effective way to coordinate arbitrary amounts of vehicles using simple logic and low requirements on communication. However, these algorithms are typically not optimal with respect to fuel consumption and should not be preferred for very small formations [14].

As fuel balancing can also be implemented by alternating the roles of leader and follower satellite, there is no real reason to opt for more complex coordination methods like virtual structure, provided that fuel optimized algorithms are implemented for formation keeping. In the remainder of this discussion, a Leader/Follower pattern will therefore be assumed.

3.3.3 Disturbances

Two formation flying satellites will drift apart when orbiting. When assuming an eccentricity / inclination separated formation, the main cause for this drift is the differential J_2 effect [16]. It causes secular drifts in the right ascension of the ascending node Ω, the argument of perigee ω, and the mean anomaly M, as well as short- and long-period oscillations in all six orbital elements (a, e, i, ω, Ω, and M_0). It is recommended to not actively control short-term oscillations as trying to control these would be an unnecessary expense of fuel [17]. Control ΔV's in the order of 10^{-2} m/s per orbit are necessary to compensate for the differential

J_2 effect [16]. However, as it is planned to not apply any other separation than separation by true anomaly, this effect will vanish as can be observed from Equations (3.14) and (3.15). In these equations it can be seen that when the inclination i, the semi-major axis a, and the eccentricity e are kept constant, there will not be a differential nodal precession rate ω_p originating from the J_2 effect.

$$\omega_p = -\frac{3}{2}\frac{R_E^2}{(a(1-e^2))^2} J_2 \omega \cos i \tag{3.14}$$

$$J_2 = \frac{2\varepsilon_E}{3} - \frac{R_E^3 \omega_E^2}{3\mu_E} \tag{3.15}$$

ε_E, R_E, ω_E, and μ_E represent Earth's oblateness, radius, rotation rate, and gravitational parameter, respectively and can be considered to be constant over the mission duration.

Instead, for the DelFFi mission, the biggest perturbation will originate from the differential drag between the Delta of Phi satellites, of which estimates are presented in detail in Section 3.3.5.

3.3.4 Formation Acquisition

This section will discuss the formation acquisition which mainly consists of two parts. These two parts are the along track distance acquisition and the orbital plane acquisition.

Orbital plane acquisition

As explained in Section 3.3.1 the same orbital plane is preferred. Before acquiring the same orbital plane the initial orbital planes of the two satellites should be determined. The main reason the two satellites have different orbital planes is due to the deployment. The satellites are deployed using a common launcher, which uses P-Pods to deploy the two satellites in cross-track direction. This deployment causes a change in orbit which is graphically displayed in Figure 3.5.

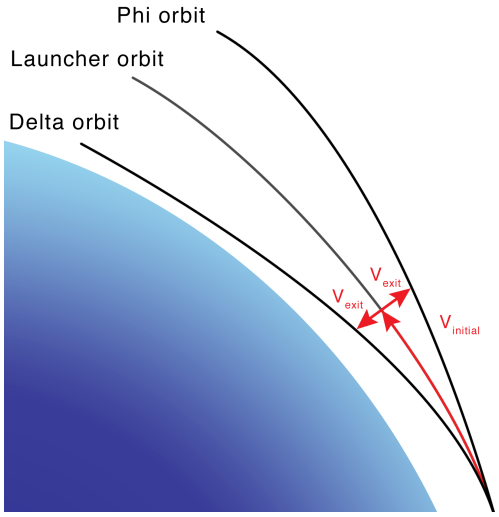

Figure 3.5: Orbital plane change due to deployment

The P-Pods release the satellites with a cross-track velocity of 1.6 m/s ,which will be accounted for after detumbling. This is done in the assuming a worst case scenario in which both satellites are ejected from the opposite directions. The velocity necessary for this is described by the relation given in Equation (3.16).

$$V_{opa} = \frac{V_e \cdot V_2}{V_1} \tag{3.16}$$

In this equation V_{opa} is the velocity necessary to regain the initial orbital plane. V_e is the exit velocity of the P-Pod and V_1 and V_2 stand for the velocity of the satellite at orbit injection and at the end of the detumbling phase respectively. Using these equations it follows that the ΔV necessary to change the orbital plane is only slightly lower than 1.6 m/s. Therefore a ΔV of 1.6 m/s is taken into account for orbital plane acquisition.

Along track distance acquisition

The formation acquisition phase is initiated directly after the detumbling phase of the satellite. For these calculations, the detumbling phase has been assumed to take 1 day, which is computed in Section 4.3.3. To acquire formation, the remaining time of the initialization phase shall be used. During this time differential drag is used to obtain the required along track distance. After detumbling, the two satellites will have an along track distance and a difference in velocity. Therefore, first the along track distance and the velocity difference have to be computed. This is done by simulating the orbits of both the satellites with different ballistic coefficients using the approach stated in Section 3.2.

The worst case scenario is when one satellite would fly in configuration 1 and the other satellite in configuration 2 of Figure 3.6. Configuration 1 is a tumble around the flight direction axis which does not change the frontal area and drag coefficient. The second configuration is for a tumble around an axis perpendicular to the orbit which causes a variation in the frontal area and drag coefficient. As the P-Pod release system releases both satellites along the same axis this worst case scenario is assumed not to be the case. However to account for possible variations in ballistic coefficients a margin of 25% is taken into account.

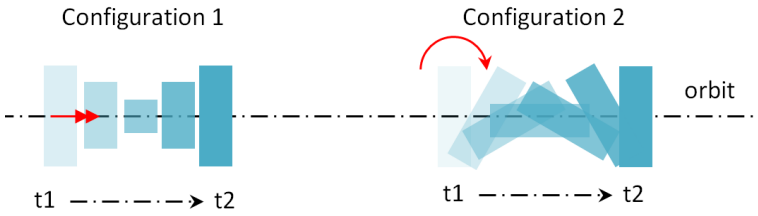

Figure 3.6: Different tumble configurations

These orbits are computed with that margin on the ballistic coefficients. Taking a C_D of 4.8 and a frontal area A of 0.035 m^2 for the second satellite and the same ballistic coefficient multiplied by 0.75 for the first satellite.

Once both orbits are known, Equation (3.17) [18] can be used to determine the difference in acceleration due to the drag difference. This drag difference is caused by the differences in ballistic coefficient $\frac{A \cdot C_d}{m_s}$. In this equation, ρ is the air density and V is the velocity of the satellites. As the two orbits are determined, the acceleration difference can be computed for each data point.

$$\Delta a_d = \frac{(A_1 \cdot C_{d_1} - A_2 \cdot C_{d_2}) \cdot \rho \cdot V^2}{2 m_s} \tag{3.17}$$

The Velocity difference ΔV is computed using Equation (3.18). Where $\Delta a_{d_{avg}}$ is the average acceleration over the detumble phase and $t_{detumble}$ is the detumble time.

$$\Delta V_{tumble} = \Delta a_{d_{avg}} \cdot t_{detumble} \tag{3.18}$$

Multiplying again by the time it is tumbling gives the along track separation $Dist_{tumble}$, see Equation (3.19).

$$Dist_{tumble} = \Delta V_{tumble} \cdot t_{detumble} \tag{3.19}$$

These equations give an along track separation of 30.8 km and a velocity difference of 0.356 m/s.

After the detumbling phase, the attitude can be controlled. With attitude control the 1000 km along track distance can be achieved using a combination of differential drag and propulsion. The propulsion is used to counteract the velocity differences between the satellites after the detumbling phase. When this is done, differential drag is used to acquire the 1000 km along track separation. This means altering the attitude of both satellites to gain another 969.2 km. The approach taken for this is to alter the attitudes such that half the distance is covered in half the available time frame. Once this is achieved the attitudes are switched around to cover the other halve. Simultaneously it will enable the satellites to put their velocity difference that was acquired during the first stage back to 0 m/s. This ensures the actual acquisition and disables the satellites from overshooting.

To compute the attitudes (angle of attack) for the differential drag, necessary to acquire the along track distance, an iteration was made. Within this iteration, the satellites angles of attack range between 0-90°. Using these angles (in radians) the corresponding frontal area and drag coefficient can be computed for each attitude with Equations (3.20) and (3.21).

$$A = 0.01\cos(\alpha) + 0.03405\sin(\alpha) \tag{3.20}$$

$$C_d = 1.8283\alpha^6 - 8.9008\alpha^5 + 16.575\alpha^4 - 15.176\alpha^3 + 5.9066\alpha^2 + 2.1592\alpha + 2.1941; \tag{3.21}$$

By extrapolating points from Figure 3.7 [19] and interpolating these points Equation (3.21) was set up. The interpolation was done using Excel.

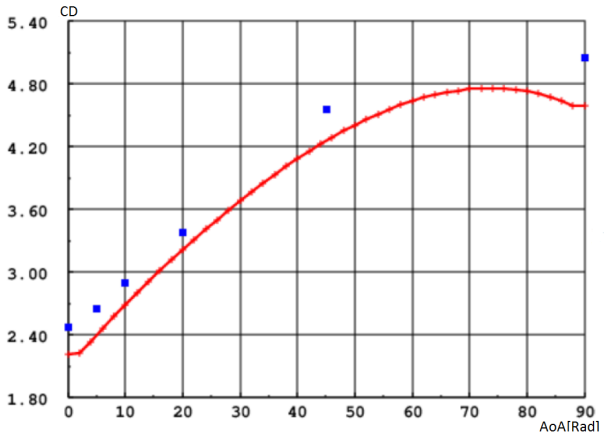

Figure 3.7: Variation of the drag coefficient with the angle of attack

Now that all frontal areas and drag coefficients can be determined, the differential drag differences can be computed. This is done using the same equations as for detumbling; Equations (3.17) to (3.19). The differential drag acceleration over time should be large enough to increase the gap by half the amount necessary over half the amount of time available.

This leads to a lot of possible configurations. However some of these already acquired the necessary distance within one day instead of the 4 days available. Since this is not what is wanted as it increases the complexity of the acquisition, a better filter was applied. This filter stated that half of the along track separation which still had to be covered should be achieved between 3.5 and 4 days. This restriction left less than 25% of all possible solutions. From these attitude configurations, together with possible pointing accuracy's for the AOCS, an optimal attitude can be determined. This attitude has been set to an α of 0° for the first satellite and 35° for the second satellite. This also requires a pointing accuracy of 2.5°. If the pointing accuracy is worse, the two satellites might not be able to acquire half the distance in half a day or overshoot that limit.

3.3.5 Formation Keeping

In this section, the procedure for formation flight maintenance is discussed and the computation of the ΔV budget is explained. The main reason for the separational drift between the satellites is due to drag differences in case the two satellites fly under different angles of attack (α). The calculations of the ΔV budget are based on a worst case scenario. In this case the attitudes are defined as following, one of the satellites flies at an α of 0° while the other one flies at an α of 90° . This can be seen in Figure 3.8. This is chosen as a worst case scenario to account for possible failure of a satellite or if, for some reason, the other satellite would have to fly with a higher angle of attack.

This assumption leads to the following data for the different satellite configurations (see Table 3.1).

These values are used as input for orbital decay calculations. This is done to determine the satellite's flight path, velocity, drag and orbital periods during the mission lifetime. The computations with respect to the ΔV, necessary to maintain formation, start at the altitude at which formation is acquired. For these computations first the difference in acceleration due to drag must be calculated. To acquire this acceleration,

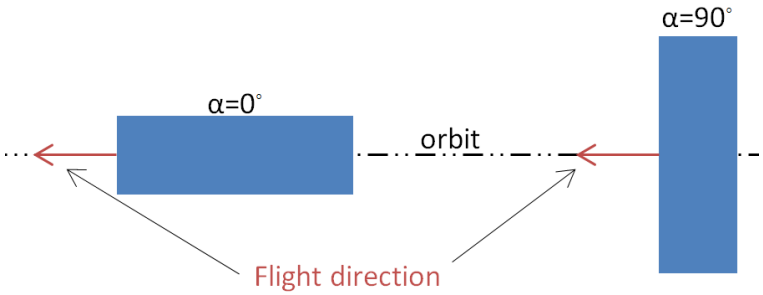

Figure 3.8: Worst case scenario for formation flight

Table 3.1: Satellite drag parameters for the different flight conditions [19]

α [deg]	C_d [-]	A [m^2]
0	2.5	0.01
90	4.5	0.034

Equation (3.17) is used. [18] Note that the density is not different, because it is considered constant over one revolution and this equation is used for 8 points per revolution.

Now that the acceleration is known, the velocity can be computed by multiplying by the period(see Equation (3.22)). This approach enables us to determine the ΔV necessary to counteract the drag difference per revolution as the drag shall be countered once per orbit.

$$\Delta V_d = \Delta a_d \cdot P \tag{3.22}$$

For the total ΔV a summation is made for all revolutions that are made during the formation flight demonstration. This directly implies that the speed difference between the satellites is put to 0 after every revolution. This gives a ΔV of 8.12 m/s. However as both satellites should do an equal amount of work only half of the ΔV is necessary which is 4.06 m/s.

The previous calculations only include the acceleration differences per revolution and the ΔV to counteract it per revolution. However they do not describe anything to counter the increase of along track distance. This increase is also caused by the drag and accumulates over time.

Since there is no possibility to have the thrusters working continuously the drag can not be fully counteracted by just setting the velocity difference to zero each revolution. Therefore an along track distance will still be accumulated over time. This along track distance is equal to $\Delta V/2 \cdot P$. Calculating this distance per day gives us an accumulated distance of about 5 km per day. This shows that the total along track separation over seven days due to this effect would not cause the satellite to go out of the control box and therefore, this distance could be neglected. However, in order to clearly demonstrate formation flight, the satellite should actively try to remain close to the center of the control box and adjustments therefore will be made. Estimates of these corrections are provided in Section 3.3.8.

3.3.6 Command Data Flow

Given that an impulsive shot strategy will be applied, the problem can be stated as follows: *"Determine and perform the impulsive shot that is required to end up in the center of the control box in some future state"*. For determining this future state, some heuristic needs to be defined that connects the current position of the leading satellite to a future position of the following satellite.

A well known heuristic is Lambert's problem. Lambert's problem is a boundary value problem for the differential equation

$$\ddot{\boldsymbol{r}} = -\frac{\mu}{r^2}\hat{\boldsymbol{r}}$$

for which the Kepler orbit is the general solution. Efforts have been made to incorporate the J_2 effect into this prediction model (J_2-perturbed Lambert problem) [20]. The suggested strategy is as follows:

1. Get the mean orbital elements of the leading satellite using analysis of GPS data

2. Predict the mean orbital elements after one period minus the temporal separation that matches the desired along track distance of 1,000 km (desired prediction) using Lambert's problem or a similar heuristic
3. Get the mean orbital elements of the following satellite using analysis of GPS data
4. Predict the mean orbital elements of the following satellite after one orbital period using Lambert's problem or a similar heuristic (expected prediction)
5. Match the desired prediction against the expected prediction and check whether the orbital elements of the expected prediction are within the centermost `<tbd>` percent of the control box with the desired prediction at its center [1]
6. If this condition is not met, the following satellite should perform a formation keeping maneuver

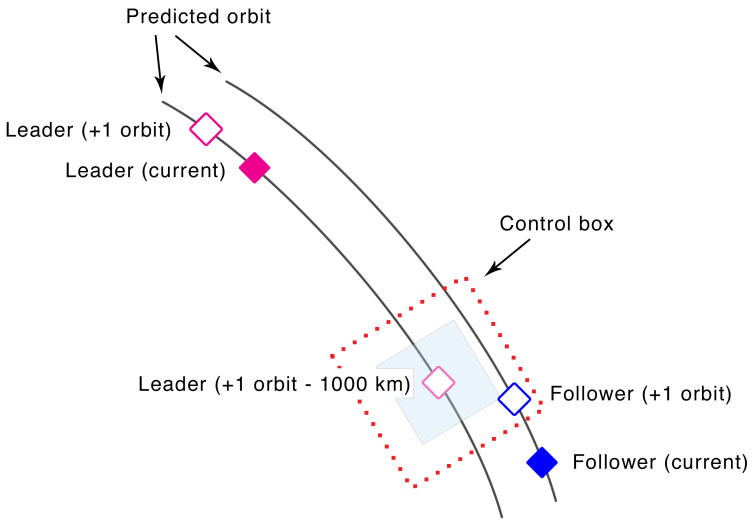

Figure 3.9: Formation flying prediction model

This procedure is shown graphically in Figure 3.9. It shows the current and predicted positions of the two satellites where the positions indicated with "Leader (+1 orbit)" and "Leader (+1 orbit - 1000 km)" differ by the along track distance. The control box is drawn around this latter position, and it is checked whether or not the predicted state of the following satellite is inside this control box. A smaller shaded area within the control box is indicated. If this smaller box is used for determining whether or not to make a corrective maneuver, the formation flying performance can be increased. It is recommended that this variable, smaller box will be used for this purpose during the formation flying mission. Its size can be decreased when it appears that the satellites can easily remain within the original control box and the maximum formation flying precision (versus acceptable fuel cost) can be assessed during the mission.

The next question that should be answered, is where these actions should take place. As no inter-satellite link is assumed, the ground station will be in the loop anyway and using the GENSO network, ground coverage will be close to 90% [21]. This means that it might be logical to do processing on Earth. Also, the OBC processing speed is in the order of 8-25 MHz. Assuming that this OBC can perform orbit analysis which will, among others, involve linear regression on many data points in order to determine the mean orbital elements, while gathering housekeeping data and mission data, is very optimistic. There is a clear reason for performing the processing on the satellites, however: If processing will be performed on Earth, it will be more difficult to switch to an inter-satellite link in future formation flying satellites that will share DelFFi's baseline design. Therefore, a scheme is suggested in which processing will be performed by the ground station, and another scheme is provided in which processing is done on board as a recommendation for future missions. These schemes are displayed graphically in Figures 3.10 and 3.11, respectively. These figures assume that the Phi satellite is the leading satellite, and the Delta satellite is the following satellite. Note again that the leader satellite does not necessarily have to be in front of the follower satellite. Furthermore, this scheme assumes the four-impulse method [14] will be used to perform corrections. This method is further explained in Section 3.3.7, and estimates are provided to demonstrate that not all four impulsive shots strictly need to be performed for this specific formation flying mission.

[1] Changing this value is an easy way to increase formation flying performance. Different values might be provided for along-track distance and cross-track distance.

Looking at Figure 3.10), it can be seen that in case of ground station processing, the GPS data from both satellites needs to be sent to Earth, where the mean orbital elements are being calculated by the ground station. Two position estimates will be made for the future position of the two satellites and a control box will be determined. If actions are necessary, the ground station will send the Follower satellite a sequence of maneuvers that need to be executed at certain times, in order to maintain the formation.

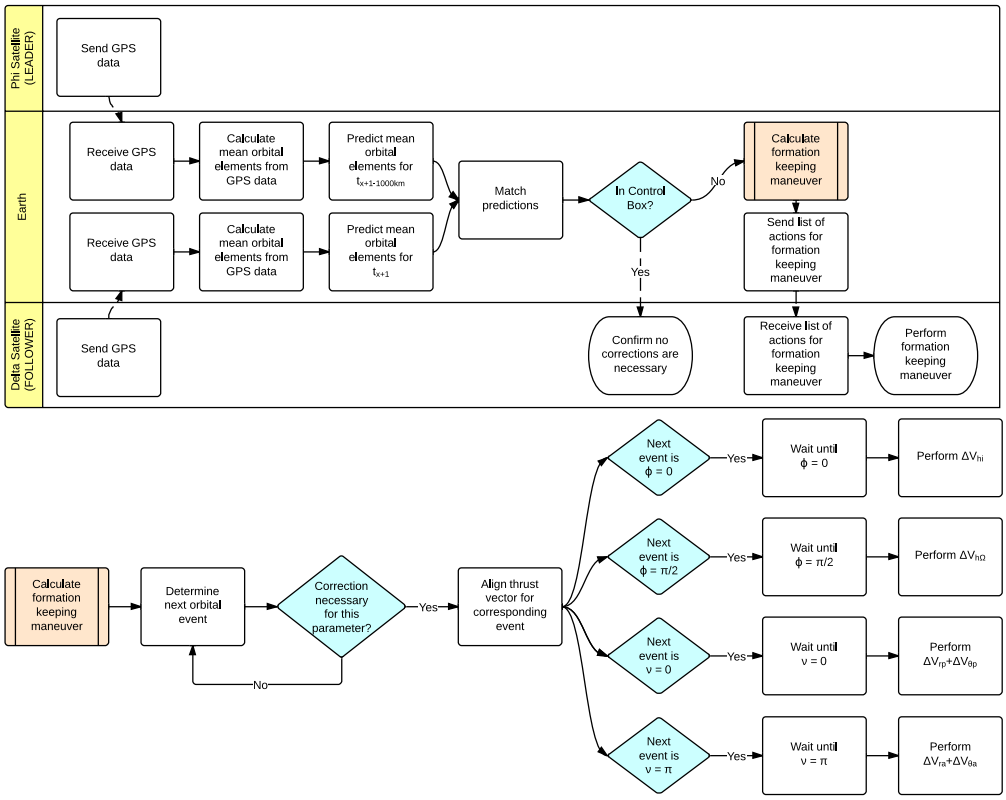

Figure 3.10: Formation flying control strategy assuming data processing on Earth

Figure 3.11 shows the same procedure for on-board processing. The key difference is that the ground station just relays the mean orbital elements (that were already calculated on-board) of the Leader satellite to the Follower satellite. Afterwards, the Follower satellite itself determines the control box based on this input and its own orbital prediction, and performs a formation keeping maneuver if necessary.

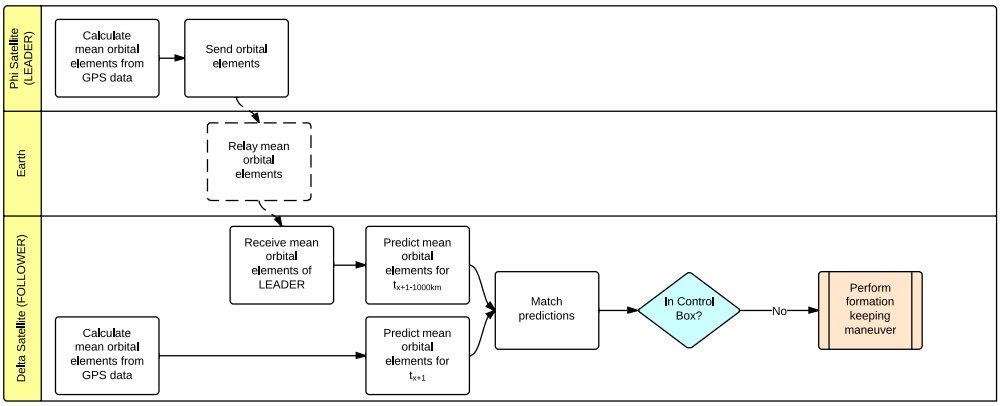

Figure 3.11: Formation flying control strategy assuming on-board data processing. The action "Perform formation keeping manuever" corresponds to the action "Calculate formation keeping maneuver in Figure 3.10.

3.3.7 Correction Scheme

There are several ways to correct the orbit of a satellite. It was already mentioned that due to heavy requirements on power, AOCS, and propulsion system, continuous control is not an option for the DelFFi mission.

A good and general method for orbit correction using impulsive shots is the four-impulse method. The four-impulse method requires four impulsive shots over the course of one orbit. The method was developed by Schaub and Alfriend for the purpose of formation flying and is able to perform adjustments in all Keplerian elements [17]. The impulsive shots that need to be performed can be summarized as follows:

1. When the argument of latitude, ϕ, is 0 (or π) radians, implement a velocity change Δv_{h_i} as mentioned in Equation (3.23) in the cross-track direction. This is to compensate for a change in inclination.

$$\Delta v_{h_i} = \frac{h}{r \cos \phi} \delta i \tag{3.23}$$

   In this equation, h is the angular momentum, r is the orbital radius, and δi is the change in inclination that needs to be made.

2. When the argument of latitude is $\pi/2$ radians, implement a velocity change Δv_{h_Ω} as mentioned in Equation (3.24) in the cross-track direction. This is to compensate for a change in right ascension of the ascending node.

$$\Delta v_{h_\Omega} = \frac{h \sin i}{r \cos \phi} \delta \Omega \tag{3.24}$$

   In this equation, $\delta\Omega$ is the change in right ascension of the ascending node that needs to be made.

3. At perigee ($\nu = 0$), implement a velocity change as mentioned in Equations (3.25) and (3.26):

$$\Delta v_{r_p} = -\frac{na}{4} \left[\frac{(1+e)^2}{\eta} (\delta\omega + \delta\Omega \cos i) + \delta M \right] \tag{3.25}$$

$$\Delta v_{\phi_p} = \frac{na\eta}{4} \left(\frac{\delta a}{a} + \frac{\delta e}{1+e} \right) \tag{3.26}$$

   In these equations, η is $\sqrt{1-e^2}$, a is the semi-major axis, M is the mean anomaly, and n is the mean motion. The former equation cancels the argument of perigee ($\delta\omega$) and mean anomaly (δM) errors, whereas the latter one cancels errors in the semi-major axis (δa) and in the eccentricity (δe).

4. At apogee ($\nu = \pi$), implement a velocity change as mentioned in Equations (3.27) and (3.28):

$$\Delta v_{r_a} = -\frac{na}{4} \left[\frac{(1-e)^2}{\eta} (\delta\omega + \delta\Omega \cos i) + \delta M \right] \tag{3.27}$$

$$\Delta v_{\phi_a} = \frac{na\eta}{4} \left(\frac{\delta a}{a} + \frac{\delta e}{1-e} \right) \tag{3.28}$$

   These equations serve the same purpose as their counterparts in Equations (3.25) and (3.26).

It should be noted that as the satellites are continuously decaying, technically speaking, there is no Kepler orbit (as a matter of fact, Keplerian orbits are always an approximation as they do not account for any perturbations). However, over the course of one or a few orbits, especially during the formation flying part of the DelFFi mission when the satellites are at their highest possible orbit, the orbits are by approximation Keplerian: The MATLAB model used to predict the orbital decay showed a decay of only 2.6 m per orbit at the end of the formation flying sequence.

3.3.8 ΔV Estimates for Secular Drifts

This section will present order of magnitude ΔV estimates that are needed to compensate the different secular drifts that might occur. This will give an initial estimate of the impact of this parameter on the ΔV budget and whether or not it should be accounted for in orbit corrections. Table 3.2 displays the values that were used to compute these estimates. They originate from the MATLAB simulation that was introduced in Section 3.2 and uses values that represent the end of the formation flying phase. A small note on eccentricity: The QB50 website mentions a circular orbit, as does the DSE project guide. However, as no orbit is perfectly circular, a non-zero value of 10^{-4} was chosen. This value represents a difference between apogee and perigee distance in the order of 1 km. It should be noted that this initial value has a much higher impact on the eccentricity than the orbital decay does, as the decay is only a few meters per orbit during the formation flying phase. It should also be noted that the along track drift values for one orbit and one day are radically different as

Table 3.2: Parameters used for calculations

Parameter	Symbol	Value
altitude	h	297 km
eccentricity	e	0.0001
decay	s_d	2.6 m/rev
inclination	i	98°
orbital velocity	V_ϕ	7.7 km/s
along track drift (one orbit)	$d_{\phi,drift}$	137 m
along track drift (one day)	$d_{\phi,drift}$	76 km

Mean anomaly As differential drag is the main contributing factor to secular drifts, the most affected orbital element will be the differential mean anomaly δM. Using Equations (3.25) and (3.27), it can be seen that the ΔV needed to correct this along track drift would be 0.25 m/s per day (with 16 orbits per day) if corrected every orbit, or 7.0 m/s if corrected daily. The big difference between these two strategies lies in the fact that due to differential drag, one satellite will keep decelerating at a faster pace than the other satellite, increasing the error rate over time. It can clearly be seen that it is recommended to perform corrective maneuvers every orbit rather than after multiple orbits.

Inclination Large changes in inclination require a lot of ΔV. This also implies that an orbit will not drift from its initial inclination that easily. As an order of magnitude estimate: Using simple trigonometry it can be shown that even when a considerable ΔV of 1 m/s would be given in the cross-track direction, the maximum cross-track separation would become a mere 8.7 km. In other words, there is no reason to expect that a difference in inclination would cause the satellites to drift out of the control box. A ΔV of 1 m/s would cause an inclination change δi of

$$\delta i = \tan^{-1} \frac{V_{cross-track}}{V_\phi} = \tan^{-1} \frac{1}{7.7 \cdot 10^3} = 1.30 \cdot 10^{-4} \text{ rad}$$

This inclination change would cause a maximum cross-track separation $d_{cross-track}$ of

$$d_{cross-track} = (R_E + h) \tan \delta i = (6378 + 297) \left(\tan 1.30 \cdot 10^{-4}\right) = 8.7 \text{ km}$$

This demonstrates that even with a relatively large change in inclination, the satellites will still remain within the control box, and there is no need to implement inclination change maneuvers.

Semi-major axis The semi-major axis is affected by the orbital decay. Any change in the semi-major axis to over 100 m will still yield ΔV impulsive shots in the order of cm/s. As the orbital decay is only a few meters per second in the worst case (which both satellites are subjected to so there is no differential effect), it is not expected that changes in the semi-major axis will need to be accounted for.

Right ascension of the ascending node Even in the occasion in which the cross-track distance becomes so large that a correction in the right ascension of the ascending node is necessary to stay within the control box, it can be observed from Equation (3.24) that the ΔV necessary for correction will be in the order of 1 cm/s (assuming $\delta\Omega$ corresponds with a change of 50 km (or equivalently 1.25 mrad) in the right ascension of the ascending node. As mentioned before, when the satellites have the same inclination, this event is very unlikely.

Eccentricity It was explained before that changes in the semi-major axis in the order of 100 m are quite unlikely. Assuming that the apogee and perigee increase and decrease with 100 m respectively, the changes in eccentricity δe are in the order of 10^{-5} (using $e = \frac{r_a - r_p}{r_a + r_p}$). Using Equations (3.26) and (3.28) it can be seen that the corresponding corrections are in the order of cm/s. A differential effect can be assumed to be even smaller as the satellites will experience similar drifts. Furthermore, the initial eccentricity assumes a difference between apogee and perigee distance in the order of 1 km. As the angular separation was demonstrated to be approximately 0.024 radians, the separation between the two satellites due to the initial eccentricity will be much smaller than 1 km. Therefore, the satellites will not periodically drift in and out of the control box due to the eccentricity.

Argument of perigee It is not expected that the differential argument of perigee $\delta\omega$ would change by any significant amount over the duration of the formation flying mission. Using Equation (3.25), it can be seen that changes up to 5 mrad can be countered using a ΔV of 1 cm/s. It should be noted that the argument of perigee only affects the position in the control box through the eccentricity of the orbit. As the eccentricity is very close to zero and differences between apogee and perigee distance are in the order of 1 km, it is not expected that the differential argument of perigee should be corrected.

Intermediate Results

Table 3.3 summarizes the results treated above. From this table, it can be seen that the only parameter that is expected to be actively controlled, is the mean anomaly. Its corrective ΔV estimates are also one order of magnitude higher than the ones caused by the other disturbances. Additionally, a smaller additional ΔV is necessary to compensate for the accumulated deceleration over time, as mentioned in Section 3.3.5. The order of magnitude of the corrections matches with estimates from How and Tillerson [16]. The provided value is only accurate when the mean anomaly is corrected every orbit. If corrections are made every day, the ΔV needed per day increases to several meters per second. It is therefore strongly recommended that corrections are made very frequently, preferably every single orbit. The two advantages of this are more accurate formation flight and lower fuel consumption. Note that all these ΔV calculations relate to the Follower satellite; the Leader satellite does not use any ΔV. Roles of Leader and Follower should be changed at least once in order to balance fuel use.

Even though the other orbital elements do not seem to need corrections during the formation flying mission, it is recommended that the functionality necessary for these corrections will still be implemented for testing purposes, as these disturbances will become more pronounced in future missions, for instance when eccentricity / inclination separation is selected to compensate the increased risk that comes with smaller separation distances.

Table 3.3: Secular differential disturbances and corrective ΔV estimates

Differential disturbance	**Symbol**	**Max ΔV estimate [m/s/orbit]**	**Correction necessary**
Mean anomaly	δM	10^{-1}	Yes
Inclination	δi	10^{-3}	No
Semi-major axis	δa	10^{-2}	No
Right ascension of the ascending node	$\delta\Omega$	10^{-2}	No
Eccentricity	δe	10^{-2}	No
Argument of perigee	$\delta\omega$	10^{-2}	No

3.3.9 Impulsive Shot Approximation Justification

Table 3.4 summarizes the inputs that were used for the following calculations. These will be derived in Section 4.4.

Table 3.4: Parameters used for burn time calculations

Parameter	**Symbol**	**Value**
satellite mass	m	3.6 kg
mass flow	$\dot{m}$	$7.84 \cdot 10^{-5}$ kg/s
exhaust velocity	w	778 m/s

The thruster burn time during the maneuvers can be obtained using the rocket equation, shown in Equation (3.29):

$$\Delta V = w \ln \Lambda \tag{3.29}$$

In this equation, Λ is the mass ratio before and after the delivery of the ΔV. It can also be expressed as $1 + \frac{\Delta m}{m}$. The maximum delivered impulsive shot is smaller than 0.02 m/s. Rewriting Equation (3.29), we can find an approximation for the expelled mass:

$$\Delta m = \left(e^{\frac{\Delta V}{w}} - 1\right) m = \left(e^{\frac{0.02}{778}} - 1\right) 3.6 = 9.25 \cdot 10^{-5} \text{ kg}$$

In this equation, the satellite mass was assumed to be constant at 3.6 kg, which is a safe assumption as it is the maximum allowed mass of the satellite. Dividing by the mass flow , the maximum burn time during formation keeping is obtained:

$$t_{burn,max} = \frac{\Delta m}{\dot{m}} = \frac{9.25 \cdot 10^{-5}}{7.84 \cdot 10^{-5}} = 1.18 \text{ s}$$

This burn time corresponds to a change in mean anomaly of 1.4 mrad or equivalently, 0.08°, the propulsion system is active in such a small part of the orbital period that the burn times can be considered to be impulsive.

3.4 Results

In this section, the results obtained from the astrodynamics calculations and formation flying strategy are discussed.

3.4.1 Orbital Decay

Figure 3.12 shows the orbital decay of the satellites during the detumbling and formation acquisition phase using the approach explained in Section 3.2. During detumbling, the satellites experience different decay rates due to the assumed difference in ballistic coefficients of 25%. After detumbling, the two satellites experience different decay rates due to the differences in attitude (angles of attack of 0 and 90°). The first part with the diverging altitudes corresponds with the situation where the Leader satellite (Delta in this case) is flying at a zero degrees angle of attack, and the converging part corresponds with the Follower satellite (Phi) flying at a zero degrees angle of attack. At the end of the phase, 1,000 km along track distance is realized.

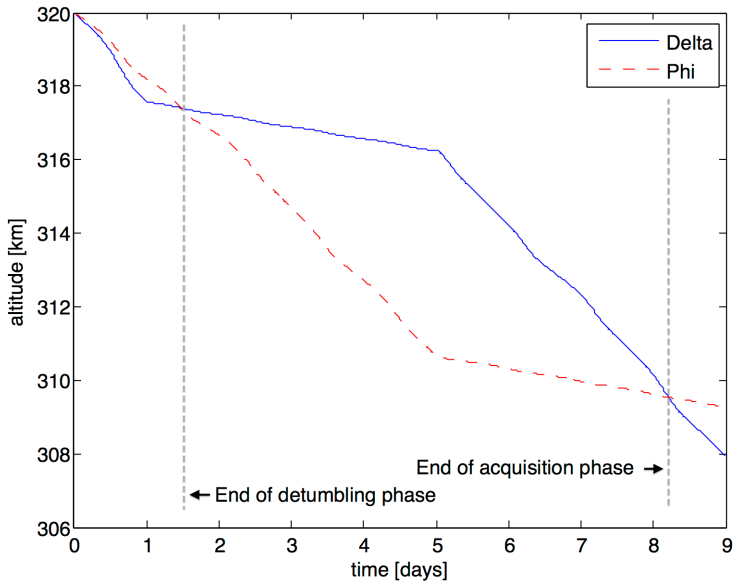

Figure 3.12: Graph of the orbital decay of the two satellites during the detumbling and formation acquisition phase, following the approach described in Section 3.2.

Figure 3.13 shows the best and worse case orbital decay of the satellites during the formation flying phase. The upper bound or best case shows the lifetime of the satellite assuming a continuous formation flight at zero degrees angle of attack. The lower bound assumes that formation flight takes place under a 90° angle of attack scheme. This worst case is not expected to be experienced, but it clearly demonstrates the importance of controlling the attitude of the satellite in order to reduce drag and increase the mission duration. The actual decay will be closer to the best case scenario, but for different reasons (thrust vector alignment being one of them) the satellite will also have to fly at different angles of attack during parts of each orbit.

3.4.2 Formation Flying

The chosen formation is an in-plane formation in which both satellites will experience almost equal disturbances. Due to this choice of orbit, the main secular drift is a drift in the mean anomaly. This drift effectively

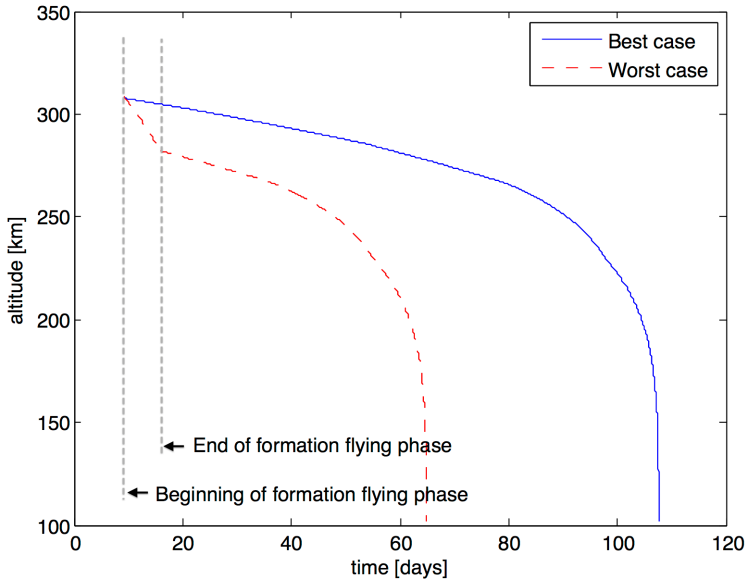

Figure 3.13: Graph of the orbital decay during the formation flying phase and onwards following the approach described inSection 3.2.

Table 3.5: ΔV budget

Maneuver	**Total ΔV needed [m/s]**
Acquisition: inclination	3.2
Acquisition: along track distance	0.36
Keeping: Velocity difference due to differential drag	8.1
Keeping: Maintaining along track distance	1.8
Total	13.5
Total (one satellite)	6.75

causes the along track distance between the two satellites to diverge, and potentially drift out of the control box (the distance can also converge in which case no action needs to be taken). Other drifts were demonstrated to be at least one order of magnitude smaller. Due to the limited formation flying duration, these drifts do not necessarily need to be accounted for. However, it is recommended that the possibility exists to counteract these effects, as future missions will most likely need to account for them.

The choice of orbit requires the satellites to maneuver back to the same inclination during the formation acquisition phase, after the satellites are being ejected from their P-PODs. The ΔV necessary for this action is 3.2 m/s for the two satellites combined. Another combined 0.36 m/s is needed to reach the required 1,000 km along track separation and to equalize the differential velocity afterwards. The actual number is higher, but will be accounted for using differential drag as was explained in Section 3.3.4.

For formation keeping, a total combined ΔV of 8.12 m/s is necessary to mitigate the velocity differences that accumulate due to differential drag, provided that an impulsive shot is performed every orbit. Another 0.25 m/s per day is needed to compensate the secular drift that comes with the differential drag.

The coordination structure used is a Leader-Follower structure, where the Follower satellite is the satellite that will perform the maneuvers. The roles of leader and follower can be alternated, and fuel balancing can therefore be realized. All ΔV maneuvers mentioned above are total numbers for the two satellites, and hence, the total requirement of one satellite is half of this amount. The budget is summarized in Table 3.5.

The satellites will communicate their position through the ground station, and the ground station will process the maneuvers that have to be performed. It is recommended for future missions to perform all processing on board, in order to develop satellites with a higher level of autonomy.

CHAPTER 4
SUBSYSTEM DESIGN

Every satellite system is composed of a number of subsystems that guarantee the proper working of the entire system during the mission. Typically on CubeSats, these subsystems are a telemetry, tracking and command (TT&C) system, a command and data handling (C&DH) system, an attitude and orbital determination system (AOCS), an electrical power system (EPS), a propulsion system and a thermal control system. The systems combined with a structure that provides structural integrity and protection from the space environment, form a satellite.

The structural analysis of DelFFi Delta can be found in Section 4.1. The design of the EPS was done in Section 4.2, whilst the design of the AOCS can be found in Section 4.3. The propulsion system was designed using the method described in Section 4.4. The TT&C design can be found in Section 4.5. The C&DH system design can be found in Section 4.6 and the thermal protection system design can be found in Section 4.7. Furthermore, a sensitivity analysis was performed to see the implications of certain changes in these subsystems w.r.t. each other. The sensitivity analysis can be found in Section 4.8.

4.1 Structural Integrity

The exact dimensions of the structure of the CubeSat are given in Table 4.1. The outer structure of the CubeSat is 10 x 10 x 34 cm. As described in the Mid-term report [4], the structure consist of an inner and outer structure. The structure is customized by TU Delft.

4.1.1 Inner Structure

The inner structure consist out of four rods and an ejection system for the re-entry capsule. The four rods are used to attach the Printed Circuit Boards (PCBs) and the components of subsystems, these are placed one at a time onto the rods. Separators are used to get the required spacing between the boards.

4.1.2 Outer Structure

The outer structure has four different parts: the bottom panel, the top panel, and two different L-shaped profiles. The parts will have sensors and components of subsystems attached. The parts, which are shown in Figure 4.1, are described below.

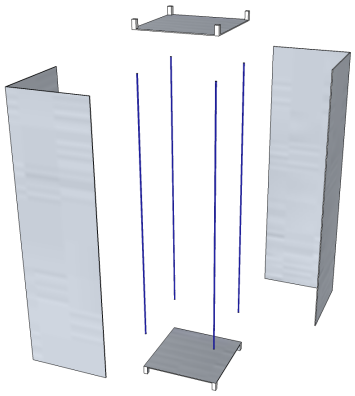

Figure 4.1: The solar panel and solar cell configuration in a deployed state

Top panel The top panel contains the FIPEX unit and one sun sensor. The FIPEX unit, provided by Von Karman Institute (VKI), is placed directly onto the top panel on the inside and will point in the direction of flight. The FIPEX will be partly outside of the satellite. Therefore, the top panel has a cutout in the middle. The details of the constraint of the FIPEX unit are described in [22, p. 79]. A sun sensor is placed on the outside of the top panel.

Bottom panel The bottom panel has a sun sensor mounted. And will be part of the ejection system for the capsule. This is described detailed in Section 5.6.

L-shaped profile, sun side The first L-shaped profile has the solar panels mounted and two sun sensors attached. Furthermore, two cutouts are required for the antennas. The antennas will deploy from both sides. In total there are 14 solar cells attached to the outside of the L-shape profile. The inside of the L-shape profile is covered in thermal tape, as described in Section 4.7.

L-shaped profile, dark side The second L-plate contains cutouts for the antennas and the nozzles. Next, two sun sensors are placed on the outside. The inside is covered in thermal tape. The deployable solar panels are mounted with the solar cells towards the outside, as described in Section 4.2. These are undeployed attached to the L-shaped profile by a resistor wire. The resistor wire is cut, by melting, which will deploy the solar panels by means of springs. At an angle of 135 degrees the panels are constrained and the spring will hold the panels in place.

4.1.3 Conclusion

For the structure 5052-H32 sheet aluminum is used [23]. The total weight of the structure becomes 630 g, where a 5% margin is taken into account. The dimensions are, as mentioned before 10 x 10 x 34 cm. The structure will be made within TU Delft and is customized to accommodate solar cells and components. The final characteristics are in Table 4.1.

Table 4.1: Budgeted quantities for the satellite's structural support

Structural Support	Value
Mass [g]	630
Dimensions (hxwxd) [cm]	10x10x34

4.2 Electrical Power System

In the final design of the EPS, the assumptions are handled and discussed. The final budget is made and the solar cell characteristics are shown. Then the calculations are done, followed by the final appearance and configuration of the power system.

4.2.1 Final power budget

In order to set up the final budget, different modes had to be established. There are four different modes: detumbling mode, normal operational mode, safe mode and formation flying mode. The total budget for every mode can be found in Table 4.2, whereas the budgets for every different subsystem per mode can be found in Chapter D. The duty cycles of the subsystems are the fraction of the orbit they should be active. The mode time stated is the time of the missions the mode is expected to be active. The normal operation mode is active when no other mode is active and the safe mode does not have time allocated, because it is unknown if and how long it will be in safe mode.

Table 4.2: Budgets for the different modes

Mode	Average power [W]	Time in mode
Detumbling mode	2.29	1 day
Normal operation mode	3.68	Continuous
Safe mode	0.98	Not allocated
Formation flying mode	3.73	7 days

The mode with the highest power requirement is the formation flying mode, this mode has a duration of 7 days with an average power of 4.5 W taking a 20% margin. Therefore, the power system is sized for a continuous power required of 4.5 W. The battery is designed to cover the peak powers.

4.2.2 Solar Cell Selection

The solar cell selection is done by comparing the top solar cells from three different suppliers; ISIS, SpectroLab and Azure Space. The data of these solar cells are shown in Table 4.3. As can be seen the Azure Space Triple Junction GaAs solar cell [24] has the best performance, which is one of the main reasons it is selected.

Table 4.3: Solar cells for CubeSats from diverent supliers.

Supplier	Solar Cell Name	Structure	Area [cm^2]	Efficiency
ISIS	ISIS CubeSat Solar Panels	GaAs	26.62	28%
SpectroLab	NeXt Triple Junction (XTJ)	GaInP2/GaAs/Ge	26.62	29.5%
Azure Space	Triple Junction GaAs	GaInP2/GaAs/Ge	30.18	30%

4.2.3 Solar Panel Configuration

In the Mid-term report [4] the first choice of the solar panels was the body-mounted configuration. However, the power budget changed and the charge and discharge losses are greater than initially accounted for. In the power budget, the major change is the AOCS which will have a duty factor of 100%. Next, the input conversion efficiency is set to 47% for eclipse and 69% for daylight as described in Section 4.2.4. Thus, the body-mounted configuration will not satisfy the power requirements and the configuration of the solar panels has changed.

Because drag has a high impact during the mission, configurations are considered which have low drag when flying with the top side towards the front. The configuration should be symmetric, so no extra disturbance torque is induced. Therefore, the aerodynamic stability is considered as is shown by [25].

As described in Section 4.3 the nominal attitude of the satellite will be in the lowest drag attitude. This leaves one degree of freedom left, which can be continuously controlled by a reaction wheel. The axis control has an accuracy of 0.5° along its long axis in sunlight, and 1 to 5 ° in eclipse. This gives the opportunity to point the solar panels toward the sun when the satellite is in daylight, while still considering the lowest drag attitude.

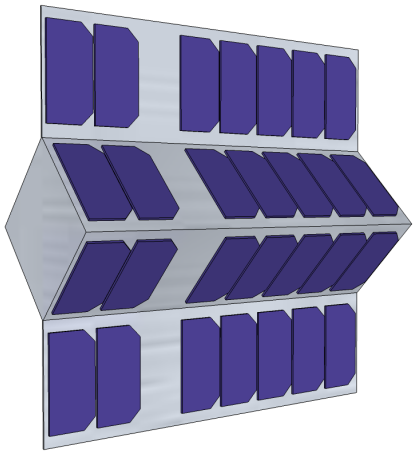

Figure 4.2: The solar panel and solar cell configuration in a deployed state

One design remains that fits all constraints and is shown in Figure 4.2. As can be seen the panels are symmetric and covered with solar cells on one side. During launch the solar panels will be attached to the sides. Therefore, when the satellite is launched from the P-POD, it can receive power from four sides as shown in Figure 4.3. This is beneficial because the power received can be used to detumble the satellite and point it towards the sun before deployment of the solar panels. The amount of solar cells needed will be determined in Section 4.2.6. The location of the solar cells are based on the sensors, antennas and nozzle allocated space.

4.2.4 Global Electric Power System

The global electric power system (G-EPS) similar to the one in Delfi-n3Xt will be used. It will supply a single voltage of 12 V to the subsystems. Between the systems there will be power converted, the conversion

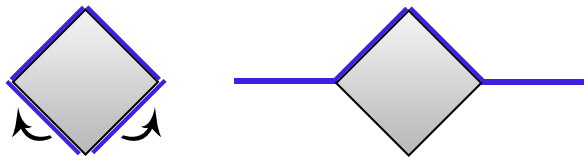

Figure 4.3: The undeployed and deployed solar panels

efficiency was taken to be 83% [26] for every step.Therefore, the input conversion of this system will be 47% for eclipse, four conversion steps, and 69% for daylight, two conversion steps.

4.2.5 Assumptions

It is assumed that the degradation will increase when the satellites altitude decreases, due to the short the mission lifetime, the degradation over its lifetime is taken to be 2%. This consists of 0.8%, which accounts for radiation during its mission-life time, and 1.2% for the aerodynamic impact [24].

During the detumbling of the satellite, all the solar cells will be able to supply power for the start-up of the satellite, even when the panels are not deployed yet.

The worst case situation is considered for the calculation,thus when the orbit is parallel to the incoming sun rays. The altitude taken for the eclipse calculations will be 150 km. When 150 km is reached it only takes 5 orbits before re-entry starts and therefore would not give a good representation.

4.2.6 Calculation

In these calculations the power delivered by the solar cells is determined and the battery is sized.

Table 4.4: Values for power subsystem

Variable		**Values**	**Units**
Effective area	A_{eff}	636.2	cm^2
Accuracy angle	α_{acc}	0.5	$^\circ$
Solar rays angle	θ	0-180	$^\circ$
Solar cell area	A_{sc}	30.18	cm^2
Solar cells per panel	N	7	–
Needed power	P_{need}	4.5	W
Battery fraction	T_b	0.55	-
Sun fraction	T_s	0.45	-
Input conversion efficiency battery	X_b	0.47	-
Input conversion efficiency sun	X_s	0.69	-
Dept-of-Discharge	DOD	0.4	-
transmission efficiency	n	0.9	-

Solar Panels The number of solar cells determines the delivered power and battery time. Therefore, the amount of solar cells and power delivered is determined by iterations. This results in 7 solar cells on each solar panel. All other values that were re-used from the Mid-term report [4] or used for the calculation are shown in Table 4.4.

The solar panels will be in the sun for about half an orbit and will rotate 180° with respect to the sun. As the power required does not change between daylight and eclipse, the average power that is required from the solar panels, which should be delivered during one orbit, can be determined. Due to the satellite orientation the satellite has half an orbit to obtain the required delivered power. Equation (4.1) determines the delivered

power.

$$\begin{aligned} P_{sp,del} &= A_{eff} \cdot \cos(\alpha_{acc}) \cdot \sin(\theta) \\ A_{eff} &= ((2 + 2 \cdot \cos(45^\circ)) \cdot A_{sc} * N \end{aligned} \tag{4.1}$$

A_{eff} is the effective area, α_{acc} is the AOCS pointing accuracy and θ is the incoming solar ray angle. For the effective area A_{sp} is the area of a solar cell and N is the number of solar cells on a panel. The results is shown in Figure 4.4.

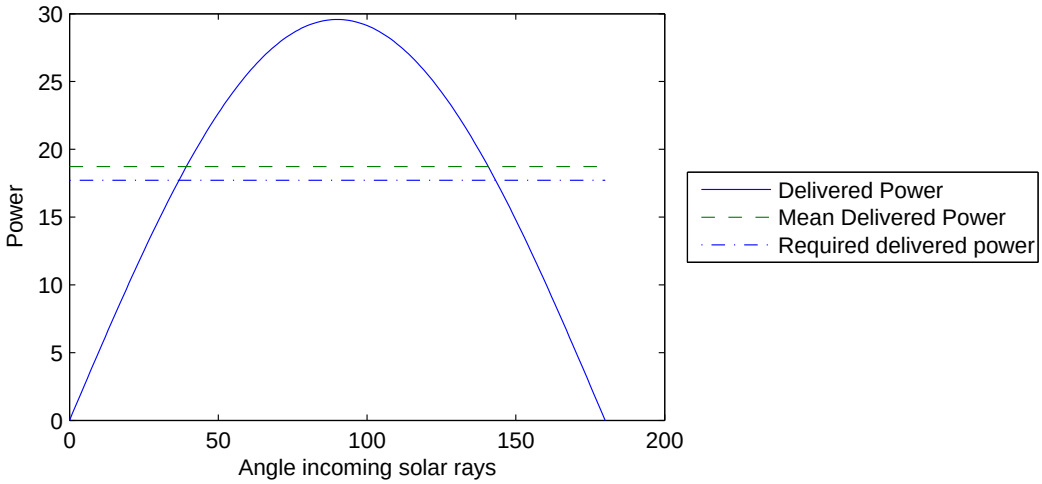

Figure 4.4: The power delivered in half an orbit, with the required power

Now the power required from the solar panels can be calculated, by using Equation (4.2). The available power should be enough to operate the satellite and charge the battery. T_b and T_s are determined from the power delivered. The battery fraction is the fraction of the orbit the solar panels do not deliver the required power.

$$P_{sp,req} = \frac{P_{need} T_b}{X_b T_s} + \frac{P_{need}}{X_s} \tag{4.2}$$

P_{need} is the average power needed, T_b is the battery fraction, T_s is the solar panel power fraction, X_b the input conversion efficiency when using the battery and X_s is the input conversion efficiency during solar panel power.

This results in an average power required of 17.72 W delivered by the solar panels in one orbit. When looking back at Figure 4.4 it can be seen that the average power delivered, 18.73 W, is sufficient.

Battery The battery is sized using the method described in [27, p. 422]. Depth-of-Discharge (DoD) depends on the number of cycles and is taken to be 40%, computed from [27, p .421]. A lithium-ion battery is commonly used for CubeSats. They have a transmission efficiency of 90% [28] . The battery capacity can then be calculated with Equation 4.3.

$$C_r = \frac{P_{need} T_b}{(DOD)n} \tag{4.3}$$

Where C_r is the battery capacity, (DOD) is the Dept-of-Discharge and n is the transmission efficiency.

With this the battery delivered capacity should be 9.5 Wh. Including the conversion efficiency of 69% it results in a actual battery capacity of 11.5 Wh. As peak powers are covered by the battery, its capacity is set to be 20 Wh. This also adds redundancy, with a fully charged battery the satellite can survive for one and a half orbit in operation mode and for more than 20 hours in safe mode.

4.2.7 Deployment

The deployment of the solar panels will be done using springs, such as the previous Delfi satellites. The solar panels will be held by a wire against the bus. Deployment is done by cutting the wires and a spring will deploy them. The solar panels should deploy 135°; this will be constrained such that a spring will keep it at its position. The deployment will be done after detumbling and pointing of the satellite.

4.2.8 Electrical Architecture

The electrical architecture is shown in Figure 4.5. The power generated by the solar panels is delivered to the EPS. Each of the solar panels has its own Maximum Power Point Trackers (MPPT) to get the most performance out of the solar cells. These are linked to a shunt which will regulate a constant voltage on the electrical bus. Next, they are linked to the local EPSs of the subsystems. The battery regulators are also linked to the G-EPS. They decide if the battery should charge or discharge. Each local EPS has a DC converter when a different voltage than the bus wiring is required.

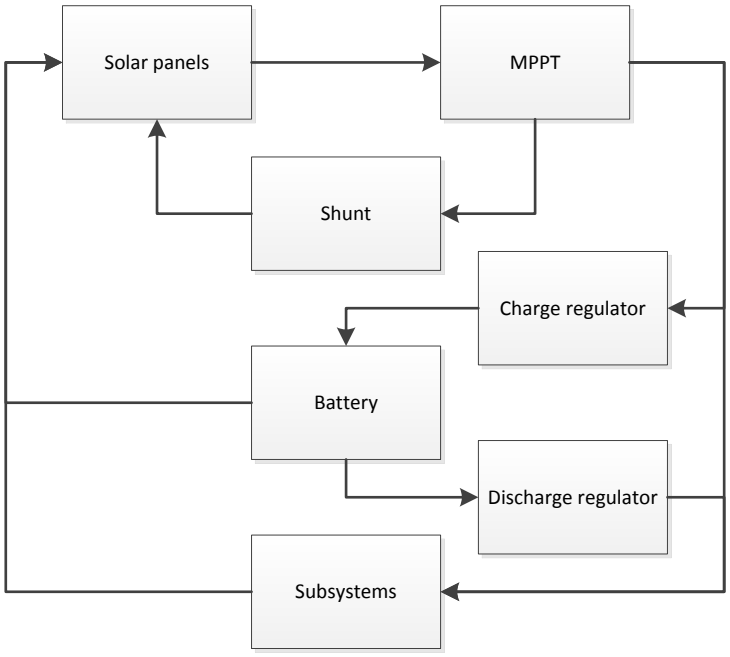

Figure 4.5: The electrical block diagram of the EPS.

4.2.9 Conclusion

The final design will consist of a G-EPS, deployed and body mounted solar panels and one battery.

G-EPS The G-EPS will be similar as the one in the Delfi-n3Xt. All solar panels will have their own power conversion to secure enough current. A regulated single supply voltage of 12 V is used for all subsystems. The main reason to go for a single supply voltage is to keep the system bus interfaces to a minimum in order to limit wiring harness and complexity and to standardize the system bus interface. The main power line is protected by the standard system bus interface. This is done because cabling can be very efficient, which saves a lot of space and weight compared to other CubeSat. The mass of the system including the cabling will be 100 grams, its thickness is 0.5 cm and it uses 63 mW.

Solar panels The solar cells are located on two deployable panels and on two body mounted panels. All panels will have 7 solar cells on one side, the configurations can best be seen in Figure 4.2. The solar panels

will be connected to the G-EPS which will convert the voltage to 12 V. The weight of all these panels combined will be 650 grams.

Battery The battery will be connected to the G-EPS and will have a capacity of 20 Wh. For the propulsion system, power from the battery will be used. The battery will have a thickness of 1.9 cm, with a mass of 140 g. The final characteristics are shown in Section 4.2.9.

Table 4.5: Final quantities for the power subsystem

Electrical Power	Value
Mass [g]	650
Dimensions (hxwxd) [cm]	10 x 10 x 2.4
Power [mW]	63

4.3 Attitude and Orbital Control System

This section will elaborate on the attitude and orbit determination and control system (AOCS). First the mission phases will be discussed. In the subsequent sections the disturbances and detumbling will be analyzed. These will be used as input for the attitude determination sensor selection, and actuator selection. First the magnetic torques will be calculated, then the best matching magnetic torquer is selected. Finally the cycle time, the total system layout and conclusion will be given.

4.3.1 Mission Phases

The satellite will experience four major phases. In chronological order these are; detumbling, formation flying, orbit maintenance and re-entry. For the AOCS, the detumbling and the orbit maintenance are the most interesting since these involve clear attitude and orbit acquisition and orbit movements. The detumbling phase starts with the ejection of the CubeSat from the P-POD, after which it will starts to tumble. Based on QB50 requirements, a maximum tumbling rate of 10 deg/s will be assumed to be the worst case scenario.

The AOCS has the duty to determine the location of the satellite exactly and keep track of the time with the GPS receiver. Also the AOCS has to perform attitude movements such that the ΔV is given in the correct direction.

When formation flying has finished, the satellite mission continues until the re-entry phase starts. During the orbit maintenance phase, the AOCS has to deal with all the disturbances and if necessary perform attitude movements. The disturbance over the complete mission that induces the highest torque is the aerodynamic drag. This increases with lower altitude.

In the last phase, the re-entry, the satellite will burn due to the enormous heat and the re-entry capsule will descend to Earth. The only thing the AOCS has to perform in this phase is position the satellite in the correct attitude and transmit the GPS coordinates as long as possible. This will provide a more accurate footprint prediction. A more detailed mission outline can be found in Chapter 2. For every mission phase calculations will be performed to understand the sizing and design of the sensors and actuators.

4.3.2 Disturbances

There are five different disturbances that will occur. These disturbances are mentioned in the Mid-term report [4] and described in more detail in the section below. The solar pressure disturbance and the nozzle misalignment do not depend on the altitude, the other three disturbances do. All initial values that were used are based on the astrodynamics model, and are shown in Table 4.6. The value of the disturbance is depended on the height: the lower the satellite will be, the higher the disturbances of the gravity gradient; the magnetic field and the atmospheric drag. From Section 3.4.2, the last orbit were active attitude control is necessary is at 150 km. After 150 km altitude the temperatures can rise due to the increase in density, and will eventually cause the AOCS to fail. Therefore, the c_p is located behind the c_m (See Chapter 6) and thus the satellite will be aerodynamically stable. The center of pressure is taken to be in the geometric center. [29]. Also, at lower altitudes the disturbances will be higher than an AOCS can possibly counter affect.

Table 4.6: Initial values for disturbances calculations.

Name		Values	Units	Remark
Solar constant	Φ	1362	W/m^2	
Speed of light	c	299,792,458	m/s	
Frontal area	A_s	0.048	m^2	Maximum effective area
Surface reflectance	q	0.6	–	Reflectance aluminum
Center of solar pressure	cp_s	0	m	From center
Center of mass	cm	0.02	m	From center
Gravitational parameter Earth	μ	$3.986 \cdot 10^{14}$	km^3/s^2	
Distance to center of the Earth	R	$6521 \cdot 10^3$	m	
Moment of Inertia, z-axis	I_z	0.0048	m^4	
Moment of Inertia, y-axis	I_y	0.0136	m^4	
Maximum deviation, z-axis	θ	45	°	
Satellite dipole	D	0.2	Am^2	
Magnetic moment of the Earth	M_E	$7.96 \cdot 10^{15}$	Tm^3	
Orbit inclination	i	98	°	
Drag coefficient	C_D	2.4	–	
Reference area	A_r	0.034	m^2	One side of the satellite
Center of drag pressure	cp_a	0	m	From center
Thrust force	F_{thurst}	$40 \cdot 10^{-3}$	N	
Distance of thrust line from mass center	x_P	$1 \cdot 10^{-3}$	m	

Solar pressure As the solar pressure does not depend on the altitude the disturbance can be easily determined. This is done with Equation (4.4).

$$T_s = \frac{\Phi}{c} A_s (1+q)(cp_s - cm) \tag{4.4}$$

This results in a maximum disturbance of $7.01 \cdot 10^{-9} Nm$.

Gravity gradient The gravity gradient is calculated with Equation (4.5). The gravity gradient is depended on the height.

$$T_g = \frac{3\mu}{2R} |I_z - I_y| \sin(2\theta) \tag{4.5}$$

This was done for different altitudes, and resulted in a small torque. The minimum, at 320 km, is $1.25 \cdot 10^{-8}$ Nm and the maximum, at 150 km, is $1.35 \cdot 10^{-8}$ Nm.

Magnetic field The magnetic field disturbance is determined with Equation (4.6). As for the gravity gradient the magnetic field varies with height.

$$T_m = D \left(\frac{M}{R^3} \lambda \right) \tag{4.6}$$

This results in a minimum, at 320 km, of $5.08 \cdot 10^{-7}$ Nm and a maximum, at 150 km, of $5.49 \cdot 10^{-7}$ Nm.

Aerodynamic drag The aerodynamic drag is determined with Equation (4.7). The disturbance increases substantially when the altitude decreases, as the air density increases.

$$T_a = \frac{1}{2} \rho C_D A_r V^2 (cp_a - cm) \tag{4.7}$$

Where ρ is the density, C_D is drag coefficient, A_r is the reference area, V is the velocity and $cp_s - cm$ is the distance between the center of pressure and the center of mass. The density and the velocity will vary with

altitude, which values were used from the astrodynamics model. In the initial orbit, the aerodynamic drag is quite low. But when descending the density quickly increases, as shown in Section 3.1, and thus the drag will increase. At 320 km the drag moment is $1.65 \cdot 10^{-6}$ Nm and at 150 km the drag moment is $1.32 \cdot 10^{-4}$ Nm.

Thruster misalignment The disturbance due to thruster misalignment comes from Equation (4.8). For this calculation, the misalignment has to be estimated.

$$T_p = F_{thrust} x_p \tag{4.8}$$

This will give a final maximum value of $4.0 \cdot 10^{-6} Nm$, although is value is high. This is only present when the propellant is expelled. This is always a very short time.

Concluding the disturbance calculations, the aerodynamic drag is the largest (Equation (4.7)). When the altitude further decreases the atmospheric drag rapidly increases. Therefore in the final stage of the mission the aerodynamic stability can be used, this is further discussed in the [29].

The total disturbance is maximum at 150 km, the value of this will be $1.32 \cdot 10^{-4}$ Nm. For higher altitudes the disturbances torques will be lower, with the minimum at 320 km being $2.18 \cdot 10^{-6}$ Nm.

4.3.3 Detumbling

After deployment from the P-POD, the DelFFi Delta will have an initial tumbling rate of 10 °/s. This tumbling rate will have to be reduced to 0 deg/s, according to requirement DELTA-ACS-2 [22].

Two approaches can be considered with respect to detumbling. The first one is to consider a fixed available torque for detumbling and calculate the amount of time required to detumble the satellite using this available torque. A second approach is to fix the amount of time available for detumbling and size the torque accordingly. The second approach is more related to the design and sizing of the actuators in the AOCS. Especially since the mission has a tight schedule (DELTA-C-4.1 to 4.7), it is more convenient to fix the amount of time available for detumbling. The Cartesian coordinate system of the satellite is shown in Figure 4.6.

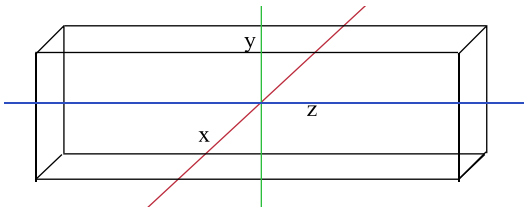

Figure 4.6: Cartesian coordinate system of the Delta satellite.

Using Euler's equations, the satellite's rotation can be described. It is assumed that the satellite is a rigid body and that there are no external disturbances acting on the satellite. The Euler equations are shown in Equation (4.9). [30, p. 224]

$$\boldsymbol{I}\dot{\boldsymbol{\omega}} + \boldsymbol{\omega} \times \boldsymbol{I}\boldsymbol{\omega} = \boldsymbol{T} \tag{4.9}$$

In Equation (4.9), $\boldsymbol{I}$ is the inertia matrix, $\dot{\boldsymbol{\omega}}$ is the angular acceleration vector, $\boldsymbol{\omega}$ is the angular velocity vector and $\boldsymbol{T}$ is the torque vector.

$$\boldsymbol{I} = \begin{bmatrix} I_x & 0 & 0 \\ 0 & I_y & 0 \\ 0 & 0 & I_x \end{bmatrix}, \qquad \boldsymbol{\omega} = \begin{bmatrix} \omega_x \\ \omega_y \\ \omega_z \end{bmatrix}, \qquad \dot{\boldsymbol{\omega}} = \begin{bmatrix} \dot{\omega_x} \\ \dot{\omega_y} \\ \dot{\omega_z} \end{bmatrix}, \qquad \boldsymbol{T} = \begin{bmatrix} T_x \\ T_y \\ T_z \end{bmatrix}$$

In scalar form, Equation (4.9) can be expressed as shown in Equations (4.10) to (4.12).

$$I_x \dot{\omega}_x - (I_y - I_z)\omega_y \omega_z = T_x \tag{4.10}$$

$$I_y\dot{\omega}_y - (I_z - I_x)\omega_z\omega_x = T_y \tag{4.11}$$

$$I_y\dot{\omega}_z - (I_x - I_y)\omega_x\omega_y = T_z \tag{4.12}$$

As mentioned earlier, the goal is to design the control torques $[T_x, T_y, T_z]^T$. Therefore, the other variables have to be known. Starting with the inertia matrix, it was assumed that each of the subsystems is a cuboid. The mass moment of inertia of a cuboid can be determined using Equations (4.13) to (4.15) [31]. The dimensions of this cuboid as well as its mass were based on the available budgets. The 3U CubeSat structure is, in contrast to the subsystems, represented as a hollow and thin-walled cuboid.

$$I_x = \sum \left[\frac{1}{12}m(d^2 + h^2) + m\left[(y - y_0)^2 + (z - z_0)^2\right]\right] \tag{4.13}$$

$$I_y = \sum \left[\frac{1}{12}m(w^2 + h^2) + m\left[(x - x_0)^2 + (z - z_0)^2\right]\right] \tag{4.14}$$

$$I_z = \sum \left[\frac{1}{12}m(w^2 + d^2) + m\left[(x - x_0)^2 + (y - y_0)^2\right]\right] \tag{4.15}$$

In Equations (4.13) to (4.15), I_x, I_y and I_z are the mass moment of inertia around principle axis x, y and z. h, d and w are the altitude, depth and width of the cuboid respectively. (x_0, y_0, z_0) are the coordinates of the center of mass and (x, y, z) are the coordinates of the cuboid's center of mass. The symbol m represents the combined mass.

The angular velocities $\boldsymbol{\omega}$ are the tumble rates after the deployment. In a worst case scenario, all three axis will rotate with 10 deg/s, such that $\boldsymbol{\omega}$ is $[0.175, 0.175, 0.175]^T$ rad/s.

The angular acceleration $\dot{\boldsymbol{\omega}}$ depends on the time that is available to detumble the initial angular velocity; the shorter time is available to detumble, the higher the deceleration should be. As a result, when assuming constant angular acceleration, Equation (4.16) can be derived.

$$\dot{\omega}_k = \frac{\omega_k}{t} \tag{4.16}$$

In Equation (4.16), $\dot{\omega}_k$ is the angular acceleration around axis k, ω_k is the angular velocity around axis k and t is the time available for detumbling for a single axis.

According to requirement DELTA-ACS-2, the satellite should not only be able to recover from a tumbling rate of 10 deg/s, but also within two days. If the three axis are detumbled separately, this would yield that there, if divided equally, is 2/3 day for each axis to detumble.

Based on the discussion before, a preliminary satellite configuration (see also Table 6.2) has been established. As a result, using Equations (4.13) to (4.15), the mass moments of inertia were determined. In the calculations of the mass moment of inertia, it was considered that the solar panels were not deployed. All the inputs for the calculations are shown in Table 4.7.

Table 4.7: Input and output for detumbling calculations

Input	**Value**
I_x, I_y	0.0228 m^4
I_z	0.0048 m^4
$\omega_x, \omega_y, \omega_z$	0.175 rad/s
t	1 days

The amount of torque required for each axis to detumble depends on the order in which the axis are detumbled. Therefore, the six possible orders in which the satellite can be detumbled are listed in Table 4.8, with the required torque per axis.

As can be observed from Table 4.8, detumbling the z-axis first will require the least amount of torque compared to situations where the x- or y-axis are detumbled first. Based on these preliminary calculations,

Table 4.8: Required detumbling torque per axis, depending on detumble sequence

Sequence	T_x [Nm]	T_y [Nm]	T_z [Nm]
$x \to y \to z$	$-5.5 \cdot 10^{-4}$	$6.9 \cdot 10^{-8}$	$1.4 \cdot 10^{-8}$
$x \to z \to y$	$-5.5 \cdot 10^{-4}$	$6.9 \cdot 10^{-8}$	$1.4 \cdot 10^{-8}$
$y \to x \to z$	$6.9 \cdot 10^{-8}$	$5.5 \cdot 10^{-4}$	$1.4 \cdot 10^{-8}$
$y \to z \to x$	$6.9 \cdot 10^{-8}$	$5.5 \cdot 10^{-4}$	$1.4 \cdot 10^{-8}$
$z \to x \to y$	$6.9 \cdot 10^{-8}$	$6.9 \cdot 10^{-8}$	$1.4 \cdot 10^{-8}$
$z \to y \to x$	$6.9 \cdot 10^{-8}$	$6.9 \cdot 10^{-8}$	$1.4 \cdot 10^{-8}$

the required torque for detumbling should be at least $6.9 \cdot 10^{-8}$ Nm, in particular for the x- and y-axis. When a margin of 10% is added, the total torque required per axis to detumble the satellite would be $7.6 \cdot 10^{-8}$ Nm.

To detumble the satellite using the magnetic torquers, a control algorithm has to be used. An often used control algorithm is the B-dot controller. This type of controller tries to minimize the derivative of the magnetic field vector measured by a magnetometer and is extremely simple [32]. A B-dot controller has been used on several nanosatellites, such as the Delfi-n3Xt, SwissCube, CAN-X1, Cute-1.7 and OPTOS [33, 34].

4.3.4 Attitude Determination

In this section the used sensors for attitude and orbit determination will be identified. Their principle of operation and their respective accuracies are explained. Together with the disturbances and detumbling moments this will serve as an input for the attitude control. The attitude determination of the CubeSat will be done using several separate systems. A Micro Electro Mechanical System (MEMS) gyroscope will be used together with fine sun sensors and magnetometers. This combination of sensors will give a precise attitude determination when the satellite is facing the sun and a slightly accurate attitude determination when in eclipse. Requirement DELTA-ACS-4 of formation flying states that the attitude determination should be at maximum 5 °.

Sun Sensor

Sun sensors detect the relative orientation with respect to the sun. This will result in a two axes attitude determination, because no measurements can be done about the sun line [35]. Sun sensors detect if the sun enters the field of view (FOV). When it does not detect the sun, it will not provide a measurement of the attitude. The FOV for a course sun sensor is 180 °. There are basically three ways to use the sun for attitude determination; solar panels, course sun sensors and digital sun sensors. The main drawback of a sun sensor is that no measurements can be performed during eclipse. Sun sensors work based on a phenomenon called 'photo-electric effect'. This comes down to when the solar cell is exposed to light at a certain frequency it produces power. The amount of current depends mostly on the frequency of the light it is exposed to, the higher the frequency the brighter the light, the higher the produced power. [36] When the attitude of the CubeSat compared to the sun is 90° it is impossible to tell if the sun is a doted light source or a spherical light source.

Solar panels In the Mid-term report [4] the best solution in terms of mass and power budget is discussed and the conclusion stated that the solar panels will be used as sun sensors. This technique is not done very often, and the pointing accuracy of solar panels as sun sensors are in the best case 3 ° [37] (using half the control box a pointing accuracy of 2.5°is needed). The risk that the pointing accuracy of solar panels is not good enough cannot be taken, since the QB50 payload and the formation flying mission depends on this pointing accuracy. Therefore the choice has been made to use sun sensors and use the solar panels as back-up. The qualification of solar panels as sun sensors can be performed with this satellite.

Digital / Fine sun sensor The digital sun sensor works differently; the sun light passes through a narrow groove onto a mask containing holes that form a binary Gray code. Below the mask is an array of solar cells. This binary readout indicates the angle of the sun relative to a plane normal to the mask and passing through the groove. The FOV is typically 128° and can reach an accuracy of up to 0.25° [38]. The Adcole fine sun sensor is very popular and can reach more accurate measurements. It contains more entrance grooves and

a reticle that has four row of grooves staggered by a quarter of the width of the reticle grooves [39]. Under the reticle are four photocells, each generating currents. These currents can be related to the sun incidence angle with.

This sensor has an FOV of 100 ° and can reach an accuracy up to 0.01 °. Specifications of CubeSat appropriate sun sensors are listed in Table 4.9.

Table 4.9: Sun sensor

Parameters	**Cubesat sun sensor** [40]	**Comtech AeroAstro** [41]	**OUFTI's MOEMS sun sensor** [41]
dimensions (hxwxd)[mm]	6 x 33 x 11	10 x 20 x 20	7 x 39 x 50
Power consumption [mW]	50	0	-
Mass [g]	5	36	24
FOV [°]	114	60	40
Accuracy [°]	0.5	1	1

From Table 4.9 the choice has been made to go for the Cubesat sun sensor for the reasons that it requires low power, it is the lightest, has the largest FOV and the best accuracy. With a FOV of 114 °, almost omnidirectional coverage can be achieved with 4 sensors placed on the longitudinal sides of the CubeSat [42]. In order to increase this even further and add some redundancy, two extra sensors are added on the top and bottom of the CubeSat.

Magnetometer A magnetometer can measure the geomagnetic field. These have flown on many CubeSats and COTS magnetometers are small, inexpensive, reliable and require little power [43]. Since the geomagnetic field is a vector quantity, the magnetometer only provides two axes of attitude measurement [35].

Also this system does have drawbacks, which can be overcome. Firstly, the Earth magnetic field has been thoroughly analyzed and is modeled accurately. It is however variable and cannot be modeled perfectly. Next to this electronics of other systems produce a magnetic field which will corrupt the measurements of the magnetometer. Thirdly the magnetic field needs to be known for all possible positions in orbit; therefore, the spacecraft must have orbit determination and a magnetic field model [43].

In [44] the new Cal Poly CubeSat electronics is tested with a HMC588L magnetometer. The electronics consist of the system board. Although the electronics and the magnetometer are slightly different from the Delta CubeSat, this information can be used as reference. The results of this test revealed that the system board induces a noticeable magnetic field when the board is active, however increased or decreased computational activity and power draw is negligible in comparison. Therefore active electronics result in a constant magnetic offset which can be accounted for.

Another source that had performed magnetometer interference measurements is the 6th workshop of the QB50 [29]. The basic conclusions that can be drawn from that workshop are the following:

- Permanent magnets will skew the magnetic field
- Brushless DC motors closer than 8 cm will affect magnetometer measurements
- Bus electronics causes interference (noise)

Since the drawbacks of this sensor can be overcome. The sensor requires very little power and volume and the accuracy is between 1° and 5 °, the choice for this sensor is clear. Since the requirements from the pointing accuracy is only needed once per orbit, when the ΔV is given, the pointing accuracy is good enough for eclipse.

The magnetometer that will be used is the Honewell HMC5843, the specifications are listed in Table 4.10. The main reason why this type has been chosen is that it has been extensively tested in a configuration which is comparable with the layout of the Delta CubeSat with respect to magnetic interference.

MEMS gyroscope A MEMS gyroscope is a small gyro, that is light weight and has low power consumption. The use of MEMS has widely grown in consumer and robotic markets. There are four different MEMS techniques; Vibratory, Tuning fork, Vibrating-wheel and Wine Glass Resonator [45], but they all use the same principle; 'by vibrating mechanical element (proof-mass) the MEMS is able to sense rotation. No rotating parts are required and therefore they are easily miniaturized. All vibratory gyroscopes are based on

Table 4.10: Magnetometer specifications of the Honewell HMC5843

Parameter	Value
Accuracy [mGauss]	10
Dimensions (hxwxd) [mm]	2 x 4 x 4
Mass [mg]	50
Power [mW]	<1

the transfer of energy between two vibration modes of a structure caused by Coriolis acceleration. This is an acceleration that arises in a rotating reference frame and is proportional to the rate of rotation. When the satellite is in eclipse the sun sensors can not be used. Therefore, in eclipse the MEMS gyroscope can be useful to determine the attitude. The big disadvantage is the bias stability (drift) of the sensor. For example, the offset is the MEMS gyroscope of the Delfi-n3Xt satellite is 20° after eclipse [46]. This means that the MEMS gyroscope will only be used for short periods of time, since for a larger period the offset will be too large to be reliable.

This sensor has been chosen since the dimensions of the system are small and can still be a redundant system for the attitude determination when the satellite is in eclipse. Furthermore it consumes very little power.

The gyroscope that is selected for the AOCS is the ADXRS646 [47]. This gyroscope includes an accelerometer. The specifications of the MEMS gyro are listed in Table 4.11. This one is chosen from [47] because it is still small, while having remarkable bias stability of 12 $^\circ/Hr$ [48].

Table 4.11: MEMS gyro specifications of the ADXRS646

Parameter	Value
Bias Stability [$^\circ/Hr$]	12
Dimensions (hxwxd)[mm]	3 x 7 x 7
Mass [g]	0.5
Power [mW]	20

4.3.5 Orbit Determination

The need from the orbit determination comes in the first place from the QB50 requirement [22] that all science data shall be tagged with location and time information, within 1 kilometer position accuracy and 1 second time accuracy (and in second place from the formation flying). Although QB50 does not require the use of a GPS receiver, no alternatives are currently present as discussed in the Mid-term report [4]. The only alternative, Corner Cube Retroreflectors (CCR) might not be fully visible during the whole pass of the tracking station and might not be suitable for orbit determination. Therefore the orbit will be measured with the use of a GPS system.

When the GPS is always in operational mode, the orbit predictions will have an high accuracy, which will be beneficial for formation flying. When this is not possible for example due to power budget constraints, the orbit determination will be less accurate.

The GPS system consist of basically two parts; a receiver and an antenna. Although those two system components can be chosen almost separately, usually the antenna and the receiver are from the same brand and type, in order to make sure that these are indeed compatible. First the receiver is discussed, then the antenna.

GPS receiver In the Mid-term report several GPS receivers were discussed for GPS RO. In order to perform just gps measurements for location and time a more simple gps receiver can be chosen than those necessary for GPS RO. The difference is that, now the GPS receivers do not have to be capable of receiving L1 and L2 signals, also it will be sufficient to track just the GPS satellites that will be visible instead of receiving the gps signals from the gps satellites which are just behind the Earth.

Different receivers have been analyzed and considered, one of the key requirements for selecting the GPS receiver was the power consumption and the volume. The selected GPS receiver is the SGR-05U. The specifications of this system are listed in Table 4.12.

Table 4.12: GPS receiver options

Parameters	**SGR-05U** [49]
Dimensions [mm] (lxwxh)	70x45x10
Power consumption [mW]	800
Mass [g]	40
Accuracy [m]	10

All GPS receivers fit in the requirement to tag the data. Therefore the GPS receiver with the least power consumption will be selected. This is the SGR-05U, although the mass and the dimensions of this receiver are not as good as those of the SSBV receiver, the power consumption is considered to be more important.

GPS antenna The antenna that is recommended with the SGR-05U receiver actually sold together with the receiver. It is an active quadrifilar antenna. An option for better performance is an active patch antenna.

Table 4.13: GPS receiver antenna

Parameter	**Value**
Dimensions (hxwxd) [mm]	13 x 13 x 40
Mass [g]	12
Power [mW]	200
Orbital position [m]	10
Orbital velocity [m/s]	0.15 m/s

In case the quadrifial antenna will not fit on the satellite a proven antenna is going to be used. This is the antenna which also served on the Can X-2 mission, the cubesat from Toronto [50]. It has already been proven that it works on other CubeSat missions. The type is AeroAntenna AT2775-103O and has the typical patch antenna dimensions of 76x76x10mm. The dimensions are different and should be taken into account.

Concluding

Table 4.14: attitude and orbit determination system specifications

Parameter	**Value**
Dimensions (hxwxd) [mm]	98 x 98 x 10
Mass [g]	83
Power [mW]	1300

The design of the attitude determination consist of three different systems, the sun sensor, the magnetometer and the MEMS gyro. Using sun sensors is the most lightweight and accurate way of determining the attitude. The best sun sensor selected is the CubeSat sun sensor, the specifications are listed in Table 4.9. Six sun sensors will be used in order to have the sun almost always in the FOV in one of the sun sensors. The accuracy of these sensors is 0.5°. The main drawback of the sun sensor is that these cannot be used during eclipse. However, the QB50 payload and the ΔV (for formating flying) can be performed outside eclipse. Therefore the objectives are not endangered when no sun sensors are used in eclipse, it is more efficient to have some kind of attitude system such that the satellite has not rotated completely during eclipse. Therefore a second and third system are selected, these are the magnetometer and the MEMS gyro because they are very light and require very low power. This is beneficial since volume and power are very limited on board of the CubeSat. The magnetometer selected is the Honewell HMC5843. The accuracy of this system is varying between 1° and 5°. This is mainly because the magnetic field of the Earth also varies. The MEMS gyro that is selected is the ADXRS646 of Analog Devices. The drift is 12°/hour which make it not very accurate in the long run. In order to be as accurate as possible in eclipse, the gyro should be reset just before going into eclipse.

The orbit determination consists of a GPS receiver and an antenna. These are the SGR-05U and the included antenna, this system will have an accuracy of 10 m and in worst case 20 m. Total values for mass, dimensions and power consumption can be found in Table 4.14.

4.3.6 Attitude Control

In the Mid-Term Report [4] the options for attitude control are investigated, the conclusion from this investigation is that the most suitable actuator set is a combination of reaction wheels and magnetic actuators. The reaction wheels provide a precise attitude control of the CubeSat and the magnetic actuators will be able to unload the reaction wheels.

Although magnetic actuators have some drawbacks:

- Only low torque can be applied
- No torque can be applied along the Earth's magnetic field
- It is difficult to use beyond LEO
- The relative high gravity gradient torque will prevent a good pointing accuracy when only using magnetic actuators.

These drawbacks can be overcome using the following strategies.

Only low torque can be applied

Depending on the system configuration the time to become stable is different, in normal operational mode, only using magnetic actuators, the accuracy is limited to 5° [41].

No torque can be applied along the Earth's magnetic field

Also the magnetic torques are constrained on a plane perpendicular to the local magnetic field. This means that it is hard to control the attitude of the satellite in this axis. Next to this fact, the disturbances will interfere with the attitude of the satellite.

It is difficult to use beyond LEO Since the altitude of the Delta CubeSat will have an initial altitude of 320 km, the satellite will not go beyond LEO and this issue will not have an influence on the mission design of the Delta satellite.

The relative high gravity gradient torque will prevent a good pointing

This will become a major issue when the satellite will have an altitude of more than 500 km [41], although the contribution will also be relative high at the initial orbit altitude of 320 km. Also recent studies [41], [51] shows that a combination of two magnetic actuators and one reaction wheel can be used to increase pointing accuracy up to 1°. The algorithm is improved by not applying the torque if the difference between the current attitude and the ideal attitude is more than 45°. When using three magnetic actuators and three reaction wheels, redundancy is built in the AOCS. Since it is of main importance for the mission that the AOCS works properly the entire mission. The total torque to overcome is larger than in the minimum case, where only two magnetic actuators and one reaction wheel form the total attitude control system.

Typically magnetic torquers are used to dump the momentum from the reaction wheels and to take care of the large moments action on the satellite. This will be the case when detumbling the satellite. As a basis for designing the actuators we will use the same protocol as the Delfi-n3Xt; this means that the magnetorquers will be used to detumble and the reaction wheels will be activated when the rotation rate is less than 1 $^\circ/s$. The advantage of using reaction wheels is that a better and smoother control of the attitude is possible, but this comes with the price of a higher power consumption [52].

4.3.7 Magnetic Torquer Sizing

Magnetic torquers are in fact solenoids that result in a torque since they are placed in the magnetic field of the Earth. The torque generated by a solenoid is given by Equation (4.17).

$$D = \frac{T}{B} \tag{4.17}$$

In Equation (4.17), D is the magnetic dipole of the torquer, T is the generated or required torque and B is the strength of the Earth's magnetic field [27].

The magnetic field strength of the Earth B is not a design parameter, since it depends on the location of the satellite in its orbit. For calculations, based on descriptions of the Earth's magnetic field in MATLAB (e.g. the function `wrldmagm`), a value of $B = 6 \cdot 10^{-5}$ T has been used. The torque T depends on the amount of torque required during the different phases of the mission. Since the magnetic torquers will be used for

detumbling of the satellite, the torque required for detumbling is considered. Using Equation (4.17), each of the magnetic torquers will have to provide a dipole moment of at least $1.5 \cdot 10^{-3}\,\mathrm{Am}^2$.

During detumbling, the satellite will be close to its initial orbit of 320 kilometers. At this altitude, the total disturbance torque will be around $1.1 \cdot 10^{-6}\,\mathrm{Nm}$. Using Equation (4.17) again, the magnetic torquers will have to provide a dipole moment of $0.02\,\mathrm{Am}^2$.

Based on [27], a safety factor of 3 to 10 times this value has been chosen to deal with worst case scenarios. If a safety factor of 10 is used, a total dipole moment of $0.2\,\mathrm{Am}^2$ is required.

However, when using torquer rods, one problem arises. To obtain full three axis control, three magnetic torquers should be placed perpendicular to each other. When looking at available torquer rods, their lengths are around 80 mm [53]. If placed perpendicular, this would take up a volume of 80x80x80 mm^3, assuming the volume would not be used by another subsystem. It is however possible to make a coil with open structure as demonstrated on the Delfi-n3Xt [33].

A Commercial off-the-shelf solution which contains two magnetic torquers and an open loop is produced by ISIS [54]. This MagneTorquer Board will produce the required magnetic dipole of $0.2\,\mathrm{Am}^2$ and will fit within the power- and mass budget. Specifications of the MagneTorquer Board by ISIS are listed in Table 4.15.

Table 4.15: ISIS MagneTorquer Board (iMTQ) [54]

Budget	Value
Mass [kg]	0.195
Peak power [W]	0.200
Volume [mm^3]	95.9 x 90.1 x 15

4.3.8 Reaction Wheel Sizing

Reaction wheels are used to perform precise satellite attitude manoeuvres and allow for smooth control of internal torques. Torques are produced on the satellite by decelerating or accelerating the reaction wheels.

Essentially, reaction wheels are torque motors with high-inertia rotors. They can spin either direction and provide attitude control about the spin axis of the motors.

For 3-axis control system, cyclic torques build up cyclic angular momentum in reaction wheels, as the wheels provide compensating torques to keep the vehicle from moving. Typically, the angular momentum capacity of a reaction wheel (limited by its saturation speed) to handle the cyclic storage during an orbit without the need for frequent momentum dumping. Thus if the reaction wheels (without magnetic torquers) deal with all the disturbances torques, assuming a momentum dumping every 0.5 orbits, the minimum momentum storage is the average disturbance of 0.5 orbits. The secular torques and the total storage capacity then defines how frequently the angular momentum must be dumped [27, 55].

The reaction wheel system consist of a Direct Current (DC) electric micro motor, a reaction wheel and power supply between those two parts. Usually, the motor dimensions are large which makes the design challenging. In order to gain full attitude control the reaction wheels must be placed orthogonality. This means that at least three reaction wheels are required. For redundancy, a fourth can be added. This one should be oriented at an axis which does not coincide with the other three axes [56]. The design of the reaction wheel should be as small and light as possible, with as much mass as possible as far as possible from the rotational axis. This can be obtained by using a thinner part on the inside and a thicker part on the outer circumference.

In order to calculate the exact dimensions and the performance the reaction wheels should have, the maximum forces from the detumbling section and disturbance section are taken. The maximum torque the actuators together with the magnetometers should overcome is the aerodynamic moment. This has a value of 9.910^{-5} Nm.

Slew torque For maximum acceleration slews [27].

$$T_s = 4\theta \frac{I}{t^2} \tag{4.18}$$

In Equation (4.18),T_s is the slew torque required, θ is the angle which the satellite will rotate [27]. The maximum moment of inertia around which the satellite have to rotate is the $0.0136m^4$, although this is without deployed solar cells. The maximum rate of slew is 180°. In order to calculate the time that is needed, it is assumed that a rotation of 180° should be performed wihtin a quarter of an orbit. The orbit time is 3257 seconds, thus a quarter corresponds to 814 seconds (at an altitude of $125km$). Using these numbers, the required torque is $2.5810^{-8}Nm$

Momentum storage reaction wheel The momentum storage of the reaction wheels will be calculated with Equation (4.19).

$$h = T_D \frac{OrbitalPeriod}{2}(0.707) \tag{4.19}$$

In Equation (4.19), h is the wheel momentum, T_D is the worst case disturbance torque, this is the sum of the worst case aerodynamic drag, the magnetic disturbance force and the thruster misalignment and is equal to 1.010^{-6} Nm. The number of 2 is used since the assumption is made that the reaction wheels should be able to store the momentum of half an orbit. This is also assumed to be the case in Delfi neXt [33] 0.707 is the average of a sinusoidal function [27]. The value of h will be in worst case $1.151349510^{-3}Nms$. When using a safety factor of 5 (which is convenient) [27], a sufficient margin for worst-case torques can be overcome. Thus a reaction wheel is needed with a momentum storage of $1.151349510^{-3}Nms$.

The maximum rotation speed is defined as the rotation speed where the design torque equals the maximum motor torque. The maximum rotation is 25250 rpm.

Reaction Wheel Selection

The dimensions of the reaction wheels, the motor and the corresponding electronics can now be determined.

Motor sizing, from [57, Table 15] a list of available motors can be found. The requirements the motor has to fulfill are

- Power consumption; 710 mW
- Momentum storage; $1.15 \cdot 10^{-3}$ Nms
- Torque $1.4 \cdot 10^{-6}$ Nm
- Rotation; clock wise and counter clock wise

When these requirements are compared to the capabilities of the Delfi-n3Xt, see Table 4.16 it can be seen that these fit the profile.

Table 4.16: Reaction wheels requirements vs. Delfi-n3Xt reaction wheel system

Parameter	Required	Delfi-n3Xt
Power consumption [mW]	-	530-710
Momentum storage [Nms]	$1.15 \cdot 10^{-3}$	$1.56 \cdot 10^{-3}$
Torque [Nm]	$5.5 \cdot 10^{-6}$	$5.5 \cdot 10^{-6}$
Dimensions [mm]	100 x 100 x -	40 x 40 x 27
Mass [g]	-	82

4.3.9 Cycle

The AOCS basically consists of three parts: the attitude determination, the orbit determination and the attitude control. During the detumbling phase, the attitude determination will be switched on, as well as the magnetic rods of the attitude control. At the end of the detumbling phase and during the rest of the satellite mission the reaction wheels will be used to deal with the smaller attitude changes. In the detumbling phase, the GPS receiver will also be operative, since it is beneficial for the formation flying mission to know already where the satellite is.

The GPS module will be active during the scientific measurements. Typically, a GPS fix will take maximum 90 seconds [58], adding a margin of 10% and the time it has to measure; 60 seconds for the QB50 payload

Section 4.6, the maximum time the GPS has to be switched-on is 159 seconds. The measurements have to be performed every 10 minutes (roughly 9 times per orbit), the GPS will thus require to be switched-on 159 of the 600 seconds. Moreover, during re-entry the GPS will stay on as long as possible to obtain a higher accuracy for the landing prediction.

After detumbling, the formation acquisition and maintenance, the satellite requires a very precise attitude determination and control. In this period, the attitude of the satellite will have to be maintained in a certain position under disturbance loads. Also there is a possibility that the attitude must be changed every orbit, due to the position of the nozzle. Next, the attitude could change such that the C_D will increase or decrease. The sun sensors, MEMS gyro and the magnetometer will determine the attitude, except for the sun sensor in eclipse. The attitude control will be performed by the reaction wheels. Again, the magnetic torquers will dump the momentum of the reaction wheels regularly. When the reaction wheels spin up to 50% of their maximum capacity, the magnetic rods will unload the momentum as soon as the attitude, such that the magnetic field and that specific torquer is perpendicular.

For formation flying the orbit should be measured as precise as possible, therefore the GPS will always be switched on. Although with less measurements the orbit calculation can be done, it will be less accurate and thus the error in the formation flying will be larger, which will increase the amount of ΔV required.

After the formation flying period, the 'normal' operational time and the re-entry, it is assumed that the satellite will remain in a 'horizontal' attitude such that the Cd is minimum. The attitude determination will be activated all the time, furthermore the attitude control will be switched on the whole time to overcome the disturbances which act on the satellite. Also when a special maneuvre has to be performed, the AOCS will be available. This can be the case when there is still some ΔV left in order to increase the mission lifetime or position the capsule into an slightly changed orbit.

The reaction wheels are designed to store momentum which corresponds with the maximum disturbances for half an orbit. When the reaction wheels are fully spinned, the moment will be dumped using the magnetic rods. The magnetic rods are thus only active during the detumbling phase and the moment dumping.

4.3.10 System Layout

The AOCS is one of the most complex and one of the most important systems on-board the CubeSat. It consist of an attitude determination system, an orbit determination system as well as a control system. The purpose of the AOCS is to stabilize the satellite in the orbit and take care of the proper attitude such that the propulsion system is pointed in the correct direction. For formation flying it is required that the ΔV is added in the correct direction, furthermore the GPS sensor requires the GPS antenna to be facing away from the Earth. The design of the AOCS is shown in Figure 4.7.

The desired attitude and orbit is compared to the measured attitude and orbit. Then the actuators in the form of the reaction wheels and the magetic torquers for the attitude are controlled by an algorithm and the orbit is controlled by the thruster. The loop closes again as the CubeSat is liable to disturbances. The attitude and orbit will be measured again and the process repeats itself.

4.3.11 Conclusion

During all phases of the mission the AOCS has to fulfill an important role, first it has to detumble the satellite, then it has perform attitude maneuvers for the formation flying objective and it has to deal with all the disturbances. The total torque that is required to detumble the satellite is $4.5 \cdot 10^{-8}$ Nm, this will be handled by the magnetic rods. In total there are five disturbances of which the aerodynamic drag is the largest. All worst case disturbances combined results in a torque of $1.0 \cdot 10^{-6}$ Nm, which every reaction wheel must be able to produce in the worst case scenario.

The AOCS is a complex system which can be divided into three parts; attitude determination, orbit determination and orbit control. The attitude determination is done by a combination of 3 different sensor systems; 6 sun sensors, 1 magnetometer and 1 MEMS gyro. In eclipse the sun sensors will not be used and will therefore have a slightly worst performance. The accuracy will be 5° in eclipse and 0.5° out eclipse.

4.4 Propulsion System

One of the primary missions of the DelFFi Delta mission is the formation flight demonstration. In order to achieve formation flight, the satellite should be able to provide a ΔV. This ΔV, which will have a value for

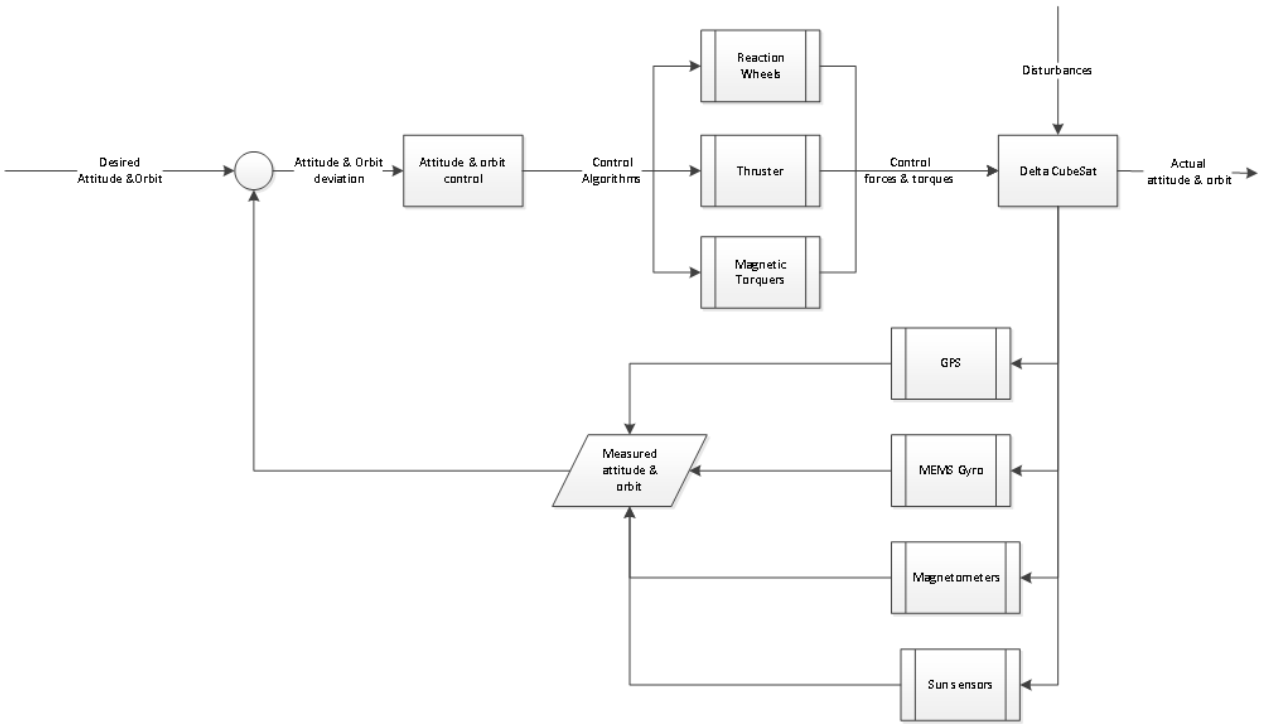

Figure 4.7: Control loop for the AOCS

Table 4.17: Final quantities for the AOCS

AOCS Subsystem	Value
Mass [g]	438
Dimensions (hxwxd) [cm]	10x10x4.2
Power (operating) [mW]	1700
Operating time description	continuous

the DelFFi mission of 15 m/s, can be delivered by the means of a propulsion system (requirement DELTA-PR-2). In this section, the design of the propulsion system for the DelFFi Delta will be described. First of all, the type of propulsion is selected. Next, a conventional propulsion system is considered, with all the gas stored in a single tank. Finally, existing propulsion systems developed by the Delft University of Technology will be analysed and adjusted to fit the requirements and budgets of the DelFFi Delta mission.

4.4.1 Types of propulsion

Depending on the mission requirements, different propulsion systems can be selected. In Figure 4.8, different types of thrusters are shown and in which ranges they are used. To provide the ΔV of 15 m/s, Cold Gas Thrusters would be the most suitable. Cold gas thrusters offer the greatest degree of simplicity of all propulsion sytems, which reduces the risk of failure. This type of propulsion consist of a cold gas which is blown down through a nozzle, resulting in a thrust [59].

4.4.2 Conventional Cold-Gas Thruster Design

The specific impulse I_{sp} of the system depends on the selected propellant gas, the sonic speed of the gas and the pressure ratio between the storage tank and the nozzle exit used. Equation (4.20) gives the relation between these different variables [61].

$$I_{sp} = \frac{C^*}{g}\left\{\left(\frac{2}{\gamma-1}\right)\left(\frac{2}{\gamma+1}\right)^{(\gamma+1)/(\gamma-1)}\left(1+\frac{P_e}{P_c}\right)^{(\gamma-1)/\gamma}\right\}^{1/2} \tag{4.20}$$

In Equation (4.20), C^* is the characteristic velocity in m/s (see Equation (4.21)), g is the gravitational acceleration in m/s^2, γ is the specific heat ratio, P_e is the exit pressure in Pa and P_c is the chamber pressure

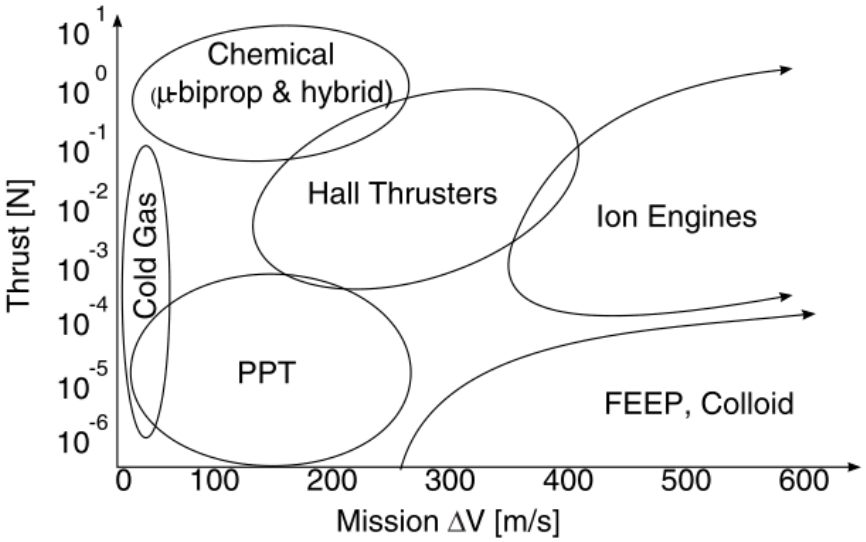

Figure 4.8: Domains of different propulsion systems [60]

in the nozzle in Pa.

$$C^* = \frac{\sqrt{\gamma RT/M}}{\gamma \left(\frac{2}{\gamma+1}\right)^{\frac{\gamma+1}{2(\gamma-1)}}} \tag{4.21}$$

In Equation (4.21), R is the general gas constant (8.31446 $\frac{\text{J}}{\text{mol K}}$), T is the temperature of the gas in K and M is the molar mass of the gas in kg/mol [61].

Using Equation (4.20) with nitrogen, oxygen and hydrogen as cold gas, the relation between the pressure ratio in the tank and the exit of the nozzle and the specific impulse is given by Figure 4.9.

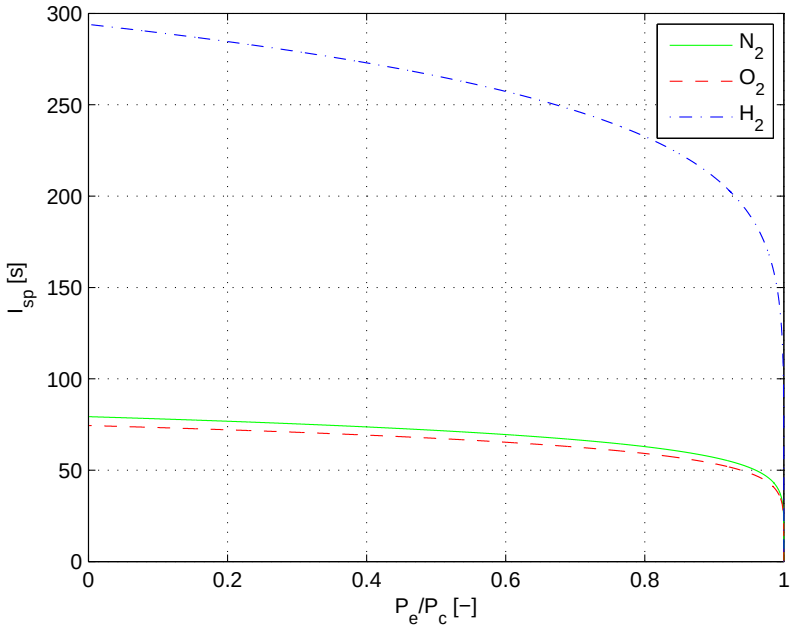

Figure 4.9: Specific impulse as a function of the pressure ratio for nitrogen, oxygen and hydrogen as cold gas propellant

The theoretic specific impulse is the specific impulse at which the gas is expanded to a vacuum. In reality, however, there will not be a real vacuum, which will result in a lower specific impulse. For the three cold

gasses, their properties used for Figure 4.9 and the theoretic specific impulse resulting from Equation (4.20) are listed in Table 4.18.

Table 4.18: Propellants and their properties, including theoretic specific impulse at 20°C

Cold Gas	**Symbol**	**Molar mass** M [g/mol]	**Specific heat ratio** γ [-]	**Specifc Impulse** I_{sp} [s]	**Propellant mass** m_p [g]
Nitrogen	N_2	28	1.404	79.3	68.7
Oxygen	O_2	32	1.4	74.4	72.7
Hydrogen	H_2	2	1.41	293.9	18.5

The rocket equation published by Konstantin Tsiolkovsky (Equation (4.22), [27, p. 690]) relates the specific impulse to the required propellant mass, when the required ΔV and total mass is known. For DelFFi Delta, the required ΔV is 15 m/s and the total budgeted mass is 3.6 kg.

$$\Delta V = g I_{sp} \ln\left(\frac{m_0}{m_0 - m_p}\right) \tag{4.22}$$

In Equation (4.22), ΔV is the change in velocity, g is the gravitational acceleration, I_{sp} is the specific impulse, m_0 is the total mass of the satellite at the start and m_p is the propellant mass.

The required propellant mass to obtain a ΔV of 15 m/s for each of the earlier mentioned cold gasses can now be determined using Equation (4.22) and are also listed in Table 4.18. Using the ideal gas law in Equation (4.23), the required volume as a function of the pressure can be determined. This is shown in Figure 4.10.

$$PV = \frac{m}{M} RT \tag{4.23}$$

In Equation (4.23), P is the pressure at which the gas is stored in Pa, V is the volume in m^3, m is the mass of the gas in kg, M is the molar mass of the gas in kg/mol and R is the general gas constant (8.31446 $\frac{\text{J}}{\text{mol K}}$)and T is the temperature of the gas in K. [62]

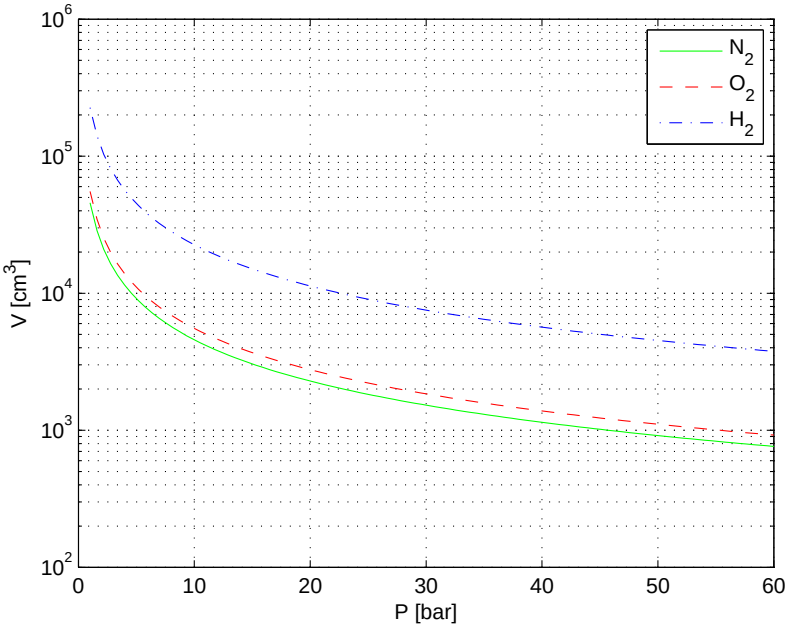

Figure 4.10: Required propellant volume as a function of the pressure in the storage tank for nitrogen, oxygen and hydrogen (20°C).

Several observations can be made from Figure 4.10. First of all, when using hydrogen as cold gas propellant, the required volume is significantly larger compared to nitrogen and oxygen at 20°C.

When assuming a spherical tank ($V = 4/3\pi r^3$), the maximum possible diameter based on the 3U CubeSat dimensions is 98 mm. This would yield that the maximum volume is 522 cm^3. As can be seen in Figure 4.10, this is not feasible for any of the gasses, unless the pressure will increase or the temperature will decrease. Decreasing the temperature is not an option, since the temperature on-board of the satellite will be controlled passively; the temperature will mainly depend on its location in the orbit. Increasing the pressure to larger values than are shown in Figure 4.10 is also not feasible; the structure will have a very large thickness and therefore a large mass. It can therefore be concluded that storage of the cold gas propellants is *not* an option in the DelFFi Delta.

4.4.3 Existing Propulsion Systems

From the previous section can be concluded that conventional cold-gas propulsion systems are not feasible for the DelFFi Delta mission. Therefore, the scope of the design will be shifted towards existing designs, especially designs created by Delft University of Technology. Delft University of Technology has two Cold Gas Propulsion systems in development: the $T^3\mu PS$ and the MEMS resistojet system. These will be discussed below. The calculated system masses are based on [63].

- The micropropulsion system developed by TNO, Delft University of Technology and University of Twente ($T^3\mu PS$ Cold Gas System) is a blow down system that uses cool gas generators, which create gaseous nitrogen which is stored in solid state in the generators. This system will be used on the Delfi-n3Xt. Using these cool gas generators, the the required tank pressure and volume can be reduced. To provide a ΔV of 15 m/s, the total system weight would be 465 g.
- The MEMS Resistojet System uses miniaturized thrusters with a nozzle throat of 5 to 10 μm. As a propellant, gaseous nitrogen is used. A laboratory test has been performed for this propulsion system. [64] To provide a ΔV of 15 m/s, the total system weight would be 700 g.

These calculated masses are outside of the available mass budget for the propulsion system. However, a recommendation made is that the cold gas generators of the $T^3\mu PS$ could be combined with the MEMS Resistojets. This combination will result in a better performance, suitable for the DelFFi formation flying mission [63].

These calculated masses are outside of the available mass budget for the propulsion system. However, a recommendation made is that the cold gas generators of the $T^3\mu PS$ could be combined with the MEMS Resistojets. This combination will result in a better performance, suitable for the DelFFi formation flying mission. The specific impulse of the MEMS Resistojet System has a reported value of 73 seconds. Resulting from Equation (4.22), the required propellant mass is 74.6 g [63].

Each of the cold gas generator has a mass of 16.3 g of which 4.21 g can be used as propellant. This yields that a total of 18 cold gas generators are required, resulting in a total mass of the cold gas generators of 293 g.

In Section 3.3.8, it has been established that the ΔV that is required for each firing of the thruster will be maximum 8-10 cm/s. As a consequence, each firing a maximum of 0.35 grams of propellant mass has to be expelled.

The contents of a single cold gas generator will be stored at a pressure of approximately 10 bar. This will result in a volume of the storage tank of 366 cm^3. If the full available area of a CubeSat will be used (e.g. approximately 95x95 mm^2), the thickness of the storage tank will be 40 mm. Note that corners of the tank will be rounded to avoid any stress concentrations which will increase the actual pressure slightly because the volume is slightly smaller. In the following calculations, this pressure increase have been neglected.

The thickness of the tank has been set to a value of 1 mm. Although no detailed structural calculations have been performed for the rectangular shape of the tank, a spherical tank shows that at the pressured used in the tank, the thickness can be very small. As can be shown in Figure 4.11, at 1 mm thickness, the stress is approximately 8 MPa. For example, aluminium alloys have a tensile strength ranging from 200 to 600 MPa, depending on the properties of the specific alloy [65]. For initial weight estimations, the aluminium alloy 6061 will be used. It has a yield strength of 110 MPa, which is sufficient. As a result, the total mass of the storage tank will be 21.9 grams.

Properties of the thrusters depend on the nozzle layout (Figure 4.12). The MEMS Resistojets have an area ratio ε of 25 [64]. Using this property, the pressure ratio over the chamber and the nozzle exit P_c/P_e can be calculated using Equation (4.24).

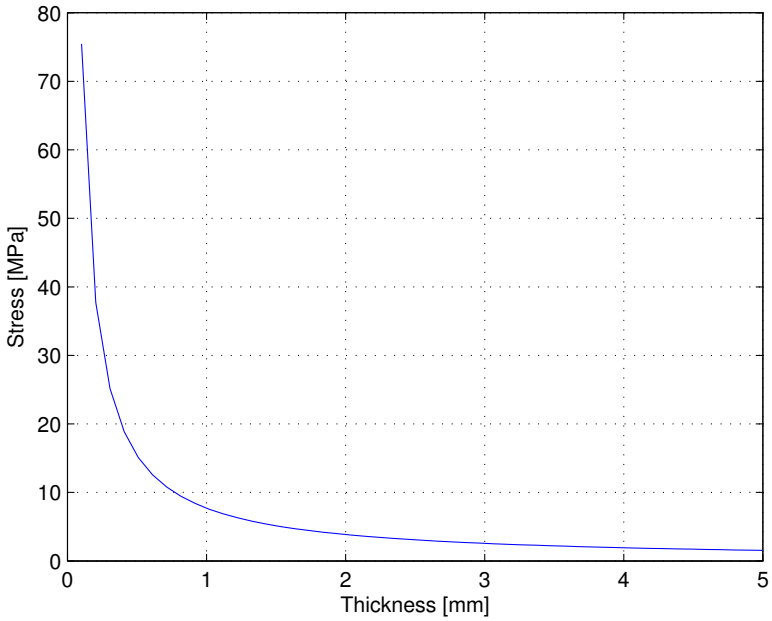

Figure 4.11: Stresses in the shell of a spherical tank (4 cm diameter) due to pressurization as a function of the thickness

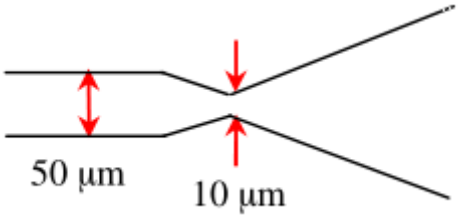

Figure 4.12: Nozzle layout; expansion ratio ε of 25 [64]

$$\frac{A_e}{A_t} = \frac{1}{C_F^0}\gamma\left(\frac{2}{\gamma+1}\right)^{(\gamma+1)/(\gamma-1)}\left(\frac{P_c}{P_e}\right)^{1/\gamma} \tag{4.24}$$

In Equation (4.24), A_e/A_t is the expansion ratio, C_F^0 is the characteristic thrust coefficient, γ is the specific heat ratio and P_c/P_e is the pressure ratio [55, p. 176]. The characteristic thrust coefficient is given by Equation (4.25).

$$C_F^0 = \sqrt{\left\{\left[\gamma\left(\frac{2}{\gamma+1}\right)^{(\gamma+1)/(\gamma-1)}\right]\frac{2\gamma}{\gamma-1}\left[1-\left(\frac{P_e}{P_c}\right)^{(\gamma-1)/\gamma}\right]\right\}} \tag{4.25}$$

Using Equations (4.24) and (4.25), a relation between the pressure ratio and the area ratio can be shown. This is visible in Figure 4.13. For an area ratio of 25, the resulting pressure ratio is 537.

Based on the pressure ratio, the resulting mass flow per nozzle can be obtained using Saint Venant equation. This equation is shown in Equation (4.26) [66].

$$\dot{m} = \frac{P_c A_e}{\sqrt{\frac{RT_c}{M}}}\sqrt{\frac{2\gamma}{\gamma-1}\left(\frac{P_e}{P_c}\right)^{(2/\gamma)}\left[1-\left(\frac{P_e}{P_c}\right)^{(\gamma-1)/\gamma}\right]} \tag{4.26}$$

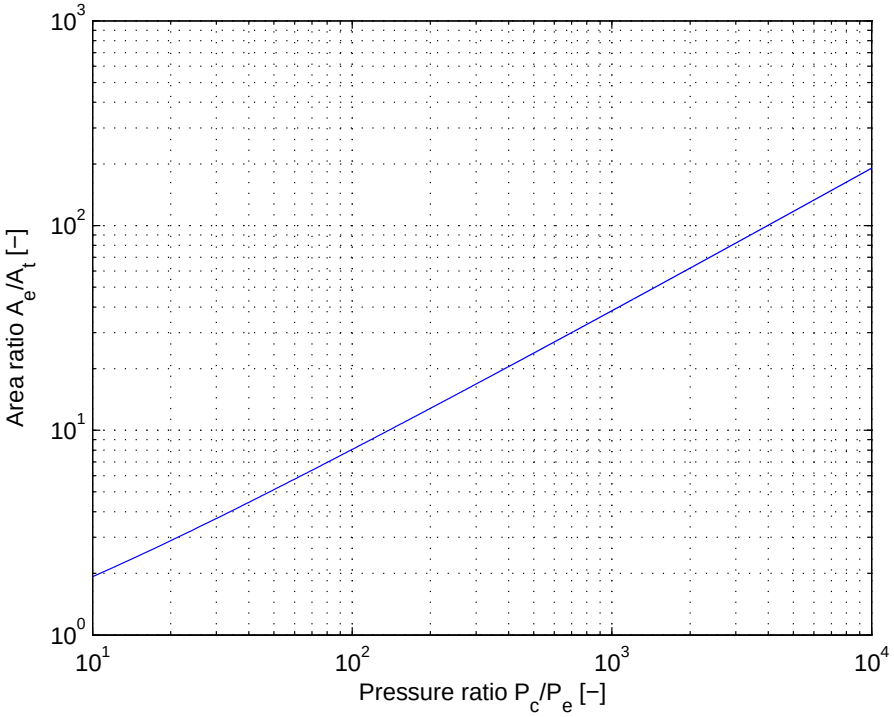

Figure 4.13: Relation between the area ratio and pressure ratio for nitrogen at 20°C

In Equation (4.26), $\dot{m}$ is the mass flow rate in kg/s, A_e is the nozzle exit area in m^2, R is the universal gas constant, M is the molar mass in kg/mol T_c is the temperature in the chamber (assumed to be 20°C, which is close to the average temperature of the satellite of 17.6°, γ is the specific heat ratio and P_e/P_c is the ratio between the pressure in the exit and the chamber [55, p. 175].

Using Equation (4.26), the pressure ratio P_c/P_e of 537, the nozzle exit area of 1500 μm^2 and the gas properties of nitrogen, the mass flow rate for this propulsion system is 3.5 mg/s. As mass is expelled from the tank, the pressure in the tank will drop. If the content of the tank is just the amount of propellant required to provide a ΔV of 8-10 cm/s (0.35 grams), the mass flow of the system would be 0.29 mg/s.

In case of a full tank (i.e. maximum pressure) and a single nozzle, the thrust time would be 100 seconds and even larger when the pressure has dropped. In an ideal case, the ΔV can be delivered as an impulsive shot, which has also been assumed in the formation flight calculations. In reality, however, this is not possible. To be as close as possible to an impulsive shot, the thrust time should be limited. Therefore, the thrust time has been limited to 15 seconds.

In case of 16 thrusters [63], the thrust time in case of a maximum pressurized tank will be 6.25 seconds, which is within the 15 seconds limit. As the pressure decreases in the tank, the thrust time will increase. When the pressure in the tank has decreased to a value of 4.17 bar, the thrust time is 15 seconds. At this pressure, 1.75 grams of propellant is left in the tank. To increase the pressure in the tank again, a new cold gas generator can be fired. This would increase the pressure in the tank to 14.1 bar and decrease the thrust time to 4.4 seconds. This process is repeated every time the pressure in the chamber reaches the value of 4.17 bar.

This approach will result in a larger pressure in the chamber than assumed before. The maximum pressure in the chamber will now be 14.1 bar. If the calculated volume will be maintained, the thickness of the tank will have to increase slightly. However, as it was concluded earlier that the tank thickness is minimal at these pressures, no changes to the design of the storage tank will be made.

The amount of thrust generated by the propulsion system mainly depends on the mass flow of the system. The mass flow of of the thrusters varies in the range from 1.5 mg/s (at a chamber pressure of 4.17 bar per nozzle) to 5 mg/s (at a chamber pressure of 14.1 bar per nozzle). The thrust of the propulsion system is given by Equation (4.27).

$$F = n\dot{m}V_e \tag{4.27}$$

In Equation (4.27), n is the amount of thrusters in the system, F is the thrust N, $\dot{m}$ is the mass flow rate kg/s and V_e is the exit velocity of the nozzle in m/s [61]. The exit velocity is given by Equation (4.28).

$$V_e = \sqrt{\frac{2RT_c}{M}\frac{\gamma}{\gamma-1}\left(1-\frac{P_e}{P_c}\right)^{\frac{\gamma-1}{2}}} \tag{4.28}$$

Using Equations (4.27) and (4.28), the total thrust of the system can be calculated. In Figure 4.14, the total thrust is shown as a function of the total mass flow for all 16 nozzles. As a result, the thrust ranges from 23 to 61 mN.

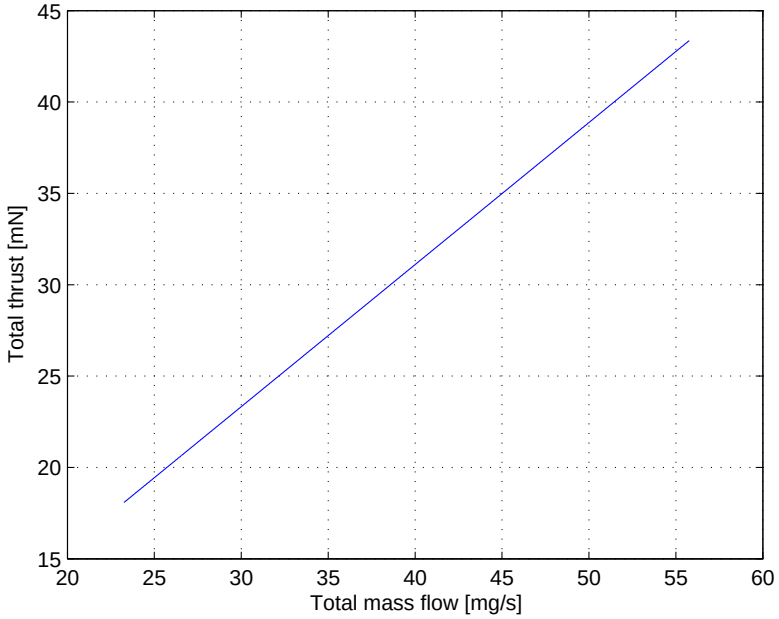

Figure 4.14: Thrust as a function of the mass flow controlled by a mass-flow controller for a total of 16 MEMS Resisojets

The power required for the propulsion system depends only on the power needed by the cool gas generators. The power to ignite the thrusters is 13.2 W for approximately 10 seconds. After ignition, thrusting would require 369 mW [67]. During idle mode, only 45 mW is required [67]. To improve the performance of the MEMS Resistojets, the propellant could be heated to 350°C, which would requires 2.5 W [68]. As a result, the specific impulse will increase from 73 seconds to 104 seconds. Because of the limited power available, this option is not considered.

4.4.4 Propulsion System Overview

Summarizing, the propulsion system for the DelFFi Delta satellite will have the following properties:

- 18 Cold-Gas Generators (293 g), which includes 75.8 g of propellant (nitrogen)
- 16 MEMS Resistojet System with a total mass of 2.6 g
- A rectangular storage tank which can store 366 cm^3 of propellant. Its mass is 21.9 g
- Maximum power usage of 13.2 W during ignition

When assuming a mass of 100 g for the wiring, valves, pipes and the PCB, the total mass of the system will be **418 g**.

4.5 Telemetry, Tracking and Command System

Communication between Delta and the ground station is essential to achieve a successful DelFFi mission. The Telemetry, Tracking and Command (TT&C) subsystem is the main actor in this process. Its main objective is to transmit data to the ground station as well as receive commands from the ground station.

Table 4.19: Budgeted quantities for the propulsion subsystem

Propulsion	Value
Mass [g]	418
Dimensions (hxwxd) [mm]	58 x 98 x 98
Power (ignition) [mW]	1320
Power (thrusting) [mW]	369
Power (idle) [mW]	45

Given these main objectives, it is important that the TT&C fulfills its function within the constraints and requirements which are described in this section. First, general information on the subsystem is presented in Section 4.5.1. As a next step, the final choices for the TT&C concerning the frequency, bandwidth, antenna, architecture as well as the modulation scheme and transceiver are shown in Section 4.5.2. Following, the link budgets for downlink and uplink are presented in Section 4.5.3.

4.5.1 General Characteristics

The following section describes the protocols used for radio amateur communication followed by the global ground station system which will be used during the mission. Finally, the data volume and data rates are explained.

Protocol Definition

Delta communicates with a global network of radio amateurs, according to the QB50 requirements [22]. Therefore, various protocols need to be considered when designing the TT&C. The most important protocol concerning the radio amateurs is the AX.25 Link Access Protocol for Amateur Packet Radio. This document focuses on the one hand on the network communication especially for radio amateurs and on the other hand on the interface requirements between different link layers and physical layer functions. Furthermore, AX.25 specifies the usable data rate, which is between 200 bps and 9600 bps [69].

The total overhead needed for the data rate is defined by two protocols focusing on radio amateur and QB50 communication [22]. The first one is the AX.25 which defines the overhead required for radio amateurs [69], the second one is the QB50 block protocol [22] defining the required QB50 protocol. With these definitions, a total overhead of 30% is used.

Global Educational Network for Satellite Operations (GENSO)

GENSO is a network of multiple ground stations that has the purpose to receive data of university satellites. Taking for example Delfi-C^3, mission data is transmitted continuously from the satellite. However, not enough ground stations are in use and therefore, the return on data relies highly on radio amateurs.

For future missions, the use of additional ground stations can lead to more data received. The GENSO network predicts around 100 ground stations to be active by 2015, providing almost global coverage [70]. Therefore, the GENSO ground station network is part of the communication system. For more information on the contact time needed to send the data see the Mid-term Report [4].

Data Volume

In the requirements of the QB50 mission [22], it has been stated that at least 8 Mb of science data [DELTA-CS-5.1] needs to be transmitted per day, in case a global ground network like GENSO is used. In accordance with the Command & Data Handling subsystem, it has been determined that in total 23 Mb per day will be sent for the QB50 payload. Additionally, the formation flying and household data needs to be transmitted. For more information see Section 4.6. Overall, the total data volume per day that needs to be transmitted is 232 Mb.

With the data volume known, it can be determined whether the data is sent continuously or in bursts. Assuming a visibility angle of 160°, the pass time of the CubeSat is at least 337 seconds per pass. During one day, the TU Delft ground station is passed at least 5 times. Based on a data rate of 4800 bps, it is not possible to transmit all the data with only one ground station. Therefore, the 232 Mb of data per day will be received by the GENSO ground stations. With this ground system, it is ensured that all data transmitted by

the CubeSat is actually received by the TU Delft. The responding link budgets to the downlink and uplink can be found in Section 4.5.3.

The TT&C is designed to send all collected data twice within one orbit, which is already considered in the total data volume of 232 Mb. This way, a margin is included to assure that the data will be received by the ground stations of GENSO. The total contact time per orbit including the margin of 100% is 72 minutes. Consequently, 9 minutes less per orbit are required for communication than the available 81 minutes.

Furthermore, the transmitted data can also be received by radio amateurs since the AX.25 protocol is used [69]. Thus, not only the radio amateurs will be rewarded for their help with previous Delfi missions, but also an additional margin is included for the ground coverage. This way it will be guaranteed that DelFFi Delta will have sufficient ground contact to transmit all the data collected.

4.5.2 System Specifications

The following section focuses on the final design choices of the TT&C subsystem. The decisions are also presented in Table 4.20. First, the frequency for the uplink and downlink is selected, then the antenna is chosen. Next, the architecture and its redundancy are presented and discussed, followed by the modulation scheme and transceiver choice.

Table 4.20: Specifications of the TT&C system

Criteria	**VHF/UHF**
Frequency [Hz]	
Downlink	$145 \cdot 10^6$
Uplink	$435 \cdot 10^6$
Downlink data rate [bps]	4800
Uplink data rate [bps]	1200
Power [mW]	1700 [28]
Mass [g]	
Transceiver	90 (two) [28]
Antennas	90 [28]
Volume [mm^3]	
Transceiver	96 x 90 x 15 [28]
Antennas	98 x 98 x 7 [28]
Costs [Euro]	6750 [28]

Frequency & Data Rate

VHF and UHF are used for downlink and uplink, respectively. As mentioned earlier, the radio amateurs are also used to receive data from the CubeSat. Therefore, the downlink frequency can be within a range of 145-146 MHz. It has been decided to use a frequency of 145 MHz, which is the frequency TU Delft already uses for satellite communication. However, compared to the Delfi-C^3 and Delfi-n3Xt communication, a slightly different frequency is used in order to prevent interference. The downlink data rate has been determined to be 4800 bps.

The TU Delft ground station gives the main constraint for selecting the uplink frequency. The uplink frequency range is 435-438 MHz, which can also be used by radio amateurs. An uplink frequency of 435 MHz has been selected that is also the current frequency used by the TU Delft ground station. The data will be sent with a data rate of 1200 bps according to the requirements [22].

Bandwidth

The bandwidth plays a crucial role when the data rate is determined under the influence of noise. A maximum bandwidth of 1000 Hz is allowed by the QB50 requirements [22]. The bandwidth can be calculated using the Shannon-Hartley theorem, found in Equation (4.29). C represents the channel capacity, B the bandwidth capacity of the channel and $\frac{S}{N}$ is the signal-to-noise ratio [71].

$$C = B\log_2\left(1 + \frac{S}{N}\right) \tag{4.29}$$

Knowing that C equals 4800 bps and $\frac{S}{N}$ equals 49.6 dB, the bandwidth for Delta can be determined using the Shannon-Hartley theorem. From Equation (4.29), a minimum bandwidth of 291 Hz will be required for the TT&C system of the Delta satellite.

Antenna

For the Delta satellite, a turnstile antenna configuration was chosen. This consist of two dipole antennas that are mounted in a 90° angle horizontally w.r.t. each other. Since two dipole antennas will be used, in total, four whip antennas will be on board of Delta. The selected antenna will be Commercial off-the-shelf and has been proven to work on previous CubeSats [28].

The same turnstile antenna will be used for uplink and downlink. This can be done since the required antenna length for downlink is 3 times the length of the required uplink antenna length. The length of the antennas will be a quarter of the wavelength of the downlink frequency. This means an antenna length of 0.52 m will be required for each whip antenna.

Architecture

The architecture of the UHF/VHF communication is shown in Figure 4.15. The on-board computer sends the telemetry to the transceiver which modulates and codes the signals that are sent to the ground. After the transceiver, the analog signal goes through the low pass filter in order to attenuate the high frequency noise signals. In the next step, the signal is sent to the antenna, which amplifies and directs it to the Earth. Each antenna block shown in Figure 4.15 represents one dipole antenna, thus, two monopole antennas. In total two duplex antennas are used. The received signal is processed through the same components in reversed order compared to the transmitted signal. This is possible since the transceiver has full duplex operation. For more information on the function of the on-board computer see Section 4.6.

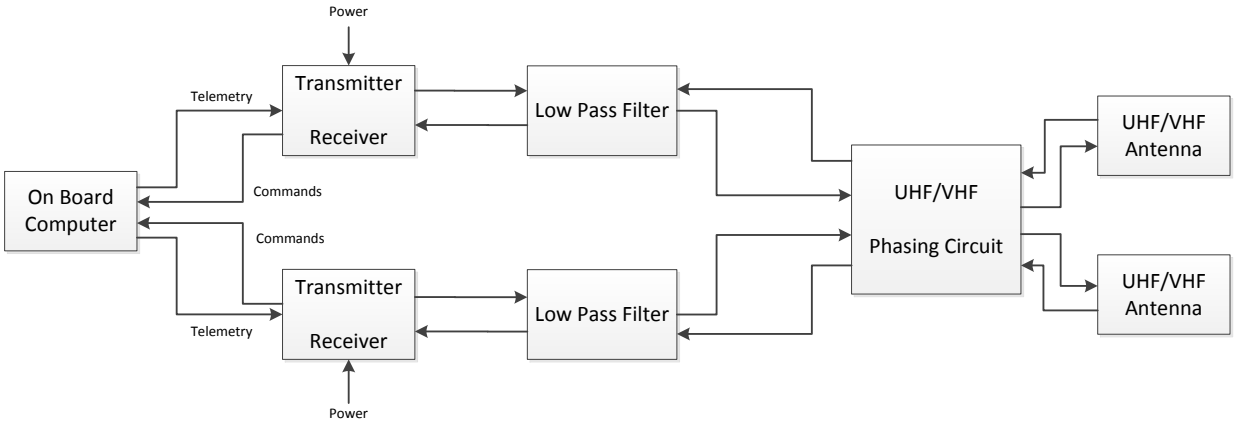

Figure 4.15: VHF/UHF communications architecture

Redundancy The TT&C subsystem is a crucial part of the CubeSat. Therefore, redundancy is an essential aspect when designing this subsystem. Looking at the architecture in Figure 4.15, one can see that the hardware is in redundant configuration. Thus, two transceivers and two low pass filters are implemented in order to have a fail-safe system.

Modulation Scheme

In principle, the data that needs to be transmitted and received is stored digitally on the on-Board Computer, but it is sent analog.

It has been decided to use Binary Phase Shift Keying, BPSK, as a modulation scheme during the Delta mission. The main idea is that information is assigned to the changed phase of the carrier signal. A 180° phase shift is used to modulate the binary information. This means that the two different binary states 0 and 1 are assigned to 0° and 180°.

The signal over time of BPSK can be determined using Equation (4.30) [72]. Here $s(t)$ is the modulation signal in time, A_mp is the amplitude of the carrier signal and f_c represents the carrier frequency. Further, ϕ_c is the carrier phase and $m(t)$ is the modulation index which takes either value 1 or -1 to transmit the binary information of 0 or 1, respectively.

$$s(t) = A_{mp} \cos(2\pi f_c t + \phi_c + \pi m(t)) \tag{4.30}$$

The main advantage of BPSK is that it has lower error rates than other modulation schemes. Because of the 180° phase shift, BPSK is very robust to noise. Even 1though the complexity of BPSK is reasonably high most modulation and demodulation parts are already COTS.

Transceiver

The transceiver that is selected for this mission is the *TRXUV VHF/UHF Transceiver*, designed by ISIS [73]. This is a full duplex Commercial off-the-shelf transceiver, meaning that the transceiver can do both telemetry and command at the same time. The specifications for this transceiver can be found in Table 4.21. This transceiver has been chosen because of the relatively low operating power, small dimensions, an interface that supports the system bus and an operating temperature range that can be achieved by Delta. Furthermore, its frequency range supports the frequencies that the Delta satellite will use for communication.

Table 4.21: Specifications of the TRXUV VHF/UHF transceiver [73]

Parameter	Value	Unit
Operating power	1.7	W
Downlink frequency	130 - 160	MHz
Downlink data rate	4800	bps
Uplink frequency	400 - 450	MHz
Uplink data rate	1200	bps
Dimensions	96 x 90 x 15	mm^3
Operating temperature	-20 to +50	°C

Since the TT&C system will be a redundant system, two of these transceivers will be implemented on the satellite. Thus, the total volume for transceivers will be twice the volume of a single transceiver. However, the power that is required for the TT&C system will still be maximum 1.7 W. This is because the redundant transceiver will only be activated in case of failure of the primary transceiver.

4.5.3 Link Budget

The link budget of a TT&C system is a tool that shows signal power and system losses throughout the communication path. For the Delta satellite, two way communication is required, which results in a link budget for the downlink, and a link budget for the uplink. The downlink budget can be found in Table 4.22 and the uplink budget can be found in Table 4.23. The link budget values were calculated using Table B.1 in Chapter B which are based on [27].

The downlink budget in Table 4.22 shows the downlink parameters, such as the frequency, data rate and modulation scheme of the downlink. Furthermore, the transmitted power, the transmitted equivalent isotropic radiated power (EIRP) of the signal, the total channel loss and received ${}^{E_b}/_{N_0}$ were calculated. Knowing the required ${}^{E_b}/_{N_0}$ for a bit-error-rate (BER) of 10^{-5}, together with the minimum link margin of 3 dB, which is required for every radio-frequency link, the final link margin can be found. This final link margin is found to be 3.7 dB, which means that the downlink can be done using the equipment that was previously mentioned.

The uplink budget parameters are shown in Table 4.22. The selected frequency, data rate and modulation scheme is presented. Further, the transmitted power, transmitted EIRP of the signal, the total channel loss and received ${}^{E_b}/_{N_0}$ were calculated. The required ${}^{E_b}/_{N_0}$ for a (BER) of 10^{-5} has been computed using [27]. Combined with the minimum link margin required for radio-frequency link, the total margin is computed. With a final link margin of 14.9 dB, it is indeed possible to have this uplink architecture with the chosen frequency and data rate.

Table 4.22: Downlink budget for DelFFi Delta

Parameter	Value	Unit
Frequency	145	MHz
Data rate	4800	bps
Modulation scheme	BPSK	-
Transmitted power	0.15	W
Transmitted EIRP	-10.3	dBW
Total channel loss	-134.1	dB
Received E_b/N_0	13.1	dB
Required E_b/N_0 for a $BER = 10^{-5}$	2.4	dB
Minimum link margin	3	dB
Final link margin	**3.7**	**dB**

More extensive link budgets can be found in Table C.1 (downlink) and Table C.2 (uplink) of Chapter C. These budgets include more information on the power profile during the entire communication path. Further, an explanation on the parameters used in the link budgets are given in Chapter B

Table 4.23: Uplink budget for DelFFi Delta

Parameter	Value	Unit
Frequency	435	MHz
Data rate	1200	bps
Modulation scheme	BPSK	-
Transmitted power	250	W
Transmitted EIRP	22.3	dBW
Total channel loss	-143.7	dB
Received E_b/N_0	24.3	dB
Required E_b/N_0 for a $BER = 10^{-5}$	2.4	dB
Minimum link margin	17.9	dB
Final link margin	**14.9**	**dB**

4.5.4 Conclusion

The final design of the TT&C consists of two transceivers and two dipole antennas. Since TT&C is a crucial subsystem for a successful mission, its main components are redundant. For example, one of the transceivers has been implemented for redundancy. With a fail-safe mechanism it is assured that data can be transmitted. Table 4.24 gives an overview of the final quantities for the TT&C in terms of mass, dimensions and power.

For communication purposes, VHF is used for downlink with a frequency of 145 MHz and a data rate of 4800 bps. Considering the uplink, a frequency of 435 MHz and a data rate of 1200 bps is chosen.

Since the data will be modulated, a modulation scheme will be used. A BPSK scheme is selected which will provide high resistant to noise due to the 180° phase shift.

Table 4.24: Final quantities for the Telemetry, Tracking and Command subsystem

TT&C Subsystem	Value
Mass [g]	270
Dimensions (hxwxd) [mm]	
Transceiver	96 x 90 x 15
Antennas	98 x 98 x 7
Power (operating) [mW]	1700
Operating time description	78%

4.6 Command and Data Handling System

The Command and Data Handling (C&DH) subsystem is a system that regulates and handles all data flows through the satellite and therefore contains all data wires. It processes the data and then sends it to the communication subsystem where it will then be transmitted down to Earth. The C&DH subsystem also stores all the data that is collected.

The C&DH subsystem is largely based on the Delfi-n3Xt design. The main reasons for this decision are the short time frame until the launch date and previous experience with the system since the Delfi-n3Xt C&DH design was based on the design of Delfi-C^3.

It will be demonstrated that the performance requirements on the Delta satellite are not higher than the performance requirements on Delfi-n3Xt. Afterwards, the main components of the C&DH subsystem will be described and an assumption on power consumption, mass, volume and data rates will be made.

4.6.1 System Specification

In this section the final hardware will be selected for the C&DH subsystem.

System Bus

The same Inter Integrated Circuit (I^{2}C) bus and Integrated Circuits (IC) as used in the Delfi-n3Xt will be used for the purpose of conveying data from one subsystem to the other. On each end of the bus, ICs are taking care of passing and accepting data through the bus. The I^{2}C bus connects all these different ICs. Using the PCF8574 ICs for interfacing with the subsystems and payloads, data rates of 100 kbps can be realized. Alternatively, the PCF8574 can be exchanged for a PCA8574 IC which uses approximately five times the power consumption of the PCF8574, which adds up to 500 μW per IC in operating mode, but also increases the maximum data rate to 400 kbps. For redundancy, Single Point of Failure (SPOF) wire failure is prevented by having dual redundant connections at each Printed Circuit Board (PCB) [74].

Microprocessor

For the microprocessor it is chosen to go with the same processor as used in Delfi-n3Xt. For redundancy, two microprocessors will be provided each with a computing frequency of 8 MHz [75]. Further, a watchdog timer is implemented to switch between the two processors in case of failure.

Data Storage

Many satellites have successfully implemented (Micro-)Secure Data (SD) solid state data storage [28]. Solid state memory is preferable as this type of memory is non-volatile, i.e. a card does not require power to retain its data. Furthermore, SD cards with increasingly large storage volumes become available as SD cards are COTS products. For consumer use, micro SD cards up to 4 GB, micro SDHC cards up to 32 GB, and micro SDXC cards up to 128 GB are available. Special radiation hardened SD cards could be used in order to withstand the radiation the satellite will be exposed to. However, this would mean increased costs and complexity, therefore, it is chosen to select a normal SD card of 2 GB as will be elaborated on in Section 4.6.2. The final design will contain two of these 2 GB SD cards for redundancy.

4.6.2 Data Rate Estimates

In order to calculate the average data rate that will be used for the bus, it is necessary to know how fast the data can be transferred back to Earth. This will be done using the VHF band assuming that all collected data will have to be sent to Earth. This maximum data rate can vary from the maximum possible data rate that the I^{2}C bus can handle (100 kbps). First, the average bus data rate is computed from the housekeeping data rate and the different payload data rates. The extensive data budget with the data rates can be found in Chapter E. This budget also includes the amount of time the payloads are activated and the housekeeping data is collected per orbit. From this, the average bus data rate could be computed as shown in Table 4.25. Considering that all data collected during the mission including a 20% margin should be stored on-board, the total storage capacity needed can be computed. Finally, the peak bus data rate is determined. This data rate is computed by taking the VHF data rate (3.36 kbps) and multiplying it by two, since it will travel twice through the bus at time of transmission and then adding the housekeeping data rate (11.56 kbps). In this case it is considered that no payloads will be active during transmission.

Table 4.25: Data parameters

Characteristics	Results
Maximum data rate I^2C	100 kbps
VHF data rate	4.8 kbps (effective 3.36 kbps)
Average bus data rate	1.34 kbps
Total storage capacity needed	1.86 GB
Peak bus data rate	18.28 kbps

When looking at the ground time, it is considered that the GENSO network will be used. This results in an almost global ground coverage (90%) by 2015 [21]. The actual ground time that is needed to send all data collected during each orbit can be calculated and as a safety precaution it is chosen to also have the ability to send data from 2 orbits during 1 orbit. So the total ground time required will be calculated for 2 orbits of data send capability in one orbit of ground time, using the average bus data rate and the total data rate of the VHF band.

If all of this is taken into account, a total ground time of 72 minutes is needed per orbit. This means that it requires about 9 min less than the available ground time of 81 minutes. The benefit of communicating in bursts instead of continuously is a reduction in power. Furthermore, there is no need to send more data at this point.

4.6.3 Volume, Mass and Power Estimates

The final power, volume and mass estimates are given in this section. It also contains the communication flow diagram.

The main power consuming elements of the C&DH subsystem are

1. microprocessor
2. data storage
3. I/O microcontrollers

At this stage, it is assumed that one processor is running at peak power, while the redundant processor is idle. The power consumption of the processors is then expected to be 100 mW [75]. SD cards have a maximum write rate of 1 MB/s to 10 MB/s, much higher than the I^2C bus rate of 100 kbps. Therefore, the power consumption of the data storage will be close to the idle rate of the card. Assuming a duty cycle of 10%, which can be realized by buffering the data with a Random-Access Memory (RAM) module, the typical power consumption will be 33 mW for micro SD cards [76]. The PCF8574 microcontrollers used in the Delfi-n3Xt have a maximum power consumption of 600 μW. It is expected that fewer than 10 are needed to connect every subsystem and payload PCB to the OBC, bringing the total to a maximum of 6 mW. Therefore, the total power consumption of the subsystem is expected to be 139 mW. A contingency of 20% should be included considering the current development stage, raising the current expected power consumption to 167 mW.

The mass estimation can best be done per part of the subsystem. The results can be seen in Table 4.26. The PCB mass includes the OBS mass [77].

Table 4.26: Mass Estimations

Part	Mass per part [g]	Total mass parts [g]
PCB	60 [75]	60
2GB micro SD card (2x)	0.5 [76]	1
Connecting cables	100	100
Total		**161**

For the volume of this subsystem it is assumed that it is only necessary to know the volume consumed by the PCB. This volume is 90 mm by 90 mm by 15 mm at this point [75].

The communication flow diagram is shown in Figure 4.16. Note that this diagram does not display the way physical connections are made. It displays which subsystems and payloads interact with each other in terms of data communication and what kinds of data are being passed.

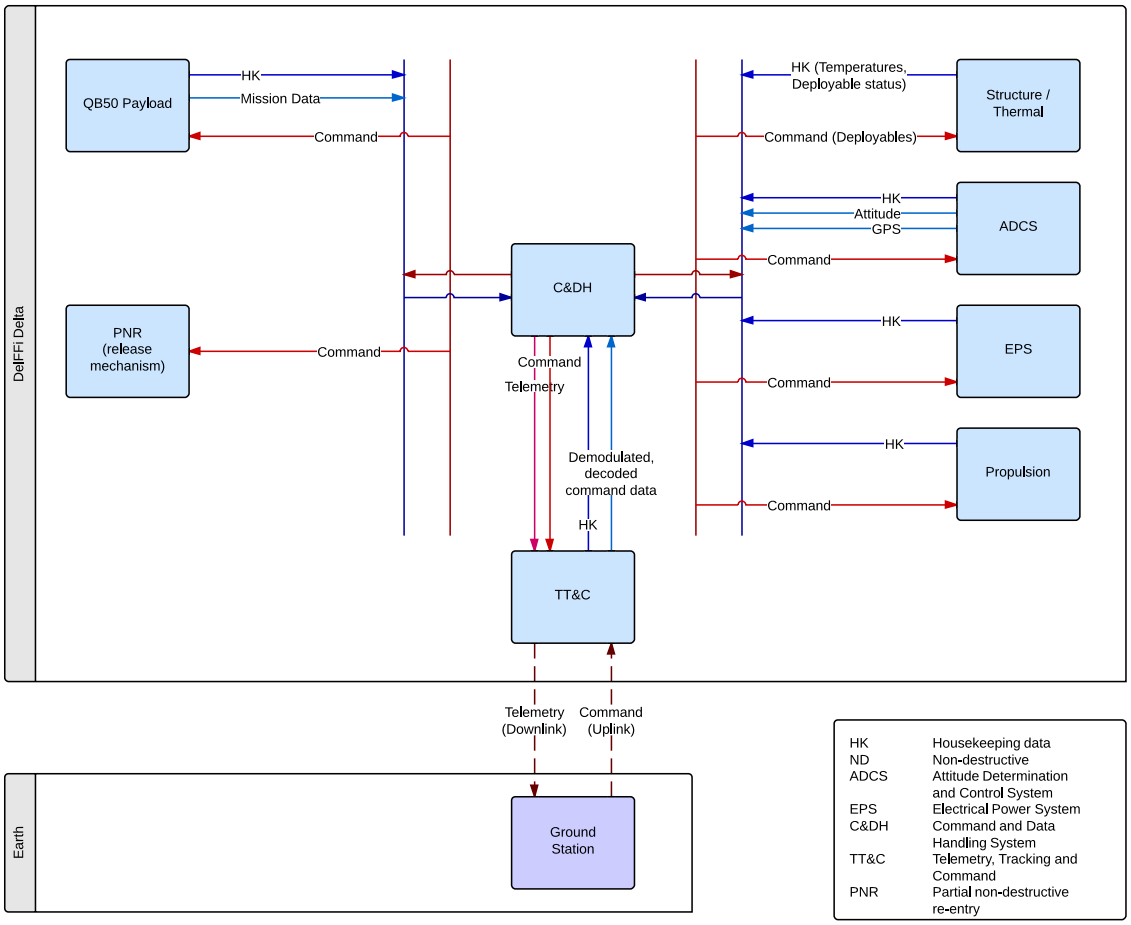

Figure 4.16: Communication Flow Diagram

4.6.4 Hardware and Software Block Diagram

The hardware and software block diagram is shown in Figure 4.17. It depicts the different systems and sensors that are connected to the command and data handling subsystem. It also shows the direction of the main data flow and the kind of data that is transferred. The final hardware representation is given in the physical appearance in Chapter 6.

4.6.5 C&DH Subsystem Overview

It was decided to use an I^2C bus using one microprocessor and another one for redundancy. Two 2 GB SD cards will be added to the system to store all data collected during the mission. The peak data rate will be 18.28 kbps during communication, and the final budget for the C&DH subsystem can be found in Table 4.27.

Table 4.27: Final quantities for the Command and Data Handling subsystem [75]

Command and Data Handling	Value
Mass [g]	161
Dimensions (hxwxd) [mm]	90 x 90 x 15
Power (operating) [mW]	167
Operating time description	Always on

4.7 Thermal Control System

Most current CubeSats have a passive thermal control, for example the previous Delfi satellites. As discussed in the Mid-term report [4] the Delta satellites thermal control is aimed to be passive. The main advantages

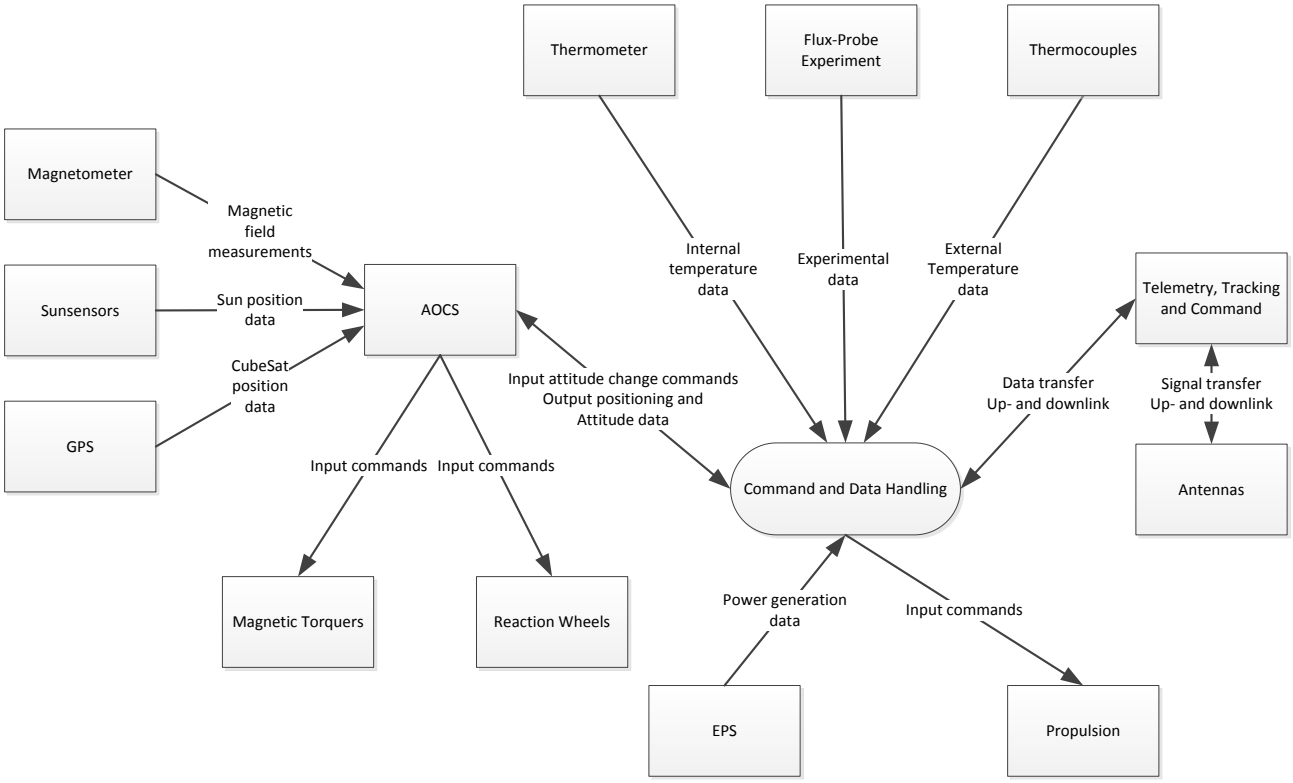

Figure 4.17: Hardware and Software Block Diagram

of a passive thermal control are the low impact on the power, volume and mass budget. As it already has been proven in spaceflight, a passive control system can be implemented in the Delta satellite.

The characteristics of the subsystem will be explained in this section. The hardware will be determined and finally the effects on the other subsystems will be described.

4.7.1 Subsystem Characteristics

The temperature is calculated by the heat balance of the incoming heat and emitted heat. The incoming heat comes from the sun, albedo, Earth's radiation and the internally dissipated heat. For the average temperature calculations, Equation (4.31) is used [55, p. 361-363].

$$T = \left(\frac{A_{planetary} J_p}{A_{surface} \sigma_{boltz}} + \frac{Q}{A_{surface} \sigma_{boltz} \varepsilon_{emit}} + \frac{(A_{solar} J_s + A_{albedo} J_a)}{A_{surface} \sigma_{boltz}} \left(\frac{\alpha}{\varepsilon_{emit}} \right) f \right)^{1/4} \tag{4.31}$$

Where A_{solar}, A_{albedo} and $A_{planetary}$ are respectively the projected areas receiving solar, albedo and planetary infrared radiation; $A_{surface}$ is the total surface area and J_s, J_a and J_p are the respected radiation intensities for solar, albedo and planetary (infrared). Finally f is the daylight fraction, σ_{boltz} is the Stefan-Boltzmann constant, α is the absorptance and ε_{emit} is the emittance.

The albedo intensity and the Earths radiation intensity are calculated using Equation (4.32) and Equation (4.33).

$$J_a = a \cdot F \cdot J_s \tag{4.32}$$

$$J_p = (IR)_{Earth} \cdot \left(\frac{R_E}{R_o} \right)^2 \tag{4.33}$$

Where a is the Earths albedo and F is the visibility factor for the albedo intensity. And IR_{Earth} is the Earth infrared radiation, R_E is the radius of the Earth and R_o is the radius of the orbit. The values that were used are shown in Table 4.28.

Table 4.28: Initial values for thermal control calculations for a altitude of 150 km.

Name		Values	Units	Remark
Projected area solar	A_{solar}	0.0424	m^2	Deployed panels neglected
Projected area albedo	A_{albedo}	0.0424	m^2	Deployed panels neglected
Projected area planetary	$A_{planetary}$	0.0424	m^2	Deployed panels neglected
Total surface area	$A_{surface}$	0.156	m^2	
Radiation intensity Earth	J_s	1371	W/m^2	
Radiation intensity albedo	J_a	67.9	W/m^2	
Infra red radiation intensity planetary	J_p	220.5	W/m^2	
average internal heat	Q	15	W	
Daylight fraction	f	0.57	–	
the Stefan-Boltzmann constant	σ_{boltz}	$5.670 \cdot 10^{-8}$	W/m^2K^4	
Absorptance	α	0.88	–	Solar cells
Emittance	ε_{emit}	0.8	–	Solar cells
Earth albedo	a	0.33	–	[55, p. 362]
Visibility factor	F	0.15(d), 0.7(e)	–	[55, p. 361]
Earth infrared radiation	IR_{Earth}	231	W/m^2	
Earth radius	R_E	$6367.5 \cdot 10^3$	m	
Orbit radius	R_o	$6517.5 \cdot 10^3$	m	

For the thermal calculations the deployable solar panels are neglected. This is done because very little heat transferred from the solar panels to the satellite bus. The Earths albedo is determined by using the Earths albedo versus the altitude graph from [55, p. 361].The temperature ranges of the different subsystem are presented in Table 4.29.

Table 4.29: Temperature ranges of the subsystems in operations.

System	Component	Temperature range
AOCS		-40 to 80°C
Power	Solar cell	-40 to 125°C
	G-EPS	-20 to 60°C
	Battery	-20 to 60°C
Propulsion		-20 t0 40°C
C&DH		-40 to 85°C
TT&C		-20 to 50°C
Structure		-40 to 80°C
Payload	VKI	-20 to 40°C
	DSE	*

* The property characteristics of PICA has no value for the minimum temperature, also there is no mentioning of problems with low temperature [78] and it is used on the outside of previous re-entry object. It is assumed the temperature can go much lower than the other systems. The maximum temperature will much higher than other systems, as it is a re-entry material.

The temperature can be calculated in maximum and no eclipse time. The maximum eclipse will be 43% of one orbit and in no eclipse the satellite will be in constant daylight.

Maximum Eclipse

In maximum eclipse, the temperature will deviate most. To simulate the temperature range the average temperature is calculated using Equation (4.31). With an eclipse of 43% the average temperature will be 17°C. As the eclipse slowly dissipates its heat, the maximum and minimum temperature are not reached,

as is shown in previous CubeSats [79]. To determine the maximum amplitude of the temperature change, Equation (4.31) is used with a daylight fraction of 1. This results in a maximum temperature of 39°C. The simplified temperature fluctuation is shown in Figure 4.18

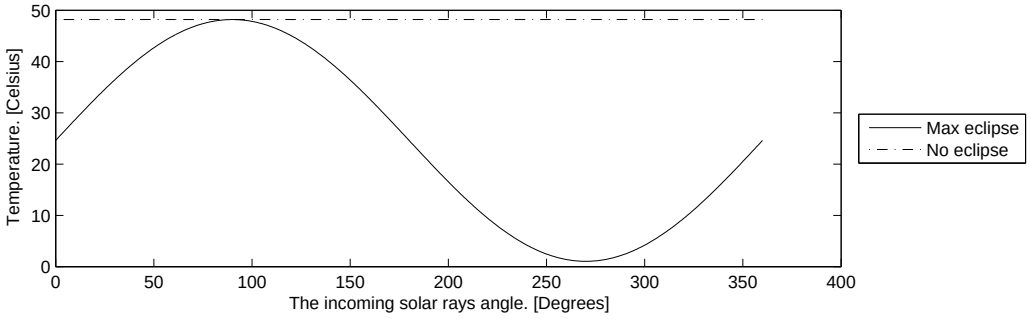

Figure 4.18: The approximated maximum thermal cycle with maximum eclipse and no eclipse.

No eclipse

In case of no eclipse, the projected area will stay the same. Therefore the temperature can be calculated easily. This is done with Equation (4.31) with a daylight of 100%. As was done before, this results in a temperature of 39° C, Figure 4.18.

The maximum temperature will be close in the QB50 payload temperature range, but as the QB50 payload requires low power, 530 mW, and will be located at a end of the satellite this maximum will not occur at the QB50 payload.

4.7.2 Hardware Selection

As shown in the calculations the average temperatures are within operating range of the different subsystems. To cope with temperature difference inside the satellite, heat radiators and thermal tape are used for passive thermal control.

On some PCB's there will be microprocessors which will generate a lot of heat due to a low conversion efficiency and small components. This can be coped with by using heat radiators which can transfer heat away from these small processors. Heat radiators will distribute the heat over a large area. Next the inside of the structure will be covered with thermal tape which can determine and dissipate heat away from the satellite.

Finally no sensor will require a very low or high temperature. With the fact that the budgets are limited this results in a passive thermal control with some components.

4.7.3 Conclusion

A passive thermal control system is used, which consist of heat radiators and thermal tape. Heat radiators are used for microchips which have a high heat generation. The thermal tape is used on the inside to add redundancy to the thermal control.The thermal tape will cover the inside of the structure. Temperature sensors are attach to the tape. Multiple systems have temperature sensors these will give a good overview of the actual heat inside the satellite, which can be used for further designs of CubeSats. As a recommendation the satellite can go to safe mode if the maximum temperature is reached, this will generate less heat and decrease the temperature with some degrees.

4.8 Sensitivity Analysis

In this section an elaboration is given on the sensitivity of the design solution for a change in major system parameters. This way the robustness of the design choices can be determined. Performing a sensitivity analysis is important to account for possible changes in requirements or subsystems during the design phase.

4.8.1 Mission Parameters

Critical parameters Next to the critical parameters that can change per subsystem also mission parameters have an influence on the mission.

- Increase of the initial altitude
- Decrease or restriction of the total allowed mass due to changes in requirements or QB50 payload
- Decrease or restriction of the total allowed volume due to changes in requirements or QB50 payload

Effects A higher initial altitude will significantly increase the mission duration. An extended mission duration affects the satellite design. First of all, this will mainly affect the power subsystem. The power system should be able to deliver the necessary power for a longer period. Therefore, degradation of the solar panels needs to be taken into account. The power system which is available now, should have no problems with an extended mission duration of five months. After this, it shall have to be slightly modified to account for the longer mission duration. Secondly, the required ΔV budget for formation flight is decreased as the formation flight will take place on a higher altitude which means less drag. Finally, all data collected is stored on board. With a significant increase in mission duration, it might be necessary to increase the storage capacity or to delete data after a certain time.

A decrease in allowed mass has an effect on all subsystems. However, a residual mass budget of 283 g is still available. As long as the decrease is less than 283 g no problem occurs. However, if for example the requirement changes to a maximum mass of 3 kg, changes need to be implemented. First of all, it is possible to reduce the redundancy which is incorporated in several subsystems. The TT&C for example was designed according to the fail-safe philosophy, therefore, a redundant transceiver is included in the structure. If after removing the redundancy the satellite still does not meet the requirement, drastic measures shall be taken. This will most likely mean discarding the re-entry capsule which would save a total of 200 g.

Similar to a decrease in mass, a decrease in allowed volume affects all subsystems. First of all note that the volume is expressed as a thickness as the thickness is the determining parameter for the volume. If the available volume would change by, for example, an increase in the QB50 payload size, it will change the overall layout of the satellite. The configuration now has a total of 17.5 mm of height left. If this would be overruled, a change in DSE mission is the most feasible thing to do. The chosen DSE mission takes up 75 mm. With respect to the TT&C, a redundant transceiver is used. If it is necessary, this redundancy can be removed leading to additional available volume.

4.8.2 Formation Flight

Critical parameters There are many parameters which can influence formation flight. The most critical ones are listed below.

- The solar activity, at the time the mission is performed, might be higher or lower than expected. In Figure 3.1 it is predicted that the mission will be done between mean and minimum solar activity. With respect to the density which is used, the changes might have an upper limit of 200% and a lower limit of 50%.
- The AOCS might malfunction and might therefore not be able deliver the pointing accuracy necessary to perform the formation flight
- The second formation flying satellite might fail
- The requirement for the formation duration could change

Effects If the density changes, the orbital decay will increase and the mission duration will decrease. This can result in two possible solutions.

- The formation acquisition should be performed faster so that the formation flight can start faster.
- The formation flying is performed at lower altitudes.

The first would mainly have an affect on the formation acquisition. More precisely, it will affect the attitude at which the satellites should fly to acquire the along track distance. Another option is to use the approach described in Section 3.3.4. Instead of using a fully passive formation acquisition, an additional ΔV budget has to be allocated for this. However, the requirement for the ΔV budget is not likely to be overruled

by this change. The formation keeping will undergo a change in required ΔV as a difference in drag is experienced.

The second, will mainly affect the formation keeping. Especially the ΔV budget required to remain in formation increases, since the drag will be significantly larger due to the increase in density and the decrease in altitude. However, as mentioned before, the ΔV budget set in the requirements is very extensive and the possibility that this will be exceeded is very small.

If the AOCS is not able to provide the necessary pointing accuracy, an additional ΔV is required to perform a more accurate formation acquisition. For formation keeping this should not have large effect as long as the determination is good enough. This because a thruster misalignment of 25° has already been taken into account. So if the determination is good enough the ΔV which is necessary can still be delivered.

If the second satellite fails, the Delta satellite is required to decrease its altitude accordingly, which will require it to deliver twice as much ΔV.

The requirement for the formation duration is very critical for the ΔV computations. If the formation flight continues for a longer period, the ΔV budget that has to be allocated will increase exponentially. This is because the formation flight should be continued at lower altitudes. These lower altitudes imply higher air density and thus higher drag.

4.8.3 Structural Integrity

The structure of the satellite is a part that is customized by TU Delft and does not have a high complexity. The dimensions are fixed and these will not change due to the heavy constraints set by the P-POD. The structure will accommodate solar cells of which four can be relocated if necessary. As the deployment system changes to a more complex system to add stiffness, the weight will increase, this can still be coped with by the mass budget, if it stays within 300 grams. There are no critical changes in the structure that will influence the design of the satellite.

4.8.4 Electrical Power System

Critical parameters Within the power system there are critical changes, that will influences the design of the subsystems or satellite.

- The power delivered by the solar cells is lower than expected
- The conversion efficiencies differ

Effects The critical changes of the EPS will have an effect on the design of the power system. Mostly the power obtained should be increased, as the power system has excess power, due to the fact it is inconvenient to mount half a solar cell. Thus, with a decrease of less than 0.5 W, there will be no impact on the design. When the power delivered decreases with 2.0 W, an additional solar cell should be fitted. This can be done by mounting a solar cell on the bottom of the satellite, which requires an additional master power point tracker for the G-EPS.

The efficiencies can either decrease or increase. When the efficiencies decrease about 3%, 1.0 W less is delivered. As described before, this can be accounted for by placing solar cells on the bottom plate. With an increase of 3% the excess power will be 2.6 W, this means that three less solar cells are needed. Another option is to use the excess power for other subsystems to enhance their performance, or to do additional measurements.

4.8.5 Attitude and Orbit Determination and Control System

Critical parameters The AOCS is a system that fulfills a crucial role in both the successful execution of the QB50 payload as well as the formation flying mission. In a less significant way it also impacts the success of the re-entry mission. During the execution of the measurements performed by the QB50 payload the FIPEX sensor should be pointed in the direction of flight, which will be the task of the AOCS. Furthermore, for formation flying, it is crucial that the ΔV will be given in the correct direction such that the orbit will be adjusted. The AOCS will assure this. During the entire mission lifetime the attitude should be controlled, this way the mission lifetime will be affected. When the satellite will start to re-enter, the preferable attitude is such that the QB50 payload will be in direction of flight. The re-entry capsule will be placed at the aft of

the satellite, which will ensure a descent without being damaged by the satellite. The parameters that could change during design are shown below.

- The attitude determination should have a pointing accuracy of better than 1.5°, at all times also during eclipse
- The AOCS should have a precision of less 1.0°, at all times also during eclipse
- The maximum rotation rate will increase 50% to 15 deg/s
- The AOCS should have a relative and absolute navigation measurement of 100 m instead of 1000 m
- The time for detumbling will be less than the 1 days that was initially allocated

Effects The changed parameters can have a big impact on the AOCS and other subsystems. When the pointing accuracy should be changed to 0.5° or better, the type of attitude determination should be changed. To solve this, a star sensor or/and Earth sensor can be used. Earth sensors like the one proposed by VKI [80] have an accuracy up to 0.18°, when the Earth is in the field of view. This sensor consumes 360 mW and is currently not implemented in the design. The increase in power will have an effect on the power acquisition, although it will not be a major issue. The size of this sensor on the other hand will create volume issues, since they take significantly more space than the MEMS gyro, magne tometer and the sun sensors combined. Another option is to use star sensors, which are very accurate like the ST-200 [81] that has an accuracy of 0.0083°. However, star sensors are quite heavy, power consuming (650 mW) and take up a lot of volume (30x30x38 mm^3). Thus, the volume and power required will increase.

When the maximal rotational rate increases about 50% from 10 deg/s to 15 deg/s, there will be no critical changes as the magentometers can still handle this rate. The torque to detumble will slightly increase, but the magnetic torquers are mainly sized on the values of the disturbance torques. Therefore, the detumbling time will hardly be influenced. Especially since the magnetic torquers are able to generate significantly larger torques than required, the detumbling time can remain the same.

The relative and absolute navigation measurements are currently performed by a GPS receiver. This receiver is accurate up to 10 meters and performs very well within the boundaries of 100 m.

If the initialization time will be shortened to less than 9 days, there is no effect on other subsystems. With the current design, the total detumbling time in the worst case scenario is 1/3 day per axis. Therefore, this will not change the layout of the magnetic rods and thus will have not an effect on other subsystems.

4.8.6 Propulsion

Critical parameters

- A larger total ΔV required
- A larger ΔV required per orbit adjustment

Effects An increase in the required ΔV for the formation flying mission will have a significant influence on the propulsion system. The amount of propellant is related to the amount of ΔV. The increase in propellant mass required for the larger ΔV will result in an increase in the number of cold gas generators that generate the propellant mass.

A larger required ΔV per orbit adjustment will imply that the amount of propellant stored in the storage tank would have to increase. As the amount of propellant increases, the storage capacity has to increase. To accomplish this, either the volume of the tank should increase or the gas should be stored at a higher pressure. Either way, the mass of the tank will increase.

4.8.7 Telemetry, Tracking and Command

Critical parameters The TT&C system does not have a large influence on the design of other subsystems. Therefore, little interference from the TT&C with other subsystems is expected. Here only the most crucial changes are considered. Less critical aspects like a change in BER or bandwidth are not considered. The reason is that already a significant margin is included in these parameters that a change does not lead to a critical effect on other subsystems. The critical changes mentioned are a result of a change in requirements.

Only the downlink is considered as a critical change, since the uplink frequency as well as the data rate is set as a requirement. A change in this requirement would not affect the TT&C of the CubeSat, but rather the ground station facilities.

- A larger downlink frequency is required.
- A higher downlink data rate is needed.

Effects If a significantly larger downlink frequency is required, the best option is to change from VHF to S-band. As a consequence, the chosen antennas will also differ. However, the antennas that are already implemented in the design will remain, since they are used to receive the uplink frequency. An additional patch antenna is required for the S-band transmission. The frequency can change to 2.4 GHz while still using the GENSO network. The downlink budget for S-band can be found in [4]. Due to the significantly higher frequencies, radio amateurs will not be able to receive the data sent from Delta. This is not needed, since the data rate of S-band is significantly higher (500 bps).

At this moment a downlink data rate of 4800 bps is used during the mission. However, if the data volume that needs to be sent increases, a larger data rate is required. Therefore, the data rate can be increased to 9600 bps. The selected transceiver is able to transmit a data rate of 4800 bps as well as 9600 bps while maintaining the same frequency. A higher data rate requires also a larger transmission power.

4.8.8 C&DH

Critical parameters

- If only one CPU is operational.
- An increase in required volume of science data of the QB50 mission to 16 Mb.

Effects If there would be only one CPU, this would mean that only half the space on the PCB board is needed. This could allow to combine the C&DH subsystem with another subsystem on the same PCB.

The increase of science data to 16 Mbit would mean that instead of measuring 9 times per orbit, one would have to measure at least 12 times per orbit. This would increase the average bus data rate to 1.69 kbps, the total needed OB storage would become 2.34 GB, the peak bus data rate would become 18.28 kbps and the total needed ground time would be 90.38 min per orbit. Since there is already redundancy taken into account with respect to the storage, meaning there is actually a total of 4 GB available, the total storage capacity can still be met. It does mean that there is less redundancy. This also goes for the total ground time. This has been calculated assuming that one would like to have the capability of sending two orbits worth of data in just one orbit. That would mean that now there would only be the capability to send 1.8 orbits worth of data in one orbit, still leaving a redundancy factor in it.

4.8.9 Thermal Control System

Critical parameters

- The temperature range will change.

Effects If the allowed maximum temperature decreases, the temperature of the satellite will be too high. Therefore, more components will be needed to dissipated the heat. This can be done by using more heat radiators. As the temperature of specific subsystems should change, the temperature of those subsystems can be controlled by means of passive thermal control. This will add extra weight.

4.8.10 Partial Non-Destructive Re-entry

Critical parameters

- Maximum mass allowed decreases
- Dimensional constraints decrease
- Heat during re-entry goes up

- Center of pressure moves forward
- Maximum allowed impact velocity decreases
- Allowed recovery time increases
- Deployment altitude changes

Effects When the maximum mass has to decrease, the only viable solution at this stage is to reduce the mass of the battery. Removing other capsule internals is not a viable solution as this would remove any possibility to recover or check the status of the capsule.

If the dimensional constraints decrease, the first aspect to look at would be the deployment mechanism. Even though it is designed to use a minimum of the available height within the satellite, it might be possible to gain a few millimeters. If that is not sufficient, the capsule would need to be redesigned. The capsule can be sized down, but not while including the same components. A first resort might be to scale the battery down, which would reduce the duration over which a position estimate can be provided. While typically not a problem if the capsule lands on ground, it would put more emphasis on recovering the capsule as quickly as possible when it would land in water.

If a more detailed analysis shows that the heat experienced during re-entry is higher than is currently predicted, countermeasures need to be taken. Even though it is expected that only 22% of the ablative heat shield will actually be lost, the temperature inside the capsule is expected to reach a maximum value of around 70°C with the current design. When it turns out that the heat shield thickness needs to increase to maintain this maximum temperature, the design might soon become impossible as the inner volume will shrink drastically with every millimeter of added heat shield thickness.

If testing shows that the center of pressure is too close to or in front of the center of mass, the two options are first, to move the center of mass even more forward or second, to adjust the outer geometry such that the center of pressure moves aft. Moving the center of mass more forward will be virtually impossible as the heaviest element, the battery, is located at the bottom of the capsule. This implies that research would need to be done on alternative capsule geometries that feature better stability.

If the allowed impact velocity decreases, the main option is to reduce the mass of the capsule as this would lower the terminal velocity. The only way to realize this would be to decrease the battery size, decreasing the recovery time window (if the capsule moves after landing). Use of a parachute was discarded earlier as the volume constraints are too restrictive to allow for one.

When the time needed for recovery increases, the beacon would need to be equipped with a larger and heavier battery in order to provide a longer battery life. Alternatively, the GPS update frequency could be reduced. This would allow for a longer recovery time, but locating the capsule will become harder.

If the deployment altitude changes, the deployment system needs to be altered as it features a rod that is supposed to melt at a certain temperature and corresponding altitude. If the deployment altitude goes down, a different rod can be chosen. However, if the deployment altitude goes up, the temperature increase might not be sufficient to start the melting process. Instead, an active deployment mechanism would need to be considered, where the OBC would actively trigger the release of the capsule.

CHAPTER 5
RE-ENTRY CAPSULE DESIGN

As a DSE mission objective three possible options where selected: GPS radio occultation, an inter-satellite link and partial non-destructive re-entry. To get to the final choice for the DSE mission, a trade-off was done in the Midterm Report [4]. The outcome was that partial non-destructive re-entry (PNR) would be the DSE mission objective.

The PNR mission, as the name describes, will make sure that a part of the satellite survives re-entry, instead of burning up like the rest of the satellite. This will be done by ejecting a re-entry capsule from the satellite that is partially made of ablative material to act as a heat shield. After landing, this capsule sends out a signal in order to retrieve it. After retrieval, analysis of the remainder of the capsule can be done.

This chapter will discuss the flight profile of the capsule during re-entry in Section 5.1. From this flight profile, a heat rate and temperature profile can be obtained, which are used in designing the thermal protection system as shown in Section 5.2. Furthermore, a safe landing needs to be achieved. This can be done with the use of a parachute and will be researched in Section 5.3. The retrieval strategy will be discussed in Section 5.4. The laws and regulations on re-entry are discussed in Section 5.5. The final layout of the re-entry capsule can be found in Section 5.6. The effect that the satellite has on the re-entry capsule is discussed in Section 5.7.

5.1 Flight Profile

The flight profile of the capsule is required for a number of reasons. First of all, the flight profile calculations form the basis for further calculations on the momentary heat rates and total heat load that are acquired during the re-entry, as will be explained in more detail in Section 5.2. Furthermore, the flight profile is required to determine the landing footprint that can be achieved using a re-entry capsule in Section 5.1.6.

5.1.1 Trajectory Types

In principle there are three different options for the re-entry trajectory: skipping, gliding and ballistic. [82] The skipping trajectory requires a controlled and advanced re-entry vehicle and system, which is not achievable within the constraints of the Delta mission.

Gliding re-entry is the re-entry case where lift is generated by the re-entry vehicle. In case of an axis-symmetrical capsule, as will be used by Delta, lift can be generated by shifting the center of gravity away from the axis of symmetry, which results in an effective angle of attack. Having a lift results in a longer flight time with a relative small heat rate, however due to a longer heat exposed time, a large heat load is achieved with the gliding flight.

During a ballistic re-entry the capsule does not generate lift, since its center of mass is on its center line opposed to the gliding re-entry. The total heat load is lower than the gliding re-entry due to shorter flight time. Furthermore, the potential footprint contains fewer uncertainties for ballistic re-entry than for gliding. Thus ballistic re-entry will be performed during the Delta re-entry.

5.1.2 Atmospheric Model

The flight profile of the capsule will depend largely on the atmospheric conditions which it will face during re-entry. Previous calculations [4] were based on an exponential atmospheric model, which was also used by [82]. This model uses the average temperature of the atmosphere during re-entry, which is 246 K. However, this is significantly different from the actual conditions. Therefore, using an exponential atmosphere model errors will be encountered in the calculations of the density and other atmospheric parameters that are needed in the flight path calculations.

Due to the rather large deviations that would be obtained using an exponential atmosphere, a more detailed atmospheric model was implemented in MATLAB: the standard atmospheric (STDATMO) model. This model was obtained from [83] and are based on the ESDU 77022 atmospheric model [84]. The inputs for this model are the altitudes for which the atmospheric (output) parameters should be known. The input and output parameters for the STDATMO model can be found in Table 5.1.

Table 5.1: STDATMO input and output parameters

Input	Altitude	Required
	Temperature offset	Not required
	Unit format	Not required
	Geometric flag	Not required
Output	Air density	
	Speed of sound	
	Temperature	
	Pressure	
	Kinematic viscosity	
	Geometric or geopotential height	

Table 5.1 shows that several output parameters are calculated with the STDATMO model. The output from this model can be used for further calculations in Section 5.1.3 and other parts of Chapter 5.

5.1.3 Derivation of Flight Profile

For a preliminary calculation of the flight profile, the method as described in [82] was used. However, in retrospect, this method could not be used for the re-entry conditions of the Delta satellite. This is mainly because the method assumes medium to large re-entry angles, something that cannot be realized during the Delta re-entry. Only a very small initial re-entry angle can be achieved. This is the result of natural decay and the ΔV that can be used to change the flight path angle for re-entry. This ΔV has a value of 8.2 m/s. This is because of the ΔV requirement of that was set up in collaboration with the Phi group was 15 m/s and 6.8 m/s of this ΔV budget it used for the formation flying demonstration (see Chapter 3. However, the required ΔV for formation flying can increase or decrease. This can happen if the atmospheric conditions and attitude of the satellite during the mission lifetime deviate from the nominal conditions. In general, the ΔV that is not used during formation flight can be used to achieve a small additional re-entry flight path angle. However, if this would not be required, thus if the natural decay of the satellite provides the landing spot that is wanted, this ΔV change is not required for the re-entry mission.

The total initial flight path angle will consist of the flight path angle that will be achieved by natural satellite decay and the flight path angle that can be achieved with the remaining ΔV from the propulsion system. The natural decay flight path angle can be calculated using the vertical velocity ($^{dh}/_{dt}$) and total velocity of the satellite. The relation between these parameters can be found in Equation (5.1).

$$\sin(\gamma) = \frac{^{dh}/_{dt}}{V} \tag{5.1}$$

In this equation, γ is the flight path angle of the capsule, $^{dh}/_{dt}$ is the vertical velocity at which the capsule approaches Earth and V is the total velocity of the capsule. The equation can be used to find the flight path angle if both total velocity and vertical velocity are known. For the initial re-entry conditions, these parameters are known from the astrodynamics calculations that were performed in Chapter 3.

As already stated above, the model that was used in [82] was not correct for the re-entry conditions that the Delta satellite will face; a new model was created in MATLAB. This model is based on discrete time steps. From the initial re-entry conditions at 90 km altitude, the capsule's flight conditions can be calculated for the entire re-entry path from 90 km altitude to sea level. The flight path is required to calculate the heat rate and heat load. The parameters that are required to calculate the heat rate and total heat load in Section 5.2 are the deceleration, the velocity and the flight time of the satellite. To get the best results during the heat calculations, these parameters should be known continuously. However, since the MATLAB model uses discrete time steps, this is not possible. Increasing the resolution of the model, by decreasing the time step size, improves the output of the model.

All calculations that were done for the new MATLAB model were based on [85]. The behavior of the re-entry capsule can be described in various reference frames. The frame that was chosen to do the simulation of the re-entry path was the vehicle carried normal Earth reference (VCE) frame. However, several parameters, such as the velocity, the drag and the lift are only known in the aerodynamic frame of the capsule. Therefore, a transformation needs to be done from the aerodynamic frame to the VCE frame. To do this, the aerodynamic frame needs to be transformed to the body frame of the capsule, which can be seen in Figure 5.1. For this case, it is not required since the angle of attack, α, and the sideslip angle, β are assumed to be zero because

the capsule is not a lifting vehicle. Therefore, the aerodynamic frame coincides with the body frame. Even if and angle of attack or sideslip angle is induced, it will be negligible. Afterwards, the heading χ, the flight path angle γ and the bank angle μ are used to transform the body frame to the VCE frame. The final transformation matrix can be found in Equation (5.2). Note that throughout the derivation of the flight path, the sine and cosine of an angle will be represented by *s(**angle**)* and *c(**angle**)*, respectively.

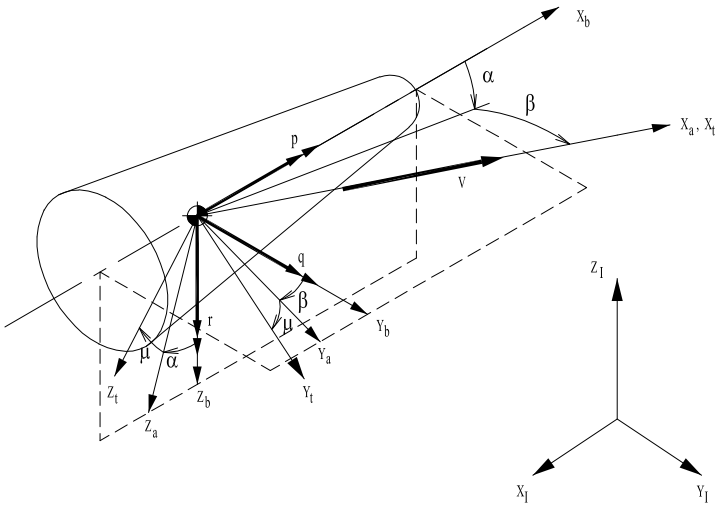

Figure 5.1: Transformation angles for aerodynamic to body frame [85]

$$T_{bE} = \begin{bmatrix} c(\gamma)s(\chi) & c(\gamma)s(\chi) & -s(\gamma) \\ -s(\mu)s(\gamma)c(\chi) - c(\mu)s(\chi) & -s(\mu)s(\gamma)s(\chi) + c(\mu)c(\chi) & -s(\mu)c(\gamma) \\ c(\mu)s(\gamma)c(\chi) - s(\mu)s(\chi) & c(\mu)s(\gamma)s(\chi) + s(\mu)c(\chi) & c(\mu)c(\gamma) \end{bmatrix} \tag{5.2}$$

In this equation, T_{bE} represents the transformation matrix from the VCE frame to the body frame. Note that to transform a vector from the body frame to the VCE frame, the transpose of this matrix should be used.

The lift, drag and velocity are defined in the aerodynamic frame. They coincide with the direction of the z-, x- and x-axis of the aerodynamic frame respectively. Therefore, in the aerodynamic frame, the lift, drag and velocity vectors will only have a component in one direction. To get the components of the velocity, lift and drag of the capsule in the body frame, respectively Equation (5.3), Equation (5.4) and Equation (5.5) can be used. These components are expressed in the north, east and down direction in the VCE frame.

$$\vec{V}_E \begin{bmatrix} V_N \\ V_E \\ V_D \end{bmatrix}_E = T_{bE}^T \begin{bmatrix} V \\ 0 \\ 0 \end{bmatrix}_b \tag{5.3}$$

In this equation, T_{bE} is the VCE to body transformation matrix, $\vec{V_E}$ is the velocity vector in the VCE frame, V_N is the north component of the velocity, V_E is the east component of the velocity, V_D is the down component of the velocity and V is the velocity of the capsule.

$$\vec{L}_E = T_{bE}^T (0.5\rho \parallel \vec{V}_E \parallel^2 A_c C_L) \begin{bmatrix} 0 \\ 0 \\ 1 \end{bmatrix}_b \tag{5.4}$$

In this equation, $\vec{L_E}$ is the lift vector in the VCE frame, T_{bE} is the VCE to body transformation matrix, ρ is the air density, $\vec{V_E}$ is the velocity vector in the VCE frame, A_c is the frontal area of the capsule and C_L is the lift coefficient of the capsule. Note that ballistic re-entry was assumed, which means that no lift will be created. However, due to small disturbances in angles, a small lift can be created. This will be implemented

in the footprint calculations.

$$\vec{D}_E = T_{bE}^T(0.5\rho \parallel \vec{V}_E \parallel^2 A_c C_D) \begin{bmatrix} -1 \\ 0 \\ 0 \end{bmatrix}_b \tag{5.5}$$

In this equation, $\vec{D}_E$ is the drag vector in the VCE frame, T_{bE} is the VCE to body transformation matrix, ρ is the air density, $\vec{V}_E$ is the velocity vector in the VCE frame, A_c is the frontal area of the capsule and C_D is the drag coefficient of the capsule.

Besides the forces that act in the aerodynamic frame, the lift and the drag, other forces act on the capsule as well. These are the gravitational force, the centripetal force and the Coriolis force. These forces are defined in the VCE frame, and therefore do not need to be transformed. The gravitational force can be computed using Equation (5.6), the centripetal force can be calculated using Equation (5.7) and the Coriolis force can be calculated using Equation (5.8).

$$\vec{F}_{g,E} = g_0 \left(\frac{R_E}{R_E + h} \right)^2 \begin{bmatrix} 0 \\ 0 \\ 1 \end{bmatrix} \tag{5.6}$$

In this equation, $\vec{F}_{g,E}$ is the gravitational force vector, g_0 is the sea level gravitational acceleration, R_E is Earth's radius and h is the altitude of the re-entry capsule.

$$\vec{F}_{cen,E} = \frac{m(V_N^2 + V_E^2)}{R_E + h} \begin{bmatrix} 0 \\ 0 \\ -1 \end{bmatrix} \tag{5.7}$$

In this equation, $\vec{F}_{cen,E}$ is the centripetal force vector, m is the re-entry capsule mass, V_N is the north component of the velocity, V_E is the east component of the velocity, R_E is Earth's radius and h is the altitude of the re-entry capsule.

$$\vec{F}_{cor,E} = 2m\omega \begin{bmatrix} V_N s(\delta) + V_D c(\delta) \\ -V_E s(\delta) \\ V_E c(\delta) \end{bmatrix} \tag{5.8}$$

The Coriolis force needs to be accounted for to describe the relative motion of the capsule due to Earth's rotation. In this equation, $\vec{F}_{cor,E}$ is the Coriolis force vector in the VCE frame, m is the capsule mass, ω is the rotational velocity of the Earth, V_N is the north component of the velocity, V_D is the down component of the velocity and δ is the latitude of the re-entry capsule.

Knowing all forces that act on the capsule during the re-entry, the resultant force that acts on the capsule can be calculated using Equation (5.9). From this resultant force, the acceleration of the capsule can be calculated (Equation (5.10)).

$$\vec{F}_{tot,E} = \vec{L}_E + \vec{D}_E + \vec{F}_{g,E} + \vec{F}_{cen,E} + \vec{F}_{cor,E} \tag{5.9}$$

All components in this equation were calculated using equations that were previously explained in this section.

$$\vec{a}_{tot,i} = \frac{\vec{F}_{tot}}{m} \tag{5.10}$$

Equation (5.10) shows that the total acceleration $\vec{a}_{tot,i}$ can be computed by dividing the total resultant force $\vec{F}_{tot,E}$ by the mass of the capsule, m. The $'i'$ in the deceleration vector states that it is the vector for the $i'th$ time step.

The distance in north, east and down direction that is traveled during a single time step can be calculated using Equation (5.11). These distances should be known to calculate the landing location of the capsule.

$$\vec{S}_i = \vec{S}_{i-1} + \vec{V}_{i-1}\Delta t + \frac{\vec{a}_{tot,i}\delta t^2}{2} \tag{5.11}$$

In this equation, $\vec{S}_i$ is the vector that includes the traveled distances in north, east and down direction, $\vec{S}_{i-1}$ is the traveled distance of the previous time step, $\vec{V}_{i-1}$ is the velocity vector in the VCE frame during the previous time step and Δt is the time step that is taken for the calculations.

Knowing the acceleration of the capsule, the velocity of the capsule after an incremental time step, Δt can be calculated, using Equation (5.12).

$$\vec{V}_i = \vec{V}_{i-1} + \vec{a}_{tot}dt \tag{5.12}$$

In this equation, $\vec{V}_i$ is the velocity of the current time step in the VCE frame. This value is calculated using the velocity of the previous time step, $\vec{V}_{i-1}$, the deceleration during the previous time step, $\vec{a}_{tot,i}$ and the time step Δt. Since all components of velocity and acceleration of the previous time step are in north, east and down direction, the new velocity of the capsule will also have velocity components in these directions, meaning it is also described in the VCE frame.

To get the new flight path angle γ and heading χ, respectively, Equation (5.13) and Equation (5.14) can be used.

$$\gamma = \arctan\left(\frac{V_E}{V_N}\right) \tag{5.13}$$

$$\chi = \arcsin\left(\frac{V_D}{\| \vec{V}_1 \|}\right) \tag{5.14}$$

Now the velocity components in the VCE frame and the rotation angles are known, these calculations can be done again. This can be repeated until the traveled distance in the down direction equals the re-entry altitude. This iteration provides a flight profile for the velocity, acceleration and flight path angle for the entire velocity range. The results of this method can be found in Section 5.1.4.

5.1.4 Flight Profile Results

The input that was used in the MATLAB model can be found in Table 5.2. These parameters are the variables that can be changed in the model. The variables in Table 5.2 are obtained from the astrodynamics calculations that were performed in Chapter 3.

Table 5.2: Initial re-entry parameters that were used for the flight path calculations

V [m/s]	dt [s]	C_{D_c} [-]	C_{L_c} [-]	χ [°]	γ [°]	μ [°]	δ [°]	m [kg]	h [m]	d [m]
7535	1.0	1.0	0.0	0.0	-0.3318	0	36.7	0.147	90000	0.096

The velocity profile for re-entry can be seen in Figure 5.2. This figure shows that in the first part of the re-entry, from 90 km to ±50 km, the total velocity is largely depending on the north velocity of the capsule. This is mainly due to the shallow re-entry angle that the capsule still has for this altitude range and the heading angle that was assumed to be zero. This can also be seen in Figure 5.3. Between ±50 km and ±35 km, both the north and down velocities have a big impact on the total velocity. In the flight path angle plot in Figure 5.3 this can be seen by a rapid increase in γ. Below 35 km, the capsule has a very high γ, which results in the fact that the vertical velocity will be the dominant factor in the total velocity. This can also be seen in Figure 5.2.

As discussed previously in this section, γ is very low in the first part of the re-entry (90 km to ±50 km). From ±50 km, γ is increasing very fast, until a final flight path of 90° is reached. This can be seen in Figure 5.3.

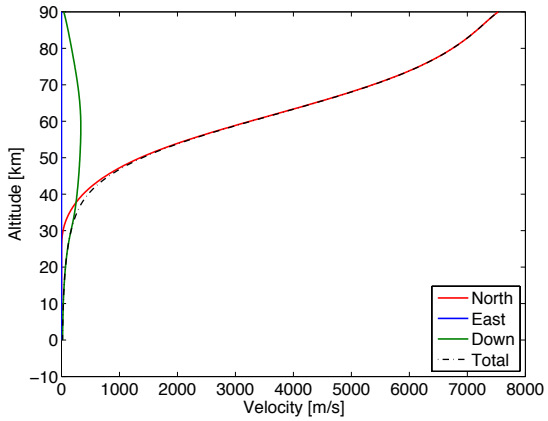

Figure 5.2: Velocity profile for ballistic re-entry

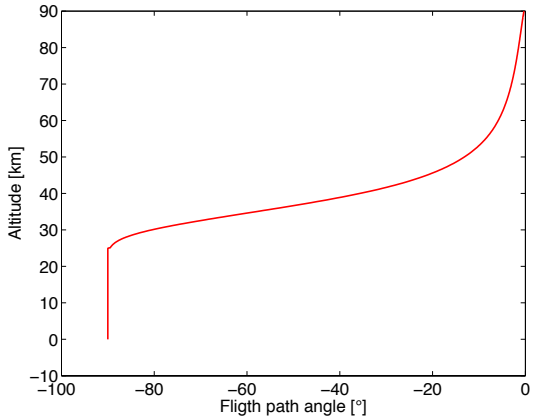

Figure 5.3: Flight path angle profile for ballistic re-entry

Figure 5.4 shows the deceleration profile for the re-entry. This profile relates to the heat rate profile in Section 5.2. Furthermore, this profile is required to determine the maximum deceleration on the capsule. This needs to be known to select the proper hardware that will be used to land and retrieve the re-entry capsule. As can be seen in Figure 5.4, the maximum deceleration is slightly lower than 8 g. This maximum deceleration happens at an altitude of approximately 60 km.

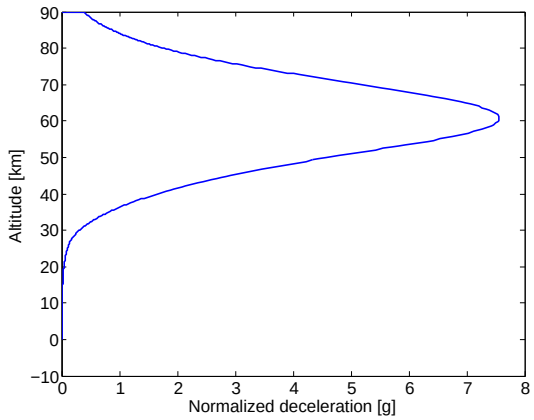

Figure 5.4: Deceleration profile for ballistic re-entry

5.1.5 Entry point

A precise altitude of the re-entry point of the capsule can be determined, since the capsule will be deployed from within the CubeSat. The capsule will be deployed at an altitude of 90 km. The re-entry point of the capsule is based on the calculations in Chapter 3. The output of these calculations will be used as the nominal conditions at which the re-entry of the capsule will be initiated.

The calculations in Chapter 3 are based on an inertial reference frame F_I. In order to determine the position of the re-entry point, a transformation from inertial to Earth-fixed reference frame will be executed. The X-axis of the Earth-fixed reference frame F_c uses the Greenwich meridian as a reference, while the inertial reference frame is fixed as can be seen in Figure 5.5.

Therefore, the Earth rotation needs to be added to the longitude values λ determined in the inertial reference frame. The latitude is not affected by the different reference frame as can be seen in Equation (5.15).

$$\begin{aligned} \lambda_C &= \lambda_F + \Omega_{Earth} t \\ \delta_C &= \delta_F \end{aligned} \tag{5.15}$$

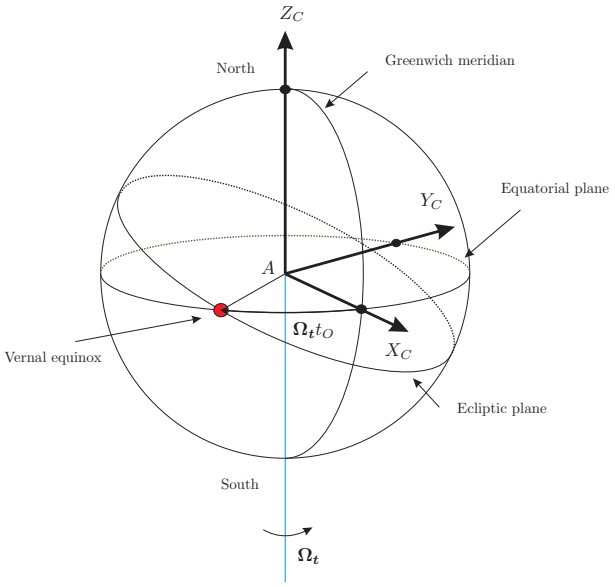

Figure 5.5: Fixed Earth reference frame [85]

After the transformation of the latitude and longitude values to the Earth-fixed reference frame, the re-entry point in the Earth-fixed frame can be determined. Knowing the final re-entry point and the flight path profile that the capsule will have, the landing location can be calculated. Together with the footprint, which is calculated in Section 5.1.6, a landing area can be calculated that will be located around the nominal landing location.

5.1.6 Footprint

In order to decrease the hazard of the capsule during re-entry, a precise footprint calculation is necessary. However, various uncertainties are involved during re-entry. To simulate these uncertainties within the footprint, a Monte Carlo simulation is used.

Monte Carlo uncertainties

During a Monte Carlo simulation a large number of samples are used to simulate a process. In this case, the possible landing spots are simulated using approximately 1200 iterations and lead to a footprint where the capsule will land with a 98% probability. Various uncertainties are considered in such a simulation to have the least possible risk.

The Monte Carlo simulation includes the following uncertainties:

- Initial flight path angle

- Bank angle
- Mass
- Density
- Lift coefficient
- Drag coefficient
- Initial velocity

With the remaining ΔV from formation flying (see Section 2.2), the flight path angle will be adjusted, however, a full control of the flight path angle is not achievable. Furthermore, the capsule mass might differ depending on how far the assumptions during the heat load determination influence the actual material that is ablated. The atmospheric density of the re-entry day also may differ from previous days, which is expressed by the uncertainty in density. Furthermore, the calculations of the flight path were done for ballistic re-entry, which implies that there is no lift. However, due to atmospheric disturbances and the fact that the geometry of the re-entry capsule can change during re-entry, a small lift is included in the Monte Carlo analysis.

Due to the short time frame that was available to do the calculations on re-entry, the winds in the atmosphere are not discussed. This could be done in a later design stage, where more time is available to calculate the impact of the winds on the landing location of the capsule. Uncertainties in the moments of inertia, the center of gravity of the capsule and the roll, pitch, yaw attitude are neglected.

Table 5.3 shows the uncertainties that were considered, their minimum and maximum value and the distribution that has been assumed. It is assumed that the samples for the velocity and density are normal distributed, since it is more likely that the nominal value will be achieved. A uniform distribution is chosen to simulate the flight path angle, bank angle, mass, lift coefficient and drag coefficient, since no information is available on the deviation of these parameters.

Table 5.3: Monte Carlo analysis variables

Variable	minimum Value	maximum Value	Distribution
Initial flight path angle [°]	0.3	0.5	Uniform
Bank angle [°]	-180	180	Uniform
Mass [g]	130	150	Uniform
Density variation [%]	-20	20	Normal
Lift coefficient [-]	0	0.1	Uniform
Drag coefficient [-]	0.8	1.2	Uniform
Initial velocity [m/s]	7150	7910	Normal

In the perfect case, more than 100 iterations per Monte Carlo criteria should be accounted for. However, due to the time constraint and the limited computing power available, only the lower and upper limits, together with the average value of the variables are used in the Monte Carlo simulation. Only the bank angle has multiple values, to account for the limits in both the x- and z- direction.

Result

Using the MATLAB script that was used in the flight path calculations, the landing spot can be calculated for each combination of the variables that are used in the Monte Carlo simulation. Doing this for the variables in Table 5.3, a footprint of 1850 km in the north-south direction by 107 km in the east-west direction was obtained. This footprint can be seen in Figure 5.6. The footprint has an oval-like shape. This is as expected, since the initial velocity was mainly in the north-south direction and not in the east-west direction.

Because of the high density of landing locations around the nominal landing spot, there is a higher probability that the capsule will land around the nominal landing location that somewhere on the outlier locations.

5.2 Thermal Protection System Design

During re-entry, the capsule is exposed to high temperatures. In order not to burn up, the capsule needs a Thermal Protection System (TPS). There are three different options for a TPS:

- Heat sink

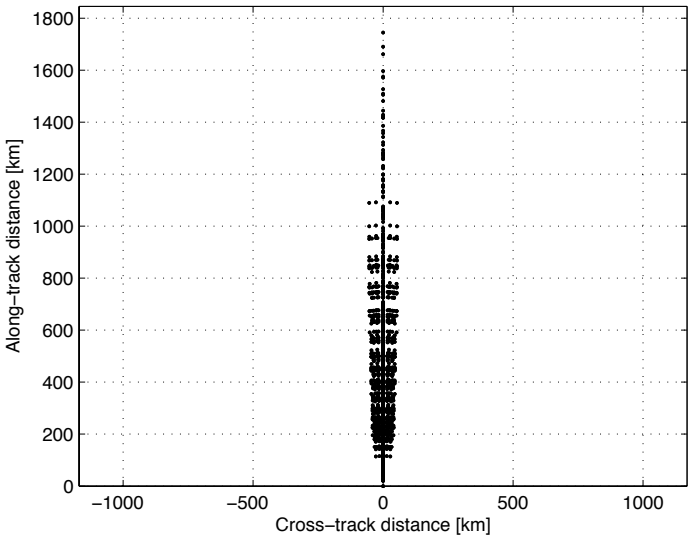

Figure 5.6: Footprint of the re-entry capsule with a ballistic re-entry

- Radiative cooling
- Ablative heat shield

When using heat sinks, additional material is used which will absorb the heat. This is not a suitable option with the given constraints of the CubeSat mission. Especially since only limited volume and mass is available on board of the CubeSat. Radiative cooling is based on thermal equilibrium, thus the same amount of heat absorbed will be radiated. This method is used mostly on re-usable spacecraft. The ablative heat shield is based on the principle of phase change. Thus, the shield material will burn up during re-entry and create a cooler boundary layer. This principle is mostly used on one-time missions and will also be used on this mission.

This section will explain the TPS design, starting with the heat rate, total heat load calculations and the wall temperature determination during re-entry in Section 5.2.1. These calculations are based on the ballistic flight calculations done in Section 5.1. Following up, the thickness of the ablative material is determined in Section 5.2.2. As a next step, the insulation is described in Section 5.2.3. Finally, in Section 5.2.4 and Section 5.2.5, the backshell of the capsule and the testing of the material is described, respectively.

5.2.1 Heat Determination

Before the total heat load acting on the capsule is determined, the heat rate is computed. This heat rate will be largest at the nose, since this is the blunt part of the capsule that will be directed in the direction of the velocity. The heat rate during re-entry q_c at the stagnation point of the capsule is determined using Equation (5.16).

$$q_c = 1.83 \cdot 10^{-4} \cdot V^3 \cdot \sqrt{\frac{\rho}{r_{crit}}} \tag{5.16}$$

V represents the velocity in m/s as can be seen in Section 5.1.4, ρ is the density at the current altitude which has been determined in Section 5.1.2. Finally, r_{crit} is the critical radius of the capsule in m. This is the capsule radius at the stagnation point. A nose radius of 0.1 m has been chosen for the capsule. The corners however have a radius of 0.01 m. Because of this, the stagnation point of the capsule will be at the corners of the capsule and not at the nose, making the corner radius the critical radius of the capsule. Calculating the heat rate for the entire altitude range, the maximum heat rate is found to be 2541 W/cm^2.

The heat rate leads to the total heat load Q by integrating it over time as can be seen in Equation (5.17).

$$Q = \int_0^t q_c dt \tag{5.17}$$

This leads to a total heat load of 35198 J/cm^2 that the capsule experiences during re-entry. With the heat rate and the total heat load, the wall temperature can be determined.

To determine the wall temperature T_w, it is assumed that the heat rate during re-entry is equal to the radiated heat rate q_r. The radiated heat rate is found using the Stefan-Boltzmann law which is given in Equation (5.18). Assuming $q_c = q_r$ leads to a safety margin, since in real life, the radiated heat rate is lower than the convected heat rate. Thus, the calculated wall temperature will be higher than in reality. This way a margin is included in the design of the TPS.

$$q_r = \sigma \cdot \varepsilon \cdot T_w^4 \tag{5.18}$$

In this equation σ represents the Stefan-Boltzmann constant of 5.67 $\cdot 10^{-8}$ W/(m^{2}K^4). The emissivity ε of the chosen material Phenolic Impregnated Carbon Ablator (PICA) is 0.8 [86]. PICA was chosen due to its low density, high emissivity and low conductance [87]. Further, the wall temperature is represented by T_w in K. It is assumed that the temperature difference between the wall temperature and the ambient temperature is equal to the wall temperature. This is a reasonable assumption since the wall temperature is significantly higher than the ambient one. PICA has been chosen as an ablative material due to its low density of 0.25 g/cm^3 and its low conductivity during ablation [88].

Setting the radiated heat rate equal to the heat rate during re-entry leads to the following relation for the wall temperature.

$$T_w = \sqrt[4]{\frac{q_c}{\sigma \varepsilon}} \tag{5.19}$$

Figure 5.7 shows the heat rate during re-entry and the corresponding wall temperature. It can be observed that the wall temperature and the heat rate have the same behavior. In the first phase of re-entry the wall temperature and the heat rate are continuously increasing until the maximum value is reached. The maximum reached wall temperature and heat rate are at an altitude of approximately 72 km.

In the second phase, the heat rate and the wall temperature decrease significantly up to an altitude of about 45 km. From that altitude on, both parameters decrease slower in value.

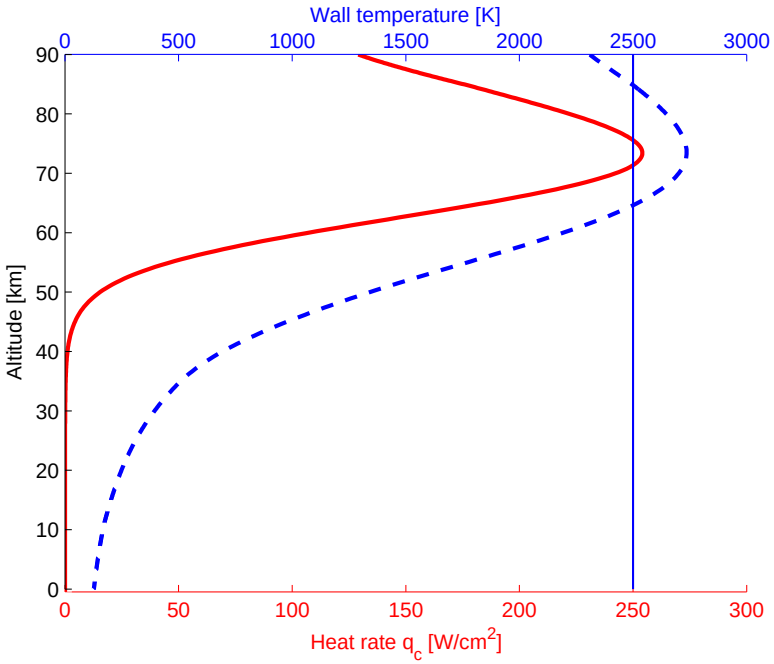

Figure 5.7: Heat rate and wall temperature during re-entry as a function of the altitude

In this figure, the red, continuous line is the heat rate, the blue, striped line is the wall temperature and the blue, vertical line is the 2500 K temperature line.

5.2.2 Ablative Thickness of PICA

Since PICA has an ablation temperature of 2500 K, the PICA layer of the TPS will not be ablating constantly. Only when the wall temperature exceeds 2500 K, the surface of the heat shield will ablate. Furthermore, all the additional heat that is generated when this temperature is achieved will be ablated. This implies that the flight path section where $T_w \geq 2500$ will only put the additional generated heat into the ablation. Therefore, not all heat generated will be put into the ablation of PICA. This results in the fact that from the heat load of 35198 J/cm^2, only 9800 J/cm^2 will be put into the ablation of PICA. Furthermore, the effective heat of ablation, H_{eff} of PICA (at these heat rates) equals 200000 J/g. This was derived from Figure 5.8.

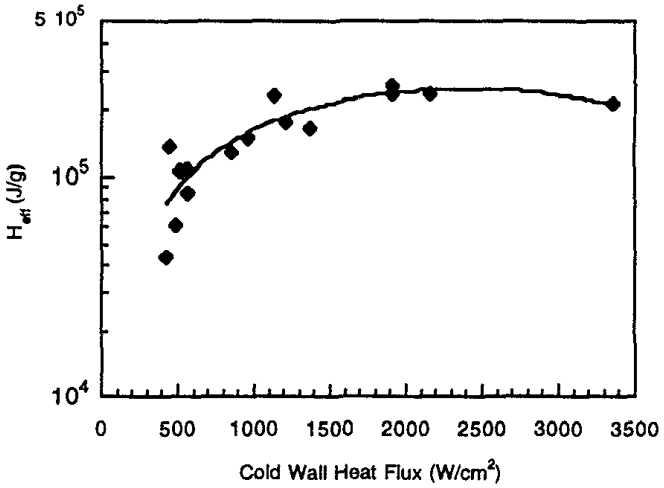

Figure 5.8: Effective heat of ablation as a function of heat rate [78]

Knowing all of this, together with the fact that the density of PICA equals 0.25 g/cm^3, the thickness of the ablated PICA can be calculated. Using Equation (5.20), this thickness was found to be 2 mm. However, close to the wall, the temperature will still be very high. Q_{abl} is the ablative heat load, H_{eff} is the effective heat of ablation and ρ_{PICA} is the density of PICA.

$$t_{abl} = \frac{Q_{abl}}{H_{eff} \cdot \rho_{PICA}} \tag{5.20}$$

Literature showed that conventional space certified insulation materials have failure temperatures of maximum 2000 K [89]. Therefore, an additional layer of PICA is applied to the heat shield for a preliminary insulation. From reference literature, this thickness was taken to be 350% of additional PICA material [90]. This gives a final PICA thickness of 9 mm.

5.2.3 Insulation Material

In order to protect the capsule from high conducted heat loads, an insulation material is required. It is needed to have in insulator since the material inside the capsule (beacon, mechanisms) should not be affected by a large inside temperature. A light weight insulation is required given the constraints of the CubeSat mission. However, since a lot of insulation materials are patented or still under development, not a lot of information on these systems can be found.

In total, three different insulation solutions are suitable for use on the re-entry capsule. These are a honeycomb structure, a multi-layer insulation material or the usage of a lightweight aerogel. For this capsule, a honeycomb structure was chosen, since it has been proven on existing flight models [90]. The thickness of the insulating layer is material dependent. However, it can be estimated by looking at the ratio of insulation material to total heat shield thickness of the Stardust re-entry capsule [90]. The rate of insulation thickness to PICA thickness is 1 to 3. This way, an internal temperature of approximately 70°C was obtained. Since the maximum allowed internal temperature of the Delta re-entry capsule is higher than this, the same ratio will be used. This has been done to add some margin to the design.

Having a 1 to 3 ratio of insulation thickness to heat shield thickness yields a honeycomb structure thickness of 3 mm. This brings the total heat shield thickness to 12 mm, including the PICA thickness (Section 5.2.2) of 9 mm.

5.2.4 Backshell

During re-entry the blunt part of the body will experience the highest calculated heat loads. Therefore, the heat shield is designed to withstand this loading.

In order to assure that the capsule has stability as it descends through the atmosphere, the center of pressure has to be above the center of mass. This is achieved by applying more mass at the bottom of the capsule, for example by positioning the battery at the bottom of the capsule.

The backshell of the capsule is exposed to significantly lower heat loading during re-entry. Therefore, the heat shield thickness can be lower in this region. Considering the calculation of the bottom heat shield, it is decided to use a 4 mm PICA heat shield at the top part of the capsule. This way the center of mass is still at the bottom, but also sufficient heat shield is provided to withstand the heat loads [91].

However, it is recommended to look into other materials for the backshell of the capsule. One option would be to select Super Light Weight Ablator (SLA), which has been used already on similar re-entry missions before [92].

5.2.5 Material Testing

With the results of the heat shield thickness, the final design needs to be tested under simulated re-entry conditions. This way the actual performance of PICA concerning ablation and thermal properties can be tested.

A suitable test is an Arc Jet Test, which can simulate the aerodynamic heating conditions during re-entry. This test will provide data on the heat flux at the stagnation point which can be used to validate the current design [93]. Furthermore, Arc Jet Testing can also give a more detailed insight into the heat shield needed due to conduction. This is already done by NASA [93]. The current design for conducted heat is based on reference missions with similar environment. Therefore, testing the design is required to show that the inner layout of the capsule is not affected by the inner temperature.

5.3 Parachute Design

This section will discuss the possibility of using a parachute recovery system to recover the capsule. First the altitude and speed at which it will deploy will be chosen, from which the parachute area can be computed. Knowing the diameter of the parachute allows for the computation of the non-deployed volume of the parachute. Finally this volume will determine whether or not there is enough space inside the capsule for all systems. If it turns out that this would not be possible, another solution will have to be found.

5.3.1 Parachute Characteristics

To make sure the capsule will return safely to the Earth, landing speed has to be sufficiently low. The first assumption is to take a maximum speed of 10 m/s and a minimum speed of 1 m/s after deployment into account. At this point three altitudes were considered for parachute deployment: 25 km, 5 km and 3 km above the ground. These altitudes are chosen to determine the difference in required parachute diameter. From the ballistic calculations the capsule speed corresponding to each altitude can be computed. This means that at an altitude of 25 km the capsule will be traveling with a speed of 107 m/s, at 5 km it will have a speed of 23.8 m/s and at 3 km the speed will be 21.4 m/s. This is still without a parachute

The parachute area can be computed using a technique from [94, p. 7-7]. Since this technique is shown in imperial units, for reference sake, this computation has also been done in imperial units. At the end of the computation the units were converted back to SI units. Therefore, the imperial values are needed and shown in Table 5.4.

According to [94], first the equivalent rate of descent at sea level needs to be calculated. This can be done using Equation (5.21).

$$V_{e_0} = V_e \sqrt{\frac{\rho}{\rho_0}} = V_e \sqrt{\sigma} \tag{5.21}$$

Table 5.4: Imperial variables

Variables	SI	Imperial
Height of 25 km	25 km	82,000 ft
Height of 5 km	5 km	16,400 ft
Height of 3 km	3 km	10,000 ft
Allowable speed	1 - 10 m/s	3.28 - 32.8 ft/s
Capsule mass	150 g	0.33 lbs

Where σ is the ratio of the density, corresponding to 82,000, 16,400 and 10,000 ft can be found in [94, p. 3-12], resulting in 0.18, 0.78 and 0.86, respectively. Note that the value for 16,400 ft has been taken at 16,000 ft.

The next step is to calculate the dynamic pressure. This is done using Equation (5.22) where x is a standardized parameter resulting from the assumption that the descent will be in equilibrium. When calculating in ft/s, x is 841.4 ft^4/lbs [94, p. 5-128].

$$q = \frac{{V_{e_0}}^2}{x} \tag{5.22}$$

Now the parachute drag area can be calculated using Equation (5.23).

$$(C_D S)_0 = \frac{m_c}{q} \tag{5.23}$$

At this point the parachute configuration is chosen. This selection is based on [94, p. 5-3]. First the possibilities were diminished when the decision was made to opt for a parachute capable of handling the highest opening forces resulting in three options: conical, bi-conical and tri-conical/poly-conical. It was decided to do the calculations with the parachute type with the highest drag coefficient: tri-conical. A drawback of tri-conical could be that it might be hard to fabricate into the right shape. The highest possible C_{D_0} that can be achieved with such a parachute is 0.96. However, for these calculations 0.9 was used to include a safety factor.

With this C_{D_0} value, the parachute surface area could be determined using Equation (5.24).

$$S_0 = \frac{(C_D S)_0}{C_{D_0}} \tag{5.24}$$

Finally, the parachute diameter can be calculated using Equation (5.25). The results for the different altitudes is given in Table 5.5. Please note that these diameters are given in meters.

$$D_0 = \sqrt{\frac{4(S_0)}{\pi}} \tag{5.25}$$

Table 5.5: Parachute diameters

Altitude	10 m/s	1 m/s
25 km	1.02 m	10.2 m
5 km	0.24 m	2.36 m
3 km	0.21 m	2.14 m

As can be seen, the impact of opening the parachute at high altitudes compared to low altitudes is quite significant. It is decided to open the parachute at an altitude of 3 km due to the smaller size of the parachute and the lower horizontal drift that the capsule will experience. Of course the parachute could be opened at a lower altitude, however, this needs to be tested in more detail. Another thing that has to be tested is the speed at which the capsule is allowed to land. For now 10 m/s is taken, because this results in a parachute diameter of 0.21 m and will only results in a 5 min drop from 3 km to the ground. However, if it turns out that the capsule can survive an impact of 17.5 m/s, which is the terminal velocity of the capsule resulting from Equation (5.26), then no parachute is necessary at all. It does have to be said that the actual final

velocity has been calculated to be 18.4 m/s using the ballistic equations. To choose not to go with a parachute would make the footprint predictions much easier and more accurate, and the decision will be made after the non-deployed volume computation.

$$V_t = \sqrt{\frac{2mg}{\rho A C_d}} \tag{5.26}$$

The final diameter is chosen to be 0.21 m. However, on the rocketman website [95] the smallest parachute diameter is 1 ft (or 0.3m), therefore this parachute is chosen as a candidate. Since COTS are more sustainable, the 1 ft parachute could be purchased. A new calculation can be done with the C_{D_0} value of ordinary amateur parachutes being 0.75 [94], which means that the existing parachutes are flat and circular. When computing using this value, for 3 km it can be found that a parachute of at least 0.235 m is needed, so 1 ft should be enough. Should one still like to go with a diameter of 0.21 m, it will have to be custom made, and a custom parachute can be more expensive and less sustainable.

5.3.2 Non-Deployed Volume

Now the volume that will be taken up by the parachute is computed. With the COTS parachute, the volume is already predefined. Since no precise information are given by [95], a number of assumptions are required. The parachute is made from nylon, which in this case has a thickness of 1 mm. This means that the total area and the total volume of the fabric becomes 730 cm^2 and 73 cm^3, respectively.

If a safety/folding factor of 50% is now taken, the volume of the non-deployed parachute can be computed to be 6 cm x 4 cm x 4.6 cm compared to the volume of the custom parachute which is 6 cm x 3 cm x 3 cm.

5.3.3 Decision

From the non-deployed computation it can be observed that the volume required to house the parachute is rather large. In fact it is so large that it would take up all the space that is currently available leaving no space for any kind of beacon or release mechanism. Therefore it has been decided not to go with a parachute. This means that instead of landing with a speed of 10 m/s the capsule will now land with a speed of 18.4 m/s. This 8.4 m/s difference can be compensated by improving the structure of the capsule such that it can survive the impact, which will require less space than putting a parachute in there.

5.4 Retrieval

The retrieval of the capsule depends on the footprint and landscape where the capsule will land. The footprint calculations in Section 5.1.6 show that the landing area is a rectangular with maximum dimensions of 1850 km (North-South) and 107 km (East-West). Also the location where the capsule will land is uncertain until a good orbit estimation can be done based on actual flight data.

Once the capsule has landed and the location is transmitted successfully, the location is known with an accuracy of 18 m due to the GPS receiver, which is discussed in Section 5.6. When the transmission of the location failed, the probability of finding a capsule of less than 10 cm in an area of 1850x107 km is practically zero. Therefore the transmission of the signal is crucial for a successful mission.

Different scenarios with their subsequent characteristics will be discussed. For each case the chances of a successful retrieval as well as an indication of the effort necessary to retrieve will be discussed. An overview of this discussion will be given in Table 5.6. For all cases the landing spot should be inspected before the capsule can be touched. This way valuable information about the landing and ablation can be gained for future missions.

5.4.1 Retrieval from Water

If the capsule lands in the water, the probability of successful retrieval depends highly on the capsule's ability to float, the chance that it will land in water is high, since 70% of the Earth is covered by water [96]. In the current design the capsule should float, although this depends heavily on the amount of PICA that will crumble off the capsule due to re-entry and impact with water.

When the capsule floats, and the transmission of the location is successful. It is simply a matter of going to the spot where the capsule is and retrieve it. Retrieval can be straightforward; Go by plane (and helicopter if necessary) as close to the landing spot as possible and then hire a boat to go to the landing spot. The probability of successful retrieval is medium for landing spots which is easy accessible (close to land) and low for landing spots which are hard to reach (middle of the ocean).

If the capsule lands in the water, and it does not float, there is a very low chance of finding the capsule. A scenario in which it could be retrieved is for example, when it will land into shallow water and it will send the location before landing into the water. This scenario is unlikely. Thus when the capsule does not float it will practically not be possible to retrieve the capsule.

5.4.2 Retrieval from Land

In the next scenario the capsule will land on ground, this makes the retrieval chance a lot higher. Also the effort to retrieve the capsule will be significantly lower. Preferably the capsule will land on a rural place like a large desert, then the chance of hitting property or humans will be minimized. Depending on which surface and landscape the capsule will land the vehicle choice for retrieval can be made. Also for this scenario, first an airplane and helicopter will be used to get as close to the capsule as possible, then a helicopter or car will be hired to collect the capsule. The probability of successful retrieval is maximal in this scenario.

When the capsule will land into an inhabited area, the capsule might be detected before the team of the Delta mission could be send there. Legislation states that every country, which is a UN member (all countries except Kosovo, Vatican and and Taiwan) has to retrieve and return the capsule if it lands on their ground (for more information see Section 5.5). Alternatively, a crew can be sent to the respective footprint location.

The cost of retrieval also depends on the distance between the landing spot and Delft. For example, if a team has to be flown to Japan, high cost should be accounted for airplane tickets as well as the cost to stay there.

Table 5.6: Retrieval options, assuming that the capsule floats

Options	Cost	Successful Retrieval
Water, close to land	Medium	Medium
Water, far away from land	High	Low
Land, sparsely populated	Medium	High
Land, densely populated	Low	Very high

5.5 Laws and Regulations

The following section presents the laws and regulations concerning space re-entry and space debris. As the CubeSat enters the atmosphere, it will burn up and only the re-entry capsule is left. Since no AOCS is on-board of the capsule, it has to be assured that no hazard is created during re-entry and landing. Different institutions focus on regulations that minimize the potential hazard of capsules and other objects re-entering the atmosphere. The United Nation Office for Outer Space Affairs is one of the leading institutions concerning Space Law. Next to this, the European Center for Space Law and the International Institute of Space Law are also involved in the regulations about space and re-entry objects. The main institution concerning safety requirements in Europe is the European Cooperation for Space Standardization (ECSS).

Within the QB50 mission, VKI is the final authority that decides over the in-flight operation and is responsible for those [97].

5.5.1 Licenses

A re-entry mission should not be a threat to the Earth environment. According to the safety policy of ECSS no damage should be created to the following [98]:

- human life
- environment
- public and private property

With this in mind, it becomes clear that different licenses are needed on national, European and international level in order to launch a vehicle into space and return it to Earth.

VKI is the operator of the QB50 mission and is therefore also responsible to file the applications for authorization. This includes achieving licenses over the launch, the orbital maneuvers and de-orbiting of the CubeSats [97].

As a Dutch university, a license is needed from the Dutch government in order to perform activities in space. Within six months after the application, it will be decided if a license will be granted [99].

5.5.2 Potential Hazard

Responsibilities The re-entry capsule does not have an AOCS on-board and therefore, the landing site is not entirely predictable during the mission. In order to keep the damage to a minimum, the capsule shall land on uninhabited land. However, if the capsule creates damage, the responsible state who launched the vehicle is responsible according to the United Nations Treaties and Principles on Outer Space [100].

Furthermore, the Space Activities Act of the Netherlands [99] states in paragraph 3.10 that

> If an incident occurs or has occurred that may jeopardize the safety of persons and goods, environmental protection in outer space, the maintenance of public order or national security, or otherwise cause damage, the license-holder shall, without delay, take the steps that can reasonably be expected of it in order to prevent the consequences of that event or, where those consequences cannot be prevented, to limit and rectify them as far as possible.

Consequently, TU Delft and Von Karman Institute will be held responsible in case of damage.

Risks Every object of the capsule can be a potential hazard, since it the re-entry is uncontrolled. The European Cooperation of Space Standardization set the requirement for atmospheric re-entry [98]:

> The space vehicle shall be designed and operated [...] such that,[...], the risk of a catastrophic event does not exceed the level of acceptable risk specified by the project [...].

In order to create the least possible damage, the footprint calculations need to include possible uncertainties during re-entry as can be seen in Section 5.1.6.

5.5.3 Capsule Retrieval

Since the capsule needs to be retrieved, use of the UN agreement on the return of objects launched into outer space by the United Nations Office for Outer Space Affairs can be made. The UN Treaties and Principles on Outer Space states in paragraph B, article 5 the following [100]:

> Each Contracting Party which [...] discovers that a space object [...] has returned to Earth in territory under its jurisdiction or on the high seas or in any other place not under the jurisdiction of any State, shall notify the launching authority [...].
>
> Each Contracting Party having jurisdiction over the territory on which a space object [...] has been discovered shall, upon the request of the launching authority [...] take such steps as it finds practicable to recover the object [...].

With this agreement, which all member countries of the United Nations signed, the help of other nations can be used to retrieve the capsule depending on the final landing spot.

5.6 Re-entry Capsule Layout

This section is discussing the layout of the re-entry capsule. First, the geometry and the general layout of the capsule will be covered. Afterwards the heat shield, landing and the cap release mechanism will be discussed. The subsequent sections will discuss the retrieval approach together with the required battery and electronics to support the retrieval. Finally, a weight estimation will be given, which will give an overview of the system. Also some recommendations will be given for future works, as this design is still at a conceptual stage. For most subsystems the approach will be to first investigate the design options and then discuss per design whether it is suitable for the capsule.

Geometry

The volume left inside the CubeSat is very small for a re-entry capsule. Usually, these are much larger and leave more room for components. One of the main challenges for the capsule is to design an aerodynamic shape and a shape which leaves enough room for all necessary components. The CubeSat is constrained by a volume of 98x98x72 mm, see Section 2.5.2. Due to this constraint, the width of the capsule is taken to be 96 mm and the height 70 mm, this way on all sides of the capsule 1 mm space is left as contingency. The outer volume is $2.81 \cdot 10^{-4}$ m^3.

The geometric shape of the re-entry capsule can be observed in Figure 5.9. Basically, it will be a body with a sphere at the bottom and a cone on top of it. It has been decided to use this geometry, as the heat rate of the capsule is smaller when the nose radius is larger [101] and a detached shock wave is created. Although a full sphere is beneficial in terms of heat distribution, it is not an option, as the required instruments and components were not expected to fit into a sphere of such a small size, therefore the bottom is flattened by using a large radius. This way the shape has an aerodynamic basis, just like the Apollo [102], the Stardust capsule [103] and the capsule of the Marco Polo R mission [104]. Although the capsule has great similarities in terms of geometry (except from the scale), no aerodynamic calculations are performed. These should be done through CFD analysis or with a test model of the capsule in order to determine properties like the c_p.

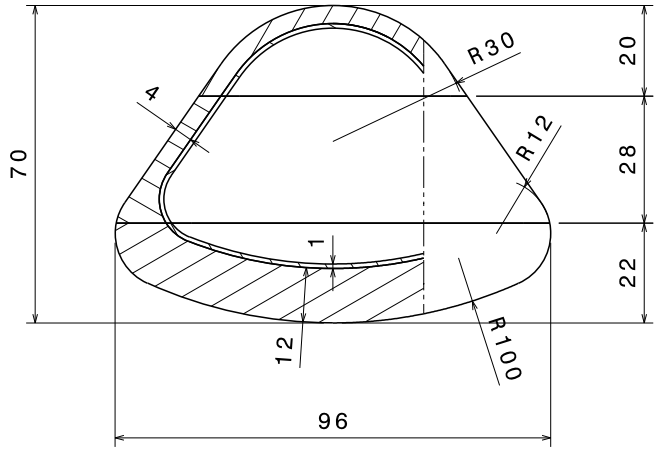

Figure 5.9: Dimensions and geometry of the re-entry capsule in millimeters

Layout

Now the geometry has been chosen, the layout of the capsule will be discussed. The capsule consist of an outer heat shield structure, which is made of an ablative material, PICA, and an insulation material, see Section 5.2. On the inside, also a sheet of 1 mm aluminum is placed. This will protect the inside of the capsule for impact. Aluminum is chosen because it is very light: 2.7 g/cm^3 [105], while still containing the properties to protect the capsule. Since only 22% of the PICA is burned during re-entry Section 5.2 it will take care of the impact protection together with the aluminum.

The inside of the capsule is filled with electronics such that the capsule can be located and be retrieved. The basic parts will be the beacon, a battery, a timer, a release mechanism and a small electronic board which connects all components. The timer will activate the system that will release the top of the capsule. The effect of this is that the antenna will be fully extended outward and make transmission of the beacon signal possible.

The outer volume is $2.81 \cdot 10^{-4}$ m^3. An inner volume of $1.4 \cdot 10^{-4}$ m^3 is left. All the components of the capsule except the heat shield should fit within this volume, volumes are listed in Table 5.7. All the components have a volumetric and mass margin of at least 10%. From an initial analysis through the CATIA model the location of the center of mass is calculated: This goes trough the two planes of symmetry and is located 23.7 mm above the lowest point of the heat shield. Figure 5.10 shows the initial allocation of volumes within the capsule.

Table 5.7 shows the volumes that were obtained from the CATIA model Figure 5.10 and component specifications (see below).

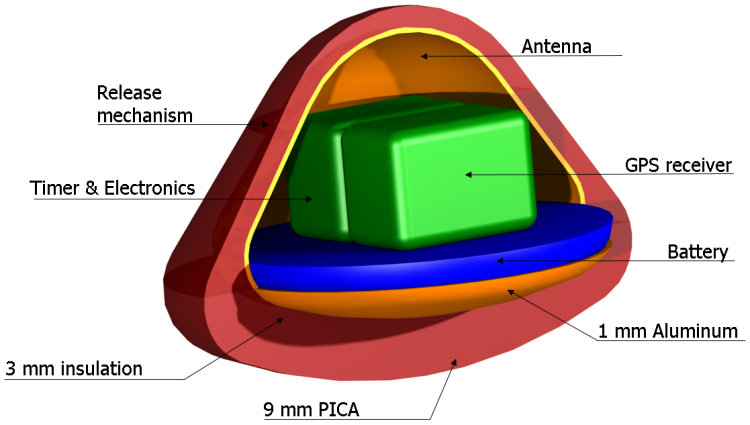

Figure 5.10: CATIA model of the proposed capsule layout

Table 5.7: Capsule volumes

Volume	Value (m^3)
Outer volume	$2.81 \cdot 10^{-4}$
Outer volume minus top hatch	$2.50 \cdot 10^{-4}$
Outer volume minus top hatch minus 22% heat shield	$2.19 \cdot 10^{-4}$
Outer volume minus top hatch minus 22% heat shield minus electronics	$1.39 \cdot 10^{-4}$
Heat shield	$1.25 \cdot 10^{-4}$
Aluminum	$0.13 \cdot 10^{-4}$
Inner volume	$1.40 \cdot 10^{-4}$
Inner volume minus top hatch	$1.25 \cdot 10^{-4}$
Electronics	$0.70 \cdot 10^{-4}$
Spare volume (inside)	$0.70 \cdot 10^{-4}$

Heat shield

For the thermal protection system it was decided to use an ablative heat shield as the capsule is going to be used only once, in particular PICA. In the Mid-term Report [4] the decision has been made to go for PICA(-X) because this material is lighter than AVCOAT. According to heat calculations in Section 5.2 and the estimations based on the Stardust mission the inner temperature will not exceed 70°C. The electronics inside the capsule should be capable of withstanding this temperature. It is recommended that the temperatures will be verified by a model to establish that the temperatures will stay the given temperature. On bottom part of the heat shield an honeycomb isolation material is used, some practical reasons this is left out of the Figure 5.10. The density of this material will be assumed to be the same PICA. An elaboration on the heat shield design is given in Section 5.2.

The mass of the heat shield can be calculated with the use of $\rho = m/V$. ρ is equal to 250 kg/m^3, the volume is known from the drawings and the heat shield calculations. This is equal to $1.225 \cdot 10^{-4}$m^3, which gives a value for the mass equal to 32 grams.

Landing

The velocity of the capsule just before landing is around 18.4m/s, as was calculated in Section 5.3 when the capsule weight is 150 gram, this was the allocated budgeted. The landing speed is relatively low and it is assumed that the capsule will survive the impact of landing on Earth. Although at this stage no calculations have been done in order to make sure that the electronics survive the landing. When no parachute is used, the landing loads have to be covered by the PICA, the insulation material and the aluminum. In order to decelerate the electronics in the capsule slower a light weight material like, foam can also be used. No requirements on the transmitter data sheet [106] can be found with respect the maximal accelerations. Therefore this phase A design should be complemented with tests that verify that the electronics works properly when the capsule lands on ground or on water. In Section 5.3 it has been explained that an parachute was not feasible due to volume constraints. This simplifies the design of the capsule; no parachute release system has to be designed and implemented. This leaves more space for the other electronics, which means a beacon with a longer battery life can be used. The decrease in mass due to the ablated heat shield

and the release of the top hatch was calculated: The total mass decrease is 12 grams (see Table 5.9). The values are calculated with the equation from Section 5.1. Therefore the actual landing velocity is 17.3 m/s with a mass of 135 grams, and the actual descending velocity will be 18.0 m/s with a mass of 147 grams, this is the speed just before the top hatch is separated from the capsule.

Cap Release Mechanism

As the beacon is located within the capsule, it will need to have an antenna which cannot remain isolated within the capsule. Therefore, some part of the capsule will need to be detached. This detachment will occur after re-entry, but before landing. The most obvious location to split the capsule is where the heat loads are estimated to be at a minimum; this is the upper part.

Given the extreme volume constraints, the size of the release mechanism needs to be kept to a minimum. At this stage, it is considered to use the flexible antenna of the beacon to serve as a spring that is applying pressure to the upper part of the capsule. The capsule will not open during re-entry as the upper and lower parts are held together internally by a wire. The wire will melt when heated by an electrical charge. The melting temperature of the wire should be higher than the inner capsule temperature experienced during re-entry.

There are different methods for determining when the upper and lower parts of the capsule need to be separated. Three candidates are pressure sensor, temperature sensor, and timer.

Pressure sensor Using a pressure sensor, the air pressure must be measured during re-entry. As soon as the satellite is at an altitude where the heat loads have reduced significantly, for instance 5 km above the Earth's surface, the sensor can trigger the release system. The potential difficulties with this solution are that a hole needs to be created in the capsule, the sensors are typically relatively large compared to the available volume, and the operating temperature is typically limited to 200°C [107].

Temperature sensor During re-entry the temperatures on the outside as well as the inside of the capsule will rise due to heat generated by decelerating from supersonic velocities. When the largest temperature has been measured by the temperature sensor the capsule is in descent. Around the height of 70 km the maximal temperature will be reached. The temperatures will be logged and analyzed by a small IC. The inner temperatures that the aluminum plate will reach was estimated at around 70°C. This is the only time when the inner temperature reaches such a high value. The temperature in the capsule and CubeSat will not be higher than 40°C Section 4.7 during the launch and mission duration. However, as neither the exact temperature inside the capsule, nor the heat propagation time are exactly known, there is a risk of triggering the release mechanism too early or too late.

Timer The time interval between capsule release and the capsule landing on Earth was estimated to be 890 seconds, as can be read in Section 5.1. The flight profile, or at least the approximate duration of the re-entry, does not depend on a lot of variables and the estimate is rather precise. This means that a timer could be set up to trigger the release mechanism at an altitude of, for example, 5 km. A timer is also the most cost, mass as well as volume efficient option and needs to be implemented anyway since the beacon needs a timer.

The timer will be triggered when the capsule leaves the satellite. After the time that corresponds to an altitude of 5 km, the timer will trigger the release mechanism.

Assembly As the cap release mechanism needs to be assembled, the capsule needs to be open in a different location to facilitate assembly. It is suggested that the lower part of the capsule should consist of two parts. The separation should be made where the capsule is at its widest. This allows for optimal accessibility during capsule assembly. The two parts should be welded together afterwards. When the aluminum structure is welded, the heat shield can be applied. The heat shield should consist of at least three parts, following the same division as the aluminum structure. These sections can be observed in Figure 5.9. The transitions will be seamless on the outside.

Charging / Triggering The beacon and the release mechanism both require power. Therefore, a battery needs to be on board to provide this power. If this battery could be charged before the capsule would be sealed, the advantage would be that no connections have to be available on the re-entry capsule, minimizing the risk of damaging the capsule during re-entry. However, the timer inside the capsule needs to be triggered upon ejecting the capsule from the satellite. No feasible solution was found at the time to initiate this timer wirelessly without consuming energy over the mission duration. Therefore, the upper part of the capsule should be equipped with two small diameter conductive rods (not shown in figures) that penetrate the capsule's heat shield. The local effect on the heat shield is expected to be marginal, but further testing should clarify whether this assumption is true. These rods will connect to the battery of the capsule on one end, and on the other end it will interface with Delta's EPS. The battery will be charged before assembly, and the satellite can recharge the battery in the time preceding the re-entry. Since this is a small battery, this recharging procedure will have a very minor impact on the power budget. Upon ejection, the disconnect in the charging circuit will also activate the timer. This situation is shown graphically in Figure 5.11. It shows which actions are being performed at which altitude and corresponding time after or before ejection.

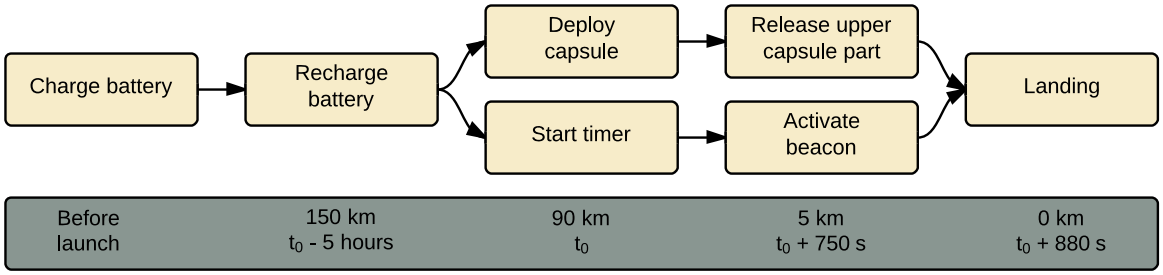

Figure 5.11: Re-entry activities as a function of altitude / time

Tracking

In order to prove that the re-entry did actually succeed, retrieval of the capsule is necessary. The beacon is one of the main electrical components inside the capsule. The key requirements for designing the beacon are the power and volume available. Four possibilities are shortly discussed; SSTS, GPS, Radio transmitter and Argos. The last option is chosen and discussed in more detail.

From the calculations in Section 5.1, a large footprint can be expected. In order to track the exact location of the landing site of the capsule four different kind of possibilities will be discussed. The first one uses of a system to track the capsule, from Earth or space, the other systems have a GPS tracker, radio transmitter and an Argos transmitter onboard.

SSTS When using a system to detect the capsule from space, a system like the Space Tracking and Surveillance System(STSS) [108] could be used. This system was built by the United States Missile Defense Agency (MDA), it's objective is to use it for space-based detection and tracking. The system uses long- and short-wave infrared sensors, which will be able to acquire and track missiles and objects during motor burning and during the boost phase of missiles. This system is compliant with other tracking systems like the Forward-Based Radar, Upgraded Early Warning Radar, COBRA DANE Radar, Transportable Radar Surveillance, Sea-Based X-band Radar and Spy-1 radar [108]. These are fixed and transportable radars and are only used in the USA, although in theory these systems can be used everywhere on Earth. The main drawback of these systems is that they probably cannot be used for civilian purposes. Next to this it is not certain that the system is able to track such small objects, due to the limited availability of public information.

GPS One possibility for a beacon is a GPS receiver on board of the capsule. A so called 'spying GPS tracker' would be suitable, since these are designed to work in all kinds of conditions and are built in mobile phone links for relaying the GPS measurements. Looking into these kinds of trackers reveals that small trackers have dimensions of: 6.4x1.9x3.2 cm [109]. These dimensions are too large to fit within the capsule. Another reason why these trackers cannot be used is that mobile phone network coverage is not global.

Radio Transmitter

A different possibility would be to have a radio transmitter as proposed in the Mid-term Report [4]. This transmitter would than be activated as soon as the capsule is deployed from the satellite to save battery.

COTS products that can be found are usually very small. One COTS product that would fit inside the capsule is the CA MODA 3750 MVS-HF [110]. This is a radio transmitter that is used in amateur rockets and has a line of sight range of 80 km and a ground range of 8 km. Another radio transmitter with a larger range is available, however, that one would need about 7 cm of space. The largest drawback of using this radio transmitter is that the range is limited to 8 (or 14.5 for the larger one) km. With the a footprint of roughly 1850x107 km a radio transmitter can be used, though the retrieval would be an expensive and time consuming process.

Argos The fourth option is to use an Argos beacon. The Argos network is mainly used to track wildlife and oceanography [111]. The Argos conventional tracking system calculates the location by measuring Doppler shift on the transmitter signal. This is a UHF signal with a frequency of 400 MHz [112]. When an Argos satellite approaches the beacon, the frequency of the beacon signal as perceived by the Argos satellite's receiver is higher than the actual transmitted frequency, and lower as it moves away. Each time the satellite receives a message from the transmitter, it measures the frequency and time-tags the arrival. In Figure 5.12a and Figure 5.12b a schematic of the principle is given. The conventional system can be augmented with GPS positioning, for which a GPS receiver will be needed. Commercial systems are available that combine both UHF transmitter and GPS receiver.

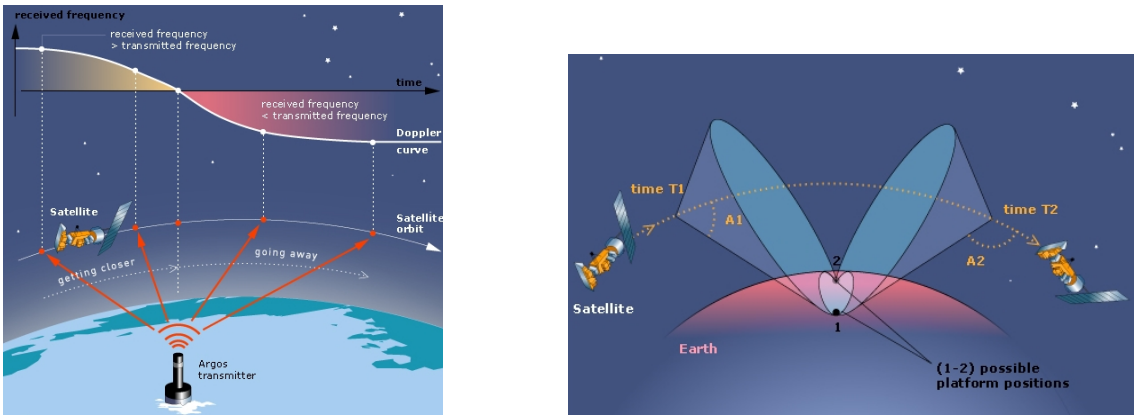

(a) Doppler shift the Argos satellite receives [112] **(b)** Exact geometric location determination [112]

Figure 5.12: Argos network layout

When the Argos transmitter is combined with a GPS module, the GPS positions are recorded in the transmitter and sent via the Argos system. This gives the benefit of obtaining an accuracy of 18 meters. Figure 5.13 shows a schematic overview of the system. This comes at the cost of a larger module, which requires more power. The smallest system available at the moment is the PTT-100, which weight is 22 grams [106]. The most important system parameters are listed in Table 5.8.

Table 5.8: Specifications of PTT-100-5 and PTT-100-22

Parameter	PTT-100-5	PTT-100-22
Power output [m]	100-300	100-500
Transmission interval [s]	45-120	45-120
Output frequency [MHz]	401.650 ±36 kHz	401.650
mass [g]	5	22
Operating temperature [°]	-5 to 45	-5 to 45
Dimensions [mm]	24x14x7.5	64x23x16.5
Accuracy [m]	350-1000m	±18

This is a COTS product, but unfortunately it just does not fit inside the capsule, since the maximum diameter of the capsule is 54 mm. Also this receiver has only a small battery with it, and a solar cell to charge the battery. Therefore, the components can be ordered separately, without the solar cell and small battery. This will be replaced with a larger battery and connected to a timer to switch the system in operational mode. It will also allow the design of the capsule to put all components in an order which is more suitable for use inside the capsule. The original PTT-100 also comes with a temperature and humidity sensor, but are

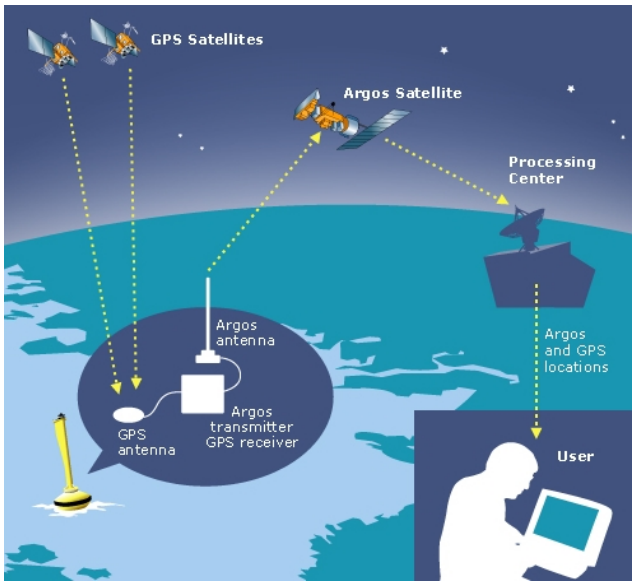

Figure 5.13: Sending gps positions using Argos [112]

not necessary to include in the redesign, since this will consume power and volume. A new battery will be designed for the capsule, and will be explained in more detail in the following section.

Battery

The manufacturer of the beacon states that a battery weighing 100 grams can provide 1,000 GPS measurements and 100 uploads to the Argos network over a three-year lifetime [106]. Battery drainage over this lifetime is therefore included. For the purpose of recovering the capsule, it would be sufficient to obtain 500 GPS measurements over 50 uploads. This would give the recovery team location information every 90 minutes if the battery needs to last two weeks. Estimating the battery at 50 grams would be a safe estimation, as the battery drain over two weeks is insignificant compared to a lifetime of three years. The volume of the battery is approximately 40 cm^3. It is recommended that the battery is tested to inspect whether it is capable of powering the transmitter for the required time.

Electronics

The tasks of the other electronics used in this system are fairly simple: They have to regulate the power from the batteries to the timer, transmitter, IC and capsule top release mechanism. These electronics should be mounted on a PCB and be interconnected. Almost the same components that are used in the PTT-100 can be used. The estimated maximum mass is 10 grams, including a contingency. Also for this section it is recommended that a more detailed electronic layout will be designed in order to inspect how much power, mass and volume this system will exactly occupy.

5.6.1 Mass

The descent of the the capsule will go into an uncontrolled descent, therefore a high chance exists that it will land in water. In order to retrieve the capsule it should float and have a lower density than water. When the capsule landed the volume is the outer volume minus 25% of the bottom part of the heat shield minus the top hatch, which will be separated before landing on Earth. It is assumed that the empty space is filled with water, this has a volume of $0.70 \cdot 10^{-4} m^3$. Using the density of water; $0.99987 grams/cm^3$, the mass will be 70 gram. The total weight of the capsule when filled with water is 211 gram. The volume of the capsule is at this point equal to the outer volume, which can be found in Table 5.7 minus the top hatch minus the burned PICA, this equals 246 cm^3. Using the density equation again, the density of the capsule is calculated when filled with water and this is equal to 0.85 kg/m^3. Thus, the capsule density is lower than the density of water. Consequently, the capsule will float in water. It has been assumed that the remained heat shield will be intact after landing into the water. All the weights will be shown in Table 5.9.

Table 5.9: Capsule weight per component

Parameter	Value [g]
Pica heat shield	35
Bottom part PICA (-25%)	17
Middle part PICA	9
Top part PICA	3
Top part aluminum	6
Protection sheet	37
Battery	50
Beacon	15
Electronics	10
Empty volume filled with water	70
Total capsule weight	147

Recommendation Perform tests such that the c_p value can be measured. The design of the outer layout can slightly change when this is not compliant with the budgets, which are stated in Section 2.5, the c_p should be above the c_m when the sharp corner is at the top.

Tests with a test model of the capsule should be done to verify that the electronics can survive the landing impact, this should be done for different landing cases; landing on water, on a rock, in snow etc. Also, the landing terrain could have an impact on the strength of the transmitter signal, this should also be tested.

In the conceptual design of the capsule [4] a data retrieval system was mentioned as a recommendation for future designs. The reason that it could be taken onboard of the capsule was done with the assumptions that a parachute was needed for the mission. Since this assumptions is not valid anymore, there might be room for an microSD card. Using a microSD card, all the data collected during the mission lifetime can be saved for redundancy. This will effect the power budget and the data flux onboard.

5.7 Capsule Deployment

During re-entry, the entire CubeSat will burn up and only the capsule remains from the original structure. The burn-up of the structure is unpredictable and can damage the entry capsule. In this section, first the reasons for a deployment of the capsule will be given, followed by the deployment mechanism.

5.7.1 Deployment Reasons

Due to the high heat load during re-entry, the CubeSat structure will burn-up. In general the burn-up of a structure during re-entry is unpredictable. Therefore, the effect on the re-entry capsule is not entirely foreseeable.

A propulsion system is positioned on-board of the CubeSat which will have propellant left as re-entry starts. As soon as the CubeSat is exposed to the high temperature and the structure starts to burn up, the propulsion system might explode. Although the low pressure in the propulsion system does not form a direct explosion threat, under the rapid changing circumstances, the behavior of the system with its propellant is unknown. Therefore, the system might explode and create debris. These debris represent a threat to the heat shield of the capsule. If the debris impact the capsule and lead to a damage in the TPS, it is not guaranteed that the capsule survives the heat loads during re-entry. Consequently, the capsule might burn up and the mission can not be carried out. Since the burn-up of the CubeSat with the re-entry capsule enclosed contains too many risks for the successful execution of the DSE mission, it is decided to deploy the capsule from the satellite before the CubeSat will burn up.

5.7.2 Deployment Mechanism

In order to accommodate deployment of the re-entry capsule during re-entry, the structure needs the ability to open. The following solution is proposed:

The re-entry capsule is located in a space at the bottom of the satellite. During re-entry, the satellite bottom will point in the opposite direction of the velocity vector. As the capsule will be located upside down within the satellite, the heat shield will be facing the velocity vector.

The bottom plate of the satellite is fitted with an adapter that fits the upper part of the re-entry capsule. It is not fixed to this adapter in any way. The bottom plate is connected to one side panel using a spring-loaded piano hinge on one side. The opposing side of the bottom plate is connected to its adjacent side plate using a hinge with a polycarbonate rod with a melting temperature of approximately `<tbd>` 150 to 200 °C. The exact desired melting temperature should be further investigated, as a deeper analysis is needed to calculate the temperature on the hinge during early re-entry stages as it is situated outside but on the rear end of the satellite.

On the side of the heat shield, the capsule is supported by a ring structure, which is connected to a small structural support inside the satellite using pre-loaded springs.

Upon re-entry, as soon as the temperature starts to rise significantly, the polycarbonate rod melts, and the bottom plate swings to the side because of the torque exetered by the spring loaded hinge. The re-entry capsule is pushed out in a straight fashion by virtue of the compression loaded springs that support the capsule from the top. It should be noted that small rotational velocities might still occur, and the re-entry capsule should be self-stabilizing nevertheless.

This mechanism is shown in Figure 5.14. The heat-triggered mechanism guarantees that during re-entry, when subsystems might be failing due to the increasing temperature, deployment of the re-entry capsule will still succeed.

Recommendation: In case extensive heat analysis shows that no temperature exists at which the polycarbonate rod (situated at the back of the satellite) can melt while the satellite is still largely intact, an active deployment technique should be used as main deployment mechanism and the deployment altitude should be slightly higher as the responsible subsystems still have to be functional. The solution suggested above can serve as a backup solution in this case.

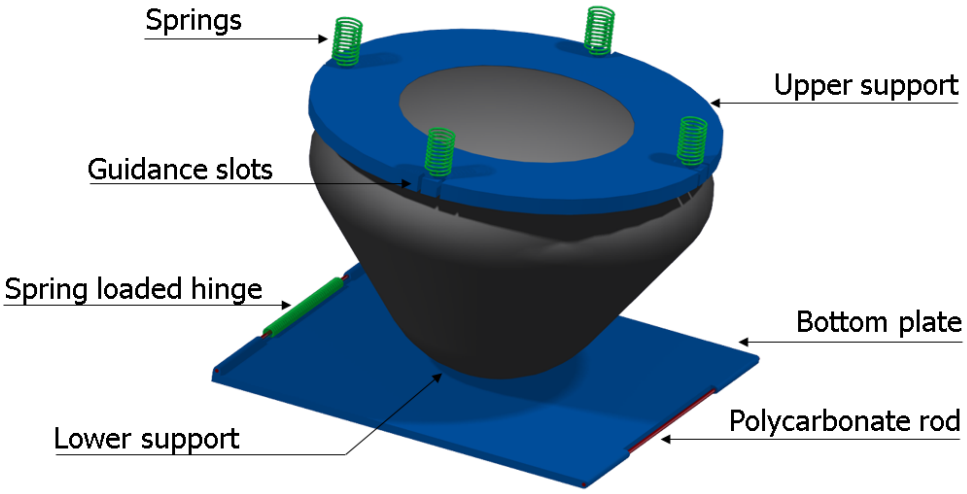

Figure 5.14: Re-entry capsule deployment mechanism

CHAPTER 6
SUBSYSTEM INTEGRATION

In the following section, the physical appearance of the CubeSat is presented. First, the layout of the satellite is determined. Afterwards, the center of mass is calculated to stay within requirement DELTA-STR-11 and finally, a visualization of the CubeSat is given.

6.1 Minimum Subsystem Separation

The minimum subsystem separation is based on the maximum deflection of the components. The PCBs are most likely to deflect, and are used to determine the maximum deflection δ. For the maximum separation calculations it is assumed the PCBs are clamped on both sides and the force will act in the middle. Therefore, $\delta = \frac{F \cdot l^3}{192 \cdot E \cdot I}$ for a clamped beam is used. The maximum force is determined with a maximum acceleration of 8.3g given by the requirement DELTA-STR-4.1. The maximum mass of a PCB was taken to be 240 grams for batteries. Other values used can be found in Table 6.1. The PCB material is a composite material composed of woven fiberglass cloth, named FR-4 [113].

Table 6.1: The value used for the maximum deflection calculations

Name	Symbol	Value	Unit
Elastic modulus	E	$2.1 \cdot 10^{10}$	Pa
Moment of inertia	I	$8.3 \cdot 10^{-12}$	m^4
Maximum force	F	32.5	N
Length of the plate	l	0.1	m

This results in a maximum deflection of 0.59 mm. The worst case scenario occurs, if both PCBs deflect towards each other. Then a minimum separation between two PCB is 1.18 mm. Including a margin, the minimum separation is set to 2 mm.

6.2 Constraints

Before the layout is determined, first the constraints are discussed. These are listed below.

The DSE capsule is placed on the bottom of the satellite.
The DSE capsule is ejected, so it is not damaged by other parts of the satellite during re-entry. Therefore it should be on the bottom.

The solar panels and solar sensors are on the outside.
The solar cells are placed as described in Section 4.2. Six solar sensors are placed one the CubeSat, one on each face.

The QB50 payload, FIPEX, will be on the top of the satellite.
As is shown in [22, p. 81] the FIPEX unit is placed on one of the ends in the direction of flight. There is a "keep out" area defined of both sides.

The nozzle of the propulsion system should be as close to the center of mass as possible.
The thruster system induces a torque, this torque increases when it is placed further away from the center of mass.

The center of mass is in the range of 2 cm of the geometric center.
As stated in requirement DELTA-STR-11.

6.3 Final Layout

With the above constraints the systems on the top and bottom of Delta are already defined. Next the nozzle of the propulsion system drives the layout. Since the propulsion system is located in the middle of the CubeSat, the other systems are placed such that the center of mass is within 2 cm of the geometric center. Finally, the Mass Moment Of Inertia (MMOI) is considered. The final layout is shown schematically in Figure 6.1.

As the layout is determined a final appearance of the satellite is made. Figure 6.2a shows the interior and Figure 6.2b shows the exterior.

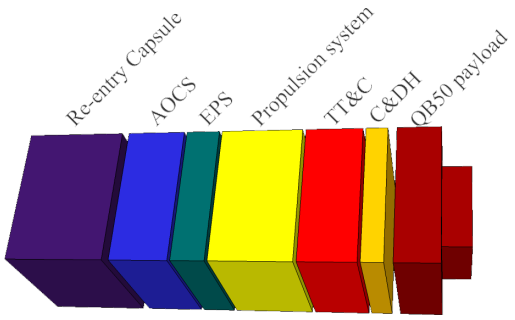

Figure 6.1: The final internal layout.

6.4 Center of Mass

The final center of mass (CoM) is calculated by using the mass of the different systems and the distances to the geometric center. It is assumed that the center of mass of the different systems is in the middle of the subsystem. The center of mass will be 1.8 cm in front of the geometric center, which is favorable for the aerodynamic stability [29]. The values show in Table 6.2 are the mass,the location and the Com in the satellite.

Table 6.2: The thickness, location and mass of the subsystems and payload of the Delta satellite.

Component	**Thickness [mm]**	**Mass [g]**	**CoM* [mm]**
QB50 payload	50	600	25
C&DH	15	161	76.5
TTL	37	270	106
Propulsion	58	418	157
EPS	24	650	200
AOCS	42	438	235
DSE payload	72	330	294
Total satellite	**340**	**3311**	18

* w.r.t. geometric center

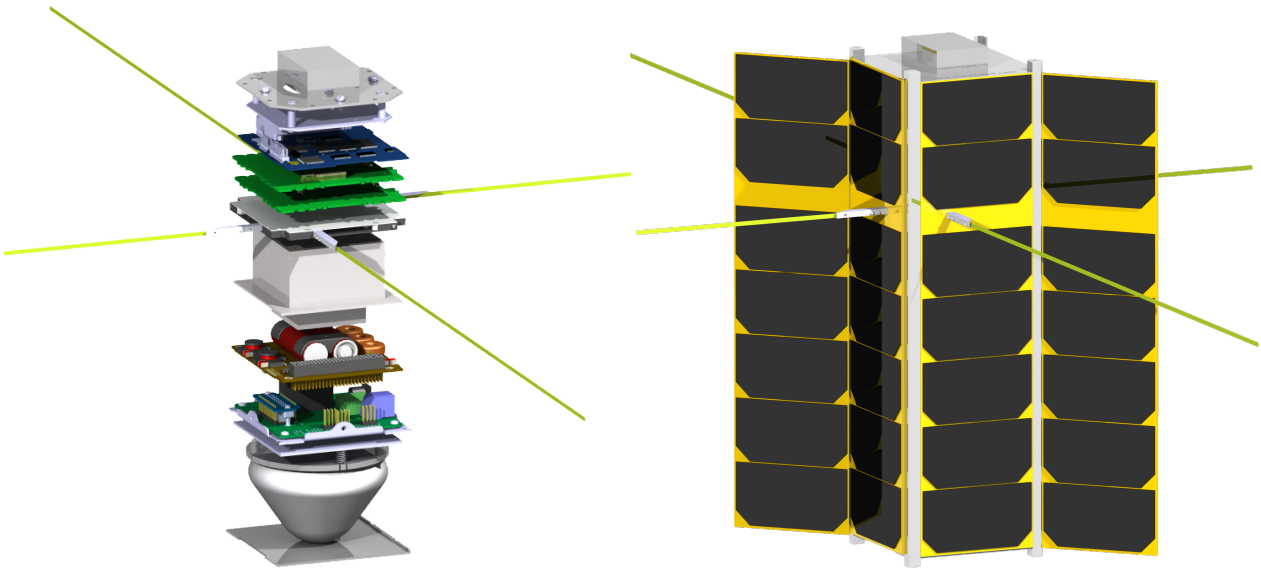

(a) The final internal appearance.

(b) The final outer appearance.

Figure 6.2: Appearance of the satellite.

CHAPTER 7
POST-DESIGN PHASE

This chapter covers the post design phase of DelFFi Delta. Before a satellite can be launched, various phases need to be passed, which is a very time consuming process. In order to prevent any delay in time or extension of the budget, these processes need to be well organized.

After the final design has been selected, the development of the satellite will take place. This is followed by the production and testing of the CubeSat. A logical sequence of the activities in the various phases is given in Section 7.1. Furthermore, the manufacturing, assembly and integration plan is presented in Section 7.2. This is followed by the logistic and operation concepts in Section 7.3. The logistic concepts focus on the locations of production and assembly of the CubeSat. The operation concepts specify the tasks of the ground segment during the operational time of the satellite. Finally, the time line of the post-design phase is shown in Section 7.4.

7.1 Project Design and Development Logic

The post design phase contains various objects that can be summarized in a project design and development logic. Figure 7.1 shows the different steps in the post design phase chronologically ordered. The post design phase can be divided into different phases: development phase, production & testing phase, operational phase and the end-of-life time.

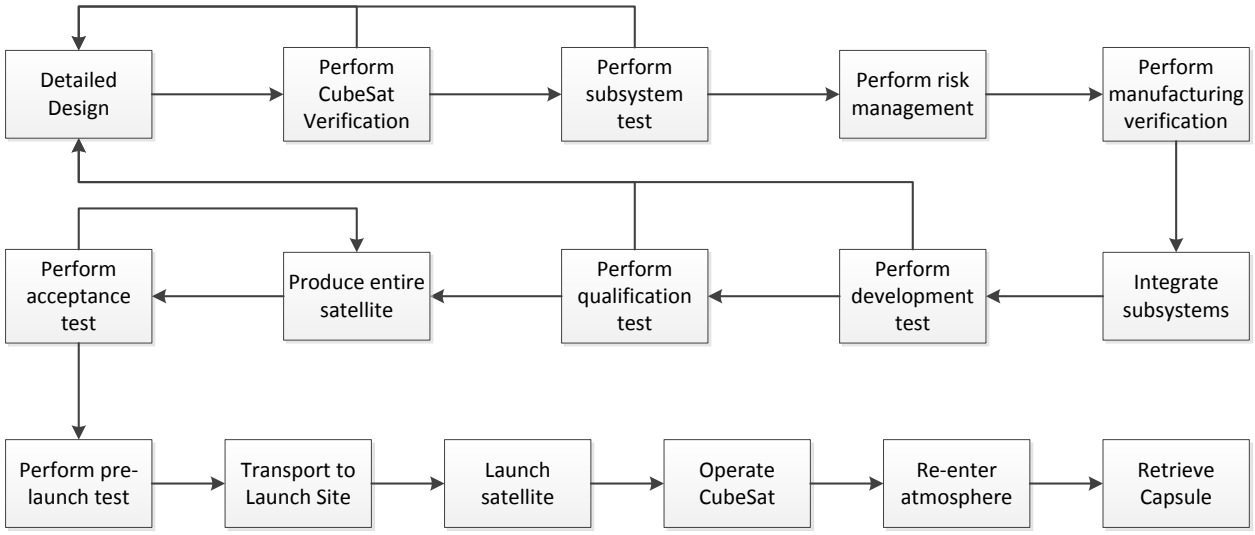

Figure 7.1: Different activities in the post design phase

After the detailed design is finished, it is verified. In case the results of the verification are not sufficient, the detailed design needs to be reworked. Otherwise subsystem tests are performed under different operational conditions.

In order to have a successful mission execution, the various risks need to be kept to a minimum and mitigated. Therefore, a risk management is performed. After the risk management, the manufacturing process is verified, which is described in more detail in Section 7.3.

As a next step, the subsystems are integrated into the satellite. More information on the subsystem integration can be found in Section 7.2. This is followed by the development and qualification test of the CubeSat. Depending on the result of the tests, the detailed design needs to be adjusted. In case of satisfying results, the flight model of the CubeSat will be produced, which will also be used for the acceptance test.

Before the CubeSat will be shipped to the launch destination, pre-launch tests will be performed, which test the operational performance of the satellite.

After the satellite is launched, it will be operational. At the end-of-life-time, the CubeSat will re-enter the atmosphere. The mission ends with the retrieval of the re-entry capsule.

7.2 Production plan

The manufacturing of the Delta satellite is done in various steps. First, the subsystems are manufactured, finally the satellite will be assembled.

For the manufacturing of the subsystems, first, the different components should be available. Some components will be COTS, others are made within TU Delft, the QB50 payload is produced by VKI and the production facility of the re-entry capsule is not yet decided on. Since the location of the production of components are decentralized, they will all be transported to the TU Delft where the assembly of the satellite take place. All subsystems and payload have a short description of their manufacturing.

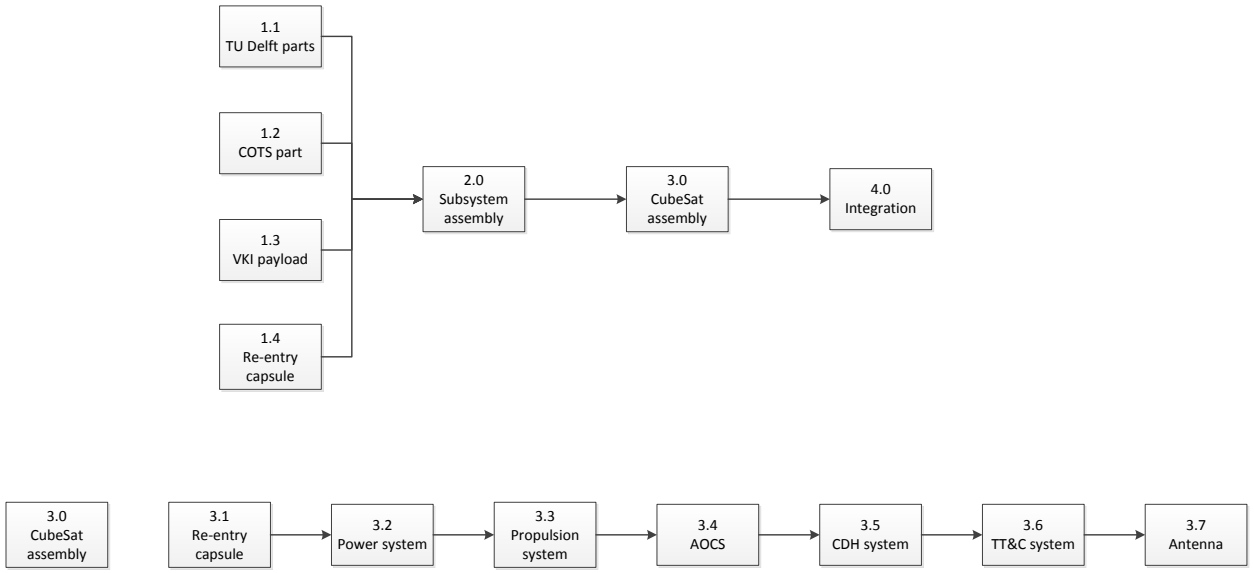

Figure 7.2: The manufacturing and assembly flow diagram

QB50 payload The QB50 payload is manufactured by VKI, no customization has to be done before it can be assembled in the satellite.

DSE payload The DSE payload will consist out of a capsule and an ejection system. The ejection system is manufactured within TU Delft. However the capsule requires more experienced people. Therefore it is manufactured with TU Delft staff and external resources. As this manufacturing is extremely novel, the manufacturing time should be determined with a large margin.

Telemetry, tracking and command system The TT&C will solely consist out of COTS products. The antennas and the transceiver will be ordered and do not require manufacturing.

Structure The structure is divided in an inner and outer structure. The inner structure only has rods which are COTS. The outer structure has two L-shaped plates and a bottom and a top plate which will be manufactured within TU Delft. One L-shape has solar cells and a sun sensor mounted on. The other will accommodate a sun sensor and a nozzle for the propulsion system. It also has the deployment systems attached for the deployable solar panels. Next, the top place has a sun sensor mounted on. Finally, the bottom plate will have the same sun sensor, however it accommodates for the capsule ejection system. The deployable solar panels are attached to the outer structure. The inside of the outer structure is fitted with temperature sensors and thermal tape.

EPS The components which will be delivered are the solar cells, batteries and components of the EPS. The final manufacturing is done within TU Delft. Solar cells will be mounted to the outer structure and on the deployable panels. The G-EPS will be manufactured on a PCB, as well as the batteries.

AOCS The AOCS has COTS products as well as products produced by TU Delft. The magnetometer and two magnetorquers are shipped from outside TU Delft. The reaction wheels and a magnetorquer is designed and manufactured within TU Delft, as well as the final manufacturing of the PCB.

Propulsion system The propulsion system consist out of the 18 MEMS thrusters and cold gas generators. The cold gas generators are COTS products, while the MEMS thrusters are produced at TU Delft. The manufacturing of a PCBs with the components are done within TU Delft.

C&DH Most of the components of the C&DH are COTS products ans some of the components are produced within TU Delft, these components will be placed on a PCB by the TU Delft.

Assembly The assembly of a CubeSat is done by placing the different subsystems and payloads onto the rods in specific order. Next the wiring is placed and finally the outer structure is placed.

7.3 Logistics and Operation Concepts

As soon as the final design has been determined and verified, the satellite will be manufactured. In Section 7.3.1, the logistic concept of the satellite assembly is explained. The logistic organization is particularly important in order to stay within the assigned schedule as well as the assigned budget. Next to the logistics, the operational functions of the ground system also need to be clarified and structured as shown in Section 7.3.2.

7.3.1 Logistic Concept

The organization of the logistics is of crucial importance in order to produce a final product within the given time and budget constraints. Figure 7.3 shows the logistic sequence from the final design until the launch of the Delta satellite in the form of a flow diagram.

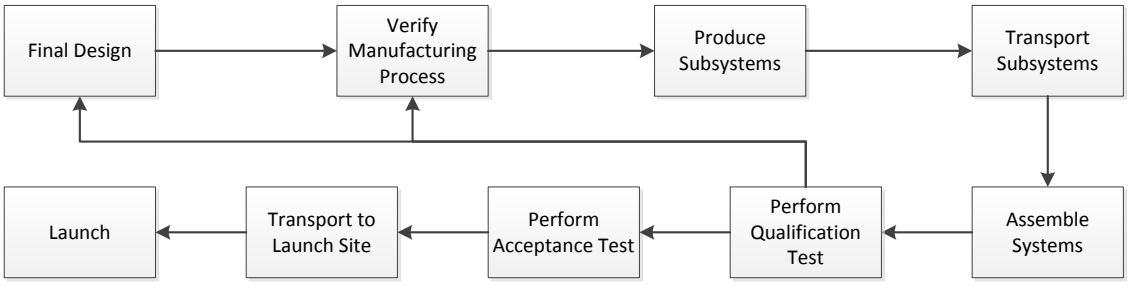

Figure 7.3: Logistic concept of the CubeSat

After the detailed design has been verified and validated, the verification of the manufacturing process can begin. During this process, the manufacturing institutes will be chosen and it will be confirmed that the manufacturing process is indeed feasible and realistic. In case this is not possible, a different manufacturing solution needs to be considered in the last step of the final design.

A vast majority of the subsystem components are COTS products. The production of these products has been decentralized and takes place at different locations around the world. However, not all subsystems will be manufactured entirely as can be seen in Section 7.2. Therefore, after all the products and subsystems are delivered to TU Delft, the remaining subsystems will be assembled.

Subsequently, a Qualification test is executed under ultimate flight conditions. This is followed by an acceptance test. During this test, the CubeSat will be verified with the given operational conditions it has been designed for. In case of deviations of the nominal performance, the malfunctioning subsystems need to be produced again.

Now that all the required tests have been performed on the CubeSat, it will be transported to the launch site.

Besides the CubeSat assembly, the ground segment establishment is also required. The GENSO ground station system will be used for communication. Since the TU Delft is part of the GENSO network, this already existing ground station will be used during the operational phase of the CubeSat.

7.3.2 Operation Concept

After setting up the logistic concept of the mission, the operation concept of the ground station needs to be established. Figure 7.4 shows the flow of the operational tasks of the ground system concerning the CubeSat performance.

Figure 7.4: Operation concept of the CubeSat ground segment

As soon as Delta has been ejected from the launcher, it needs to be assured that the CubeSat is operational. The antenna for communication and the solar cells will deploy autonomously and after different operational tests are performed by the ground station, Delta will be fully operational. The ground segment will provide the satellite with software upgrades during its operational life time to prevent malfunction of the systems. Another important aspect of the ground segment is the communication to control and support the CubeSat. Throughout the life time of Delta, there will be no maintenance on the CubeSat.

7.4 Post-Design Planning

After the Phase A design of the satellite, Delta is further designed. This post DSE phase is divided in different phases. In Figure 7.5, the Gantt chart of the post-DSE phase is shown. As can be seen the first post DSE phase is the development phase, followed by the production and testing phase. The production and testing phase is done in parallel with the ground segment. The operation phase is the phase that involves testing, shipping of the final satellite and the launch. Finally, there is a post-mission phase, where the re-entry capsule is retrieved.

Development phase In the development phase, the Delta satellite is designed in detail and fully verified. Finally, risk management is performed. There is a margin included in case of delays.

Production and testing phase During the production and testing phase, the subsystems and the satellite will be produced, assembled and tested. These test are used for validation and subsystems are integrated.

Ground segment The ground segment consists out of setting up the ground station, and managing the human resources for this ground station.

Pre-mission phase The pre-mission phase involves acceptance testing, shipping of the final satellite. Further, it includes the launch of the rocket and ends when the satellite is deployed.

Mission operation phase The mission operation will contain the most important part of the mission, the actual performing of the objectives. As can be seen this involves the measurements for the VKI and the formation flying. The phase ends with re-entry.

Post-mission phase The purpose of the post-mission phase is the retrieval of the capsule. This phase will end if the capsule is retrieved or when the capsule is not found after a specific period.

ID	Task Name	Duration	Start	Finish
1	**1 Development phase**	**170 days**	**Mon 8-7-13**	**Wed 25-12-13**
2	1.1 Detailed design	80 days	Mon 8-7-13	Thu 26-9-13
3	1.2 CubeSat verification	30 days	Thu 26-9-13	Sat 26-10-13
4	1.3 Risk management	30 days	Sat 26-10-13	Mon 25-11-13
5	1.4 Margin	30 days	Mon 25-11-13	Wed 25-12-13
6	**2 Production and testing phase**	**392 days**	**Wed 25-12-13**	**Wed 21-1-15**
7	2.1 Subsystem production and testing	30 days	Wed 25-12-13	Fri 24-1-14
8	2.2 Subsystem intergration	30 days	Fri 24-1-14	Sun 23-2-14
9	2.3 Manufactering verification	30 days	Sun 23-2-14	Tue 25-3-14
10	2.4 Satellite assembly	30 days	Tue 25-3-14	Thu 24-4-14
11	2.5 Development testing	14 days	Thu 24-4-14	Thu 8-5-14
12	2.6 Test analyis	40 days	Thu 8-5-14	Tue 17-6-14
13	2.7 Qualification testing	14 days	Tue 17-6-14	Tue 1-7-14
14	2.8 Test anabyis	30 days	Tue 1-7-14	Thu 31-7-14
15	2.9 Satellite production	93 days	Thu 31-7-14	Sat 1-11-14
16	2.10 Acceptance test	21 days	Sat 1-11-14	Sat 22-11-14
17	2.11 Margin	60 days	Sat 22-11-14	Wed 21-1-15
18	**3 Ground segment**	**68 days**	**Mon 30-6-14**	**Sat 6-9-14**
19	3.1 Ground station set-up	60 days	Mon 30-6-14	Fri 29-8-14
20	3.2 Human resources	40 days	Mon 28-7-14	Sat 6-9-14
21	**4 Pre-mission phase**	**96,33 days**	**Wed 21-1-15**	**Mon 27-4-15**
22	4.1 Pre-launch test	10 days	Wed 21-1-15	Sat 31-1-15
23	4.2 Test analysis	7 days	Sat 31-1-15	Sat 7-2-15
24	4.3 Shipping	13 days	Sat 14-2-15	Fri 27-2-15
25	4.4 Launch	3 days	Wed 15-4-15	Sat 18-4-15
26	4.5 Satellite deployment	2 days	Sat 18-4-15	Mon 20-4-15
27	4.6 Margin	7 days	Mon 20-4-15	Mon 27-4-15
28	**5 Mission operation**	**124,01 days**	**Mon 27-4-15**	**Sat 29-8-15**
29	5.1 Detumbling	0,8 days	Mon 27-4-15	Tue 28-4-15
30	5.2 Initialization	1 day	Mon 27-4-15	Tue 28-4-15
31	5.3 Formation flying	15 days	Tue 28-4-15	Wed 13-5-15
32	5.4 VKI measurments	123 days	Tue 28-4-15	Sat 29-8-15
33	5.5 Re-entry	0,01 days	Sat 29-8-15	Sat 29-8-15
34	**6 Post-mission phase**	**28 days**	**Sat 29-8-15**	**Sat 26-9-15**
35	6.1 Capsule retrieval	14 days	Sat 29-8-15	Sat 12-9-15
36	6.2 Margin	14 days	Sat 12-9-15	Sat 26-9-15

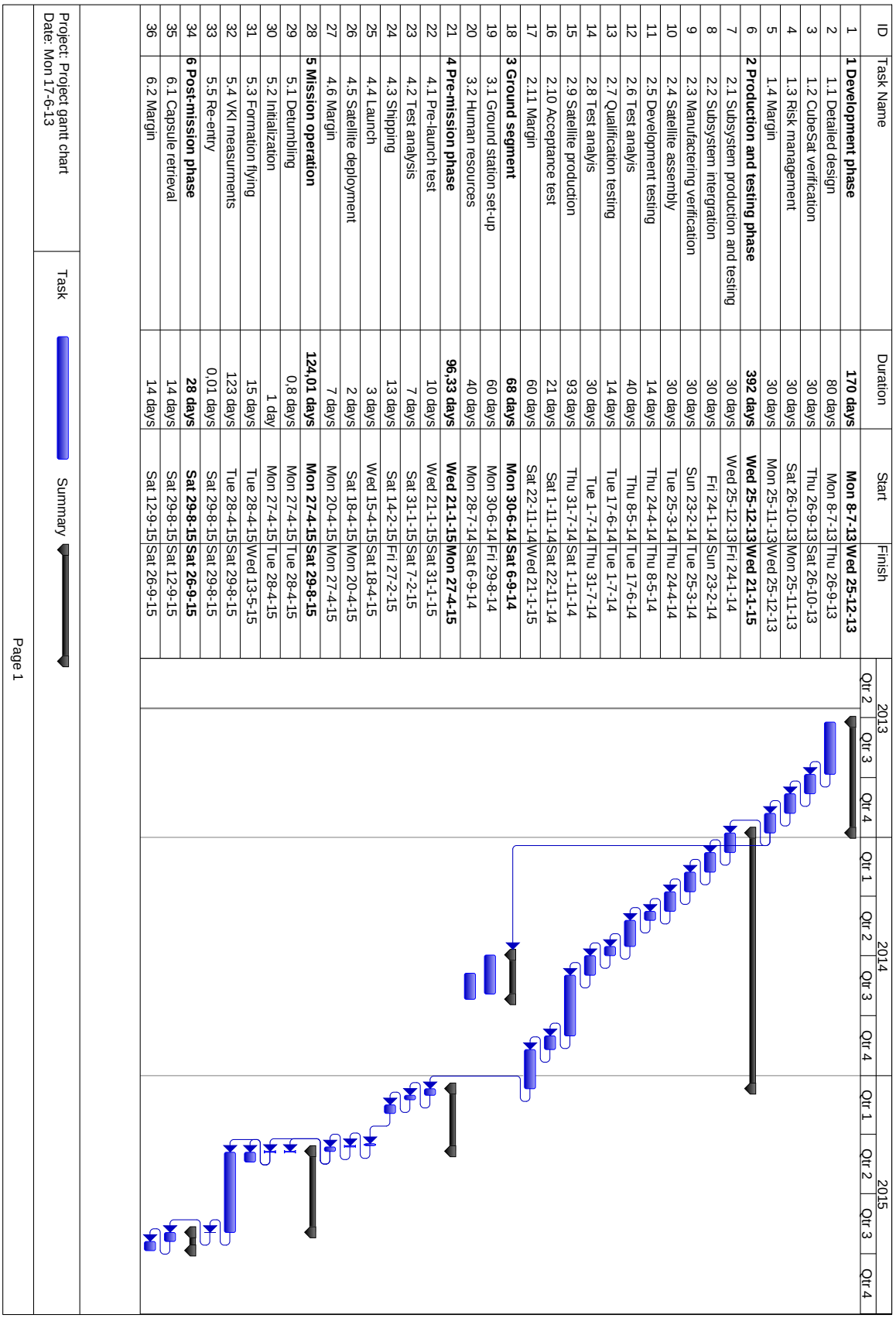

Figure 7.5: The Gantt chart for the post design phase

CHAPTER 8

SUSTAINABLE DEVELOPMENT STRATEGY

In a time where resources are becoming more and more scarce, sustainability becomes more important. The most famous definition of sustainable development is the following:

> *Sustainable development is development that meets the needs of the present without compromising the ability of future generations to meet their own needs.* Brundtland Commission, 1987 [114]

Applying the definition of the Brundtland Commission to nanosatellites implies that they should provide a certain desired function (e.g. observing) using as little resources as possible. This can be achieved in several ways.

8.1 Resources

The following section covers how sustainability is realized within the used resources. This ranges from Commercial off-the-shelf products up to the choice of the heat shield material. In general, the partial non-destructive re-entry mission objective can be used for future CubeSat missions without creating an extra CubeSat which demonstrates the feasibility of that concept.

8.1.1 COTS

A majority of the subsystems uses products that are already developed instead of developing products especially for a certain mission or spacecraft. These products are called Commercial off-the-shelf (COTS).

Using COTS products will reduce the development, testing and manufacturing costs significantly. Especially since mostly previously in-flight tested products have been selected for this mission which also leads to a reduction in risk of failure of these components. Table 8.1 gives an overview of the used COTS products in the various subsystems.

Table 8.1: Selected Commercial off-the-shelf products

Subsystem	**Product**
Structure	Rods
Power	Solar cells Batteries
AOCS	Magnetic torquers Magnetometer Sun sensors GPS receiver
Propulsion	Cold Gas generators
TT&C	UHF/VHF antenna Transceiver
C&DH	SD cards
Thermal	Thermal Tape

8.1.2 Launcher

A launcher is used to put the CubeSat into the desired orbit. Before the final altitude is reached, the launcher crosses the various atmospheric layers and pollutes these segments. Thus, it is of crucial importance to keep the effect of the launcher to a minimum. Therefore, 50 CubeSats are launched at the same time which minimizes the pollution on the different layers of the atmosphere by the launch vehicle.

8.1.3 Heat Shield

During re-entry, the capsule is exposed to large heat loads, therefore, a thermal protection system is needed to prevent damage to the capsule.

A Phenolic Impregnated Carbon Ablator (PICA) heat shield is used for the capsule. Despite the low density of the material, it has a high resistant to heat loads. In previous tests, it could be observed that less than one centimeter has been ablated during re-entry [115]. This means that a significant lower amount of material is needed compared to other methods of TPS.

Due to the low amount of ablated material, PICA can also be reused in case the initial PICA layer is thick enough. In case the heat shield survives re-entry without damage, the capsule can then be reused for future missions.

It has been determined that during the ablation of PICA different gases are created [116]. Two gases are toxic when inhaled by humans: cyanide and hydrogen cyanide. During ablation only a small amount of mass is ablated and therefore, the ecological footprint is kept to a minimum. Since the ablation process occurs at an altitude of about 60 km, the gases disperse in the upper atmosphere. Furthermore, the heat shield rapidly cools at lower re-entry, which means that no emission occurs at low altitudes, leaving no danger for humans.

8.1.4 Miniaturization

Throughout the design of the subsystems, COTS products are used if possible. However, there are also subsystems that do not consist of COTS, since these products are not suitable for the given mission. One of these subsystems is propulsion. The propulsion system on board of the CubeSat has been specifically designed to perform formation flying. With the demonstration that further miniaturization of components is feasible, the road is paved for future CubeSat mission. Propulsion has not frequently been done before on CubeSats, therefore, this mission can provide a propulsion system for future satellites.

8.2 Space Debris

Another aspect of sustainability is to mitigate space debris, this way orbits can be used for future missions without an increase in risk [117].

The United Nation guidelines on space debris mitigation state on that topic that

> *the long-term presence of spacecraft (...) in LEO after the end of the mission should be limited.* [117]

The low initial orbit altitude (320 km) will assure that the CubeSat will burn up after the scientific missions have been completed. Thus, no space debris will remain in orbit which is beneficial for future space missions (see the second part of the quote of the Brundtland Commission). Furthermore, the natural decay of the CubeSat does not require an additional end-of-life disposal which leads to a saving in resources.

CHAPTER 9
COST ANALYSIS

In the following chapter, a cost analysis is performed. Due to the increasing demand in low cost satellites, CubeSats opened an entire new market. To get an impression on the existing products as well as the potential new markets that can be set up with the DelFFi mission, a market analysis is performed in Section 9.1. This is followed by a cost break-down structure in Section 9.2, which presents the costs of the post-DSE phase. Finally, the financial budget for the material as well as the man hours is shown in Section 9.3.

9.1 Market Analysis

Besides being an educative platform, CubeSats are also very cost efficient products to perform missions. Therefore, the nanosatellite market is constantly growing. A major advantage of these satellites is that multiple CubeSats can be launched with one launcher, thus, the launch costs per satellite are significantly lower compared to other satellites.

Even though the nanosatellite market is already advanced, there is still enough room for new, more efficient products. Next to subsystems that can be further developed, also new technology can be demonstrated with CubeSats.

The aim of nanosatellites is to perform missions which are now exclusively executed on larger, heavier satellites. Thus, demonstrating that a concept that has been used on larger satellites can also be performed on nanosatellites leads to an entire new market especially in the field of sustainability.

9.1.1 Competitors

Various manufacturer of CubeSats sell COTS products, which make the CubeSat a low cost satellite. These manufacturers take up the majority of the CubeSat market.

COTS products have the advantage that the development costs are significantly decreased and therefore lead to a reduced total hardware cost. Consequently, a majority of the CubeSats launched and to be launched consist of COTS product. It should always be kept in mind that since CubeSats are low cost products, also larger risks can be taken, which means that redundancy of components is of less importance compared to more expensive missions. The average costs per CubeSat per kg is US$ 560,000 in 2011 [118] including development, hardware and launch costs. Six of the 16 CubeSats launched, where designed with student participation.

However, there is always the option to make components more efficient in terms of performance, weight and costs. Considering the available propulsion COTS products, none meet the requirements for the DelFFi Delta mission. Therefore, a propulsion system developed by TU Delft, University of Twente and TNO will be used which has the potential to become a COTS product.

Moreover, the scientific value of CubeSat demonstrations delivers a wide variety of opportunities. Even though formation flying has been demonstrated on larger missions, it has not yet been done on CubeSats, which will lead to an entire new market segment.

9.1.2 Current Markets

The market for nanosatellites was started at the beginning of the space age, however small. In 2000 the CubeSat standard was developed by California Polytechnic State University and Stanford University and many nanosatellites were based on this standard, this led to a growth in nanosatellite market. In 2012 the number of launches was 35 [119, p. 7]. Between 2000 and 2012 59% of the nanosatellites were designed by the civil sector, such as Universities. The government designed 30%, either by defense or non-defense.

With the standardization of the CubeSat the COTS products market has grown, which makes it more beneficial to design and manufacture COTS. For the current market the COTS products most of the time consist out of miniaturized technology, which keeps improving. However, not all subsystems has a many OTS products, such as propulsion system. This gives a opportunity to show this technology and improve on the capabilities of CubeSats.

9.1.3 Future Markets

With larger projects, such as the QB50 project, the number of CubeSat launches a year is expected to grow. [119, p. 10] shows that most of the announced nanosatellites will be 1 to 3 kg, which are mostly CubeSats. Therefore, the market for nanosatellites is assumed to increase [119, p. 6]. As is expected the number of nanosatellites launched is expected to grow to 121 to 188 satellites in 2020. From the announced nanosatellites an average growth of 16.8% per year over the next seven years will occur. With unannounced satellites this is expected to be 23.4% [119, p. 13].

This will give many opportunities to design COTS products which can be used for the future CubeSats. This can be seen by the current suppliers of COTS for CubeSats, as they expected an increase of growth in the upcoming seven years [119, p. 11].

The Delta satellite has several subsystems or components of subsystems that can be used in future designs. This can be favorable for future TU Delft missions as well as other CubeSats. Next the technology shown, such as formation flying, demonstrates future use for CubeSats.

The PNR objective can show a cheap manner to test re-entry, this could be very beneficial for future studies.

9.2 Cost Break-down Structure

The Cost Break-down Structure (CBS) contains all cost elements of the post-DSE project activities and was derived from the Project Design & Development logic. It has mainly been used to develop the financial budget. The CBS is somewhat broader however, since not everything mentioned will have to be covered by the TU Delft. This mainly includes launch costs. The CBS is shown in Figure 9.1.

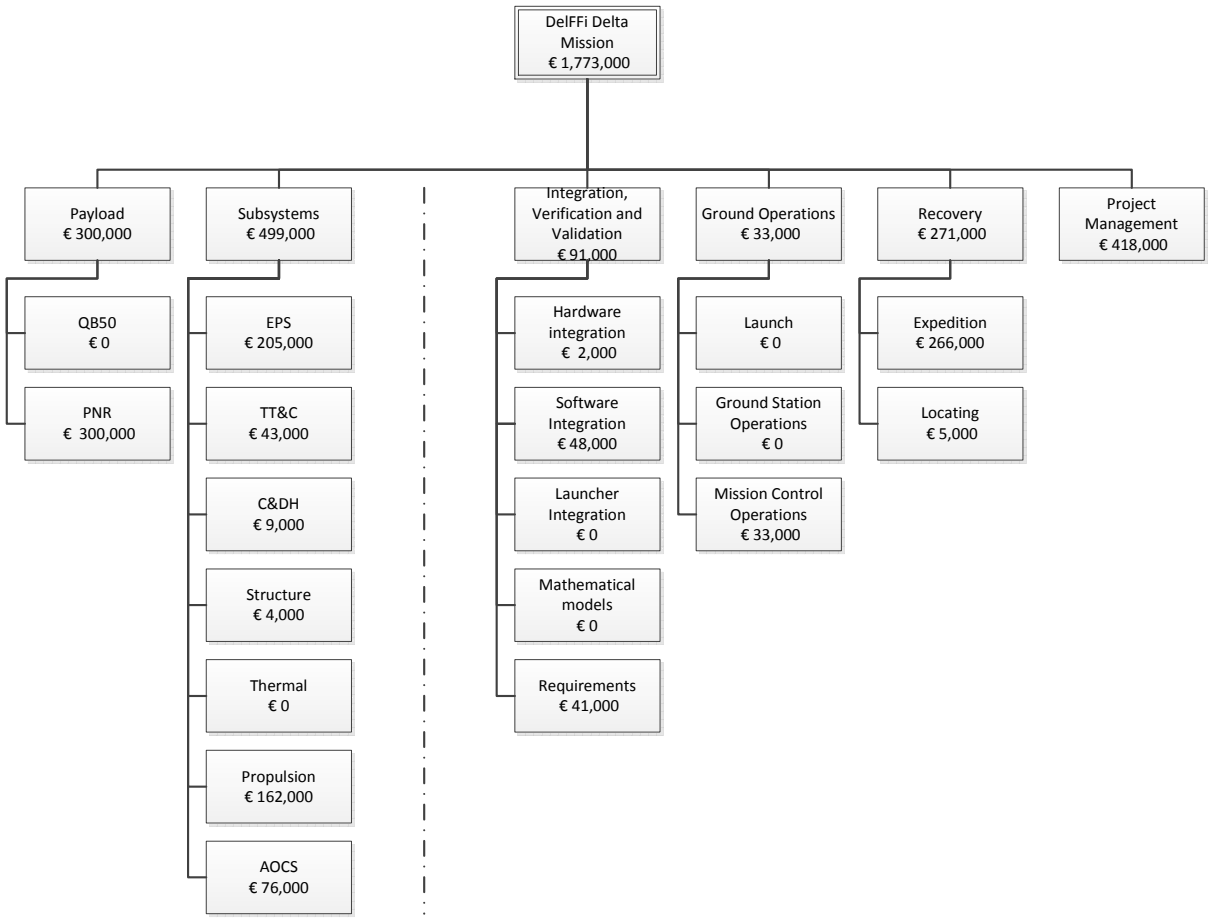

Figure 9.1: Cost Break-down Structure

9.3 Financial Budget

The financial budget for the material is an analog-based estimation. This implies using the cost of a similar item and adjusting it for differences in size or complexity. The main advantage of using this method is the possibility of using it on all levels of detail in the system. The drawback of this method is the assumption that a similar item exists. However, as this is a CubeSat, all the main components and material costs can be estimated this way. This is done in Table 9.1. For the final budget it has been taken into account that all subsystem material costs will have to be doubled to account for the building of a test model.

Table 9.1: Material costs

Subsystems	Description	Cost per part [€]	Amount of parts	Total cost [€]
AOCS				
	GPS	12,000.00	1	12,000.00
	Magnetometers	11,000.00	1	11,000.00
	Magnetorquers	1,200.00	3	3,600.00
	Reaction wheels	11,430.86	1	11,430.86
Structure				
	Outer structure	1,715.07	1	1,715.07
Thermal				
				0.00
EPS				
	Solar panels	2,750.00	36	99,000.00
	Control board and batteries	3,300.00	1	3,300.00
TT&C				
	Transciever board	8,500.00	2	17,000.00
	Antennas	4,500.00	1	4,500.00
C&DH				
	Micro SD Card	8.20	2	16.40
	OBC	4,500.00	1	4,500.00
	Connection (Ribbon) Cables	2.24	3	6.72
Propulsion				
	Micropropulsion system	81,000.00	1	81,000.00
Total				
				249,000

For the payloads this is a different story. The QB50 payload is given to us by the Von Karman Institute. So no budget is necessary for this payload. The re-entry capsule however is hard to estimate. All smaller elements such as the batteries and beacon can be estimated however the TPS and isolation material costs are hard to predict. This because no data on costs for the PICA material is available. However it can be assumed to be a material only made on demand due to the small amount of applications in which it is used. This will drive the price for the material. The price will mainly include the production process and time. For the re-entry capsule the price has been set to €300,000.00 to have enough room for the material and manufacturing costs.

Furthermore the man-hours have to be included as well, the man hours for the research and development stage can be found in Table 9.2. In this table the manager and other staff members earn the same. This is mainly because there is no difference between them, they are just assigned to different tasks. A gross wage of €60,- per hour has been used to estimate the costs of these staff members. This is based on the gross wage used for the cost estimation of the Delfi-n3Xt.

The production stage consists of hardware and software integration. When considering hardware integration, it is assumed that this will mainly be done by students. However a supervisor is still necessary to guide the project. For hardware integration a time slot of one week is reserved which means the supervisor has to

Table 9.2: Man hour costs

	Description	Cost per hour [€]	hours	Total cost [€]
Staff members	Manager	60.00	3328	199,680.00
	other staff members (4)	60.00	3640	218,400.00
Project members	students (9)	0.00	89600	0.00
Total				**418,000**

be available during that week. For software integration it was found that for small spacecraft it generally includes 1.9% of the total costs [120]. This is however if the total costs include the launcher which is typically 21% of the total costs. Re-evaluating the values, the software integration would take around 2.4% of the two million euros budget. The production costs are listed in Table 9.3.

Table 9.3: Production costs

	Description	Cost per hour [€]	hours	Total cost [€]
Hardware Integration	Supervisor	60.00	32	1,920.00
Software Integration	Software			48,101.27
Total				**50,000**

Finally the post mission and operation costs have to be accounted for. These consist of the retrieval of the re-entry capsule, the ground station operations and mission control operations. The latter one is assumed to be performed by students with the use of the facilities available at the university. However also here a supervisor will be necessary. Therefore, a supervisor is assigned to this for 4 months, which is slightly more than the expected lifetime of the satellite. This is done to account for possible increases in mission duration. For the ground station, the one available at TU Delft is used, which would not imply additional costs for TU Delft. The additional costs that come with the retrieval of the capsule consist of several parts. These parts, together with the values of the ground station operation and mission control operation costs are given in Table 9.4. For the retrieval, an expedition duration of one month is accounted for. The costs were estimated using worst case landing spots and different means of transportation which may be necessary. Furthermore, nine people are assumed to go on this expedition as their are nine people in the DSE group, however as these will probably be different people, a wage is included. As mentioned before in Section 5.6, the satellite is tracked using the Argos network. To gain access to this network a sum of €5,000 has to be allocated [112].

Table 9.4: Post-DSE costs

	Description	Cost per unit [€]	units	Total cost [€]
DSE-mission	Flight	2,237.26 per person	9 persons	20,135.34
	Hotel	4,034.35 / person	9 persons	36,309.13
	Car	973.00 / car	2 cars	1,946.00
	Boat	5,207.50 / boat	1 boat	5,207.50
	Food and drinks	900.00 / person	9 persons	8,100.00
	Capsule tracking			5,000.00
	Man-hours	60.00 / hour	3240 hours	194,400.00
Ground station operation		0.00	550.4	0.00
Mission control operations		60.00	550.4	33,024.00
Total				**304,000**

All of these costs bring the total cost of this mission to €1,773,000. This includes two times the material costs for all the subsystems to create a test model and a margin of 10%. This margin is taken to account for possible errors in the budget estimation due to the nature of an analog-based estimation.

CHAPTER 10

VERIFICATION & VALIDATION

In order to make sure that the mission will be feasible, all the requirements should be met and should be validated against legitimate criteria, this will be the main topic of this chapter.

First all the updated requirements will be given in the same section as the compliance matrix. This matrix will give an overview of which requirements are met at this point and which are not. The next section will discuss the verification and validation of the astrodynamics section. The last section of this chapter is the verification and validation of the re-entry code.

10.1 Requirements

In this section the verification procedure of the requirements is outlined. Firstly, the compliance matrix including the updated requirements are outlined. Then, the four ways in which verification of the requirements can be performed will be explained. Then, the method of verification is explained for all requirements.

10.1.1 Compliance Matrix

This section contains the compliance matrix. It is a matrix in which all requirements are checked when they have been met and otherwise it is explained why they were not met yet. Consequently all requirements are updated. The updates mainly consist of filling in the already known values of <tbd>. In order to keep the matrix manageable not all abbreviations shown in Table 10.1 are used in the code of the requirement itself. Every code in the list consists of the mission code written out and the last abbreviation letters of the full code. The requirement discovery tree can be found in the Baseline Report [1]. The requirements are separated into technical requirements and non-technical requirements (or constraints).

Table 10.1: Abbreviations Requirements Discovery Tree Codes

Abbreviation	Meaning	Explanation
D/DELTA	Delta	The name of the mission
T	Technical	Technical requirement
C	Constraint	Constraint or Non-Technical requirement
GS	Ground Station	Used for mission control or subsequently Ground Station
SS	Space System	The entire space system
LA	Launcher	Used for the launcher system
PAY	Payload	Used for the payload system of the satellite
SB	Space Bus	Used for the Space Bus system
ACS	Attitude & Orbital Control System	Used for the attitude control, guidance and navigational system subsystem
PWR	Power	Used for the power subsystem
PR	Propulsion	Used for the propulsion subsystem
COM	Communication	Used for the communication subsystem
STR	Structure	Used for the structural subsystem
CD	Command and Data	Used for the command and data handling subsystem

Technical requirements

This section states the updated technical requirements.

MISSION CONTROL

☑ **DELTA-GS**	Mission control shall communicate with the satellite via ground stations

☑ **DELTA-GS-1A**	There shall be at least 1 ground station positioned on Earth used by the mission
☑ **DELTA-GS-1.1**	Mission control shall communicate with every ground station via an internet connection
~~**DELTA-GS-1.4**~~	~~The ground station shall receive data~~ *This requirement has become redundant*
~~**DELTA-GS-1.5**~~	~~The ground station shall send data~~ *This requirements has become redundant*
☑ **DELTA-GS-2**	The ground station shall handle data as received from the satellite
☐ **DELTA-GS-2.1**	The ground station shall store <tbd> Mb of data *This depends on the ground station, since the GENSO network will be used*
☐ **DELTA-GS-2.1.1**	The ground station shall store data for <tbd> days *This depends on the ground station, since the GENSO network will be used*
☑ **DELTA-GS-2.2**	The ground station shall receive data with a rate of 4.8 kb/s
☑ **DELTA-GS-2.3**	The ground station shall send data with an rate of 1.2 kb/s
☐ **DELTA-GS-2.4**	The ground station shall process <tbd> Mb of data *This depends on the ground station, since the GENSO network will be used*
☑ **DELTA-GS-2.5**	The ground station shall use the Global Educational Network for Satellite Operations
☑ **DELTA-GS-4**	The TU Delft ground station shall receive a volume of at least 8 Mb of science data per day from the DelFFi Delta satellite

SPACE SYSTEM

☑ **DELTA-SS**	The space system shall consist of a launcher and the DelFFi satellites

LAUNCHER

☑ **DELTA-LA**	The launcher shall bring the DelFFi Delta and DelFFi Phi satellites into orbit
☑ **DELTA-LA-1**	The launcher shall insert the DelFFi satellites into an initial orbit at an altitude of 320 km
☑ **DELTA-LA-2**	The launcher shall insert the DelFFi satellites into an initial inclination of 98°
☑ **DELTA-LA-3**	The launcher shall not interfere with the orbit of the DelFFi satellites upon re-entry
☑ **DELTA-LA-5**	The launcher shall insert the DelFFi satellites into an initial orbit with an eccentricity of 0

PAYLOAD

☑ **DELTA-PAY**	The satellite payload shall operate in a space environment
☑ **DELTA-PAY-1**	The satellite payload shall include measurement equipment for thermospheric observations as specified by the Von Karman Institute
☑ **DELTA-PAY-1-1**	The QB50 science data shall be tagged with the location and time information, within 1 kilometer position accuracy and 1 second time accuracy
☑ **DELTA-PAY-2**	The satellite payload shall fit within the triple unit, 3U, CubeSat
☑ **DELTA-PAY-3**	The satellite shall house the QB50 payload, which has a mass of 600 g
☑ **DELTA-PAY-5**	The satellite payload shall withstand a temperature range from -20°C to 40°C in operational mode

☑ **DELTA-PAY-6**	The satellite payload shall withstand a temperature range from -30°C to 65°C in standby mode
☑ **DELTA-PAY-7**	The DSE mission payload shall not interfere with the QB50 mission and primary payload

SPACE BUS

☑ **DELTA-SB-ACS**	The satellite bus shall contain an attitude control, guidance and navigational system
☑ **DELTA-SB-PWR**	The power subsystem shall provide power for the DelFFi Delta satellite
☑ **DELTA-SB-PR**	The propulsion subsystem shall propel the DelFFi Delta satellite
☑ **DELTA-SB-COM**	The satellite bus shall communicate with the ground stations
☑ **DELTA-SB-STR**	The satellite bus shall provide structural integrity for the subsystems and payload
☑ **DELTA-SB-CD**	The command and data handling (C&DH) system shall handle data

ATTITUDE CONTROL, GUIDANCE AND NAVIGATIONAL SYSTEM

☑ **DELTA-ACS**	The satellite bus shall contain an attitude control, guidance and navigational system
☑ **DELTA-ACS-1**	The attitude control system shall have a pointing accuracy of 2.5 ° in all directions
☑ **DELTA-ACS-2**	The satellite bus shall have a maximum rotation rate of 10 rad/s in all directions
☑ **DELTA-ACS-3**	The guidance and navigational system shall have a relative and absolute navigation measurement accuracy of 1 km
☑ **DELTA-ACS-4**	The attitude determination system shall have an accuracy of 2.5 ° in all directions
☑ **DELTA-ACS-5**	The guidance and navigational system shall have the capability to maintain formation flying
☑ **DELTA-ACS-5.1**	The guidance and navigational system shall maneuver DelFFi Delta and DelFFi Phi within 1000 km along track distance
☑ **DELTA-ACS-5.2**	The guidance and navigational system shall maneuver the DelFFi satellites within a control window of100 ± 10 km with respect to each other
☑ **DELTA-ACS-5.5**	The guidance and navigational system shall keep the Delta and Phi satellites in formation flying when the ACS of the Phi satellite fails
☑ **DELTA-ACS-5.6**	The guidance and navigational system shall demonstrate an active controlled formation flying demonstration for 7 days

POWER SYSTEM

☑ **DELTA-PWR**	The power subsystem shall provide power for the DelFFi Delta satellite
☑ **DELTA-PWR-1**	The power system shall store 20 Wh of energy
☑ **DELTA-PWR-2**	The power subsystem shall provide a peak power of 15.73 W
☑ **DELTA-PWR-3**	The DelFFi Delta satellite shall survive in a powered down state without charging of the power system, inspection or functional testing for a period of up to 24 months
☑ **DELTA-PWR-4**	No electronics shall be active during launch
☑ **DELTA-PWR-4.1**	The energy storage shall be fully deactivated during launch or launch with a discharged energy storage system

☑ **DELTA-PWR-5**	The power subsystem shall provide an average power of 4.5 W
☑ **DELTA-PWR5.1**	The power subsystem shall provide an average power of 2.1 W to the attitude control, guidance and navigational subsystem
☑ **DELTA-PWR-5.2**	The power subsystem shall provide an average power of 0.063 W to the power subsystem
☑ **DELTA-PWR-5.3**	The power subsystem shall provide an average power of 0.255 W to the propulsion subsystem during formation flying
☑ **DELTA-PWR-5.4**	The power subsystem shall provide an average power of 0.25 W to the structure subsystem
☑ **DELTA-PWR-5.5**	The power subsystem shall provide an average power of 1.7 W to the communication subsystem
☑ **DELTA-PWR-5.6**	The power subsystem shall provide an average power of 0.167 W to the command and data handling subsystem
☑ **DELTA-PWR-5.7**	The power subsystem shall provide an average power of 0.530 W to the QB50 payload
☑ **DELTA-PWR-5.8**	The power subsystem shall provide an average power of 0 W to the DSE payload

PROPULSION SYSTEM

☑ **DELTA-PR**	The propulsion subsystem shall propel the DelFFi Delta satellite
☑ **DELTA-PR-1**	Total stored chemical energy shall not exceed 100 Wh
☑ **DELTA-PR-2**	The propulsion subsystem shall provide a total ΔV of 15 m/s
☑ **DELTA-PR-3**	The thrusters shall have a maximum misalignment of 25 ° with respect to the normal plane of the satellite surface

COMMUNICATION SYSTEM

☑ **DELTA-COM**	The satellite shall communicate with the ground stations
☐ **DELTA-COM-1**	The antenna gain shall be at least <tbd> dB *This is not appropriate for 2D omni-directional antennas because they have no gain*
☑ **DELTA-COM-2**	The signal to noise ratio for the spacecraft shall be at least 2.4 dB
☑ **DELTA-COM-3**	The satellite shall have two-way communication with the ground station
☐ **DELTA-COM-6B**	The contact time shall be at least 36 min per orbital period *This requirement can not be checked yet because the exact number of ground stations in the GENSO network at the time of launch is not exactly known yet*
☑ **DELTA-COM-6.1**	The satellite uplink shall be at least 1.2 kb/s
☑ **DELTA-COM-6.2**	The satellite downlink shall be at least 4.8 kb/s
☑ **DELTA-COM-6.3**	The satellite downlink signal shall carry a unique identifier
☑ **DELTA-COM-7**	The satellite shall send data
☑ **DELTA-COM-8**	The satellite shall receive data

STRUCTURE

☑ **DELTA-STR**	The satellite bus shall provide structural integrity for the subsystems and payload
☑ **DELTA-STR-1**	The satellite bus shall have outer dimensions of 100.0 ±0.1 x 100.0 ±0.1 x 340.5 ±0.3 mm at launch
☑ **DELTA-STR-1.1**	The satellite bus shall be designed to prevent cold-welding to the launch vehicle
☑ **DELTA-STR-1.2**	Deployables shall be constrained by the satellite bus

☐ **DELTA-STR-3**	The lowest natural frequency of the satellite bus shall be higher than 90 Hz *This is something that will have to be tested with a real life test model*
☑ **DELTA-STR-4**	The satellite bus shall withstand the operational loads
☐ **DELTA-STR-4.1**	The satellite bus shall withstand 8.3g during launch in x-, y-, and z-direction *This is something that will have to be tested with a real life test model or can be compared to the Delfi-n3Xt after it is launched*
☑ **DELTA-STR-4.2**	The satellite bus shall withstand 37 mN of on-board thruster force during operational lifetime
☐ **DELTA-STR-4.3**	The satellite structure shall posses the characteristics as per Table 3 of [22] *This is something that will have to be tested with a real life test model*
☐ **DELTA-STR-4.4**	The satellite structure shall posses the characteristics as per Table 4 of [22] *This is something that will have to be tested with a real life test model*
☐ **DELTA-STR-4.5**	The satellite structure shall posses the characteristics as per Table 5 of [22] taking into account the shock loads damping during propagation within the spacecraft structure *This is something that will have to be tested with a real life test model*
☑ **DELTA-STR-5**	The satellite shall use space compatible materials
~~**DELTA-STR-5.1**~~	~~Space compatible materials shall withstand 70 *mSv* amount of radiation~~ *This requirement turned out to be irrelevant*
~~**DELTA-STR-5.2**~~	~~Space compatible materials shall withstand all temperatures within <tbd> temperature range~~*This requirement tunred out to be irrelevant*
☑ **DELTA-STR-6**	The satellite bus shall provide thermal control
☑ **DELTA-STR-6.1**	The satellite bus shall operate within $-20°$C to $+40°$C temperature range
☑ **DELTA-STR-6.1.1**	The attitude control, guidance and navigational subsystem shall operate within $-20°$C to $+40°$C temperature range
☑ **DELTA-STR-6.1.2**	The power subsystem shall operate within$-20°$C to $+60°$C temperature range
☑ **DELTA-STR-6.1.3**	The propulsion subsystem shall operate within $-20°$C to $+40°$C temperature range
☑ **DELTA-STR-6.1.4**	The structure subsystem shall operate within$-40°$C to $+80°$C temperature range
☑ **DELTA-STR-6.1.5**	The communication subsystem shall operate within $-20°$C to $+50°$C temperature range
☑ **DELTA-STR-6.1.6**	The QB50 payload shall operate within $-20°$C to $+40°$C temperature range
☑ **DELTA-STR-6.1.7**	The command and data handling subsystem shall operate within $-20°$C to $+85°$C temperature range
☑ **DELTA-STR-7**	The satellite shall have an available volume of 500 cm^3 to allocate the QB-50 payload
☑ **DELTA-STR-9**	The satellite bus shall provide integration options for subsystem integration
☑ **DELTA-STR-10**	The satellite shall have a maximum total mass of 3.6 kg
☑ **DELTA-STR-11**	The satellite center of gravity shall be located within a sphere of 20 mm from its geometric center

COMMAND AND DATA HANDLING SYSTEM

☑ **DELTA-CD**	The command and data handling (C&DH) system shall handle data
☑ **DELTA-CD-1**	The processing speed shall be ¿ 8 MHz
☑ **DELTA-CD-2**	The C&DH system shall have a data storage capacity of 1.9 GB
☑ **DELTA-CD-3**	The satellite shall collect orbit data and log telemetry every 60 seconds
☐ **DELTA-CD-4**	The satellite systems shall power-on within 30 minutes after deployment *Only the AOCS, C&DH and Power system will be activated immediately after deployment, the rest of the systems will be activated after the detumbling fase, so after 1 day*
☑ **DELTA-CD-5A**	The satellite shall send the data which is needed by ground control
☑ **DELTA-CD-5.2**	The satellite shall send a volume of at least 8 Mb of science data per day to the ground station network
☑ **DELTA-CD-5.3**	The ground station shall be able to request and obtain additional data from the satellite
☑ **DELTA-CD-6**	Any computer clock used shall exclusively use Coordinated Universal Time (UTC)/Greenwich Mean Time (GMT) as time reference
☐ **DELTA-CD-7**	During pre-launch processing and launch, the spacecraft on-board equipment and ground support equipment (GSE) shall sustain the electromagnetic fields of up to 10 V/m (TBC) within 10 kHz to 40 GHz *This is something that will have to be tested with a real life test model*

Non-technical requirements

In this section all updated non-technical requirements are listed.

BUDGET	
☑ **DELTA-C-1**	The cost of the entire mission shall be within budget
☑ **DELTA-C-1.1**	The development, production and operational costs shall not exceed 2 million euros
~~**DELTA-C-1.2**~~	~~The operational costs shall not exceed <tbd> euros~~ *This requirements was double*
☑ **DELTA-C-1.3**	Phase 0 and A shall be completed within 3600 man-hours
SAFETY	
☑ **DELTA-C-2**	The safety of the mission shall be guaranteed
~~**DELTA-C-2.1**~~	~~The satellite shall have a predicted minimum close approach of <tbd> m with respect to other objects~~*This is something that did not have to be taken into account after all*
☑ **DELTA-C-2.2**	When the satellite is not in normal operational mode, communication mode detumbling mode or formation flying mode, the satellite shall go into safe mode
☑ **DELTA-C-2.3**	No pyrotechnics shall be installed on the satellite
SUSTAINABILITY	
☑ **DELTA-C-3**	The mission shall be sustainable
☑ **DELTA-C-3.1**	The satellite shall be out of orbit within 25 years after end of life
☑ **DELTA-C-3.2**	The satellite shall contain no hazardous materials, as found in [121]
☑ **DELTA-C-3.4**	The satellite shall not use any materials that have a potential to degrade during the 2 year storage after assembly

☑ **DELTA-C-3.6**	Satellite materials shall satisfy the low out-gassing criterion
☑ **DELTA-C-3.6.1**	Total Mass Loss (TML) shall be less than or equal to 1.0%
☑ **DELTA-C-3.6.2**	Collected Volatile Condensable Material (CVCM) shall be less than or equal to 0.1%
☑ **DELTA-C-3.7**	The satellite shall create no unnecessary space debris during deployment and operation

SCHEDULE

☐ **DELTA-C-4**	The mission shall be completed on schedule *At this point, this requirement is not satisfied yet because the process has not been finished*
☐ **DELTA-C-4.2**	The satellite shall be launched in April 2015 *This can still be changed by QB50 and will also depend on the company launching the satellites*
☐ **DELTA-C-4.2.1**	The production and verification of the satellite shall be completed at least 3 months before launch *At this point, this requirement is not satisfied because the process has not been finished*
☐ **DELTA-C-4.2.2**	The launcher vehicle shall be available at least <tbd> days before launch *This will depend on the company launching the satellites*
☑ **DELTA-C-4.3**	Phase 0 and A shall be completed before July, 2nd 2013
☑ **DELTA-C-4.4**	The satellite shall have an initialization time of maximum 9 days after orbit injection
☑ **DELTA-C-4.5**	The formation flying demonstration shall have a duration of 7 days
☑ **DELTA-C-4.6**	The formation flying demonstration shall be performed directly after satellite initialization
☑ **DELTA-C-4.7**	The mission operation life time will be 3 months

Key and Killer Requirements

This section will show the key requirements from the list stated in the previous section. Since during the process of making the requirements list, the possibility of the requirement was already taken into account, there are no killer requirements to be found.

The key requirements consist of the stated requirements:

- ☑ **DELTA-PAY-1** The satellite payload shall include measurement equipment for thermospheric observations as specified by the Von Karman Institute
- ☑ **DELTA-ACS-4** The guidance and navigational system shall have the capability to maintain formation flying
- ☑ **DELTA-PWR-5** The power subsystem shall provide an average power of 4.5 W
- ☑ **DELTA-STR-1** The satellite bus shall have outer dimensions of 100.0 ±0.1 x 100.0 ±0.1 x 340.5 ±0.3 mm at launch
- ☑ **DELTA-STR-10** The satellite shall have a total mass of 3.6 kg
- ☑ **DELTA-C-4.7** The mission operation life time will be 3 months

10.1.2 Verification of Requirements

The different verification methods for every requirement have been discussed in the Midterm report [4]. In this section the focus will lie on the verification that could be done in the DSE period, this will mainly be analysis. First the key requirements are going to be discussed, after which the requirements that were found to be critical are verified. Finally the requirements that can be verified due to analysis will be discussed.

Key Requirements

The key requirements are verified as stated:

- **DELTA-PAY-1** In the final satellite payload, the QB50 payload has also been included and it has been shown that there is enough space to allocate this.
- **DELTA-ACS-4** The AOCS has been designed for a precision accuracy of 2.5°, and sensors and actuators have been chosen accordingly.
- **DELTA-PWR-5** A test has not been performed yet however, the calculations performed on the power analysis confirm that the requirement will be met, because this also includes a margin.
- **DELTA-STR-1** From computer drawings it has been observed that the dimensions are met.
- **DELTA-STR-10** The satellite itself has not been weighed yet, however the weight estimations show that the satellite mass is within the 3.6 kg.
- **DELTA-C-4.7** The mission operation life time will be 3 months.

Critical Requirements

- **DELTA-GS-4** Since the GENSO network will be used, a volume of 8 Mb can be received by the ground stations.
- **DELTA-LA-1** From the TU Delft it has been determined that the final altitude will indeed be 320 km.
- **DELTA-PAY-3** The final mass for the sensors have been set by VKI.
- **DELTA-PAY-5** The payload sensors have been selected by VKI to meet this requirement.
- **DELTA-PAY-6** The payload sensors have been selected by VKI to meet his requirement.
- **DELTA-ACS-1** The computer models have shown that the AOCS can obtain and maintain a pointing accuracy of 2.5°, and the sensors have been selected accordingly.
- **DELTA-PR-1** This has not been measured yet because the test model has not been made, however the propulsion system has been sized such that the total chemical energy will not exceed 100 Wh.
- **DELTA-COM-2** This has not been tested yet, however the link budget shows that the signal to noise ratio shall be at least 2.4 dB.
- **DELTA-STR-6.1** According to the thermal calculations the bus shall stay withing the temperature range.
- **DELTA-CD-1** The specifications have shown that the processing speed is indeed 8 MHz.
- **DELTA-CD-5.2** Since the extensive data budget shows that the total amount of science data send per day will be 12 Mb, this meets the 8 Mb requirement

Other Requirement

All other requirements that could be verified by the use of analysis have been verified at this stage of the design and development process. The list of verification methods per requirement can be found in the Midterm report [4]. All other requirements will be verified at a later stage during development and production of the satellite. In the compliance matrix most of the requirements could be checked off because they have been taken into account during the satellite design phase, however they should still be verified.

The analysis has been perform using computer models, simulations and CATIA drawings. At the beginning of the production stage, a test model will have to be produced which will be used to test, demonstrate and inspect. At that stage all other requirements can be verified before the final satellite is build, however the requirements that should be verified first when the test model is ready are: PWR-1, PWR-2, PWR-5, PR-2, PR-3, STR-4.1 and STR-4.2. This should be done, because they either are not verified yet by analysis or may take a long time to be redesigned if the requirement is not met afterall.

10.2 Astrodynamics

This section will handle the verification and validation of the astrodynamics code. As not many results are to be found on this subject, the verification is done using the plots to check whether the parameters behave as expected or not. The validation is split up into different parts, the part for formation keeping is done based on a paper published by E. Gill [18]. The density model is checked by comparing the air density values for the expected solar activity to the air density values for mean and low solar activity [122].

Verification

Figure 10.1a shows the density compared to the altitude which is encountered over the mission duration. Therefore note that the relationship shown also includes a time component. This is explains why there is a slight deviation from the expected linear relation between density and altitude. Taking a close look at Figure 10.1a there are huge deviations in the density on about the same altitude, at the beginning of the curve. These can be explained by realizing the effect the time component has on this curve. This time component influences the density in terms of solar activity at that time. More time is spend at higher altitudes, as the decay rate increases over time. This explains the extreme variations in the beginning of the curve as more points are set up for these altitudes and therefore, more variations due to time are apparent. The altitude curve, Figure 10.1b, shows the four different parts of the flight.

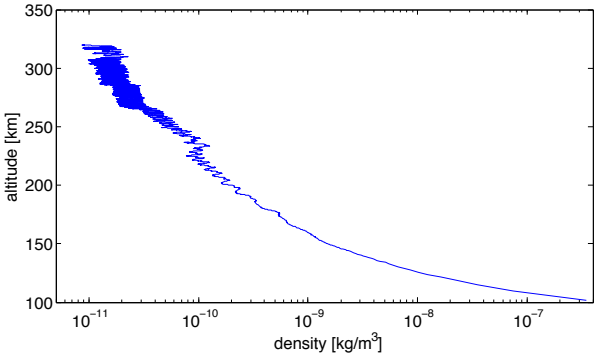

(a) Density change over altitude

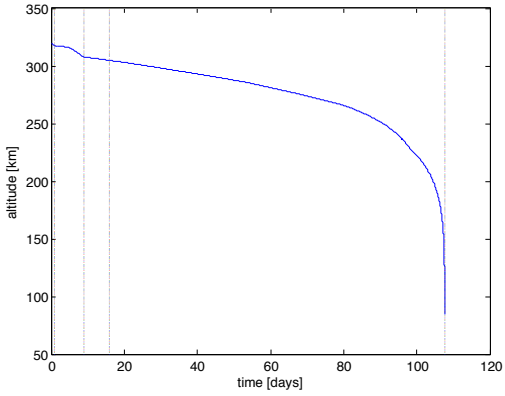

(b) Altitude change over time

Figure 10.1: Orbital decay parameter

First the detumbling phase is shown which has a duration of approximately one day. The second part is the formation acquisition which is described in the 8 days after the detumbling phase. Next the formation flight is described, in this graph an optimal formation flight is described. The formation flight lasts for 7 days. Finally the further decay is described until one orbit in which it would reach the 90 km boundary. This graph clearly shows how the orbital decay is affected by the change in attitude. As expected the larger the angle of attack the faster the decay. This is most clearly seen in the acquisition phase where the first four days are in optimal flight condition (α=0°). Where the last four days of the acquisition phase are performed under an angle of attack of 35° (α=35°) . Furthermore it is clear that the decay under the same angle of attack goes faster the lower the altitude. This is because the increase of air density which implies an increase in drag at lower altitude.

The velocity is expected to decrease due to the drag. In the Figure 10.2 this is shown. When comparing it to the altitude curve given by Figure 10.1b it is clear that the velocity and the altitude are related to each other. When looking at the equations stated in Section 3.2 it can be seen that the equation for the velocity decay is based on the equation for the altitude decay. Therefore it is logical that both curves look similar. When looking at the values it can be seen that the velocity only drops about 200 m/s. The reason for this small amount is mainly due to the exchange between potential and kinetic energy. If the satellite drops in altitude, the satellite increases its velocity. However as the drag is still the determining factor the velocity will still decrease according to the drag.

To validate the atmospheric model the density values from the script are compared to the density values for mean and low solar activity [122]. As explained earlier the expected solar activity for 2015 was converted back to an earlier time where the same solar activity was present. From that the air density would be expected to lay between mean and low solar activity therefore it is compared to both these cases. The validation is done by comparing the values for five different altitudes. This comparison can be seen in Table 10.4

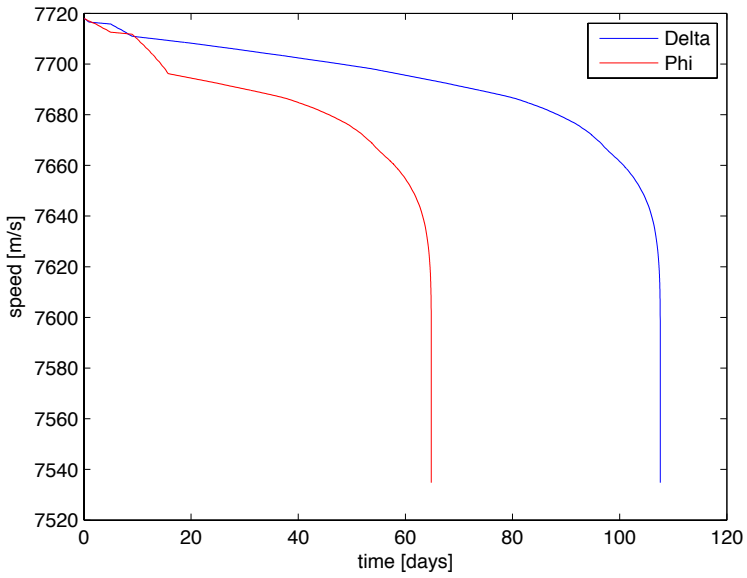

Figure 10.2: Velocity change over time

Table 10.4: Density comparison

	Density		
Altitude [km]	**Model [kg/m^3]**	**Mean solar activity [kg/m^3]**	**Low solar activity [kg/m^3]**
320	$8.9453{\cdot}10^{-12}$	$1.72{\cdot}10^{-11}$	$4.21{\cdot}10^{-12}$
300	$1.7954{\cdot}10^{-11}$	$2.58{\cdot}10^{-11}$	$7.22{\cdot}10^{-12}$
280	$2.0756{\cdot}10^{-11}$	$3.94{\cdot}10^{-11}$	$1.27{\cdot}10^{-11}$
260	$6.0915{\cdot}10^{-11}$	$6.16{\cdot}10^{-11}$	$2.30{\cdot}10^{-11}$
240	$6.5135{\cdot}10^{-11}$	$9.91{\cdot}10^{-11}$	$4.31{\cdot}10^{-11}$

Looking at Table 10.4 it can be stated that the values for the density model used within the code are realistic. They also tend to go more and more to the low solar activity values which is good as the predicted curve for solar activity along time is going to the minimum as well.

Validation

For formation keeping Equation (3.17) is checked using a paper of E. Gill [18]. In this paper the values in Table 10.5 are used. According to there computations, this produces a ΔV of 0.1 m/s per day for an altitude of 300 km. Using Equations (3.6) and (3.17) combined with the values from Table 10.5 the same values for the ΔV are obtained.

Table 10.5: Input values for validation of astrodynamics code

Parameter	**Value**
ρ [kg/m^3]	$35{\cdot}10^{-12}$
A/m [m^2/kg]	0.01
C_d [-]	2.3

The same equations are used for the formation acquisition to determine the attitude positions. Therefore the formation acquisition is validated as well.

10.3 Re-entry Code

Since the calculations for the ballistic and gliding re-entry were done with MATLAB, the code needs to be validated. Since the initial re-entry calculations were done by deriving a model from [82], the new MATLAB model should have the same output as the model from [82]. Therefore, the same input as [82] was used to validate the re-entry code. If the output is the same, the model will be validated.

Ballistic re-entry

The input values that were used to calculate the ballistic re-entry parameters in [82] can be found in Table 10.6. From these values, the outputs were calculated with MATLAB and can be found in Table 10.7. These were then compared with the output values that were obtained in [82].

Table 10.6: Input values for calculating the ballistic re-entry parameters

Input parameter	g_0 [m/s^2]	R [m^2/s^{2}K]	T [K]	γ [°]	V_E [m/s]
Value	9.81	287	256	-20	7000
Input parameter	C_D [-]	C_f [-]	d [m]	m [kg]	
Value	1	0.08	0.3	115	

Table 10.7: MATLAB output values for the ballistic re-entry parameters

		$\frac{V}{V_E}$ [-]	h [m]
$q_{c_{max}}$	Laminar	0.85	h'+7900
	Turbulent	0.77	h'+4510
Maximum heat flow $\frac{dQ}{dt}$		0.72	h'+2951
Maximum deceleration $\left(\frac{a}{g}\right)_{max}$		0.61	h'

Table 10.8: Output values for the ballistic re-entry parameters for the model from [82]

		$\frac{V}{V_E}$ [-]	h [m]
$q_{c_{max}}$	Laminar	0.85	h'+7910
	Turbulent	0.77	h'+4526
Maximum heat flow $\frac{dQ}{dt}$		0.72	h'+2919
Maximum deceleration $\left(\frac{a}{g}\right)_{max}$		0.61	h'

After comparing Table 10.7 with Table 10.8, slight differences between the altitude values are noticed. The differences between the altitude values can be linked to the step size that was used for the time steps. Furthermore, a small adjustment had to be made to the MATLAB script to avoid singularities in the output, which induced a small error. However, since the errors in the altitude are very small, the model can be assumed to be properly working.

CHAPTER 11
CONCLUSIONS AND RECOMMENDATIONS

In the following chapter the main conclusions with respect to the DelFFi mission are drawn. Moreover, various recommendations are given for future research and development, in order to further improve the design of the CubeSat.

11.1 Conclusions

The purpose of this project is to show the steps and decisions that were taken during the Phase-0 design of one of the new satellites of TU Delft, the Delta CubeSat. The design is performed on a subsystem-level. The main conclusions that were drawn are stated below.

Astrodynamics Formation acquisition starts after the detumbling phase. The formation flying will start after the initialization period of 9 days. At this point the satellites will haven an along track distance of 1000 km. The formation flight is done by the Leader-Follower structure, at which the role of the leader and follower will be alternated. The formation flying demonstration is performed for 7 consecutive days. The ΔV needed for this In-Orbit Demonstration is 6.75 m/s per satellite. After the formation flight the satellite will have acquired the attitude with the lowest drag, in order to increase the mission lifetime. After this, the satellite will decay due to the high aerodynamic drag and the low altitude in approximately 3.5 months, after which it will re-enter the atmosphere.

Subsystems The subsystems within the Delta satellite are designed to a component level design. Most of the subsystems have COTS components, due to the standardization of the CubeSat. However, for some components customized or even custom made parts were used. To obtain the required power delivered from the solar cells, two deployable solar panels are used together with solar cells on the body of the satellite. All solar cells are located on one side of the satellite. Therefore, the Delta satellite is pointed along its long axis in an attitude direction with respect to the sun. This will be done by the AOCS, which uses three magnetictorquers and three reaction wheels as actuators, and a magnetometer , a mems gyro and six sun sensors for attitude determination. After detumbling the satellite will be kept in a lowest drag attitude, this means the top of the satellite will be in direction of flight. The orbital location is measured by a GPS sensor. The propulsion system, capable of a delivering ΔV of 15 m/s, is used for the formation flying mission. It consists of 18 Cold-Gas Generators, 16 MEMS Resistojets and a storage tank. The thrust line of the nozzles of the Resistojets will be as close to the center of mass as possible, which means only a low disturbance torque is induced. Therefore, the propulsion system is located in the middle of the satellite. This means the satellite needs to rotate 90° to have the nozzle facing the line of flight, which is required to deliver the ΔV.

Partial non-destructive re-entry The re-entry capsule will be deployed by a deployment mechanism that was custom designed for this mission. The deployment will happen from the rear of the satellite and the capsule will be deployed with the heat shield in the direction of the velocity. After deployment, the capsule will re-enter the atmosphere. The heat shield consists out of a 9 mm layer of PICA, which is a heat resistant ablator, and a thermal insulation layer of 3 mm will protect the capsule from the heat that is generated during re-entry. The capsule will land with a terminal velocity of 18 m/s in a landing zone with a footprint of 1850 km by 107 km. To locate the capsule, the Argos network will be used. The hardware that is required to use this network are a GPS receiver and a UHF transponder to communicate with the Argos satellites. These components are fitted inside the capsule.

Post-design phase The post-design phase will include a more detailed design of the subsystems and the re-entry capsule for the PNR mission. Recommendations to improve the designs of the subsystems and the capsule can be found in Section 11.2.

Cost analysis The cost analysis includes a market analysis, which concluded that the markets for nanosatellites are continuously growing. A growth of the nanosatellite market of 16.8% to 23.4% per year is expected during the next seven years. The financial budget that was created for this report concluded that the DelFFi Delta mission will stay within the € 2,000,000 budget during design, launch, operation and retrieval of the capsule. The total costs of the Delta mission are estimated to be € 1,772,000. This includes a 10% margin to include growing costs.

Sustainable development strategy The sustainability analysis that was conducted concluded that the two main parameters that influence the sustainability of the satellite are resource management and space debris mitigation. Resource management will be done by using a large amount of COTS, launching all 50 CubeSats with one launcher and an effective use of the data communication. Space debris mitigation is done by using the fact that the satellite will have an orbital decay that makes sure that the satellite will burn up in the atmosphere at end-of-life. This is a result of the low initial altitude at which the satellites will be launched. Because of this, no additional space debris will be created during this mission.

11.2 Recommendations

This section lists recommendations for further design implementations, which can lead to an improved design of the CubeSat structure, the formation flying mission and the partial non-destructive re-entry.

11.2.1 Formation Flying

- *Perform more research on decay equations.* Currently, the decay equations are based on energy methods and circular orbits. Although due to the small eccentricity of the orbits they can be assume circular, the parameters are not related with a continues circular orbit. This mainly has an influence on the velocity. As the velocity of a circular orbit should increase as it descends, the actual velocity of the Delta satellite will drop. This implies that an error is induced. Therefore more accurate decay equations have to be found for better estimations of all the orbit parameters over time.
- *Explore the possibility of differential drag use for formation keeping.* Currently active propulsion is used for formation keeping. However, it might be possible to do this with the use of differential drag. For this design of the satellite active propulsion was chosen to enable faster response to possible changes. However, the possibility of differential drag will also be shown during the acquisition phase. Therefore it might also be possible to use it for the formation keeping.
- *Process formation flying control data on-board.* Due to the use of a small, energy efficient On-Board Computer, it was not feasible to perform full mean orbital element estimation and calculate control data on board of the satellites. Instead, a scheme was supposed with the ground station in the loop, which is not problematic for this mission as the orbital data was relayed through Earth anyway. Future missions might have an inter-satellite link and it would be useful and perhaps even more energy efficient to calculate the required data on board. This would realize a more autonomous form of formation flying, paving the road for future missions consisting of multiple satellite constellations. An alternative scheme with the ground station out of the loop was already presented in Figure 3.11.

11.2.2 EPS

- *Look for and test for better conversion efficiencies.* The current electric power system, loses a lot of power due to the conversion between the wiring bus, batteries, G-EPS and subsystems. With better efficiencies the required power delivered can be lower, what result in a larger margin on the power and there for more redundancy.

11.2.3 AOCS

- *Perform a better research on the aerodynamics of the satellite.* The satellite will experience a lot of drag, therefore the aerodynamic stability give a clear indication of the attitude at the lower altitudes.
- *Perform GPS radio occulation.* With the use of a GPS receiver and antenna it is possible to do some more measurements like GPS radio occultation (RO) measurements. Such a mission has been explained in the mid-term report [4] and can actually be done next to a Partial Non-Destructive Re-entry mission. The choice has been made to focus on one mission only, this way one mission will be properly worked out instead of two missions halfway due to time constraints. Although GPS RO can be done, it comes at the cost of selecting slightly different components and a higher power use. In this case the receiver and antenna will be replaced with the Novatel 6-15 and the AeroAntenna AT2775-103O. The receiver has almost the same dimensions but the antenna does quite differ, this should be taken into account.

11.2.4 Propulsion

- *Investigate the possibilities of propellant heating.* If the propellant is heated, the specific impulse could increase to 104 seconds [68]. This would result in less propellant mass required. However, the influence of internal heating on the satellites temperature needs to be investigated as well. Another aspect that needs to be considered is the amount of required power for the heating of the propellant.

11.2.5 TT&C

- *Look for a transceiver PCB that has a redundant system in one board.* Currently, two transceiver PCBs are implemented in the CubeSat to provide redundancy. However, there should also be the option to have a completely redundant transceiver system installed on only one PCB. This requires more research.
- *Fit an inter-satellite link in this or a future satellite design.* There are advantages to equipping formation flying satellites with inter-satellite links: Near real-time feedback on satellite positions can be achieved, allowing for missions with more stringent requirements on formation flying capabilities.

11.2.6 C&DH

- *A final check has to be done on the different sensors to make sure the data rates are correct.* At this point, the time the sensors have to be active has been chosen, however it should be checked if this has been done correctly. It could be, that the data rate will oscillate with a lower constraint of 8 MB/s because the sensors do not have to be active for the amount of time that is specified in this report.
- *Make sure that getting household data every minute for one second will be enough or is even too much.* When the final subsystems have been build, one could do a final check to see if the amount of household data that is transmitted by the satellite is enough to get an accurate picture of the current satellite situation.

11.2.7 Physical Appearance

- *Perform an accurate center of mass calculation when the subsystems are fully detailed designed.* With more detailed subsystems the center of mass can be determined with more precision. This is important, because it should be within 2 cm of the geometric center. Next the center of mass should be in front of the center of pressure to ensure a aerodynamic stability.

11.2.8 Partial Non-Destructive Re-entry

- *Look into more detail for a different backshell ablator material.* At this moment PICA is used as a heat shield throughout the capsule. However, due to the lower heat load also a different material can be used for example Super Light weight Ablator SLA. This material has been used already on different other re-entry missions.
- *Consider more uncertainties in the footprint calculations.* The footprint calculations are based on the main uncertainties. But, there are more uncertainties which are not considered like a shift in center of mass, a deviation in attitude during re-entry etc. More advanced footprint calculations can implement these uncertainties and lead to a more precise footprint calculation.
- *Perform more detailed Monte Carlo simulation.* The Monte Carlo simulation determines the footprint of the re-entry capsule landing. For this report, the simulation was done with approximately 1200 data points. This was done because the time and computing power was not available to make the footprint for more data points. However, to perform an optimal Monte Carlo simulation, at least 10,000 data points should be used. This could be done in a later stage of the design, if more computing power is available. Furthermore, additional variables can be implemented during the simulation such as the translational and rotational state of the earth.
- *Feasibility of crash scenario* No detailed calculations have been made on the crash impact of the capsule. This can be done in a further stage of the design.
- *Extensive thermal analysis of re-entry and capsule.* This document presents expected values that were established through literature and basic analysis tools. In order to accurately size the heat shield geometry and thicknesses, a more thorough analysis should be performed.

REFERENCES

[1] M. Akerboom, J. Hess, T. Talboom, F. Paradis, M. Deklerck, A.-T. Schulz, S. Petrovic, T. Rijndorp, and R. Wildvank, "DelFFi Delta & Phi: Two Nanosatellites for Formation Flying in Low-Earth Orbit, Baseline Report.".

[2] "QB50 website." https://www.qb50.eu/index.php/project-description. Accesed on: 19-06-2013.

[3] A. Smith, "Sensor Selection Working Group Final Report." https://www.qb50.eu/sswg_report.pdf, United Kingdom, 2012. Accessed on: 15-06-2013.

[4] M. Akerboom, J. Hess, T. Talboom, F. Paradis, M. Deklerck, A.-T. Schulz, S. Petrovic, T. Rijndorp, and R. Wildvank, "DelFFi Delta & Phi: Two Nanosatellites for Formation Flying in Low-Earth Orbit, Mid-Term Report.".

[5] NASA, "NRLMSISE-00 Emperical Model of the Atmosphere: Statistical Comparisons and Sceintific Issues." http://ntrs.nasa.gov/archive/nasa/casi.ntrs.nasa.gov/20020038771_2002061046.pdf, December 2001. Accessed on: 27-06-2013.

[6] D. D. Hathaway, "Solar Cycle Prediction." http://solarscience.msfc.nasa.gov/predict.shtml. Accessed on: 03-05-2013.

[7] National Oceanic and Atmosphereic Administration, "Index of Geomagnetc Data Indices." ftp://ftp.ngdc.noaa.gov/STP/GEOMAGNETIC_DATA/INDICES/KP_AP, 2004. Accessed on: 24-05-2013.

[8] QB50, "Frequently Asked Questions of QB50." www.qb50.eu/index.php/faq. Accessed on: 31-05-2013.

[9] MathWorks, "Orbital Parameters to Cartesian Coordinates." http://www.mathworks.com/matlabcentral/fileexchange/39494-geodetic-and-geocentric-coordinates/content/orb2eci.m. Accessed on: 21-05-2013.

[10] MathWorks, "Cartesian to Geodetic Coordinates." http://www.mathworks.com/matlabcentral/fileexchange/7941-convert-cartesian-ecef-coordinates-to-lat-lon-alt. Accessed on: 21-05-2013.

[11] R. Braeunig, "Rocket & Space Technology, Orbital Mechanics." http://www.braeunig.us/space/orbmech.htm. Accessed on: 03-05-2013.

[12] C. Sabol, R. Burns, and C. A. McLaughlin, "Satellite Formation Flying Design and Evolution," *Journal of Spacecraft and Rockets*, vol. Vol. 38, 2001.

[13] S. DAmico and O. Montenbruck, "Proximity Operations of Formation-Flying Spacecraft Using an Eccentricity/Inclination Vector Separation," *Journal of Guidance, Control, and Dynamics*, vol. 29, 2006.

[14] K. Alfriend, S. R. Vadali, P. Gurfil, J. How, and L. Breger, *Spacecraft Formation Flying: Dynamics, Control, and Navigation*. Butterworth-Heinemann, 2009.

[15] W. Ren and R. W. Beard, "Virtual Structure Based Spacecraft Formation Control With Formation Feedback," *AIAA Guidance, Navigation, and Control Conference and Exhibit*, 2002.

[16] J. P. How and M. Tillerson, "Analysis of the Impact of Sensor Noise on Formation Flying Control," tech. rep., Analysis of the Impact of Sensor Noise on Formation Flying Control, 2001.

[17] H. Schaub and K. T. Alfriend, "Impulsive Feedback Control to Establish Specific Mean Orbit Elements of Spacecraft Formations," *Journal of Guidance, Control, and Dynamics*, vol. 24, 2001.

[18] E. Gill, P. Sundaramoorthy, J. Bouwmeester, and B. Sanders, "Formation Flying to enhance the QB50 Space Network," in *Small Satellite Systems and Services Symposium (4S)*, (Funchal, Portugal), 2010.

[19] Von Karman Institute, "QB50 Welcome, Practical Aspects and Status of the project," January 2013. Presentation on 5th QB50 Workshop.

[20] R. Engels and J. Junkins, "The gravity-perturbed Lambert problem: A KS variation of parameters approach," *Celestial mechanics*, vol. 24, no. 1, pp. 3–21, 1981.

[21] European Space Agency, "GENSO." http://www.genso.org. Accessed on: 20-06-2013.

[22] F. Singarayar, *QB50 System Requirements and Recommendations*. QB50, 3 ed., 2013.

[23] ASM Aerospace Specification Metals Inc., "Aluminum 5052-H32." http://asm.matweb.com/search/SpecificMaterial.asp?bassnum=MA5052H32. Accessed on: 21-06-2013.

[24] Azurespace, "30http://www.azurspace.com/images/pdfs/HNR_0003384-00-01.pdf, 2012. Accessed on: 16-06-2013.

[25] S. Arnold, "Qbx - The CubeSat Experimen." http://digitalcommons.usu.edu/cgi/viewcontent.cgi?filename=0&article=1090&context=smallsat&type=additional. Accessed on: 04-06-2013.

[26] Clyde Space, "EPS datasheet." http://www.clyde-space.com/documents/2818. Accessed on: 21-06-2013.

[27] J. R. Wertz and W. J. Larson, eds., *Space Mission Analysis and Design*. New York, NY: Springer, 3rd ed., 2007.

[28] ISIS, "CubeSatShop." http://www.cubesatshop.com/. Accessed on: 24-05-2013.

[29] L. Visagie, "6th QB50 Workshop," in *ADCS Design and interface specification*, 2013.

[30] A. H. de Ruiter, *Spacecraft Dynamics and Control*. Wiley, 2012.

[31] A. Bedford and W. Fowler, *Engineering Mechanics: Dynamics*. Pearson, 2008.

[32] T. W. Flatley, W. Morgensten, A. Reth, and F. Bauer, "A B-Dot Acquisition Controller for the RADARSAT Spacecraft," tech. rep., Goddard Space Flight Center, 1997.

[33] J. Bouwmeester, T. Hoevenaars, D. Choukroun, and J. Reijneveld, "Design and verification of a very compact and versatile attitude determination and control system for the Delfi-n3Xt nanosatellite," in *Proceedings of the 4S Symposium*, (Slovenia), pp. 1–15, 2012.

[34] A. Sofyali and R. Aslan, "Magnetic Attitude Control of Small Satellites: A Survey of Applications and A Domestic Example," 2011.

[35] M. E. Pittelkau, "Sensors for attitude Determination," *Encyclopedia of Aerospace Engineering*, 2010.

[36] Y. Winetraub, S. Bitan, U. dd, and D. A. B. Heller., "Attitude Determination Advanced Sun Sensors for Pico-satellites," p. 10, 2006.

[37] U. Kvel, E. Kulu, T. Scheffler, silver Latt, and M. Noorma, "Magnetic Attitude Control Algorithms For Estcube-1," in *IAC-12-B4.5.12*, 2012.

[38] J. R. Wertz, *Spacecraft attitude determination and control*. Reidel Publishing Company, 1991.

[39] Adcole, "Two-axis fine sun sensor system." http://adcole.com/two-axis-fss.html, June 2013. Accessed on: 20 June 2013.

[40] ISIS, "CubeSat Sun Sensor." http://www.cubesatshop.com/index.php?page=shop.product_details&flypage=flypage.tpl&product_id=104&category_id=7&keyword=sun+sensor&option=com_virtuemart&Itemid=69. Accessed on: 07-06-2013.

[41] V. Francois-Lavet, "Study of passive and active attitude control systems for the OUFTI nanosatellites," master thesis, University of Liege, Place du Vingt Aout 7 4000 Liege, Belgium, May 2010. Supervisor: Prof. Christophe Geuzaine.

[42] A. Scholz, P. J. Miau, and P. J. Juang, "Miniature Digital Sun Sensor for Application in Nano- and Picosatellites," in *CubeSat Developers Workshop*, 2008.

[43] J. A. Bowen, "On-board orbit determination and 3-axis attitude determination for picosatellite applications," Master's thesis, Faculty of California Polytechnic State University, 2009.

[44] J. D. Foley, "Calibration and characterization of cubesat magnetic sensors using a helmholtz cage," Master's thesis, Faculty of California Polytechnic State University, December 2012.

[45] S. Nasiri, "A critical review of MEMS Gyroscope Technology and Commercialization status." http://invensense.com/mems/gyro/documents/whitepapers/MEMSGyroComp.pdf, June 2005.

[46] J. Bouwmeester, G. Brouwer, E. Gill, G. Monna, and J. Rotteveel, "Design Status of the Delfi-n3Xt Nanosatellite Project," in *Proceedings of the61st International Astronautical Congress*, (Prague, Czech Republic), 2010.

[47] Analog Devices, "MEMS Inertial Sensor." http://www.analog.com/static/imported-files/selection_tables/MEMS_Inertial_Sensors_Selection_Tables.pdf, November 2012. Accessed on: 20-06-2013.

[48] Analog Devices, "High Stability, Low Noise Vibration Rejection Yaw Rage Gyroscop," tech. rep., Analog Devices, 2012.

[49] Surrey Satellite Technology LTD, "Space GPS Receiver: SGR-05U Datasheet." http://www.sstl.co.uk/getattachment/97ae8ccc-024d-4376-a99d-7d3c2266a7f7/SGR-05U-05P. Accessed on: 15-05-2013.

[50] R. Bishop, D. Hinkley, D. Stoffel, D. Ping, and P. Straus, "First Results from the GPS Compact Total Electron Content Sensor (CTECS) on the PSSCT-2 Nanosat," in *26th Annual AIAA/USU Conference on small satellites*, 2012.

[51] M. J. Sidi, *Spacecraft dynamics and Control: a practical engineering Approach*. Cambridge University Press, 1997.

[52] J. Li, M. Post, T. Wright, and R. Lee, "Design of Attitude Control Systems for CubeSat-Class Nanosatellite," *Journal of Control Science and Engineering*, vol. 2013, pp. Article ID 657182, 15 pages, 2013.

[53] ZARM Technik, "Magnetic Torquers for Micro-Satellites Datasheet." http://www.zarm-technik.de/downloadfiles/ZARMTechnikAG_CubeSatTorquers_web2010.pdf. Accessed on: 11-06-2013.

[54] ISIS Space, "ISIS MagneTorquer Board (iMTQ) Datasheet." http://www.isispace.nl/brochures/ISIS%20iMTQ%20Brochure%20v12.11.pdf, 2013. Accessed on: 12-06-2013.

[55] P. Fortescue, J. Stark, and G. Swinerd, *Spacecraft System Engineering*. Wiley, 2003.

[56] G. P. Candini, F. Piergentili, and F. Santoni, "Miniaturized attitude control system for nanosatellites," *Acta Astronautica*, vol. 81, pp. 325–334, 2012.

[57] G. Eriksson, "A Research Study and Design Concept to Improve Reaction Wheels for Precision CubeSat Attitude Control," Master's thesis, Lulea University of Technology, 2012.

[58] M. Hess, A. Helm, L. Cacciapuoti, S. Feltham, R. Much, R.Nasca, and O. M. M. Gribkov, "The ACES GNSS Subsystem and its Applications," tech. rep., Astrium Space Transportation, April 2010.

[59] J. Mueller, R. Hofer, and J. Ziemer, "Survey of propulsion technologies applicable to CubeSats," tech. rep., California Institute of Technology, 2010.

[60] R. L. Bayt, "Analysis, Fabrication and Testing of a MEMS-based Micropropulsion System," Master's thesis, Massachusetts Institute of Technology, 1999.

[61] A. Anis, *Remote Sensing - Advanced Techniques and Platforms*, ch. Cold Gas Propulsion System - An Ideal Choice for Remote Sensing Small Satellites, p. 462. InTech, 2012.

[62] Y. A. Cengel and M. Boles, *Thermodynamics - An Engineering Approach*. McGraw-Hill, 2010.

[63] A. Cervone, B. Zandbergen, J. Guo, E. Gill, W. Wieling, F. T. Nardini, and C. Schuurbiers, "Application of an Advanced Micro-Propulsion system to the DelFFi Formation Flying Demonstration Within the QB50 Mission," in *Proceedings of the 63rd International Astronautical Congress*, (Naples, Italy), pp. 1–8, 2012.

[64] M. Mihailovic, T. Mathew, J. Creemer, B. Zandbergen, and P. Sarro, "Mems Silicon-Based Resistojet Micro-Thruster for Attitude Control of Nano-Satellites," in *Transducers'11*, (Beijing, China), 2011.

[65] I. Polmear, *Light Alloys: Metallurgy of the Light Metals*. Butterworth-Heinemann, 1995.

[66] B. Zandbergen, "Rocket Propulsion." Lecture, March 2012. Internal publication.

[67] Delfi Space, "Micropropulsion Payload." http://www.delfispace.nl/index.php/delfi-n3xt/micropropulsion-payload. Accessed on: 18-06-2013.

[68] T. V. Mathew, B. Zandbergen, M. Mihailovic, J. Creemer, and P. Sarro., "A silicon-based MEMS Resistojet for Propelling Cubesats." Presentation, 2011.

[69] W. Beech, D. E. Nielsen, and J. Taylor, "AX.25 Link Access Protocol for Amateur Packet Radio," July 1998.

[70] European Space Agency, "GENSO - Project Background." http://www.esa.int/Education/Project_background. Accessed on: 22-05-2013.

[71] C. E. Shannon, "Communication in the Presence of Noise," *Proceedings of the IRE*, vol. 37, pp. 10–21, 1949.

[72] Circuit Design, Inc., "Circuit Design, competence in radio solutions." http://www.cdt21.com/resources/default3.aspp. Accessed on: 03-06-2013.

[73] ISIS, "TRXUV VHF/UHF Transceiver." http://www.isispace.nl/brochures/ISIS_TRXUV_Transceiver_Brochure_v.12.5.pdf. Accessed on: 11-06-2013.

[74] N. Cornejo, J. Bouwmeester, and G. N. Gaydadjiev, "Implementation Of A Reliable Data Bus For The Delfi Nanosatellite Programme," p. 8, 2009.

[75] Delft University of Technology, "Onboard computer." http://delfispace.nl/index.php?option=com_content&view=category&layout=blog&id=15&Itemid=19. Accessed on: 16-05-2013.

[76] DoubleTap Technology Ltd., "Micro-SD Specification." http://www.dtt8.com/images/micro-sd%20specification.pdf. Accessed on: 16-05-2013.

[77] "Onboard Computer." http://delfispace.nl/index.php?option=com_content&view=category&layout=blog&id=15&Itemid=19.

[78] H. K. Tran, C. E. Johnson, D. J. Rasky, F. C. L. Hui, M.-T. Hsu, and Y. K. Chen, "Phenolic Impregnated Carbon Ablators (PICA) for Discovery class missions," *Thermophysics Conference*, 1996.

[79] E. Gill, J. Bouwmeester, J. Guo, and N. von Storch, "Delfi-C3 Five Years in Orbit." Presentation, 2013.

[80] V. Lappas, "QB50 ADCS + GPS." https://www.qb50.eu/download/3rdQB50Workshop_presentations/07-ADCS%202.2.12-Lappas-3rdQB50Workshop.pdf, Februari 2012. Accessed on: 27-05-2013.

[81] Berlin Space Techologies, "ST-200 Miniaturised Autonomous Star Tracker." http://www.berlin-space-technologies.com/index.php?id=42. Accessed on: 20-06-2013.

[82] E. Mooij, "Re-entry Trajectories." Delft University of Technology. Internal publication.

[83] S. Sartorius, "STDATMO: Standard Atmosphere Function." http://www.mathworks.com/matlabcentral/fileexchange/28135-stdatmo-standard-atmosphere-function/content/stdatmo.m. Accessed on: 05-06-2013.

[84] J. A. Pearson, "U.S. Standard Atmosphere 1976," tech. rep., National Aeronotics and Space Administration, National Oceanic and Atmospheric Administration, United States Air Force, 1976.

[85] J. Mulder, W. van Staveren, J. van der Vaart, E. de Weerdt, A. in't Veld, and E. Mooij, "Flight Dynamics." TU Delft, March 2013. Internal publication.

[86] R. Wernitz, M. Fertig, G. Herdrich, S. Lhle, M. Winter, and H.-P. Rser, "Assessment of PWT Conditions for the STARDUST Post-Flight Evaluation,"

[87] J. Thornton, W. Fan, E. Ghandehari, M. Stachpoole, and J. Chavez-Garcia, "PICA Variants With Improved Mechanical Properties." http://ntrs.nasa.gov/archive/nasa/casi.ntrs.nasa.gov/20110014590_2011015184.pdf. Accessed on: 31-05-2013.

[88] D. Olynick, Y.-K. Chen, and M. E. Tauber, "Forebody TPS Sizing with Radiation and Ablation for the Stardust Sample Return Capsule," *American Institute of Aeronautics and Astronautics*, 1997.

[89] O. R. Evans, "Aerogel Insulation for the Thermal Protection of Venus Spacecraft." http://www.sbir.gov/sbirsearch/detail/355873, 2006. Accessed on: 13-06-2013.

[90] K. M. McNamara, D. J. Schneberk, D. M. Empey, A. Koshti, D. E. Pugel, I. Cozmuta, M. Stackpoole, N. P. Ruffino, E. C. Pompa, O. liveras, and D. A. Kontinos, "X-ray Computed Tomography Inspection of the Stardust Heat Shield," tech. rep., NASA Johnson Space Center, 2008.

[91] E. Venkatapathy, C. E. Szalai, B. Laub, H. H. Hwang, J. L. Conley, and J. Arnold, "Thermal Protection System Technologies for Enabling Future Sample Return Missions,"

[92] M. Finckenor, "Optical Property Measurements on the Stardust Sample Return Capsule."

[93] M. A. Covington, J. M. Heinemann, and H. E. Goldstein, "Performance of a Low Density Ablative Heat Shield Material," *Journal of Spacecraft and Rockets*, vol. 45, pp. 237–247, 2008.

[94] T. W. Knacke, *Parachute Recovery System Design Manual*. Para Publishing, first ed., 1992.

[95] http://http://www.the-rocketman.com/chutes.html.

[96] University of Michigan, "Human Appropriation of the World's Fresh Water Supply." http://www.globalchange.umich.edu/globalchange2/current/lectures/freshwater_supply/freshwater.html, April 2006. Accessed on:21-06-2013.

[97] K. Vanderhauwaert, "Some legal aspects of the QB50 project," June 2013.

[98] European Cooperation for Space Standardization, *Space product assurance - Safety*. 2009.

[99] United Nations Office of Outer Space, "Rules Concerning Space Activites and the Establishment of a Registry of Space Objectives (Space Activities Act)." http://www.oosa.unvienna.org/oosa/en/SpaceLaw/national/netherlands/space_activities_actE.html. Accessed on: 21-06-2013.

[100] United Nations Office for Outer Space Affairs, *United Nations Treaties and Principles on Outer Space*. 1968.

[101] J. J. Sellers, W. J. Astore, R. B. Giffen, and W. J. Larson, *Understanding Space*. McGraw-Hill, 2013.

[102] J. N. Moss, C. E. Glass, and F. A. Greene, "Blunt body aerodynamics for hypersonic low denisty flows," September 2006.

[103] W. H. Willcockson, "Stardust sample return capsule design experience," *Journal of Spacecraft and Rockets*, vol. 36, 1999.

[104] European Space Agency, "Marco Polo - R." http://sci.esa.int/science-e/www/object/index.cfm?fobjectid=49559, May 2013. Accessed on: 12-06-2013.

[105] The engineering toolbox, "Metals and alloy densities." http://www.engineeringtoolbox.com/metal-alloys-densities-d_50.html. Accessed on: 17-06-2013.

[106] Microwave Telemetry, Inc, "PTT-100 22 gram Solar Argos/GPS PTT." http://www.microwavetelemetry.com/bird/solarArgosGPS_22g.cfm, June 2013. Accessed on: 17-06-2013.

[107] M. Specialities, "XPC10 High temperature miniature Pressure sensor," tech. rep., Measurement Specialities, 2013.

[108] U.S. Department of Defense, "The Ballistic Missle Defense System (BMDS)." http://www.mda.mil/system/system.html. Accessed on: 14-06-2013.

[109] Deluxe CCTV Video Surveillance, "Deluxe CCTV Video Surveillance, Real time trackers." http://www.deluxecctv.com/catalog/real-time-trackers/spark-nano-gps-spy-tracker-988.html. Accessed on: 18-06-2013.

[110] Walston Retrieval. http://www.walstonretrieval.com/sub-3.htm. Accessed on: 24-05-2013.

[111] Telonics Inc., "Telonics." http://www.telonics.com/index.php. Accessed on: 17-06-2013.

[112] F. Jacq, "ARGOS worldwide tracking and environmental monitoring by SATELLITE." http://www.argos-system.com/html/system/how_it_works/tracking_en.html. Accessed on: 17-06-2013.

[113] D. T. Siewert, D. S. Liu, D. D. R. Smith, and M. J. C. Madeni, "Properties of Lead-Free Solders." http://www.plasticsintl.com/datasheets/Phenolic_G10_FR4.pdf.

[114] World Commission on Environment and Development, "Our Common Future," 1978.

[115] S. Nowlin and L. Thimons, "Surviving the heat: the application of phenolic impregnated carbon ablators," 2013.

[116] National Aeronautics and Space Administration, "Final Environmental Assessment for the Origins, Spectral Interpretation, Resource Identification, and Security-Regolith Explorer Mission," March 2013.

[117] United Nations Office for Outer Space Affairs, *Space Debris Mitigation Guidelines of the Committee on the Peaceful Uses of Outer Space*. 2010.

[118] K. Woellert, P. Ehrenfreud, A. Ricco, and H. Hertzfeld, "CubeSats: Cost-effective science and technology platforms for emerging and developing nations," *Advances in Space Research*, vol. 47, pp. 663–684, 2011.

[119] D. DePasquale and J. Bradford, "Nano/Microsatellite Market Assessment." http://www.sei.aero/eng/papers/uploads/archive/SpaceWorks_NanoMicrosat_Market_Feb2013.pdf. Accessed on: 21-06-2013.

[120] A. NASA, "Cost Estimating Module." http://orion.asu.edu/Class Accessed on: 01-07-2013.

[121] Environmental Protection Agency (EPA), "Hazardous Waste." http://www.epa.gov/osw/hazard/wastetypes/pdfs/listing-ref.pdf, March 2008. Accessed on: 25-04-2013.

[122] R. Braeunig, "Rocket & Space Technology, Atmosphere Properties." http://www.braeunig.us/space/atmos.htm. Accessed on: 03-05-2013.

APPENDIX A

FUNCTIONAL FLOW DIAGRAMS

This chapter shows the functional flow diagram as well as the functional breakdown structure.

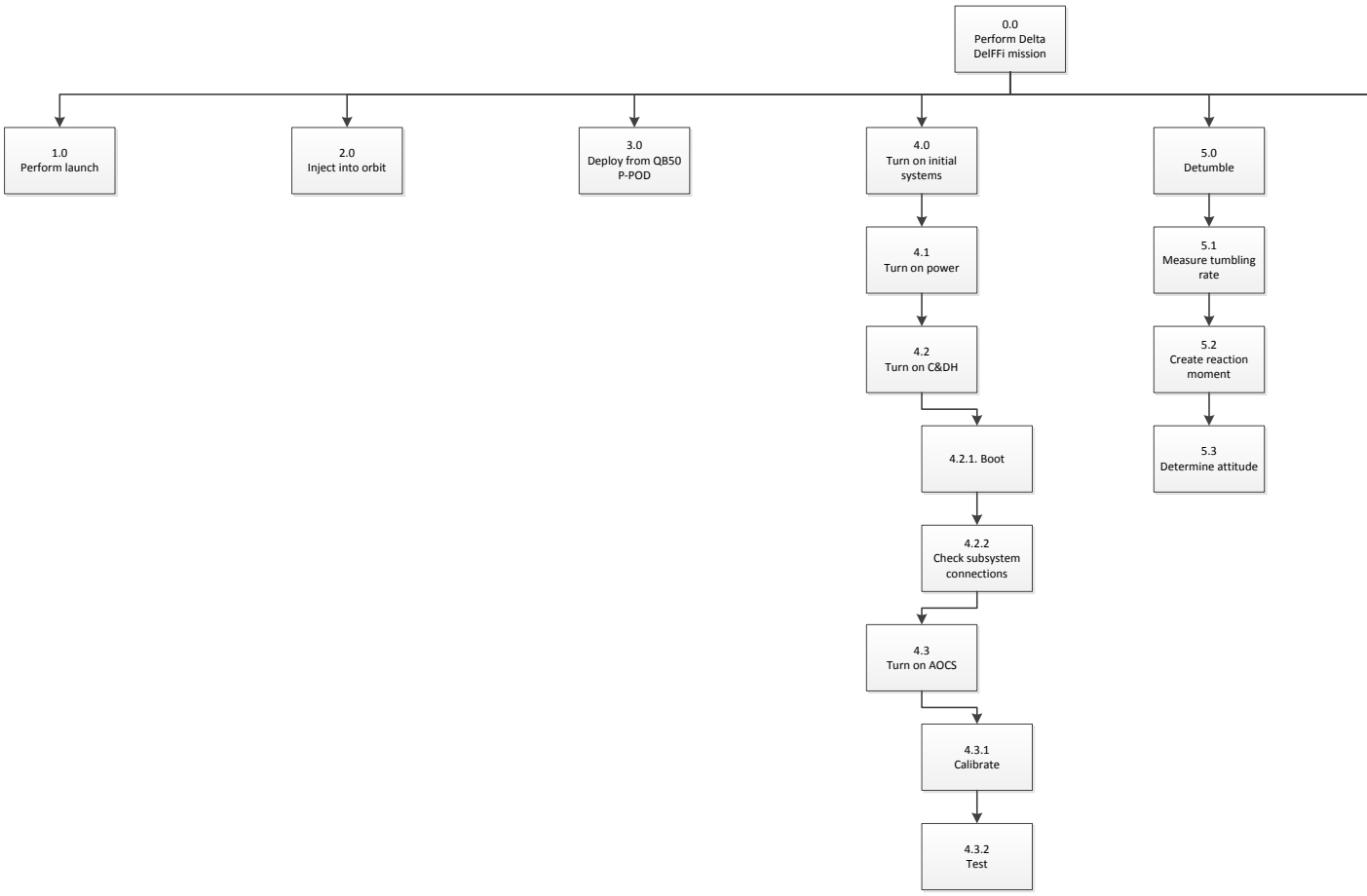

Figure A.1: Functional breakdown diagram

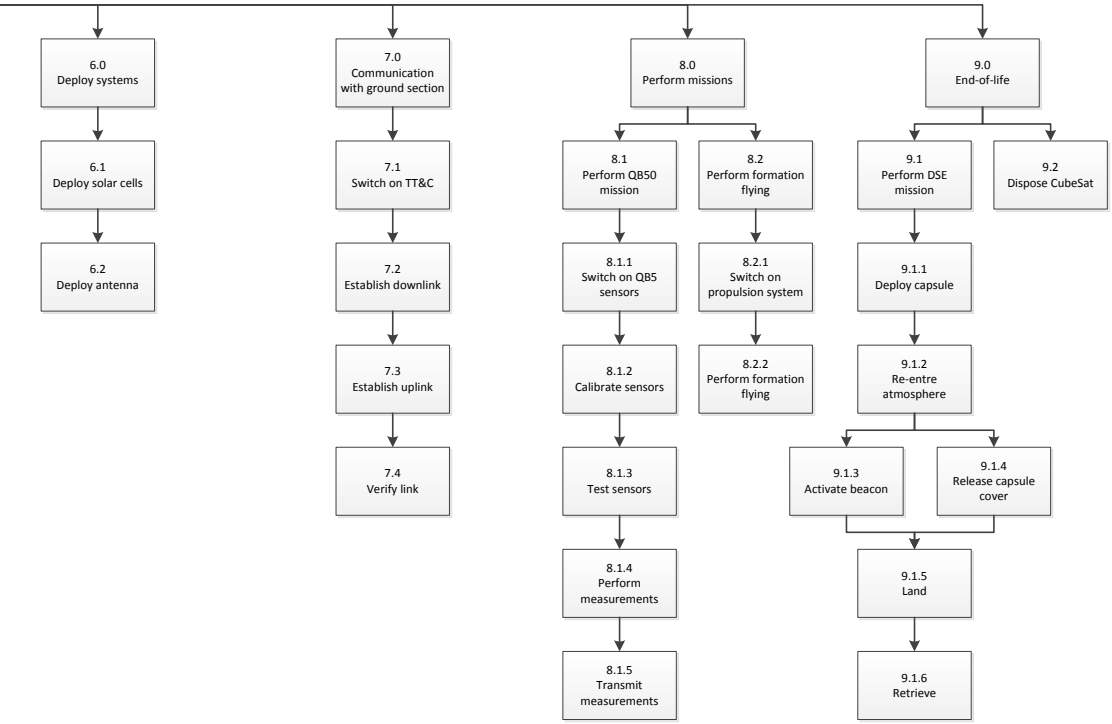
6.0
Deploy systems
6.1
Deploy solar cells
6.2
Deploy antenna
7.0
Communication with ground section
7.1
Switch on TT&C
7.2
Establish downlink
7.3
Establish uplink
7.4
Verify link
8.0
Perform missions
8.1
Perform QB50 mission
8.1.1
Switch on QB5 sensors
8.1.2
Calibrate sensors
8.1.3
Test sensors
8.1.4
Perform measurements
8.1.5
Transmit measurements
8.2
Perform formation flying
8.2.1
Switch on propulsion system
8.2.2
Perform formation flying
9.0
End-of-life
9.1
Perform DSE mission
9.2
Dispose CubeSat
9.1.1
Deploy capsule
9.1.2
Re-entre atmosphere
9.1.3
Activate beacon
9.1.4
Release capsule cover
9.1.5
Land
9.1.6
Retrieve

Figure A.2: Functional flow diagram (part 1)

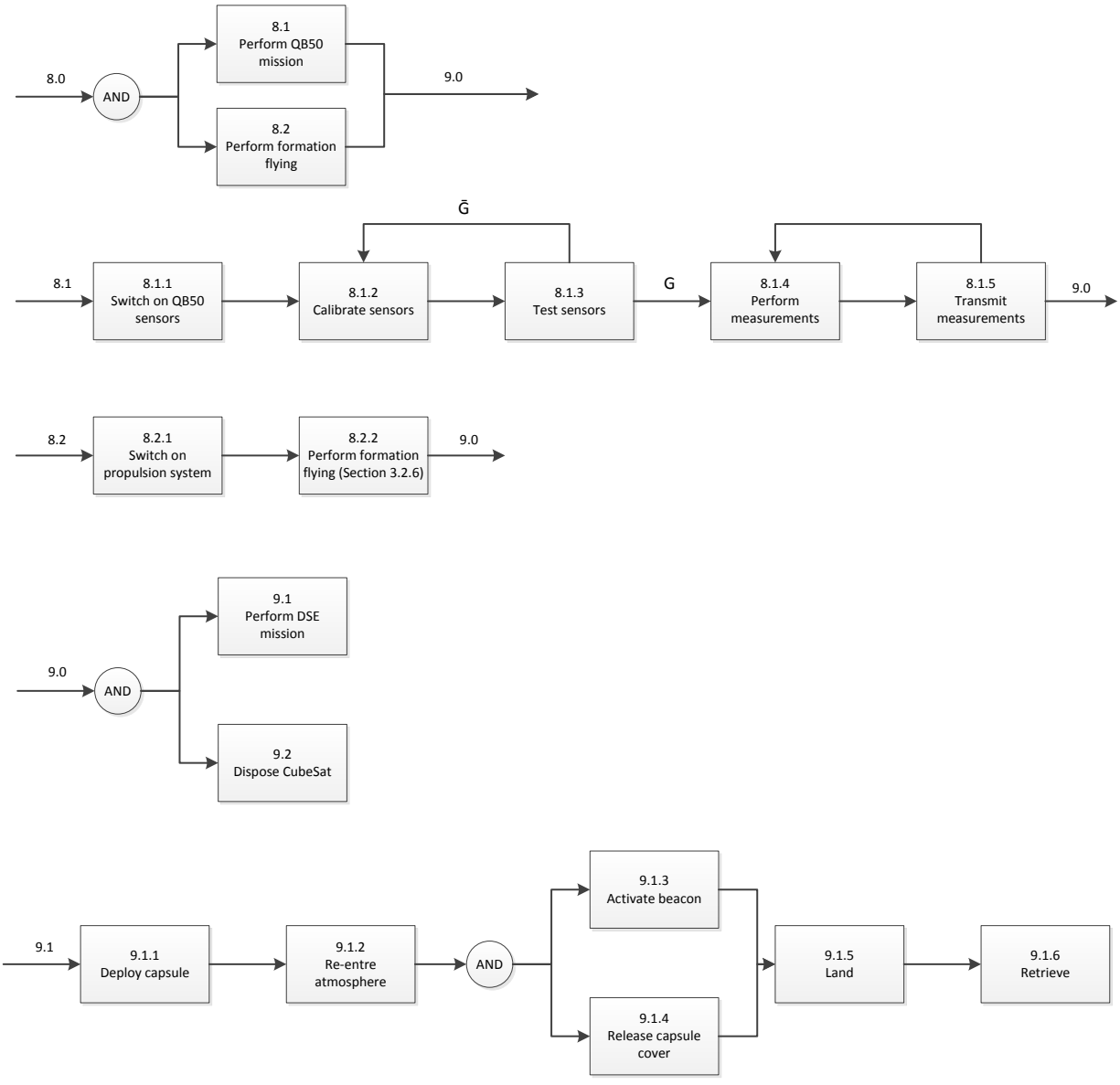

Figure A.3: Functional flow diagram (part 2)

APPENDIX B

LINK BUDGET PARAMETER CALCULATIONS

Table B.1 shows the parameters that are used in the link budgets, together with their variable name, units and an equation to calculate them. Some variables that are used in the equations, but are not explained are the signal wavelength λ, the signal frequency f, the Earth radius R_e, the visibility angle γ_v, the orbital altitude h, the system noise temperature T_S and the implementation losses L_{imp}.

Table B.1: Equations that are used in the link budget

Parameter	**Symbol**	**Unit**	**Equation**	**Eq. number**
Transmitter power	P	dBW	$10 \cdot \log(P)$	1
Transmit antenna length	d_t	m	$\frac{\lambda}{4}$	2
Transmit antenna beamwidth	θ_t	deg	$\frac{21}{f_{GHz} \cdot d_t}$	3
Transmit antenna pointing loss	L_{pt}	dB	$-12 \cdot \left(\frac{e_t}{\theta_t}\right)^2$	4
Peak transmit antenna gain	G_{pt}	dBi	$44.3 - 10 \cdot \log(\theta_t^2)$	5
Net transmit antenna gain	G_t	dB i	$G_{pt} + L_{pt}$	5
Equivalent Isotropic Radiated Power	$EIRP$	dBW	$P + L_l + G_t$	6
Propagation path length	S	km	$R_e \cdot cos(180 - \gamma_v) + \sqrt{R_e^2 \cdot cos^2(180 - \gamma_v) + (R_e + h)^2 - R_e^2}$	7
Space loss	L_s	dB	$147.55 - 20 \cdot \log(S) - 20 \cdot \log(f)$	8
Receive antenna beamwidth	θ_r	deg	$\frac{21}{f_{GHz} \cdot d_r}$	9
Receive antenna pointing loss	L_{pr}	dB	$-12 \cdot \left(\frac{e_r}{\theta_r}\right)^2$	10
Receive antenna gain	G_r	dBi	$G_{rp} + Lpr$	11
Energy-per-bit to noise ratio	$\frac{E_b}{N_0}$	dB	$P + L_l + G_t + L_{pr} + L_s + L_a + G_r + 228.6 - 10 \cdot \log(T_s) - 10 \cdot \log(R)$	12
Carrier-to-noise density ratio	$\frac{C}{N_0}$	dB-Hz	$EIRP + L_s + L_a + \frac{G_r}{T_s} + 228.6$	13
Link margin	$Marg.$	dB	$\frac{E_b}{N_0} - req.\frac{E_b}{N_0} + L_{imp}$	14

Propagation & Polarization Loss The propagation & polarization loss L_a is determined using [27, p. 564]. First, the downlink will be considered. With a downlink frequency of 145 MHz, the theoretical one way zenith attenuation is -0.03 dB. Continuing with the uplink, a frequency of 435 MHz is selected. This frequency corresponds to about -0.03 dB.

Energy to Noise Ratio The required energy to noise ratio can be found using with [27, p. 561]. The probability of bit error has been previously determined to be 10^-5, furthermore, BPSK was chosen as a modulation scheme in Section 4.5. Therefore, a required energy to noise ratio of 2.4 dB is need.

APPENDIX C

EXTENSIVE LINK BUDGETS FOR TT&C

Table C.1 and Table C.2 show the downlink and uplink budget, respectively, in more detail. These values were calculated using the equations in Chapter B.

Table C.1: Downlink budget for DelFFi Delta

	Parameter	Value	Unit
General	Transmission frequency	145	MHz
	Output power	0.15	W
	Orbital altitude	320	km
	Data rate	4800	bps
	Modulation scheme	BPSK	-
	Minimum elevation	20	deg
	Coding gain	0	dB
Transmitter	Power amplifier output	-8.2	dBW
	Transmitter line loss	-2	dB
	Transmit antenna pointing loss	-0.02	dB
	Transmitted EIRP	-10.3	dB
Channel	Path loss	-133.8	dB
	Attenuation loss	-0.3	dB
	Total channel loss	-134.1	dB
Receiver	Pointing offset	-5.4	dB
	Implementation loss	-4	dB
	System noise temperature	221	K
Received $\frac{E_b}{N_0}$		13.1	dB
Required $\frac{E_b}{N_0}$ for $BER = 10^{-5}$		2.4	dB
Minimum link margin		3	dB
Final link margin		**6.7**	**dB**

Table C.2: Uplink budget for DelFFi Delta

	Parameter	Value	Unit
General	Transmission frequency	435	MHz
	Output power	250	W
	Orbital altitude	320	km
	Data rate	1200	bps
	Modulation scheme	BPSK	-
	Minimum elevation	20	deg
	Coding gain	0	dB
Transmitter	Power amplifier output	24.0	dBW
	Transmitter line loss	-2	dB
	Transmit antenna pointing loss	-0.02	dB
	Transmitted EIRP	22.3	dBW
Channel	Path loss	-143.4	dB
	Attenuation loss	-0.3	dB
	Total channel loss	-143.7	dB
Receiver	Pointing offset	-12.2	dB
	Implementation loss	-4	dB
	System noise temperature	614	K
Received $\frac{E_b}{N_0}$		24.3	dB
Required $\frac{E_b}{N_0}$ for $BER = 10^{-5}$		2.4	dB
Minimum link margin		17.9	dB
Final link margin		**14.9**	**dB**

APPENDIX D

EXTENSIVE POWER BUDGET

Table D.1: Detumbling mode

Subsystem	Component	Duty Factor	Required power [W]
Power	G-EPS	100%	0.063
C&DH	OBC	100%	0.167
TT&C	UHF	0%	0
	VHF	0%	0
AOCS	Magnetic torquers	100%	0.2
	Sun sensors (6x)	100%	0.15
	Magnetometer	100%	0.001
	Reaction wheels	100%	0.71
	GPS	100%	1
Propulsion	Thrusters	0%	0
	Standby system	0%	0
Payloads	QB50	0%	0
	DSE	0%	0
System bus	Sensors	0%	0
Total			2.291

Table D.2: Normal operational mode

Subsystem	Component	Duty Factor	Required power [W]
Power	G-EPS	100%	0.063
C&DH	OBC	100%	0.167
TT&C	UHF	100%	0.2
	VHF	78%	1.17
AOCS	Magnetic torquers	20%	0.04
	Sun sensors (6x)	100%	0.15
	Magnetometer	100%	0.001
	Reaction wheels	75%	0.53
	GPS	100%	1
Propulsion	Thrusters	0%	0
	Standby system	0%	0
Payloads	QB50	20%	0.11
	DSE	100%	0
System bus	Sensors	100%	0.25
Total			3.68

Table D.3: Safe mode

Subsystem	Component	Duty Factor	Required power [W]
Power	G-EPS	100%	0.063
C&DH	OBC	100%	0.167
TT&C	UHF	100%	0.2
	VHF	10%	0.15
AOCS	Magnetic torquers	0%	0
	Sun sensors (6x)	100%	0.15
	Magnetometer	100%	0.001
	Reaction wheels	0%	0
	GPS	0%	0
Propulsion	Thrusters	0%	0
	Standby system	0%	0
Payloads	QB50	0%	0
	DSE	0%	0
System bus	Sensors	100%	0.25
Total			0.981

Table D.4: Formation flying mode

Subsystem	Component	Duty Factor	Required power [W]
Power	G-EPS	100%	0.063
C&DH	OBC	100%	0.167
TT&C	UHF	100%	0.2
	VHF	100%	1.17
AOCS	Magnetic torquers	10%	0.02
	Sun sensors (6x)	100%	0.15
	Magnetometer	100%	0.001
	Reaction wheels	75%	0.53
	GPS	100%	1
Propulsion	Thrusters	0.2%	0.026
	Standby system	99.8%	0.045
Payloads	QB50	20%	0.11
	DSE	0%	0
System bus	Sensors	100%	0.25
Total			3.73

APPENDIX E

EXTENSIVE DATA BUDGET

Table E.1: Data information

Type of data	Times active/orbit	Seconds active/activation	Total time/orbit [min]
QB50 Payload	9	60	9
GPS for tagging	9	60	9
Formation Flying	1	60	1
Housekeeping			
AOCS	90	1	1.5
EPS	90	1	1.5
GPS	90	1	1.5
Thermal	90	1	1.5
TT&C	90	1	1.5
Propulsion	90	1	1.5
Total			10.5

Table E.2: Data rates

Type of data	Data rate [kbps]	Collected data/orbit [kb]
QB50 Payload	1.4752	796.6
GPS for tagging	8.9	4,806
Formation Flying	10	600
Housekeeping		
AOCS	2.636	237.24
EPS	0.005	0.45
GPS	8.9	801
Thermal	0.005	0.45
TT&C	0.005	0.45
Propulsion	0.005	0.45
Total		7,242.65